MOLECULAR MECHANISMS THAT DIFFERENTIATE DENDRITIC AND AXONAL GROWTH

by

Xin Wang

A dissertation submitted in partial fulfillment
of the requirements for the degree of
Doctor of Philosophy
(Molecular, Cellular and Developmental Biology)
in The University of Michigan
2014

Doctoral Committee:

Assistant Professor Bing Ye, Co-Chair
Assistant Professor Catherine A. Collins, Co-Chair
Professor Kenneth M. Cadigan
Assistant Professor Orie Shafer
Professor Kristen J. Verhey
Associate Professor Haoxing Xu

DEDICATION

To my family and friends, especially my parents and grandmother.

ACKNOWLEDGEMENTS

I would very much like to first thank my graduate mentors, Drs. Catherine A. Collins and Bing Ye, who both offered me the priviledge to work in their laboratories, intensive guidance towards my research and invaluable career advice. I am thankful for their patience, generosity, and openess throughout my doctoral study. I have also learned and benefit tremendously from their insights and enthusiasm towards developmental neurobiology research, writing and presentation skills, as well as the persistency and optimism facing difficulty. Without their support and encouragement, this thesis would not have been possible.

I would also like to thank my thesis committee members: Drs. Kenneth M. Cadigan, Orie Shafer, Kristen J. Verhey and Haoxing Xu. I am grateful for their in-depth comments on my research projects not only at each thesis committee meeting, but also whenever I seek for their help and expertise. In addition, I really appreciate the research opportunities rotating in Dr. Robert Denver's lab and Dr. Haoxing Xu's lab.

My research projects were carried out in close collaboration with outstanding colleagues at the University of Michigan. I sincerely thank the following lab members: Xin Xiong, Ronny Ewanek, Susan Klinedinst, Bibhudatta Mishra, Jung Hwan Kim, Wei Zhou, Jin Chang, Limin Yang, Sara Robinson, Mouna Bazzi, Rose Coolon, Gabriella Stern, Takuya Kaneko and Mostafa Ghannad-Rezaie from Nikolaos Chronis's lab at Biomedical Engineering Department for collaborating and co-authoring with me. I am especially thankful to have Xin Xiong, Wei Zhou, Jin Chang, and Ronny Ewanek as passionate friends at work. In addition, I appreciate the critical comments from Drs. John Kuwada, Roman Giger, Hisashi Umemori, Yukiko Yamashita, Chen-yu Lee, Ting Han on manuscripts of my research papers. Furthermore, this thesis benefits greatly from the reagents generously shared by Drs. Tadashi Uemura, Adrian Moore, Michele Crozatier,

Tzumin Lee, Larry Zipursky, Chunlai Wu, Kendal Broadie, Chun Han, Liqun Luo, and Yuh Nung Jan.

Through the course of my graduate study, I have been fully supported by the MCDB department. My special thanks are devoted to Mary Carr who is always patient and helpful with any questions I have. I also benefit a lot from the thoughtful advice and kind help from the chairs of graduate studies: Drs. Anuj Kumar and Laura Olsen, and MCDB departmental chairs: Drs. Richard Hume and Pamela Raymond. Lastly, I am honored and thankful to receive the graudent research grant and travel grants from Rackham.

Lastly, I am grateful to have my family and friends stand by me, especially my parents and my grandmother. My parents are also my best friends with unconditional love and firm support. My grandmother was a primary school teacher who first taught me to read and write.

PREFACE

This theis consists of the research projects I conducted in Prof. Catherine A. Collins's lab and Prof. Bing Ye's lab from May 2008. The objective was to delineate the regulatory mechanisms that differentiate dendritic and axonal growth during neuronal morphogenesis in *Drosophila*.

Chapters 2, 3 and 4 were respectively published in *PLOS Bio.* (2013; 11(6): e1001572), *J Neurosci*. (2013; 33(31): 12764 –12778), and *Neuron* (2013; 78: 827-838). Chapter 5 is currently in preparation and wil be submitted by Dec 2013.

Chapter 2 presents the first in vivo evidence that a single pathway, the conserved Wnd/DLK pathway, can oppositely regulate dendrite and axon growth. It is reprinted from *PLOS Biology*, Volume 11, Xin Wang, Jung Hwan Kim, Mouna Bazzi, Sara Robinson, Catherine A. Collins, and Bing Ye. Bimodal control of dendritic and axonal growth by the dual leucine zipper kinase pathway, e1001572, Copyright (2013), with minor modifications. I performed all the experiments and contributed to all the figures in the publication. I wrote the manuscript with Dr. Bing Ye. Dr. Jung Hwan Kim contributed to fly strains. Mouna Bazzi and Sara Robinson contributed to analyses of dendritic morphology. Dr. Catherine A. Collins contributed to reagents and provided critical comments on the manuscript.

Chapter 3 investigates the endogenous functions of Wnd/DLK pathway in axon and dissects the downstream components that mediate its diverse roles. It is reprinted from *Journal of Neuroscience*, Volume 33, Susan Klinedinst, Xin Wang, Xin Xiong, Jill Haenfler, and Catherine A. Collins. Independent pathways downstream of the Wnd/DLK MAPKKK regulate synaptic structure, axonal transport, and injury signaling, pg. 12764-12778, Copyright (2013), with minor modifications. Dr. Jill Haenfler generated the $jip1^{ex}$ fly line. I made the original observations and characterization of the synaptic defects in

jip1^{ex} mutants. Dr. Susan Klinedinst confirmed *jip1*^{ex} phenotypes, uncovered the involvement of downstream MAPK p38b, and systematically dissected the independent downstream pathways involved in synaptic development versus injury response. Dr. Xin Xiong performed the nerve injury assays. Dr. Susan Klinedinst and I wrote the manuscript with Dr. Catherine A. Collins.

Chapter 4 describes the instructive role of the Down syndrome cell-adhesion molecule (Dscam) in axonal presynaptic growth, but not dendritic growth. It is reprinted from *Neuron*, Volume 78, Jung Hwan Kim, Xin Wang, Rosemary Coolon and Bing Ye. Dscam expression levels determine presynaptic arbor sizes in *Drosophila* sensory neurons, pg. 827-838, Copyright (2013), with minor modifications. Dr. Jung Hwan Kim and I contributed equally to the results in the publication and wrote the manuscript together with Dr. Bing Ye. Rosemary Coolon contributed to the generation of transgenic flies.

Chapter 5 unconvers that a dendrite-specific regulator, the Krüppel-like factor Dar1 determines multipolar dendritic structure. It will be submitted as a research article titled as "The Krüppel-like factor Dar1 determines the multipolar organization of neuronal processes ". The authors are listed as Xin Wang, Jung Hwan Kim, Gabriella Sterne, and Bing Ye. I made the original observations, analyzed the data and wrote the manuscript with Dr. Bing Ye. Dr. Jung Hwan Kim performed the microarray experiments. Gabriella Stern performed and analyzed the experiments of overexpressing Dar1 in PDF neurons and in *sw* ^{ts} heterozygous RN2 neurons.

TABLE OF CONTENTS

LIST OF TABLES

LIST OF FIGURES

Chapter 1
Introduction

The nervous system controls how we perceive and respond to the world, and allows us to learn and remember. The highly complex nervous system is assembled from individual neural circuits, such as sensory and motor circuits that process sensory stimuli and control animal behaviors, respectively. Ramon y Cajal proposed that nerve cells (now termed “neurons”) are the building blocks that transmit signals in neural circuits and that neural signals pass through a neuron from the dendrites to the soma and then to the axon. This well accepted concept has been termed the “neuron doctrine”, and we now know that "neurons" transmit information in the form of electric and chemical signals.

A neuron typically contains dendrites as the input compartment for receiving information and axons as the output compartment for distributing information (Figure 1.1). These two subcellular compartments are distinguishable from each other in electric excitability, morphology, microtubule orientation, as well as distribution of specific molecules and organelles (1, 2) (Figure 1.1). For instance, action potentials are mainly present in the axons but not in dendrites; whereas organelles such as Golgi outposts are specifically distributed to dendrites but not to the axon (Figure 1.1). Such a two-part design of neurons, achieved through the neuronal polarization process, provides structural basis for unidirectional information transmission in the nervous system.

The developmental events during neuronal polarization have been investigated in details by a number of mammalian and *Drosophila* studies (3-5). In essence, the separation of dendrites and axons requires two steps: specification of the dendrites and the axon, and differential growth of dendrites and the axon (Figure 1.2). During the specification step, dendrites and the axon assume their respective compartmental identities (2, 4). In the differential growth phase, the dendrites and axon develop their own characteristic branches to form the final branching patterns and establish synaptic connections (1).

Since the initial study of the polarization of hippocampal neurons in culture in the 1980s (2, 3), major efforts have aimed at understanding how axon-dendrite are specified. Less is known about the mechanisms underlying the differential growth of dendrites and axons, which is the focus of my thesis work. Knowledge of regulatory mechanisms that differentiate dendritic and axonal growth provides insights into understanding how the remarkable diversity of neuronal morphology is achieved in the nervous system. At the end of axon-dendrite specification, the dendritic and axonal morphologies are simpler compared to those in mature neurons. During the second differential growth phase, some types of neuron, such as Purkinje cells, exhibit more dendritic growth than axonal growth. As a result, these neurons form more elaborative dendritic branches than axonal branches. In contrast, some types of neurons, such as some motor neurons, assume more axonal growth than dendritic growth, resulting a larger axonal size than dendritic size. Therefore, the regulatory mechanisms that operate in the differential growth phase play a major role in determining the final dendritic and axonal morphologies of mature neurons, and thus underlie the morphological diversity observed in the nervous system. Moreover, the discovery of the underlying molecular mechanisms provides potential therapeutic targets for developing strategies to treat nerve injury or neurological disorders with subcellular precision. Reactivating the growth machineries that operate during development might restore injured and defective dendrites and axons observed in these conditions.

In this Chapter, I will review the molecules that control axon-dendrite specification in the first step, and those that operate during the differential growth phase. In the following Chapters 2-5, I will elaborate on my thesis projects studying the functions of DLK, Dscam, and Dar1 in differentiating dendritic and axonal growth in *Drosophila* larval nervous system.

1.1 Molecular mechanisms that establish neuron polarity.

A major system to study the establishment of neuron polarity is embryonic hippocampal neurons in culture (3). Within a day after plating, round-shaped hippocampal neurons (defined as stage 1) extend several minor processes (defined as stage 2), one of which subsequently undergoes rapid outgrowth and becomes the axon

(defined as stage 3). The rest processes assume dendritic identity and grow in the following days (defined as stage 4) (2, 3). It is hypothesized that certain organelles or molecules that are asymmetrically distributed before the morphological symmetry breaks might establish neuronal polarity.

At the organelle level, the centrosome, Golgi apparatus, and endosomes cluster together at a specific area in the cell body before the appearance of any neurites (6). This confined area marks the first sprouting neurite, which subsequently becomes the axon (6). These observations raised the possibility that the centrosome-Golgi-endosome cluster determines the axon specification. This hypothesis is supported by the findings that inactivating centrosome-directed activities, such as microtubule nucleation, inhibited axon initiation; whereas more centrosomes induced the appearance of multiple axons (6). However, the role of centrosome-directed activities in establishing neuron polarity was not confirmed by further in vivo evidence (4, 7-10). For instance, in *Drosophila* mutants that lack centrioles, neuron polarity axis was established as normal (4).

At the molecular level, a number of proteins such as c-Jun N-Terminal Kinase (11), phosphatidylinositol-3 kinase (PI3K) (12, 13), the Par3/Par6 complex (12, 14), LKB1-STRAD kinases(15), were found to be enriched in the particular neurite that subsequently becomes the axon in stage 2-3 and required for axon formation of cultured hippocampal neurons. Using cultured hippocampal neurons in combination with a stripe assay, Shelly et al. has recently uncovered that the cytosolic cyclic adenosine monophosphate (cAMP) and cyclic guanosine monophosphate (cGMP), which reciprocally regulate each other, play opposite roles in axon-dendrite specification (16) (Figure 1.3). Specifically, cAMP promotes axon initiation but suppresses the formation of dendrites; whereas cGMP causes opposite effects (16) (Figure 1.3). Furthermore, the activities of cAMP and cGMP are respectively inhibited and upregulated by the secreted ligand Semaphorin 3A (Sema3A) (Figure 1.3), suggesting Sema3A functions in an early step of neuronal polarization (17). The downstream effectors of Sema3A-cGMP/cAMP involve the protein kinase A (PKA) and LKB1 (17) (Figure 1.3).

Importantly, several of the molecules identified in vitro, such as the LKB1-SAD kinases and Sema3A, have been demonstrated to be indispensable for axon initiation of mammalian cortical neurons in vivo (15, 17, 18). For instance, conditional knock out of

the serine/threonine kinase LKB1 in the cerebral cortex caused a dramatic reduction of axon initiation in pyramidal neurons (18). LKB1 promotes axon initiation by phosphorylating and activating the downstream SAD-A and SAD-B kinases (18), which have been shown to phosphorylate microtubule-associated proteins and to establish neuron polarity (19).

In addition to these mammalian studies, a recent *Drosophila* study has revealed a critical role of cytokinesis remnants in the initial break of the symmetry (4). Using time-lapse imaging of the *Drosophila* sensory neurons of the notum, Pollarolo et al. found that a single neurite started to outgrow within several minutes after neuron birth (4). Strikingly, within 3 minutes after cytokinesis, a series of cytokinesis remnants: RhoA and Aurora Kinase, phosphatidylinositol 4,5-bisphosphate, Bazooka (Par-3), cadherin–catenin were sequentially recruited to a specific site pre-marking the formation of the first neurite (4). Overexpressing a dominant negative DE-cadherin or transient inactivation of DE-cadherin immediately after mitotic division inhibited first neurite sprouting (4). This study demonstrates that mitotic-inherited molecules likely function earliest to establish neuron polarity. It will be interesting to test whether it is a general mechanism that operates in other neuronal types of *Drosophila*, as well as mammalian neurons.

In summary, the specification of the axon and dendrites involves multiple intrinsic and extrinsic molecular mechanisms. It needs further genetic dissections to determine whether different molecules function in parallel or in the same pathway. Moreover, it is possible that different neuron types employ distinct molecular mechanisms to establish neuronal polarity.

1.2 Regulatory mechanisms of differential growth phase

Once dendrites and the axon are specified, these two compartments undergo differential growth phase, which is a critical step for establishing the final morphology and functions of mature neurons.

1.2.1 Regulatory mechanisms that maintain neuron polarity

The differential growth phase is subject to multiple regulations. First, the newly specified dendrites and axon need to maintain their compartmental identities. In both

vertebrate and invertebrate neurons, the plus end of microtubule in axon is always distal towards the cell body, termed "plus-end-out"; whereas in dendrites, the microtubule orientation is mixed with "plus-end-out" and "minus-end-out" orientations (20-22) (Figures 1.1 and 1.4). In *Drosophila* dendritic arborization (da) neurons, microtubule orientation is predominantly minus-end-out in the proximal dendrites but more mixed in the distal dendrites (20, 22) (Figure 1.4). Similar observations have been found in *C. elegans* neurons (23).

Motor proteins are critical for maintaining microtubule polarity and molecular identities of dendrites and the axon. The minus-end directed motor protein, dynein, regulates axonal microtubule orientation in *Drosophila* da neurons (21). Loss of the *dynein light intermediate chain* (*dlic2*) resulted the appearance of minus-end-out microtubule orientation, dendritic Golgi outpost, and dendrite-specific molecules in axons (21) (Figure 1.4). In contrast, the plus-end directed motor protein kinesin-1 regulates the minus-end-out microtubule orientation in the dendrites of *C. elegans* neurons (23). Loss of *unc-166*/*kinesin-1* caused the accumulation of synaptic vesicles and presynaptic proteins in dendrites (23) (Figure 1.4). Further in vitro assays suggest that kinesin-1 might maintain the dendritic microtubule polarity by gliding the plus-end-out microtubules out of the dendrites (23).

1.2.2 Dedicated mechanisms that differentiate dendritic and axonal growth

With their compartmental identities maintained, the dendrites and axon differentially grow. Prior studies have uncovered a number of molecular mechanisms that regulate dendritic or axonal growth (24, 25). For instance, differential regulation at subcellular level can be achieved through "dedicated mechanisms", referring to regulators that specifically promote or inhibit one compartment without affecting the other end (26) (Figure 1.5).

A number of regulators have been identified to control either dendrite-specific growth or axon-specific growth. Gaudillière et al. found that the basic helix-loop-helix transcription factor NeuroD, which is regulated by neuronal activity and phosphorylated by CaMKII, specifically promotes dendritic growth in cultured primary granule neurons (27) (Figure 1.5). Similarly, the bone morphogenetic protein growth factor BMP7/

osteogenic protein-1 (OP-1) induces dendritic growth in cultured sympathetic neurons, which normally form a single axon in vitro (28), and enhances dendritic growth of cultured hippocampal neurons (29) (Figure 1.5). In contrast, the transcriptional complex p300-SnoN specifically promotes axonal growth of cultured granule neurons (30) (Figure 1.5).

Despite these observations demonstrating the existence of dedicated mechanisms in vitro, the dedicated functions of these regulators have not yet confirmed by in vivo studies. One technical difficulty lies in the single-cell-labeling and long-distance tracing of total dendritic and axonal structures of a single neuron in the mammalian nervous system. In contrast, the much smaller *Drosophila* nervous system offers a great opportunity for analyzing the in vivo functions. Importantly, *Drosophila* are amenable to advanced genetic techniques, such as flip-out (31, 32) and Mosaic analysis with a repressible cell marker (MARCM) (33). Both flip-out and MARCM techniques allows single-cell labeling in vivo. Moreover, the MARCM technique enables genetic manipulations at single cell resolution, which is widely used in my thesis work.

The *Drosophila* larval class IV dendritic arborization (C4da) sensory neurons are an instrumental system to compare dendritic and axonal growth. The dendrites and axon of C4da neurons are easy to visualize with the highly specific marker *pickpocket* (*ppk*)-eGFP (34). From a genetic screen using the C4da system, several dendrite-specific regulators were identified (5). These regulators were named as Dar (Dendritic arbor reduction) proteins. Among them, three regulators of ER-to-Golgi transport were found to be dedicated to dendritic growth in vivo: Dar2, Dar3, and Dar6 (5) (Figure 1.5). Their mammalian homologs are Sec23, Sar1 and Rab1, which regulates ER-to-Golgi transport via the COPII vesicles (35). Consistent with the studies about the role of Dar3 in *Drosophila* C4da neurons, Sar1 is indispensable for dendrite-specific growth in cultured hippocampal neurons (5). This study reveals a fundamental difference in the reliance on secretory pathway between dendritic growth and axonal growth.

In addition to secretory pathway related proteins, a *Drosophila* Krüpple-like transcription factor, Dar1, was also identified from this genetic screen. Dar1 promotes microtubule-based dendritic growth without altering the axonal terminals (36) (Figure 1.5). Interestingly, different from other dendritic regulators studied so far, Dar1 is

selectively expressed in the multipolar neurons but undetectable in unipolar and bipolar neurons (See Chapter 5). Multipolar, bipolar and unipolar are three basic morphological types of neurons that have been observed in both vertebrate and invertebrate nervous system. These three types of neuron morphologies differ in the number of primary dendrites: multipolar neurons, such as the most mammalian CNS neurons, and *Drosophila* da neurons, typically develop more than one primary dendrites; bipolar neurons, such as bipolar cells in vertebrate retina and external sensory neurons in *Drosophila* PNS, normally form a single primary dendrite; unipolar neurons, such as the vertebrate dorsal root ganglion (DRG) neurons and the majority of invertebrate CNS neurons, extend a primary neurite that later bifurcate into dendrites and the axon. Loss-of-function, gain-of-function analyses demonstrate that Dar1 switches multipolar versus bipolar/unipolar dendritic morphology without changing cell-fate or axonal targeting and growth (See Chapter 5). Strikingly, overexpressing the mammalian homolog KLF7 in *Drosophila* unipolar neurons was also able to induce ectopic primary dendrites formation (See Chapter 5). Knock-down of KLF7 in mammalian cortical neurons also resulted more bipolar-shaped pyramidal neurons (data not shown). Further microarray analysis suggests that Dar1 regulates the transcription of dynein-related genes to determine multipolar neuron morphology. Since dynein complex has been demonstrated to couple nucleus and leading dendrites and critical for bipolar-multipolar-transition of cortical neurons, we speculate that Dar1/KLF7 might also function by couple the nucleus and dendrites. Collectively, Dar1/KLF is, so far, the only post-mitotic molecular link that distinguishes these basic dendritic morphology types (See Chapter 5).

On the axon side, Drac1, the *Drosophila* homolog of the small GTPase Rac, is required for axonal outgrowth but not for dendritic growth (37) (Figure 1.5). Rac functions with other GTPases Rho, cdc42 to regulate actin cytoskeleton (38). Overexpressing a dominant-negative form of Drac1 inhibited axonal growth of *Drosophila* PNS neurons without affecting the dendrites (37). In mammalian purkinje cells, overexpressing a constitutively active form of human Rac1 impairs axon terminal growth without affecting overall dendritic growth (39). These results show that Rac1 is an axon-dedicated regulator(Figure 1.5).

Additionally, we found that the Down syndrome cell adhesion molecule Dscam specifically promotes axonal growth in C4da neurons. Loss of *Dscam* caused a dramatic reduction in presynaptic growth at the axonal terminals of C4da neurons (See Chapter 4). In contrast, overexpressing Dscam induced exuberant presynaptic overgrowth C4da neurons (See Chapter 4). Therefore, Dscam instructs presynaptic growth. However, neither loss of *Dscam* nor gain of *Dscam* altered dendritic growth of C4da neurons (40) (See Chapter 4). Taken together, Dscam specifically promotes axon terminal growth in C4da neurons. Whether Dscam functions as an axon-dedicated regulator in other types of neurons remain to be elucidated.

1.2.3 Bimodal mechanisms that differentiate dendritic and axonal growth

In addition to dedicated mechanisms, another possible strategy to differentially alter dendritic and axonal growth is to direct their development in opposite manners. We termed this mode of regulation as "bimodal regulation" (41) (Figure 1.6). Unlike dedicated regulators, bimodal regulators might coordinate dendritic and axonal growth,

Prior to our study (See Chapter 2), three bimodal regulators were identified in mammalian neuronal cultures. For instance, Sema3A, which was mentioned above to specify dendritic and axonal identities during the initial stage of neuronal polarization (17, 42) (see section 1.1), also promotes dendritic growth but restricts axonal growth in later stages of cultured hippocampal neurons (17) (Figure 1.6). In addition, knockdown of a CLIP (cytoplasmic linker protein)-associated protein (CLASP), CLASP2, caused axonal overgrowth but impaired dendritic extension in cultured cortical neurons (43)(Figure 1.6). In contrast, overexpressing a dominant-negative form of the GTPase Rit inhibited axonal growth but led to more extensive dendritic growth in hippocampal neurons (44)(Figure 1.5).

In Chapter 2, we present the first in vivo evidence supporting the existence of a bimodal regulator. The evolutionarily conserved dual leucine zipper kinase (DLK) pathway regulates axonal growth, regeneration and degeneration (45-53), and organizes presynaptic structures at the axon terminals (54) (See Chapter 3). This DLK pathway consists of two major components. The first component is an E3 ubiquitin ligase named Pam/Highwire/RPM-1 (PHR). PHR targets the second component, DLK, for protein

degradation (45, 47). Upregulated DLK expression or activity, caused either by loss of PHR or overexpressing DLK, causes axon terminal overgrowth in different neurons in *C.elegans*, *Drosophila*, and mammals (41, 45, 48, 55-58). Moreover, recent studies have uncovered that loss of *DLK* blocks new axon outgrowth after nerve injury (46, 50-52, 59). Despite these exciting studies that possess great therapeutic potential to treat nerve injury, it is unknown whether or how DLK functions in dendritic growth. In Chapter 2, we demonstrate that overabundant DLK promotes axonal growth but negatively regulates dendritic branching of C4da neurons in *Drosophila* (41)(Figure 1.6). Therefore, DLK functions as a bimodal regulator in vivo, which might be important for coordinating dendritic and axonal growth after nerve injury. Previous studies found that DLK protein level is up-regulated by axonal injury (50, 51). Our study suggests that upregulated DLK restrains dendritic growth and might further facilitate axonal regeneration in respond to injury.

A bimodal regulator must act on distinct downstream components in dendrites and axons to achieve the dichotomous effects. For instance, although CLASP2 is present in both dendritic and axonal growth cones of cultured cortical neurons, it exhibits two microtubule-binding activities: it binds to both the plus end and the lattices of microtubules (60, 61). It is possible that these two different microtubule-binding activities mediate the dichotomous actions by CLASP2 on dendritic and axonal outgrowth, considering the fact that dendrites and the axon contain distinct microtubule organizations (62). In contrast to CLASP2, the DLK is localized in the soma and axonal terminals, but absent in dendritic branches (41) (See Chapter 2). We further demonstrated that the dendritic and axonal regulations by DLK were achieved through two divergent downstream transcriptional programs (41) (See Chapter 2). Transcription factor, Fos, is specifically required for the axonal regulation by DLK(41) (See Chapter 2); whereas the transcription factor Knot specifically mediates the dendritic regulation by DLK(41) (See Chapter 2). Further studies will be aimed at identifying the transcriptional targets that directly regulate dendritic and axonal growth.

1.3 Summary

Neuronal polarization is fundamental for establishing connectivity and communication in the nervous system. This developmental process is also essential for generating the diversity of neuronal morphology observed in the nervous system. Neuronal polarization is achieved through a sequential of temporal events and subjects to multiple regulations. First, the axon and dendrite identities are specified by a number of molecules, such as protein kinases, cAMP/cGMP, and cytokine remnants. Motor proteins, such as kinesin-1 and dynein are critical for maintaining the compartmental identities. Committed to their compartmental fates, the nascent dendrites and axon continue to grow and assume distinct morphologies. The molecular mechanisms that differentiate dendritic and axonal growth can be categorized into "dedicated" and "bimodal" mechanisms. Dedicated mechanisms control the growth at one compartment without affecting the other. Bimodal mechanisms alter dendritic and axonal growth in opposite manners. Moreover, it is likely these distinct regulatory modes converge to pattern the dendritic and axonal architectures of a neuron.

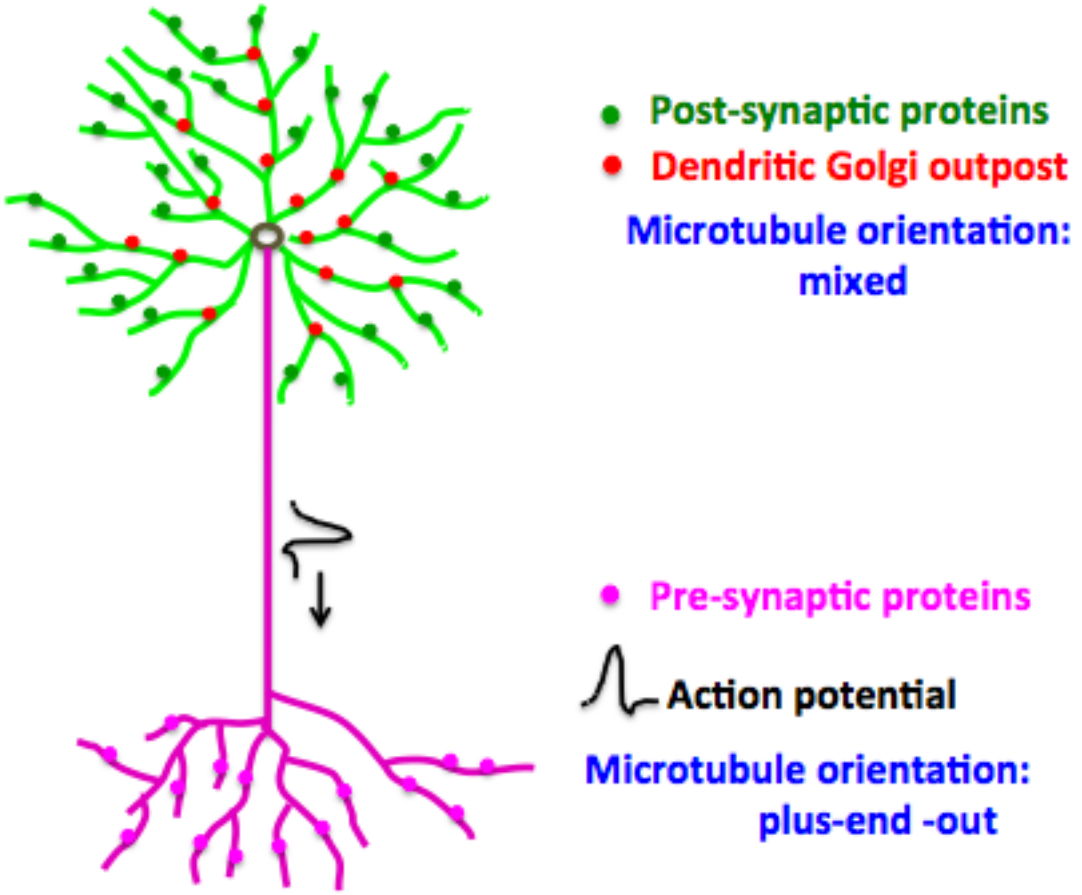

Figure 1.1 A schematic illustration of the two-part design of neurons.
In addition to the cell body, a neuron typically develops several dendrites to receive input signal, and form a single axon to send output signal. These two compartments are different in multiple aspects, such as the specific distribution of molecules and organelles, the propagation of action potentials, and microtubule orientations. The dark circle indicates the soma; the green and magenta processes indicate the dendrites and the axon respectively.

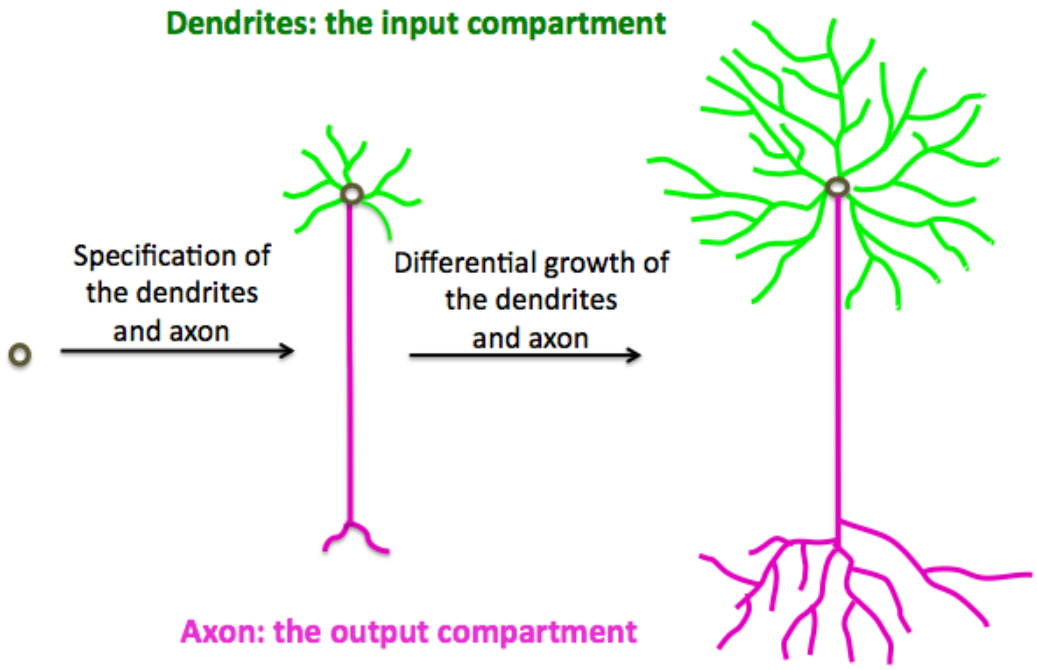

Figure 1.2 A schematic illustration of the two steps of neuronal polarization. Neuronal polarization is achieved in two steps. First, the nascent neuron (dark circle) projects several processes, one of which assumes rapid growth and typically becomes the axon (2, 3). The rest neurites then become dendrites as labeled by dendritic molecular markers (2, 3). After acquiring their compartmental identities, the axon and dendrites extend additional branches to form the final branching patterns (2, 63). The dark circle indicates the soma; the green and magenta processes indicate the dendrites and the axon respectively.

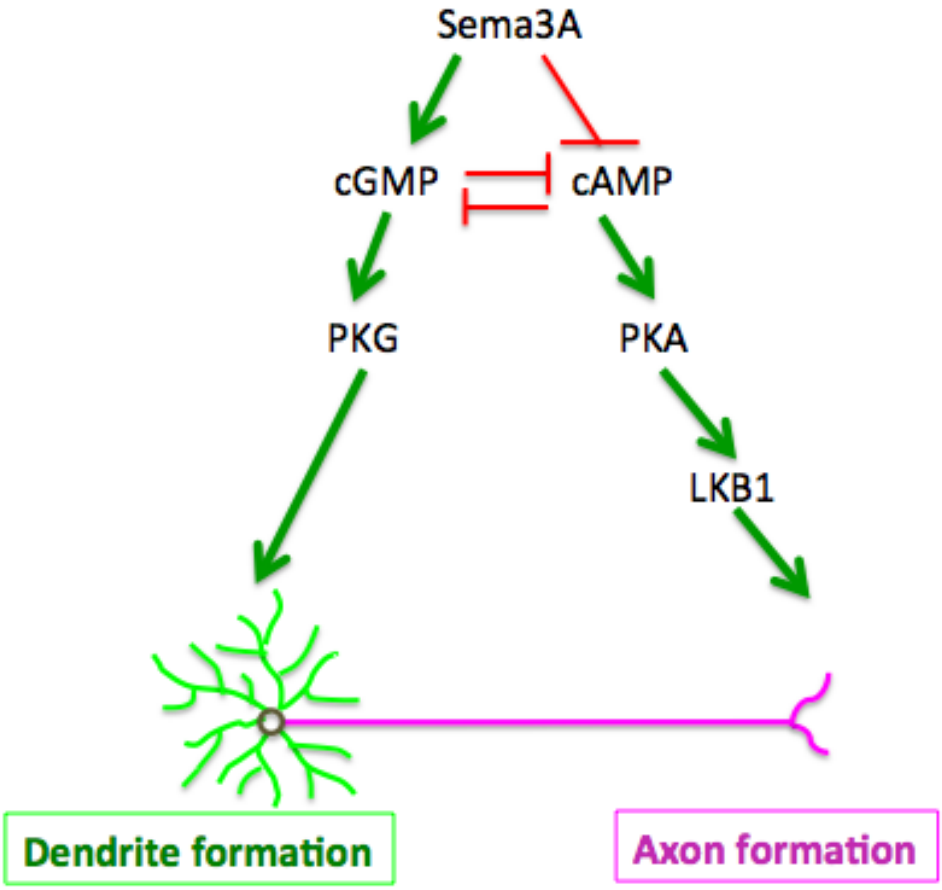

Figure 1.3 Sema3A-cAMP/cGMP pathway controls the establishment of neuronal polarization.
The cyclic adenosine monophosphate (cAMP) and cyclic guanosine monophosphate (cGMP) antagonize each other's activity and conversely regulate axon and dendrite formation in a nascent neuron (16). Sema3A, an extrinsic secreted ligand, upregulates cGMP but inhibits cAMP activities to promote dendrite formation(17). cGMP activates downstream kinase PKG; whereas cAMP activates downstream kinase PKA, which subsequently phosphorylates the LKB1 kinase(16). LKB1 has been demonstrated essential for axon initiation both in vitro (15, 64) and in vivo (18).

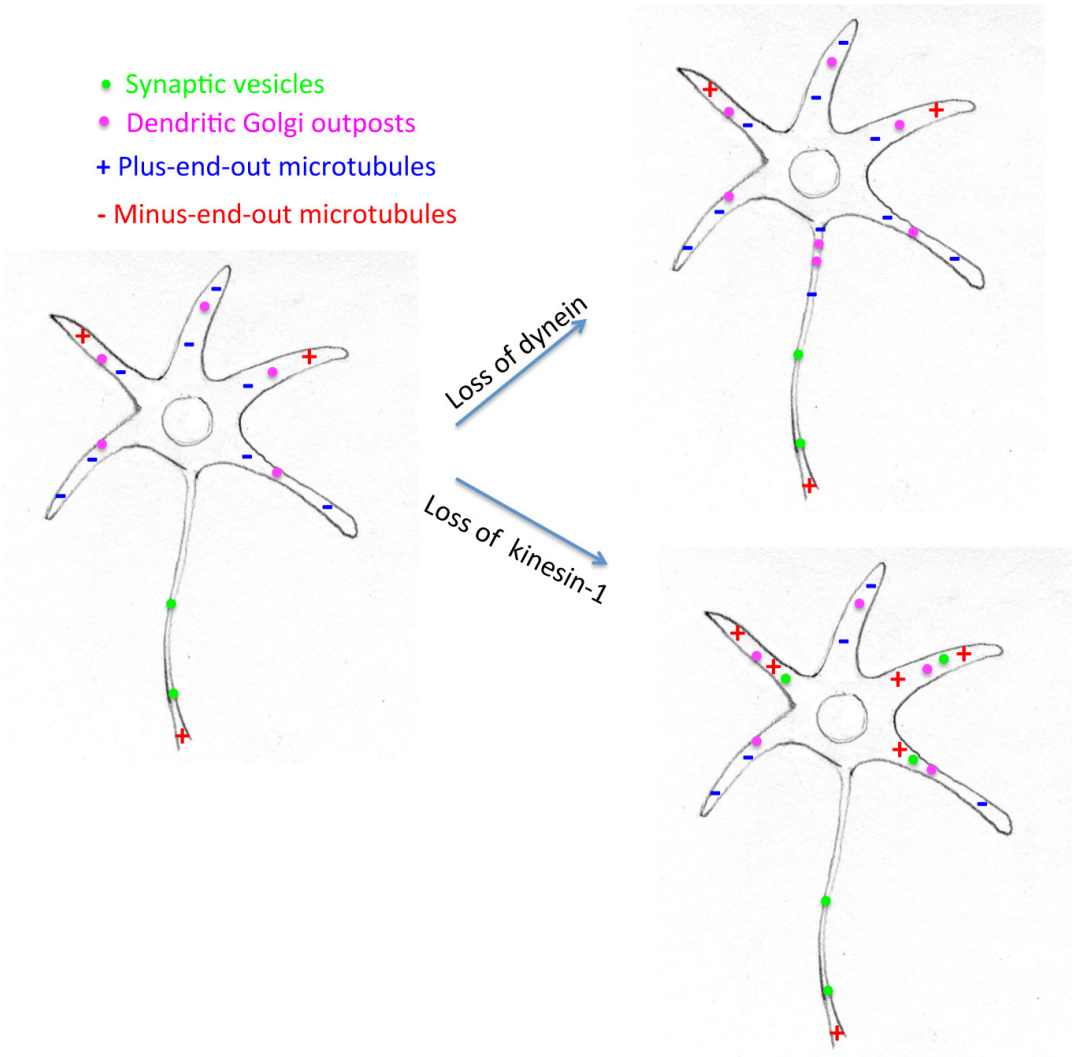

Figure 1.4 Motor proteins are required to maintain neuronal polarity.
After axon and dendrites acquire their compartmental identities, motor proteins such as dynein and kinesin-1 actively maintains the microtubule polarity in dendrites and axons. In a wild type neuron, the microtubules in the axon are always plus-end-out, whereas both plus-end-out and minus-end-out microtubules have been found in dendrites. In certain types of vertebrate, *Drosophila* and *C.elegans* neurons, the microtubule orientation in proximal part of dendrites is mostly minus-end-out(20, 22, 23). Loss of dynein function led to minus-end-out microtubules in the axon (21), whereas loss of *kinesin-1* caused plus-end-out microtubules in the dendrites (23). Consequent to the disrupted microtubule polarity, dendrite- or axon-specific molecules and organelles become mislocalized in these compartments.

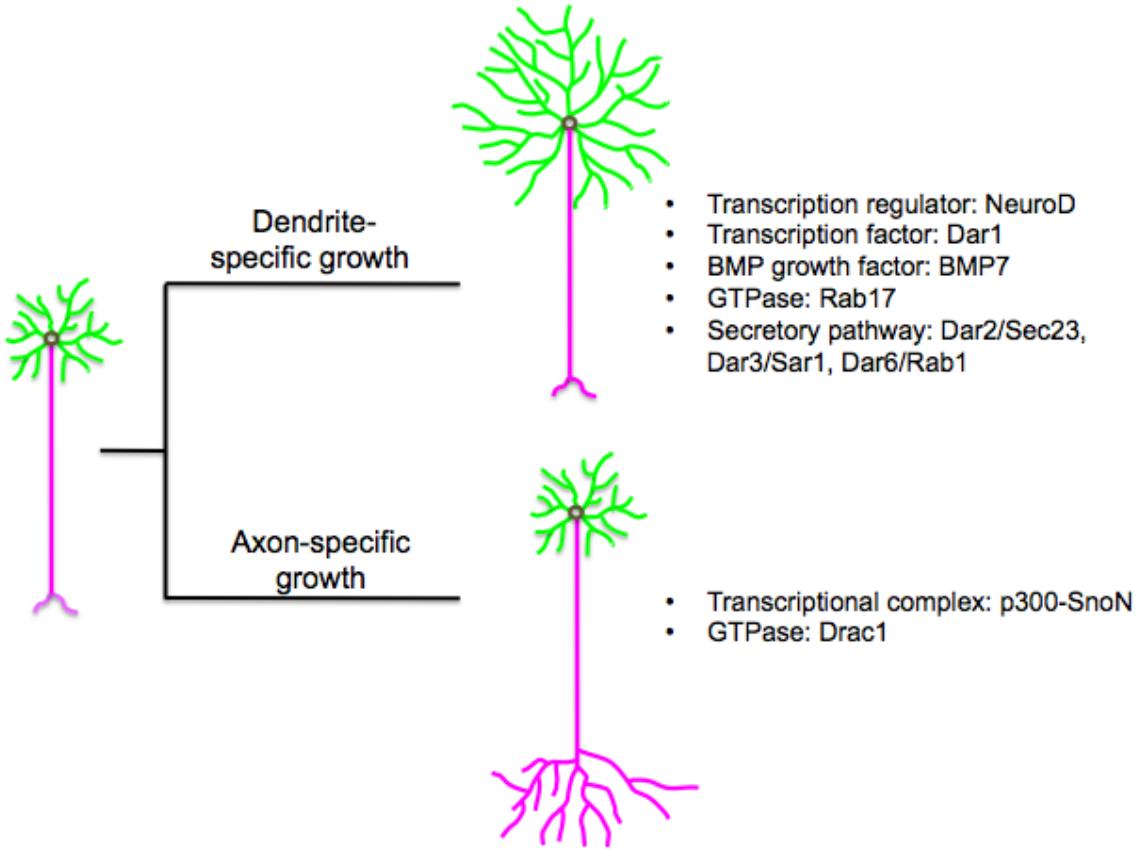

Figure 1.5 Dedicated mechanisms of dendritic and axonal growth.
Listed are previously known regulators that dedicate to either dendrite specific growth or axonal specific growth. The dark circle indicates the soma; the green and magenta processes indicate the dendrites and the axon respectively.

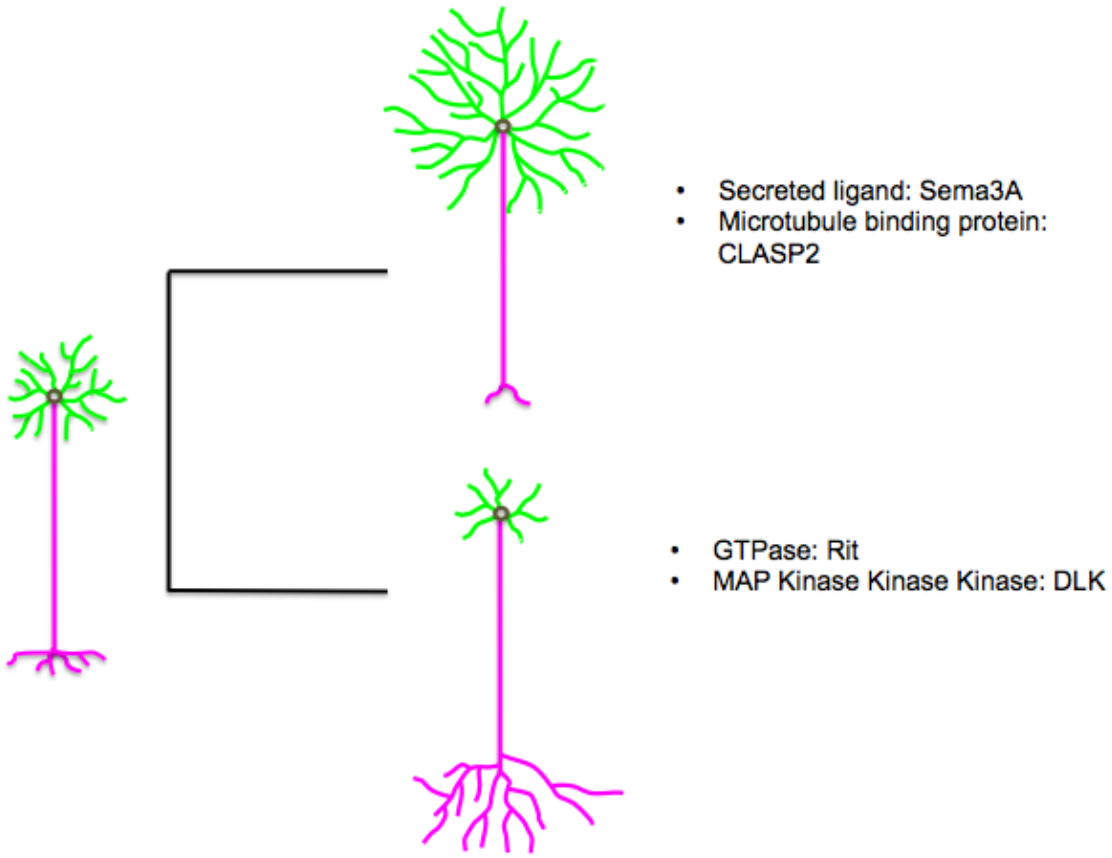

Figure 1.6 Bimodal regulation of dendritic and axonal growth.
Several bimodal regulators have been identified to oppositely alter dendritic and axonal growth. Sema3A and CLASP positively regulate dendritic growth but restrict axonal growth (17, 43), whereas Rit and DLK exert the opposite actions on these two compartments (41, 44). The dark circle indicates the soma; the green and magenta processes indicate the dendrites and the axon respectively.

Chapter 2

Bimodal control of dendritic and axonal growth by the dual leucine zipper kinase pathway[1]

2.1 Abstract

Knowledge of the molecular and genetic mechanisms underlying the separation of dendritic and axonal compartments is not only crucial for understanding the assembly of neural circuits, but also for developing strategies to correct defective dendrites or axons in diseases with subcellular precision. Previous studies have uncovered regulators dedicated to either dendritic or axonal growth. Here we investigate a novel regulatory mechanism that differentially directs dendritic and axonal growth within the same neuron in vivo. We find that the dual leucine zipper kinase (DLK) signaling pathway in *Drosophila*, which consists of Highwire and Wallenda and controls axonal growth, regeneration and degeneration, is also involved in dendritic growth in vivo. Highwire, an evolutionarily conserved E3 ubiquitin ligase, restrains axonal growth but acts as a positive regulator for dendritic growth in class IV dendritic arborization neurons in the larva. While both the axonal and dendritic functions of *highwire* require the DLK kinase Wallenda, these two functions diverge through two downstream transcription factors, Fos and Kn, which mediate the axonal and dendritic regulation, respectively. This study not only reveals a previously unknown function of the conserved DLK pathway in controlling dendrite development, but also provides a novel paradigm for understanding how neuronal compartmentalization and the diversity of neuronal morphology are achieved.

---

[1] Modified after the research article originally published in *PLOS Bio.* (2013; 11(6): e1001572) with authors listed as Xin Wang, Jung Hwan Kim, Mouna Bazzi, Sara Robinson, Catherine A. Collins, and Bing Ye

2.2 Introduction

The separation of the dendritic and axonal compartments in neurons is prerequisite to the function of neural circuits. Although the difference between dendrites and axons is a cornerstone of modern neuroscience, as theorized in the "neuron doctrine" by Ramon y Cajal (65), our molecular understanding of how neuronal compartmentalization is achieved remains limited. This knowledge, however, is crucial for understanding the assembly of neural circuits. Moreover, it is needed to develop strategies that will correct defective dendrites or axons with subcellular precision, and to alter the wiring of neural circuits in animal models in order to interrogate the functions of the nervous system.

Previous studies have demonstrated the existence of regulators dedicated to dendrite or axon growth in the same neuron, referred to as "dedicated mechanisms" herein. For instance, the transcription complex, p300-SnoN, specifically promotes axon growth in the cerebellar granule neurons (30). In contrast, transcription factor NeuroD is dedicated to dendritic growth in mammalian cerebellar granule neurons (27). Likewise, bone morphogenetic protein 7 (BMP7) specifically promotes dendritic growth in several types of neurons in culture (28, 29). In *Drosophila*, the transcription factor Dendritic arbor reduction 1 (Dar1) promotes dendritic, but not axonal, growth (36). In addition, dendritic and axonal growth exhibit differences in their dependence on the secretory pathway (5).

Besides the dedicated mechanisms, another way to differentiate dendritic and axonal growth is through bimodal regulators that control dendritic and axonal growth in opposite directions (17, 42-44). Different from the dedicated mechanisms, the bimodal mechanisms may provide coordinate growth of the two neuronal compartments. However, how the function of a molecule or signaling pathway diverges into distinct dendritic and axonal regulations is poorly known.

In this study we report that the dual leucine zipper kinase (DLK) signaling pathway is a novel bimodal regulator for dendritic and axonal growth in vivo. The core players in the DLK signaling pathway are the DLK and the Pam/Highwire/RPM-1 (PHR) family of E3 ubiquitin ligases that suppress DLK expression. The PHR-DLK signaling

module plays an important role in axon development, as demonstrated by studies in *C. elegans* (47, 55, 56), *Drosophila* (45, 57, 58), zebrafish (66, 67), and mammals (48, 68, 69). Loss of the *Drosophila* homologue of DLK-1, Wallenda (Wnd), suppresses the axonal overgrowth caused by loss of the PHR protein Highwire (Hiw) (45, 57). Consistently, overexpression of Wnd promotes axonal growth of motoneurons in *Drosophila* larvae (45). In *Drosophila* adult mushroom body neurons, Hiw-Wnd pathway is required for the segregation of axon branches in response to guidance cues (70). In addition to the roles in axon development, recent studies have discovered a conserved function of the DLK pathway in axon regeneration (46, 50-52, 59) and degeneration in several species (53, 71-73). Although these exciting findings have established critical roles for the DLK pathway in axon development, regeneration, and degeneration, whether the DLK pathway regulates dendrites remains unknown.

Here we show that the DLK pathway directs the growth of axons and dendrites in opposite directions in the class IV dendritic arborization (C4da) neurons in *Drosophila*. By inhibiting Wnd functions, Hiw restricts axonal growth but promotes dendritic growth. The opposite effects of the Hiw-Wnd pathway on axons and dendrites are achieved through two distinct transcription factors: Fos, which mediates the regulation of axonal growth, and Kn, which mediates the regulation of dendritic growth. Collectively, these results demonstrate that a single signaling pathway can differentiate dendritic and axonal growth through two independent transcriptional programs.

2.3 Results

2.3.1 *hiw* plays a dichotomous role in differentiating dendrite and axon growth

All functional studies of the PHR-DLK pathway in neurons have so far focused on axons. We first set out to determine whether the PHR gene *hiw* is involved in dendrite development using *Drosophila* as a model system.

The C4da neurons in *Drosophila* larva are a well-established in vivo system for studying the molecular mechanisms of dendrite and axon development. The dendrites and axons of these neurons are distinguishable from each other at both molecular and organelle levels in a way that resembles mammalian neurons (25). Moreover, these neurons are amenable to single cell genetic manipulations (25, 34), which is important for

comparing dendritic and axonal development in vivo. In each hemi-segment of a larva, there are three C4da neurons (ddaC, v'ada, and vdaB), whose cell bodies are located respectively in the dorsal, lateral, and ventral parts of the body wall. The axons of the three C4da neurons extend to the ventral nerve cord (VNC) where the terminals form a ladder structure (Figure 2.1A). At single-cell resolution, the axon terminal of each C4da neuron consists of an anterior projection that extends within one segment length. ddaC and vdaB neurons also extend a contra-lateral branch (74) (Figure 2.1A'). Collectively, the axon terminals of the three C4da neurons form a fascicle that connects two adjacent neuropils (Figure 2.1A').

To examine the role of *hiw* in dendritic development, we labeled the C4da neurons in *hiw* mutant larvae using a C4da-specific marker, *ppk-CD4::tdTomato* (34, 75). We found that dendritic growth was dramatically reduced in the null allele $hiw^{\Delta N}$, and to a lesser extent, in the hypomorphic hiw^{ND8} mutants (Figure 2.2 A and B). Both total length and number of termini of dendrites were significantly reduced in $hiw^{\Delta N}$ and hiw^{ND8} mutants (Figure 2.2 B).

Consistent with the known function of *hiw* in suppressing axonal growth (57, 58), *hiw* mutations led to exuberant growth of axon terminals in C4da neurons. In *hiw* mutant larvae, thickened connective fascicles were observed in the C4da neuropil ladder (Figure 2.1B). In wild-type larvae, there was no hemi-segment that contained more than three longitudinal connectives between the axon entry point of abdominal segment 5 (A5) and that of A6 (Figure 2.1A', B and D). In contrast, 100% of *hiw* mutant C4da neuropils exhibited more than three connectives (Figure 2.1 B and D), which could either arise from an increased number of axon branches from neurons in the same segment or from overextended axons that normally remain in other segments.

Our further analysis showed that the effects of *hiw* mutations on dendritic and axonal growth are not a result of defective dendrite and axon identities. The axon-specific marker, Kinesin-β-galactosidase (21, 76), remained exclusively localized to the axons of C4da neurons that were mutant for *hiw* (Figure 2.3A). Furthermore, the initial growth and pathfinding of axons to the VNC or the extension of minor dendritic processes remained unaltered in embryos devoid of both maternal and zygotic *hiw* (Figure 2.3B). Thus, *hiw* appears to be dispensable for early development, including the initial specification of

axon and dendrite. Taken together, these results suggest that *hiw* plays a dichotomous role in differentiating dendrite and axon growth after their identities have been specified.

2.3.2 Hiw regulates dendritic and axonal growth in a cell-autonomous manner

Previous studies of axon development have discovered both cell-autonomous (45, 58) and non-cell-autonomous roles of *hiw* (70). To determine whether *hiw* functions cell-autonomously in C4da neurons and to examine the axon and dendrite defects at single-neuron resolution, we generated *hiw* mutant neurons with the Mosaic Analysis with a Repressible Cell Marker (MARCM) technique (33). Consistent with the reduced dendritic growth in *hiw* mutant larvae, we observed a reduction of high-order dendritic branches in *hiw* loss-of-function mutant neurons (Figure 2.2 C). Moreover, fewer dendritic branches arrived at the segment border as compared to wild-type. *hiw* mutations caused a 43% reduction in total dendrite length and 40% reduction of the number of dendrite termini (Figure 2.2 E). In contrast to their dendritic defects, *hiw* mutations resulted in a 2.4-fold increase of axon terminal length (Figure 2.2 D and F) as compared to wild-type. The axon terminals of *hiw* mutant neurons typically spanned multiple segments, whereas the vast majority of wild-type C4da neurons extended axonal branches between their own segments and the anterior neighboring segments (Figure 2.2 D). Noticeably, although the axon terminals of *hiw* mutant neurons grew exuberantly, they preserved normal guidance within the contralateral axis of C4da neuropil tracts.

In agreement with the MARCM results, overexpressing Hiw in C4da neurons rescued both dendritic and axonal defects in *hiw* mutant larvae to a level comparable to wild-type (Figure 2.4), further confirming that the loss of *hiw* in C4da neurons is responsible for the dendritic and axonal defects. Overexpression of Hiw alone did not significantly alter axonal or dendritic growth (Figure 2.4), suggesting that *hiw* is necessary but insufficient to instruct dendritic growth and restrict axon growth. Taken together, these results demonstrate that Hiw functions as an intrinsic bimodal regulator of dendritic and axonal growth in C4da neurons.

2.3.3 Wnd mediates the functions of Hiw on both axonal and dendritic growth

Two parallel downstream pathways are known to mediate axon overgrowth induced by loss of PHR proteins. First, the PHR orthologs in *C. elegans* (*rpm*-1) and *Drosophila* (*hiw*) suppresses the worm *dlk-1* and the fly *DLK wallenda* (*wnd*), respectively, to restrain axonal growth in motoneurons (45, 47). Second, the worm *rpm-1* regulates a trafficking pathway that consists of the Rab guanine nucleotide exchange factor (GEF) GLO-4 and the Rab GTPase GLO-1, which restrict axon termination in mechanosensory neurons and synaptogenesis in motoneurons (77). In order to delineate the mechanism underlying the bimodal control of dendritic and axonal growth by *hiw*, we tested the involvement of these two pathways in axon and dendrite growth in C4da neurons. While *wnd* loss-of-function mutations on their own did not alter overall organization of axonal terminals (Figure 2.1C-D) or dendritic morphology (Figure 2.5), they completely suppressed both axonal and dendritic defects caused by *hiw* mutations (Figures 2.1 C-D and 2.5). These observations suggest that *wnd* acts downstream of *hiw* to promote axonal growth and inhibit dendritic growth.

Consistent with this model, overexpression of Wnd in C4da neurons induced extensive axon terminal overgrowth and profoundly reduced dendritic branching in C4da neurons (Figures 2.1 C-D and 2.5). In contrast, overexpression of a kinase-dead (KD) form of Wnd resulted in morphologically normal C4da neurons (Figures 2.1C-D and 2.5). Hence, increased expression of the Wnd kinase is sufficient to inhibit dendritic growth and promote axonal growth.

We also examined the potential involvement of the Rab trafficking pathway by testing *Drosophila* homologs of *glo-4* and *glo-1* in axon and dendrite development in C4da neurons. In *C. elegans*, *glo-4* mutants exhibited axon overextension similar to that in *rpm-1* mutants (77). Overexpressing the Rab GTPase Glo-1, which is activated by Glo-4, partially rescued axon termination defects in *rpm-1* mutants (77). The *Drosophila* homologs of *glo-4* and *glo-1* are *claret* (*ca*) and *lightoid* (*ltd*), respectively (78). The *ca* mutant MARCM clones devoid of maternal contribution exhibited axons and dendrites that were indistinguishable from wild-type clones (Figure 2.6 A-D). In addition, overexpressing Ltd failed to rescue either axon or dendrite defects in *hiw* mutants (Figure 2.6 E-H). These results suggest that *Drosophila* C4da neurons use the DLK (Wnd)

pathway, rather than the Ca-Ltd vesicle trafficking pathway, to mediate *hiw* function in axonal and dendritic growth.

2.3.4 The Fos transcription factor mediates the Hiw-Wnd control of axonal growth

How might the Hiw-Wnd pathway control axonal and dendritic growth differently in the same neurons? In *Drosophila* motoneurons, the Hiw-Wnd pathway requires the transcription factor Fos (45). Fos is phosphorylated by Bsk (JNK) (79), which positions it as the downstream kinase of the Wnd-Hep7-JNK kinase cascade (45). Overexpressing a dominant negative form of Fos partially suppresses axonal overgrowth at the NMJ of *hiw* mutants (45). Because of this, we decided to examine whether Fos is required by Wnd to promote axonal growth.

To test the role of Fos in C4da neurons with loss-of-function mutants, and to bypass lethality caused by *fos* null mutations kay^1 (80, 81), we generated kay^1 MARCM clones in the presence or absence of a *UAS-Wnd* transgene that overexpresses Wnd (OE Wnd). kay^1 alone did not alter axonal growth (Figure 2.7A), but completely suppressed the axon overextension caused by Wnd overexpression (Figure 2.7 A and C), which suggests that *fos* is required for Wnd-induced axonal overgrowth. In contrast to the axonal role of Fos, kay^1 did not block the dendritic reduction caused by Wnd overexpression. The total dendritic length of MARCM clones that overexpressed Wnd in the kay^1 background (OE Wnd + kay^1) was indistinguishable from that of Wnd-overexpressing clones (Figure 2.7 B, B' and C), and the number of dendrite termini was further reduced from that of Wnd-overexpressing clones. Interestingly, the kay^1 mutation alone caused a mild reduction in dendritic length and branch number (Figure 2.7 B, B' and C). This result suggests that, although Fos does not mediate the dendritic functions of the DLK pathway, it plays a minor role in supporting dendritic growth. Taken together, these results suggest that Wnd acts through Fos to specifically promote axonal growth.

2.3.5 Wnd suppresses the expression of the transcription factor Knot

In order to understand how the function of DLK pathway diverges into dendritic and axonal regulations, we hypothesized that the divergence occurred at the transcriptional level, and therefore tested the transcription factors that are known to

regulate dendritic growth in da neurons. Among them, the Krüppel-like factor Dar1, the homeodomain transcription factor Cut (Ct) and zinc-finger transcription factor Knot (Kn, as known as Collier) have been shown to be essential for dendritic growth in C4da neurons. Loss-of-function mutations in each of these transcription factors severely reduce dendritic growth in C4da neurons (36, 82-85). We first tested whether expression levels of these transcription factors in C4da neuron nucleus were altered in *hiw* loss-of-function mutants. No significant difference in the levels of Dar1 (36) or Cut (82) was observed between wild-type and *hiw* mutant C4da neurons (Figure 2.8 A-C). In contrast, the nuclear levels of Kn, which belongs to the evolutionarily conserved Collier/Olf1/EBF (COE) family, were significantly reduced in both *hiw* mutant neurons and Wnd-overexpressing neurons (Figure 2.9 A and B)

Kn is required for the expression of the ENaC ion channel Pickpocket (Ppk) in C4da neurons (83-85). *Kn* loss-of-function mutations reduce *ppk* transcription (83), and suppress *ppk* promoter activity as assayed with a *ppk-eGFP* transgene (84, 85) (Figure 2.9 D). Furthermore, misexpression of Kn induces ectopic *ppk-eGFP* expression in neuron types that do not normally express *ppk-eGFP* (83-85). Therefore, the *ppk-eGFP* transgenes may be used as readout for Kn transcriptional activity. Consistent with the reduced Kn expression by *hiw* mutations or Wnd overexpression, we found a 37% reduction in *ppk-eGFP* fluorescence intensity in the soma of *hiw* mutant C4da neurons and a 68% reduction in those of Wnd-overexpressing neurons (Figure 2.9C and D).

Furthermore, overexpressing Kn rescued the reduced expression of *ppk-eGFP* in *hiw* mutant or Wnd-overexpressing neurons (Figure 2.9 C and D). The correlation between *ppk-eGFP* fluorescence intensity and Kn levels suggests that the Hiw-Wnd pathway controls Kn transcriptional activity by regulating its protein levels. Nevertheless, it does not rule out the possibility of post-translational regulation of Kn activity by Hiw-Wnd. Taken together, Hiw suppresses Wnd function, thus maintaining high levels of Kn protein in C4da neurons, which is required for dendritic growth.

2.3.6 Knot mediates the Hiw-Wnd control of dendritic growth

It has been demonstrated that loss-of-function mutations of *kn* cause reduction in dendritic length and branch numbers (83-85). We tested potential genetic interactions

between *hiw* and *kn* in controlling dendritic growth. C4da dendrites developed normally in both $hiw^{\Delta N/+}$ heterozygous and $kn^{KN4/+}$ heterozygous larvae (Figure 2.10 A and B), in which Kn expression and *ppk-eGFP* levels remained comparable to wild-type (Figure 2.10 C-E). In contrast, the $hiw^{\Delta N/+}$; $kn^{KN4/+}$ trans-heterozygous larvae exhibited dramatically reduced dendritic growth (Figure 2.10 A and B), revealing a strong genetic interaction between *hiw* and *kn*.

We investigated the nature of the genetic interaction by epistasis analysis. Kn overexpression resulted in a mild 16% reduction of C4da dendritic length (Figure 2.11 A-B), possibly due to destabilized microtubules as a result of increased expression of the microtubule severing protein Spastin (36, 85). Nevertheless, overexpressing Kn in $hiw^{\Delta N}$ MARCM clones ($hiw^{\Delta N}$ + OE Kn) rescued dendritic defects from 45% of reduction to 25% in dendritic length, and from 44% of reduction to 29% in dendrite termini number, as compared to wild-type (Figure 2.11 A-B), suggesting that Kn acts downstream of Hiw to control dendrite growth.

In contrast, Kn overexpression had no effect on axonal growth in either wild-type or *hiw* mutant MARCM clones (Figure 2.11 C and D). Taken together, our results suggest that the Hiw-Wnd pathway acts through Kn to regulate dendritic, but not axonal, growth.

2.3.7 Kn endows neurons with the ability to respond to Wnd regulation of dendritic growth

There are four classes of dendritic arborization (da) neurons in *Drosophila* larva, which are categorized based on the complexity of dendritic branching (86). *Hiw* mutations elevated the expression of *puc*-lacZ (87), a reporter for Wnd activity (51), in all four classes (Figure 2.12), suggesting that the Hiw-Wnd pathway is functional in all these neurons. However, Kn is only expressed in the class IV, and undetectable in other classes of da neurons (83-85). If *hiw* acted via Kn to control dendritic growth, *hiw* mutations would not alter the dendritic morphology in class I (C1), class II (C2) and class III (C3) da neurons. Indeed, we observed that *hiw* mutant MARCM clones of C1-C3 da neurons all exhibited normal dendritic growth (Figures 2.13 C and D, 1.14 C and D, 1.15 C and D), even though Hiw still restricts axonal growth in these neurons (Figures 2.13A and B,

2.14A and B, 2.15A and B). These observations further suggest that the Hiw-Wnd pathway regulates dendritic growth in Kn-expressing neurons.

We next determined whether Kn expression endows neurons with the ability to respond to dendritic growth control by Wnd. Consistent with previous reports that ectopic expression of Kn in class I da (C1da) neurons leads to excessive dendritic branching and extension (84, 85), the total dendrite length was increased by 55% and the number of dendritic branches was doubled in the C1da neurons overexpressing Kn (OE Kn) compared to wild-type. Such dendritic overgrowth was considerably reduced when Wnd was overexpressed in the same neurons (Figure 2.16 A and B), with the increase in total dendrite length inhibited from 55% to 10%. As a control, a kinase-dead form of Wnd failed to suppress Kn-induced dendritic overgrowth.

Similar to the effects in C4da neurons (Figure 2.9 A-B), we detected a reduction of the nuclear Kn levels in C1da neurons expressing both Kn and Wnd (Figure 2.16 C-D). It is noteworthy that, in these C1da neurons, Kn was expressed by the Gal4/UAS system, which bypasses endogenous transcriptional control. Thus, up-regulated Wnd kinase is likely to suppress Kn expression via post-transcriptional mechanism. Collectively, these results suggest that Hiw-Wnd pathway regulates dendritic growth in Kn-expressing neurons by controlling the expression of Kn.

2.4 Discussion

In this study, we found that a single signaling pathway, consisting of the PHR E3 ubiquitin ligase Hiw and its downstream dual leucine kinase Wnd, serves not only as a negative regulator in axon growth but also as a positive regulator in dendrite growth in vivo. This is the first report, to our knowledge, to show a role for the DLK pathway in dendrite development. We further discovered that the functional divergence of this pathway is achieved through two transcription factors, Kn and Fos, which mediate the dendritic and axonal regulation, respectively.

Three distinct modes of regulations of axonal and dendritic growth

Taking into account the current study with previous studies, three distinct modes of axonal and dendritic growth regulation have been identified: shared, dedicated and bimodal (Figure 2.17).

Shared mechanisms co-promote or co-inhibit the growth of axons and dendrites. Molecular controls that operate in shared mechanisms include cytoskeleton regulators like MAP1B (Futsch) (88), histone deacetylase HDAC6 (89, 90), and β-hexosaminidase (91).

Dedicated mechanisms provide the basis for specifically regulating the morphogenesis of only axons or only dendrites. Molecular controls at work in dedicated mechanisms can be divided into: 1) axon-dedicated mechanisms, including p300 and SnoN transcription complex (30); and 2) dendrite-dedicated mechanisms, including transcriptional factors NeuroD (27) and Dar1 (36), growth factor BMP7 (28, 29), and small GTPase Rab17 (92). Manipulation of dedicated mechanisms leads to specific changes in the growth of either axons or dendrites, but not both. Thus, axonal growth per se does not regulate dendritic growth, and vice versa.

In contrast to dedicated mechanisms, bimodal mechanisms oppositely regulate axons and dendrites, and may serve to coordinate the growth of these separate compartments. Previous studies of different types of neuronal cultures have discovered three bimodal regulators: Sema3A (17, 42), CLASP2 (43), and Rit (44). In this study we have identified an in vivo bimodal regulatory mechanism that involves DLK kinase. The bimodal action of the DLK signaling pathway is achieved through two 'dedicated' transcriptional programs. These two programs are likely to be independent because manipulating their activities rescues either dendritic or axonal defects, but not both, in *hiw* mutants. We also observed that transgenic Hiw and Wnd were present in the axon terminals in addition to the cell body but not in dendrites (Figure 2.18), raising the intriguing possibility that elevated Wnd function in the axon terminals might impact transcriptional activities in the cell body, and consequently influence dendritic growth.

It is likely that various bimodal controls exist in different neuron types. Moreover, it is possible that these bimodal controls intersect with each other. For instance, since the actions of Sema3A are mediated through cGMP/cAMP levels (17), another bimodal regulator might also influence cGMP/cAMP levels. It will be interesting to determine

whether cGMP/cAMP are involved in PHR-DLK pathway for bimodal control of dendritic and axonal growth.

The DLK pathway may coordinate dendritic and axonal growth after axon injury

Despite the requirement of DLK functions in axonal growth after axon injury (46, 50-52, 59), DLK is dispensable for axonal growth during development in the neuron types examined so far (45, 47). Consistently, we find that loss of *dlk/wnd* does not alter either dendritic growth or axonal terminal length in *Drosophila* C4da neurons. Rather, the overabundance of DLK/Wnd caused by defective PHR/Hiw functions leads to axonal overgrowth as well as dendritic reduction. Since axon injury leads to an overabundance of DLK/Wnd function (50, 51), it is conceivable that the elevated activity of DLK/Wnd induced by axon injury not only promotes axon regeneration (46, 50-52, 59), but also restrains dendritic growth or prunes existing dendritic branches to compensate for the increased demand of membrane or cytoskeleton supplies for axonal growth. This notion is consistent with previous studies that show dendrite retraction following axotomy in *Drosophila* da neurons (93) and mammalian cultured neurons (94, 95).

Two transcription programs directed by Kn and Fos endow bimodal regulation of PHR-DLK pathway

Although it is known that the zinc finger transcription factor Kn is essential for dendritic growth, the signaling mechanism that regulates Kn in neurons is unknown. In this study, we show that Kn specifically mediates dendritic regulation by the PHR-DLK pathway, which is supported by three lines of evidence. First, *kn* genetically interacts with *hiw* and functions downstream of *hiw* and *wnd* to regulate dendritic growth. Second, the Hiw-Wnd pathway regulates Kn expression in C4da neurons. Third, the Kn expression pattern is consistent with the presence of the Hiw-Wnd regulation of dendrite growth. Kn is selectively expressed in a subset of neurons (83-85, 96). Consistent with Kn expression pattern, *hiw* mutations caused dendrite defects only in the Kn-expressing class IV neurons, and not in the other classes of da neurons that lack Kn. Interestingly, ectopic expression of Kn in class I neurons, which do not normally express Kn, is

sufficient to endow the Hiw-Wnd regulation. These results strongly suggest that the PHR-DLK pathway regulates Kn to control dendrite development.

In contrast to Kn, the transcription factor Fos specifically mediates axonal regulation through Hiw-Wnd pathway. We found a two-fold role for *fos* in neuronal development. On the one hand, eliminating *fos* specifically causes dendritic reduction without affecting axon terminal length in C4da neurons. This indicates that endogenous Fos is specifically required for dendritic growth during normal development. On the other hand, the requirement of *fos* could switch to be axonal when augmented Wnd activity leads to exuberant axonal growth.

In summary, Hiw-Wnd pathway can exert bimodal or dedicated control over dendritic and axonal growth, depending on the presence of the transcription factors that mediate its subcellular compartment-specific functions. If transcription factors for both dendritic and axonal growth are present, Hiw-Wnd signaling functions as a bimodal modulator (Figure 2.19). This model provides guidance for further investigation of the molecular basis of the diversity of neuronal morphology and the differential development of dendrites and axons.

2.5 Materials and methods

2.5.1 Fly stocks

$hiw^{\Delta N}$ (58)*; hiw^{ND8}* (58)*; UAS-Hiw::GFP* (58)*; wnd^{1}* (45)*; wnd^{3}* (45)*; UAS-Wnd* (45)*; UAS-Wnd^{K188A}* (45)*; UAS-Wnd^{KD}::GFP* (45); *kay^{1}* (97)*; ca^{1}, FRT^{82B}* (98)*; UAS-ltd::YFP* (99)*; kn^{1}*(100); *kn^{KN4}* (100)*; UAS-kn* (83, 101)*; ppk-eGFP* (34)*; ppk-CD4::tdTomato* (75)**;** *ppk-CD4::tdGFP* (75)*; ppk-Gal4* (102); *UAS-Kinesin::βGal* (76); *puc*-lacZ (87); *UAS-RedStinger* (103).

2.5.2 MARCM analyses

The MACRM analyses were performed as previously described (36). For MARCM analyses of *hiw* mutations in four classes of da neurons, the *tubP-Gal80, hs-flp, FRT^{19A}; $Gal4^{21-7}$, UAS-mCD8::GFP* virgins were mated with males of *$hiw^{\Delta N}$,FRT^{19A}*.

For MARCM analyses of *kay^{1}* mutant, overexpressing Wnd, and overexpressing Wnd in *kay^{1}* mutant C4da neurons, the *hs-flp; ppk-Gal4, UAS-mCD8::GFP; FRT^{82B}*

tubP-Gal80 virgins were mated with males of (1) *UAS-Wnd*; FRT^{82B} (2) FRT^{82B} kay^{1} and (3) *UAS-Wnd*; FRT^{82B} kay^{1} respectively.

For MARCM analyses of ca^{1} mutations, the homozygous FRT^{82B} ca^{1} virgins (to remove maternal contribution of wild-type Claret) were mated with males of *hs-flp; ppk-Gal4, UAS-mCD8::GFP;* FRT^{82B} *tubP-Gal80.*

To overexpress Kn in wild-type C4da neurons or in $hiw^{\Delta N}$ mutant C4da neurons, the *tubP-Gal80, hs-flp,* FRT^{19A}*;; ppk-Gal4, UAS-mCD8::GFP virgins* were mated with males of FRT^{19A}*;;UAS-Kn* and $hiw^{\Delta N}$ FRT^{19A}*;;UAS-Kn* respectively.

2.5.3 Immunostaining and Confocal Imaging

Embryos and third instar larvae were dissected and immunostained as previously described (5). The following primary antibodies were used: mouse anti-GFP (Invitrogen, 1:2000), chick anti-GFP (1:2000), rabbit anti-RFP (Rockland, 1:2000), guinea pig anti-Knot (gift from Adrian Moore, 1:1000), rat anti-Elav (DSHB, 1:500), guinea pig anti-Dar1 (1:1000) (36), rabbit anti-Cut (1:1000) (104), rabbit anti-βGAL (Cappel, 1:5000), and mouse anti-βGAL (DSHB, 1:100).

Confocal imaging was performed with a Leica SP5 confocal system. Only da neurons from abdominal segment 4 to 6 were imaged for quantification of dendrites and axons to ensure consistency.

To compare protein expression levels in C4da neurons, larvae of different genotypes in the same experimental group were processed simultaneously. The same setting for image acquisition was applied to the same experimental group and signal saturation was minimized. Fluorescence intensities of different genotypes were normalized to wild-type (Figures 2.8, 2.9, 2.10 and 2.12) or the OE Wnd^{KD} control group (Figure 2.16).

2.5.4 Quantifications and Statistical Analysis

To quantify protein levels, mean fluorescence intensity of the region of interest in each channel was measured with NIH ImageJ software. For axon terminal and dendritic morphology, manual tracing was conducted with Neurolucida software. Branches shorter

than 5 μm were excluded. For consistency, da neurons located between segment A4 and A6 from size-matched third instar larvae were imaged and analyzed in all experiments. In all of the bar charts of quantification, the numbers in the bars indicate the sample numbers. Values and error bars indicate mean ± SEM. Two-tailed unpaired student *t*-test was used. p values were indicated as: Not significant (NS): $p>0.05$, *: $p < 0.05$, **: $p < 0.01$, ***: $p < 0.001$.

2.6 Acknowledgements

We thank Drs. Tadashi Uemura, Adrian Moore, Michele Crozatier, Chunlai Wu, Chun Han and Yuh Nung Jan for sharing reagents, and Dr. John Kuwada, Dr. Roman Giger, Gabriella Sterne, and Ting Han for critical reading of earlier versions of the manuscript. This work was supported by grants from the National Science Foundation (IOS-0842701) (www.nsf.gov) and NIH (R01NS069844) (www.nih.gov) to C.C., and from NIH (R00MH080599 and R01MH091186) (www.nih.gov), the Whitehall foundation (www.whitehall.org), and the Pew Scholars Program in the Biological Sciences (www.pewtrusts.org) to B.Y.

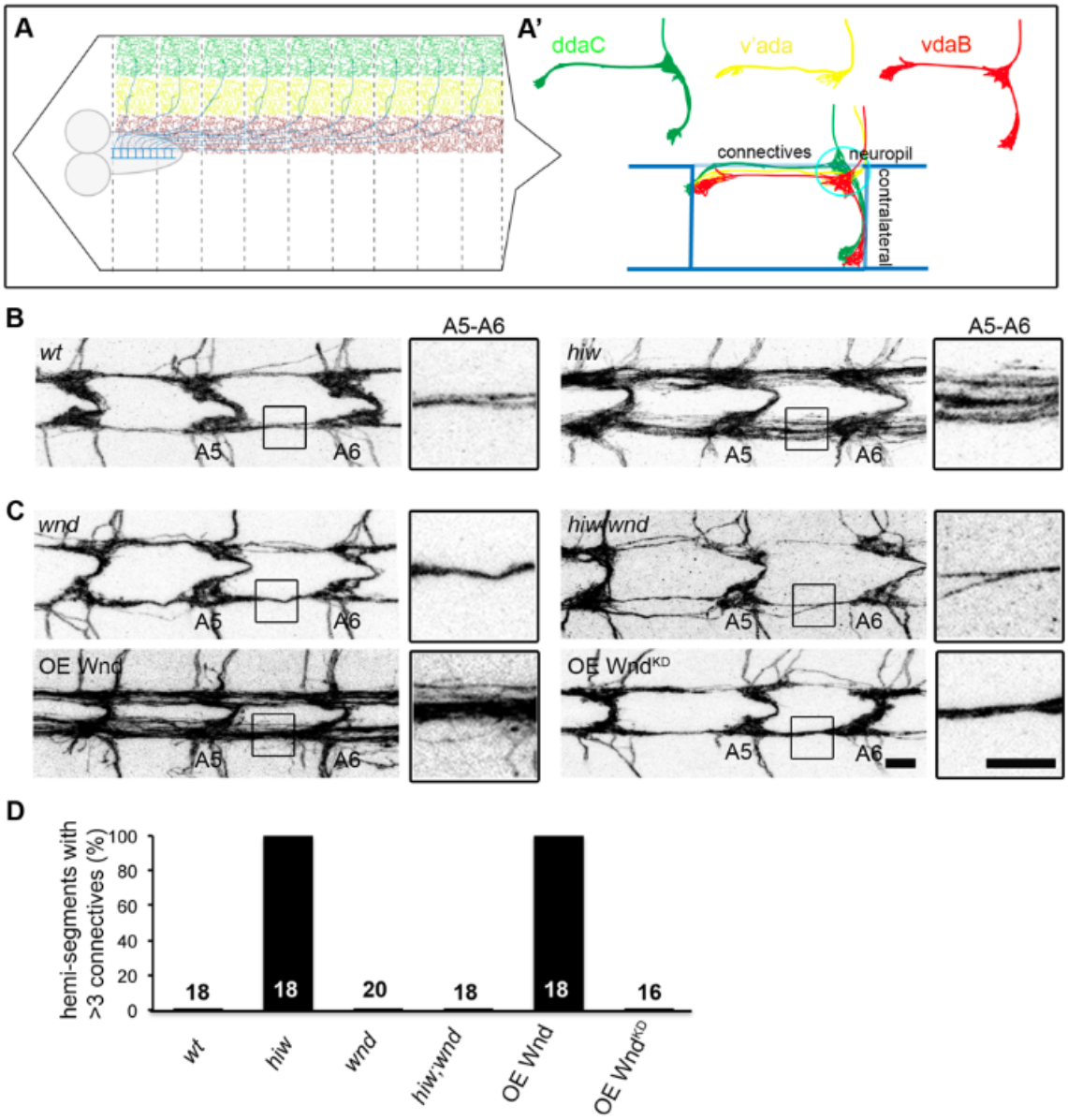

Figure 2.1 Hiw-Wnd signaling pathway operates in C4da neurons to regulate axon terminal growth.

(A) A schematic of the C4da neuron system in *Drosophila* larvae. The cell bodies of the three C4da neurons, ddaC (green), v'ada (yellow) and vdaB (red), are located from dorsal to ventral, a pattern that is repeated in each hemi-segment. The dendrites of these three neurons tile the body wall, and their axons (blue) fasciculate to enter the VNC. The C4da axon terminals form a ladder-like structure in VNC. (A') Illustrations of representative axon terminals of individual ddaC, v'ada, and vdaB (top) and their arrangement in the C4da neuropil (blue) (bottom). (B) *hiw* mutations induce axon overgrowth in C4da neurons. Shown are representative images of C4da neuropil between segment A4 and A6 of wild-type (*wt*) and $hiw^{\Delta N}$ homozygotes (*hiw*). (C) Loss of *wnd* blocks axonal overgrowth in *hiw* mutants, and Wnd overexpression induces axon overgrowth. Shown are representative images of C4da neuropil between segment A4 and A6 of the following genotypes: (1) wnd^{1}/wnd^{3} (*wnd*); (2) $hiw^{\Delta N}$; wnd^{1}/wnd^{3} double mutants (*hiw; wnd*); (3)

Wnd overexpression by *ppkGal4* (OE Wnd); (4) overexpression of a kinase dead form (K188A) of Wnd by *ppkGal4* (OE $Wnd^{KD)}$. (B-C) The magnified views of boxed area between A5 and A6 are shown on the right of each genotype. Scale bar=5μm. (D) Percentage of hemi-segments with more than three connectives between A5 and A6.

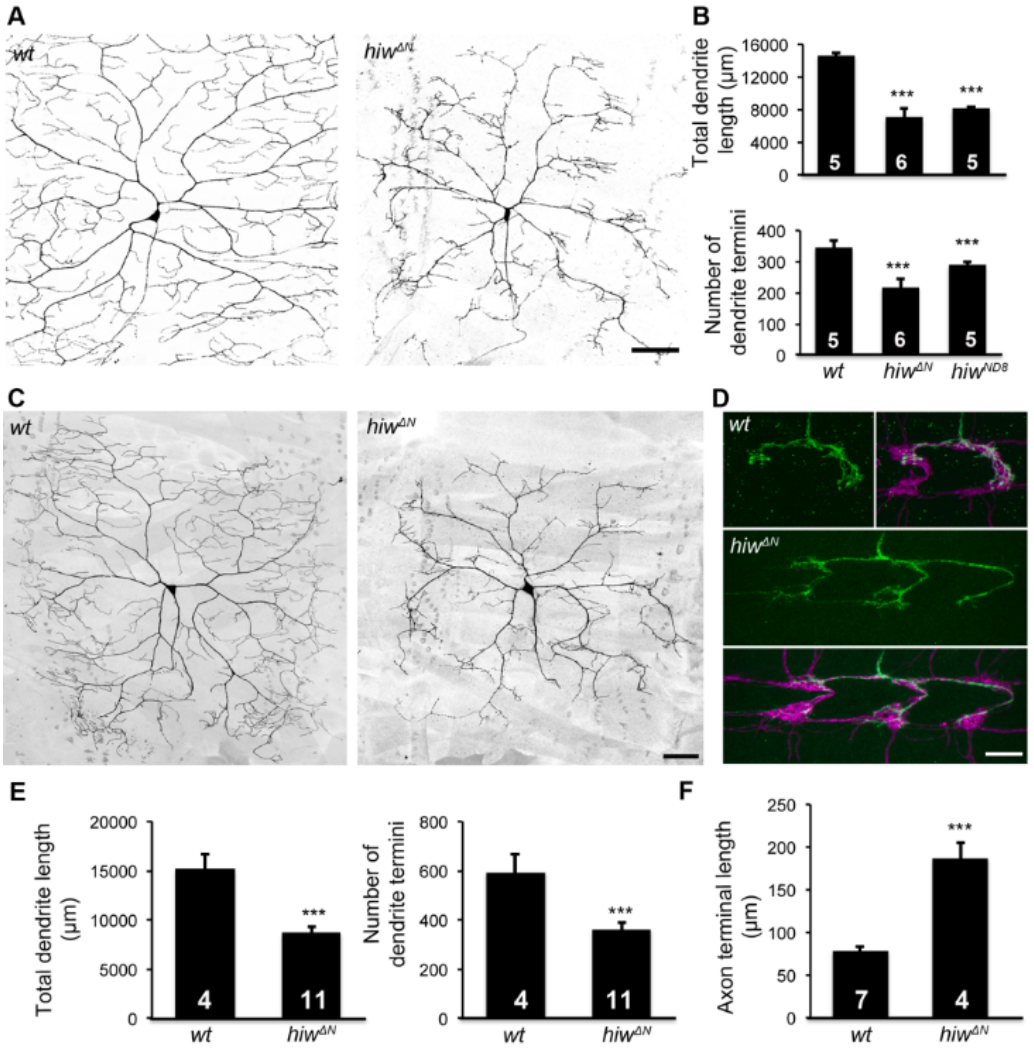

Figure 2.2 Hiw differentially regulates dendrite and axon growth in C4da neurons. (A) Dendrites of the C4da neuron ddaC in *hiw*$^{\Delta N}$ homozygous mutant larvae are reduced, as compared to *wild-type* (*wt*). C4da neurons were labeled by the C4da marker *ppk-CD4::tdTomato*. Scale bar=100μm. (B) Bar charts showing the quantification of total dendrite length (top), number of dendrite termini (bottom) of ddaC in *wt*, *hiw*$^{\Delta N}$, and *hiw*^{ND8} larvae. Sample numbers are shown in the bars of the bar charts throughout this paper. (C-D) *hiw* mutant MARCM clones exhibit impaired dendritic growth and overgrowth of axon terminals. (C) Representative dendrites of *wt* and *hiw*$^{\Delta N}$ mutant ddaC neurons. Scale bar=50μm. (D) Representative axon terminals of a single *wt* ddaC and a single *hiw*$^{\Delta N}$ mutant ddaC. The axon terminals of wild-type ddaC clones (green) extend within one segment length of the C4da neuropil (magenta) labeled by *ppk-CD4::tdTomato*. The axon terminals of *hiw*$^{\Delta N}$ mutant clones (green) expand over multiple segment lengths of the C4da neuropil (magenta). Scale bar=10μm. (E) Quantification of total dendrite length (left) and number of dendrite termini (right) of *wt* and *hiw*$^{\Delta N}$ MARCM clones. (F) Quantification of axon terminal length of *wt* and *hiw*$^{\Delta N}$ MARCM clones.

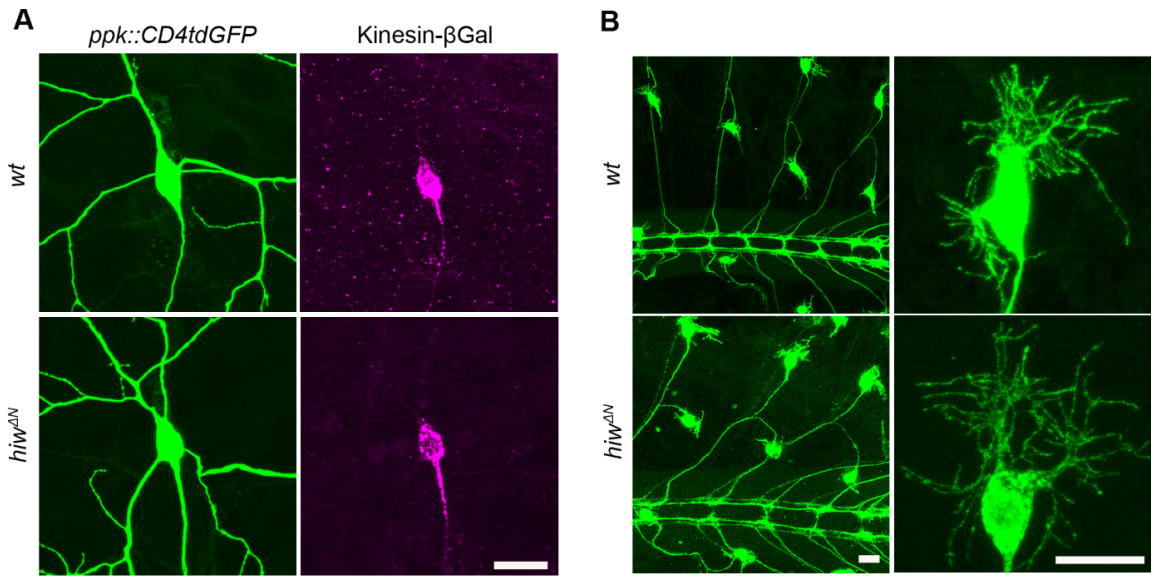

Figure 2.3 Hiw is dispensable for axon specification and early axon and dendrite development.
(A) Loss of *hiw* does not alter axon or dendrite identity. Axon-specific marker Kinesin-β-galactosidase (Magenta) exclusively localizes to the axons of C4da neurons labeled by *ppk-CD4::tdGFP* (green) in *wt* and $hiw^{\Delta N}$ larvae. Scale bar=20μm. (B) Loss of *hiw* does not affect axon pathfinding into the VNC (left panels) or early dendritic extension in stage 16 embryos (right panels). These results were collected from embryos devoid of both maternal and zygotic *hiw* functions. Scale bar=10μm.

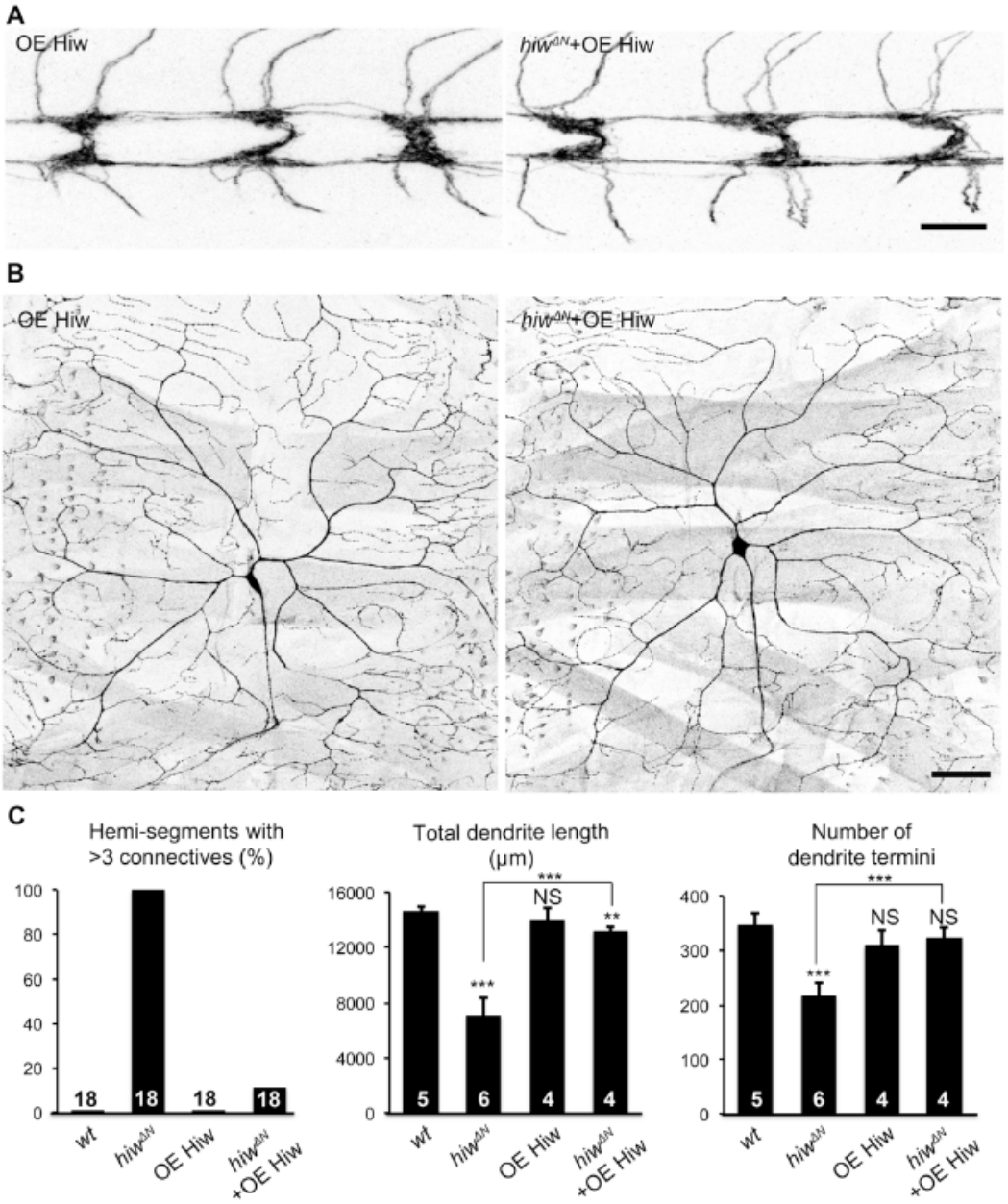

Figure 2.4 Hiw is required cell-autonomously for dendritic and axonal growth in C4da neurons.

(A-B) Overexpressing Hiw exclusively in C4da neurons does not alter axon terminal growth or dendritic growth, but restores the axonal and dendritic defects in $hiw^{\Delta N}$ mutants. Shown are representative A4-A6 neuropils (A) and ddaCs dendrites (B) of following genotypes: (1) overexpressing Hiw by *ppkGal4* (OE Hiw); (2) overexpressing Hiw by *ppkGal4* in $hiw^{\Delta N}$ homozygous mutants ($hiw^{\Delta N}$ + OE Hiw). Scale bar in (A): 10μm. Scale bar in (B): 50μm. (C) Bar charts showing the percentage of hemi-segments with more than three connectives between A5 and A6 (left), total dendrite length (middle) and number of dendrite termini (right). Samples of *wt* and $hiw^{\Delta N}$ that are used for statistical analysis are the same as those in Figure 2.2.

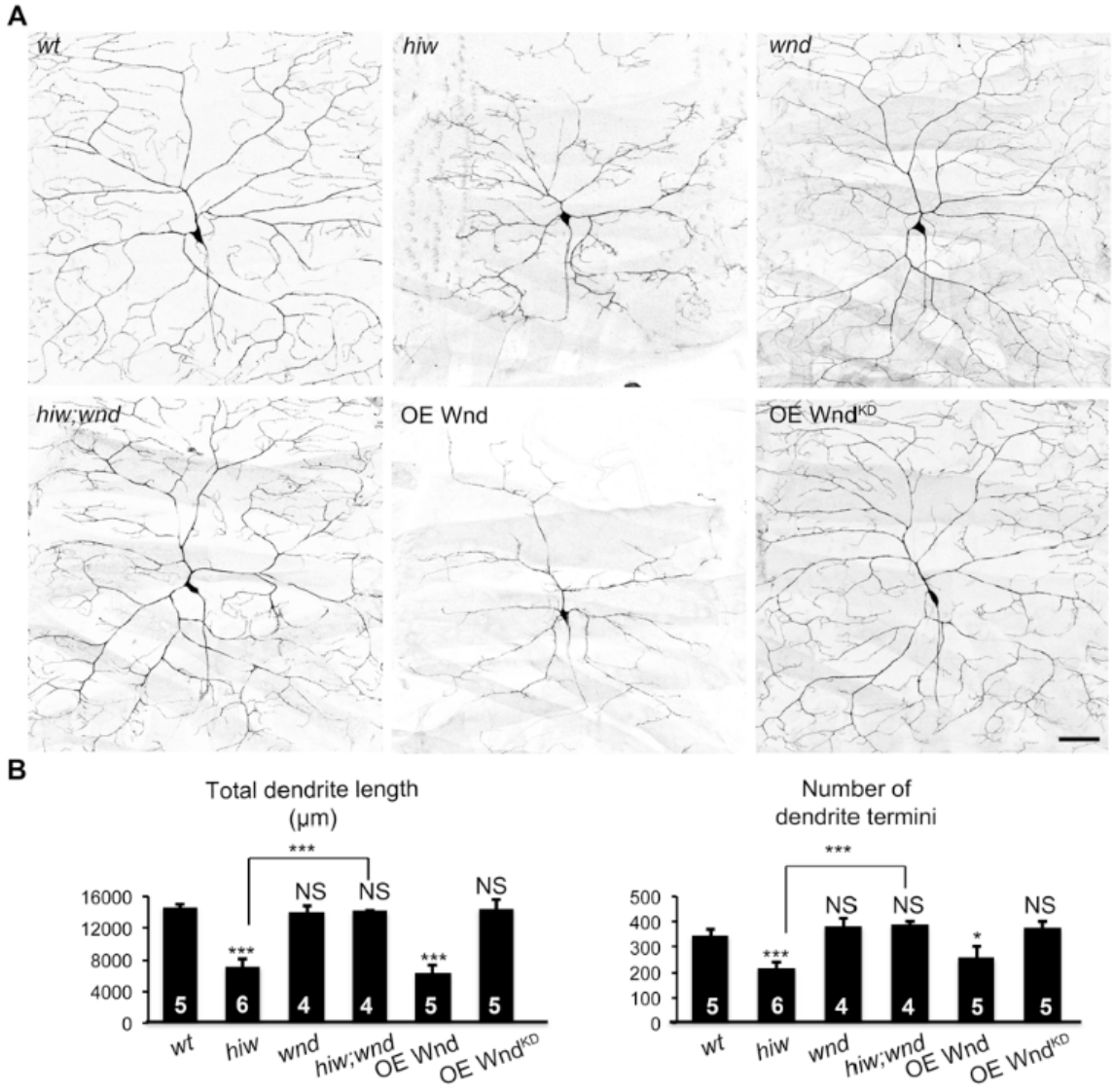

Figure 2.5 Wnd mediates the functions of Hiw on dendritic growth.
(A) Loss of *wnd* blocks dendrite reduction in *hiw* mutants, and ectopic Wnd restrains dendritic growth. Shown are representative dendrites of ddaC neurons, labeled by *ppk-CD4::tdTomato*, of the following genotypes: (1) *wt*; (2) $hiw^{\Delta N}$ homozygotes (*hiw*); (3) wnd^{1}/wnd^{3}(*wnd*); (4) $hiw^{\Delta N}$; wnd^{1}/wnd^{3} double mutants (*hiw; wnd*); (5) overexpressing Wnd by *ppkGal4* (OE Wnd); (6) overexpressing a kinase dead form (K188A) of Wnd by *ppkGal4* (OE $Wnd^{KD)}$. Scale bar=50μm. (B) Bar charts showing the quantification of total dendrite length (left) and number of dendrite termini (right). Samples of *wt* and $hiw^{\Delta N}$ that are used for statistical analysis are the same as those in Figure 2.2.

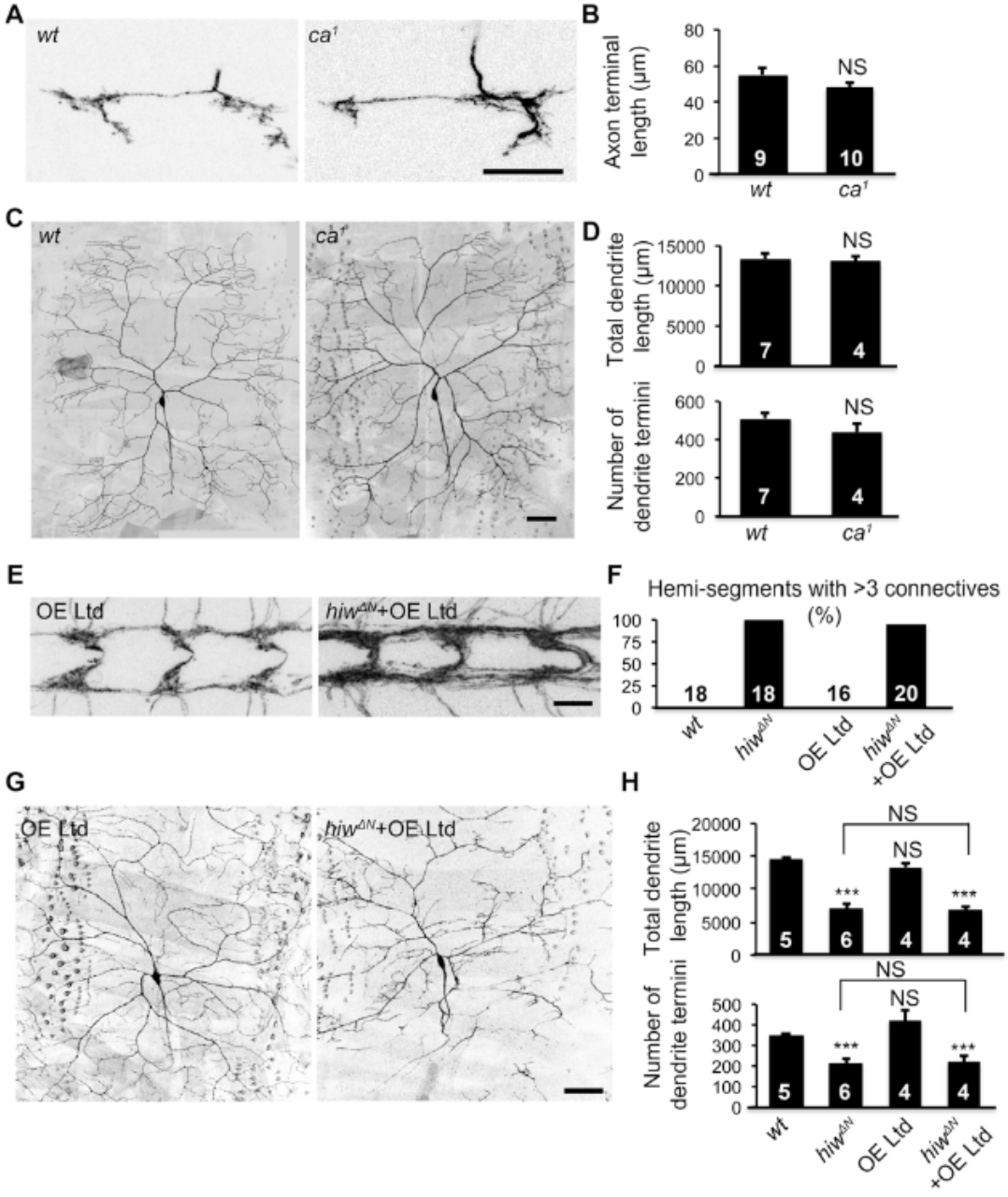

Figure 2.6 The Ca-Ltd trafficking pathway is dispensable for dendritic and axonal growth.

(A-D) *Claret* (*ca*) is not required for either axonal or dendritic growth. Representative axon terminals (A) and dendrites (C) of ddaC MARCM clones in *wt* (FRT^{82B}) and ca^{1} (ca^{1}, FRT^{82B}) are shown. Maternal contribution of *ca* was removed by using homozygous ca^{1}, FRT^{82B} mutant females in the MARCM cross. (B and D) Quantification of axon terminal length (B), total dendrite length (D: top) and number of dendrite termini (D: bottom) of *wt* and ca^{1} MARCM clones. Samples of *wt* used for statistical analysis are the same as those in Figure 3. (E-H) Overexpressing Ltd fails to rescue axon or dendrite defects in in $hiw^{\Delta N}$ mutants. Shown are representative A4-A6 neuropils (E) and ddaCs dendrites (G) of the following genotypes: overexpressing Ltd by *ppkGal4* (OE Ltd), and

overexpressing Ltd by *ppkGal4* in $hiw^{\Delta N}$ homozygotes genetic background ($hiw^{\Delta N}$ + OE Ltd). (F and H) Bar charts showing the percentage of hemi-segments with more than three connectives between A5 and A6 (F), total dendrite length (H: top) and number of dendrite termini (H: bottom). Samples of *wt* and $hiw^{\Delta N}$ that are used for statistical analysis are the same as those in Figure 2.1 and 1.2. Scale bar in (A and E): 10μm. Scale bar in (C and G): 50μm.

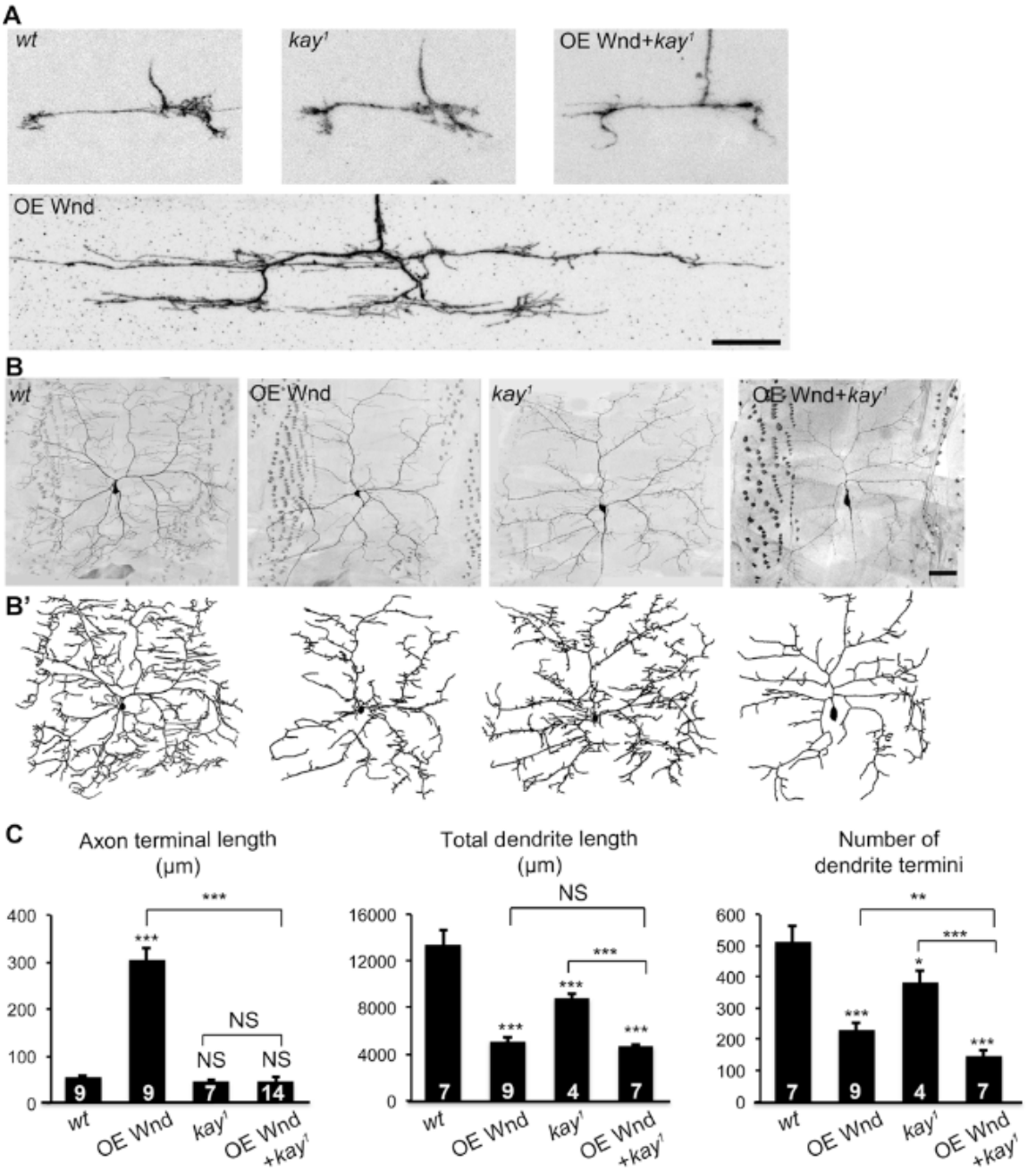

Figure 2.7 Transcription factor Fos specifically mediates axonal overgrowth induced by Wnd.

(A) Loss of the *Drosophila fos*, *kay*, blocks axonal overgrowth caused by Wnd overexpression. Shown are representative axon terminals of ddaC MARCM clones of following genotypes: (1) *wt*; (2) overexpressing Wnd with MARCM (OE Wnd); (3) kay^{1}; (4) overexpressing Wnd in kay^{1} genetic background with MARCM (OE Wnd + kay^{1}). Scale bar=10μm. (B-B') kay^{1} impairs dendritic growth in *wt* genetic background and exacerbates the dendritic reduction caused by Wnd overexpression. Shown are representative dendrites (B) and tracings (B') of ddaC MARCM clones of indicated genotypes. Scale bar=50μm. (C) Bar charts showing the quantification of axon terminal length (left), total dendrite length (middle) and number of dendrite termini (right).

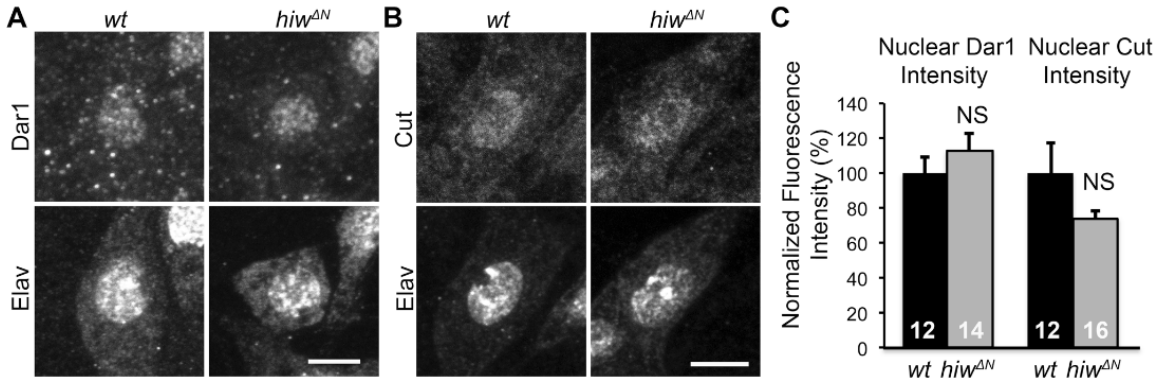

Figure 2.8 Normal Dar1 and Cut expression in *hiw* mutants.
(A) Dar1 nuclear expression levels are comparable between *wt* and $hiw^{\Delta N}$ mutants. Shown are representative immunofluorescence of ddaC neurons stained with antibodies against Dar1 (top) and Elav (bottom). (B) Cut nuclear expression levels are comparable between *wt* and $hiw^{\Delta N}$ mutants. Shown are representative immunofluorescence of ddaC neurons stained with antibodies against Cut (top) and Elav (bottom). (C) Quantification of nuclear immunofluorescence intensity of Dar1 (left) or Cut (right) normalized to nuclear Elav immunofluorescence intensity.

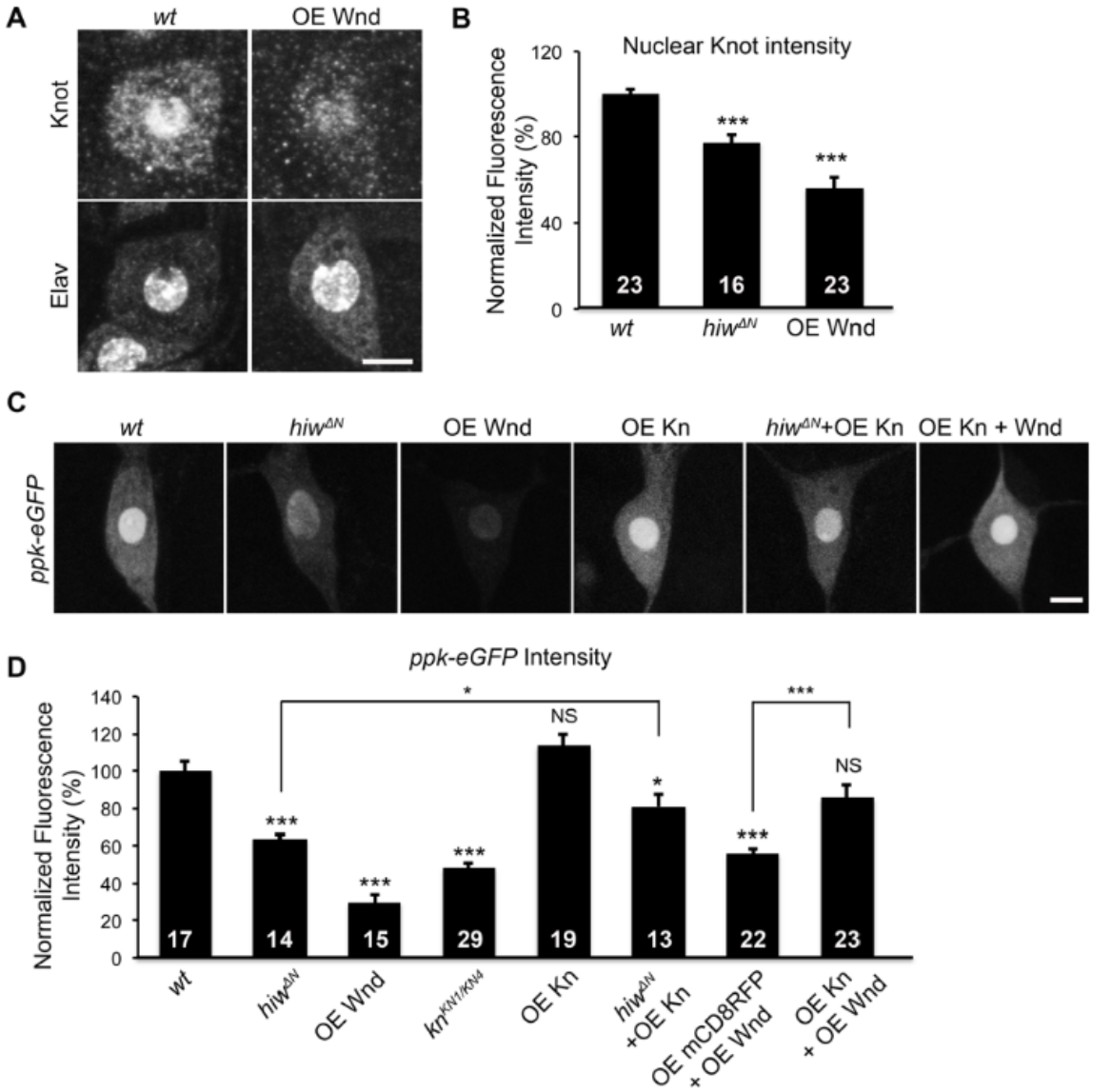

Figure 2.9 Hiw-Wnd pathway regulates the expression and transcriptional activity of the C4da-specific transcription factor Kn.

(A) Overexpressing Wnd attenuates the nuclear Kn expression levels. Representative immunofluorescence images of *wt* and Wnd-overexpressing (OE Wnd) ddaC neurons labeled with antibodies against Kn (top) and Elav (bottom). Scale bar=5μm. (B) Quantification of the immunofluorescence intensity of nuclear Kn normalized to that of nuclear Elav in *wt*, $hiw^{\Delta N}$ and OE Wnd neurons. (C) Wnd overexpression down-regulates the promoter activity of the ENaC ion channel *pickpocket* (*ppk*), a known target of Kn. Representative ddaC neurons labeled with *ppk-eGFP* in neurons of the following genotypes: 1) *wt*; 2) $hiw^{\Delta N}$; 3) OE Wnd; 4) OE Kn; 5) $hiw^{\Delta N}$ +OE Kn; 6) OE Kn + OE Wnd. Scale bar=5μm. (D) Quantification of *ppk-eGFP* fluorescent intensity in neurons of the following genotypes: 1) *wt*; 2) $hiw^{\Delta N}$; 3) OE Wnd; 4) $kn^{KN1/KN4}$; 5) OE Kn; 6) $hiw^{\Delta N}$ +OE Kn; 7) OE mCD8RFP +OE Kn; 8) OE Kn + OE Wnd.

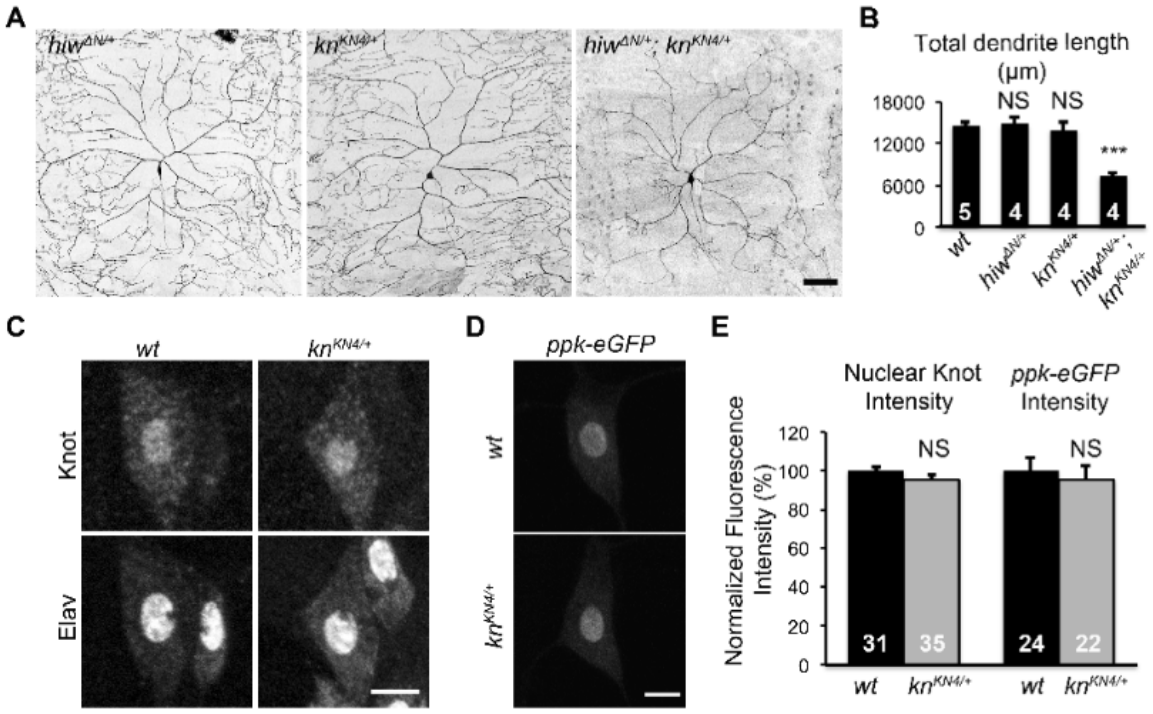

Figure 2.10 *hiw* and *kn* genetically interact.
(A) *hiw* and *kn* interact genetically. Shown are representative dendrites of the following genotypes: (1) $hiw^{\Delta N}$ heterozygote ($hiw^{\Delta N/+}$); (2) kn^{KN4} heterozygote ($kn^{KN4/+}$); (3) $hiw^{\Delta N}$ and kn^{KN4} trans-heterozygote ($hiw^{\Delta N/+}$; $kn^{KN4/+}$). Scale bar= 50µm. (B) Quantification of total dendrite length of denoted genotypes. *wt* samples used for statistical analysis are the same as those in Figure 2.2. (C) Knot nuclear expression levels are unaltered in $kn^{KN4/+}$. Shown are representative immunofluorescence of ddaC neurons stained with antibodies against Knot (top) and Elav (bottom). (D) *ppk-eGFP* levels are unaltered in $kn^{KN4/+}$. Representative ddaC neurons labeled with *ppk-eGFP* in *wt* and $kn^{KN4/+}$. (E) Quantification of nuclear immunofluorescence intensity of Knot normalized to nuclear Elav immunofluorescence intensity (left) and *ppk-eGFP* fluorescent intensity (right). Scale bar=5µm.

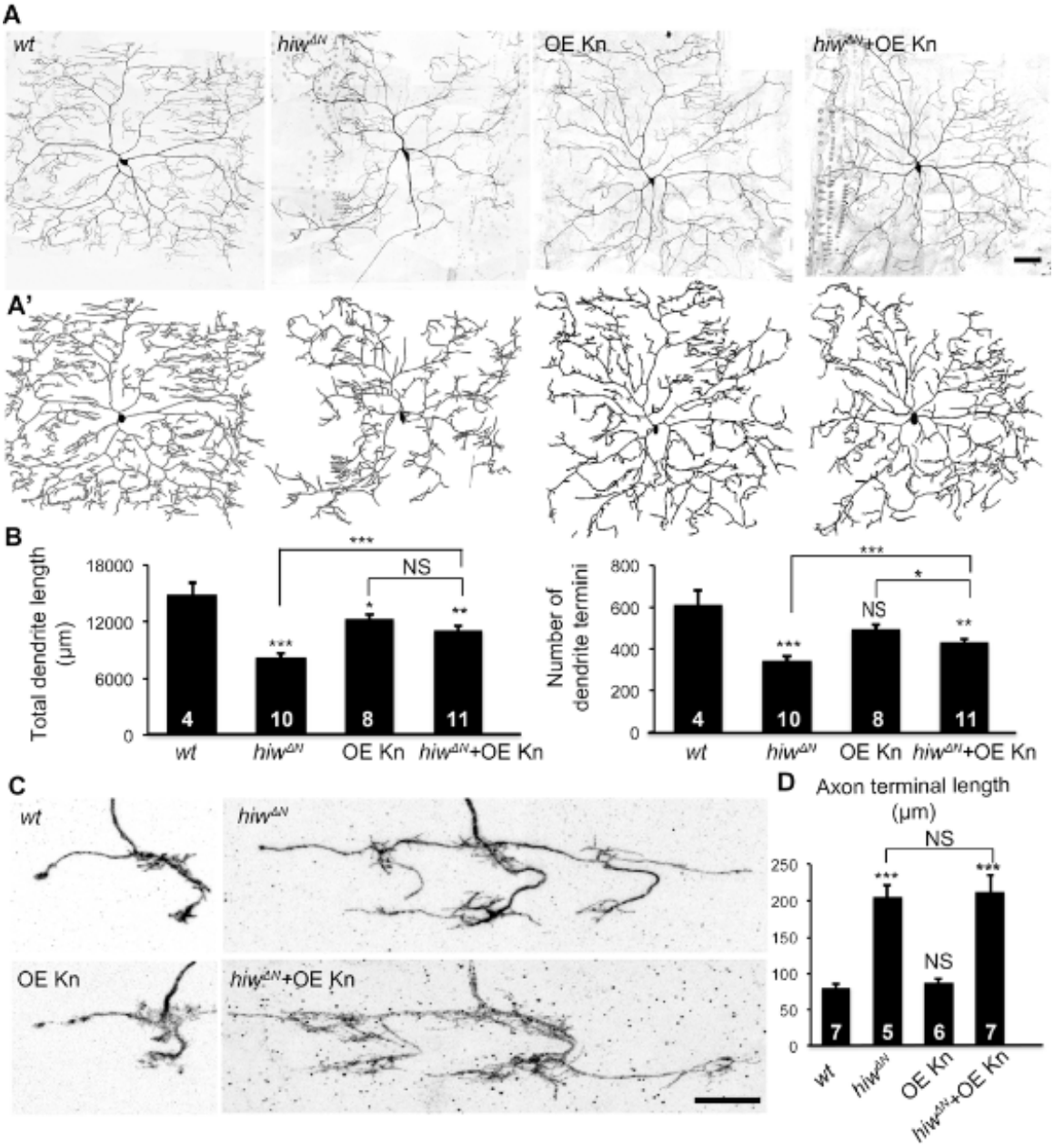

Figure 2.11 Kn specifically mediates Hiw regulation of dendritic growth.
(A and A') Overexpressing Kn partially rescues dendritic defects in *hiw*$^{\Delta N}$ mutants. Representative dendrites (A) and tracings (A') of ddaC MARCM clones of following genotypes: (1) *wt*; (2) *hiw*$^{\Delta N}$; (3) overexpressing Kn with MARCM (OE Kn); (4) overexpressing Knot in *hiw*$^{\Delta N}$ genetic background with MARCM (*hiw*$^{\Delta N}$ + OE Kn). Scale bar=50μm. (B) Quantification of total dendrite length (left) and number of dendrite termini (right). (C) Overexpressing Kn does not alter axon terminal morphology in *hiw*$^{\Delta N}$ mutants. Shown are representative axon terminals of ddaC MARCM clones of the indicated genotypes. Scale bar=10μm. (D) Quantification of the length of axon terminals.

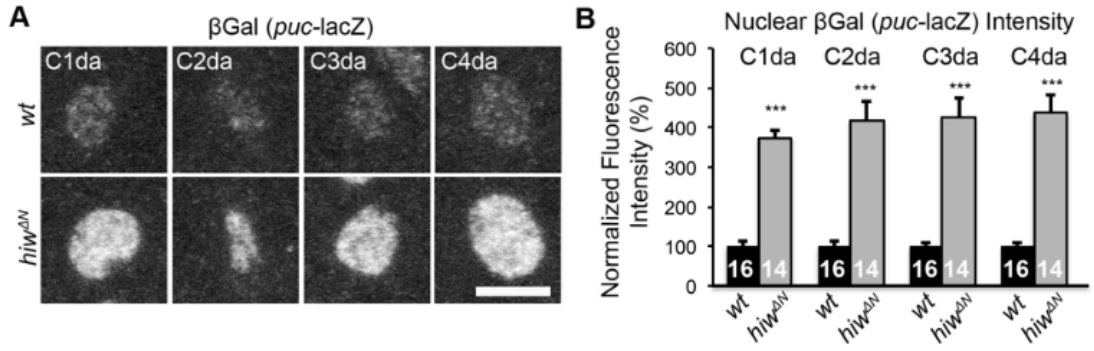

Figure 2.12 Hiw functions in all four classes of da neurons.
(A) The expression of *puc*-lacZ, a reporter for Wnd activity, is elevated by *hiw* mutations in class I-IV da neurons. Shown are representative immunofluorescence of C1da (ddaE), C2da (ddaB), C3da (ddaF) and C4da (ddaC) neurons stained with an anti-βGal antibody. Scale bar=5μm. (B) Quantification of nuclear immunofluorescence of β-Gal expressed by *puc*-lacZ.

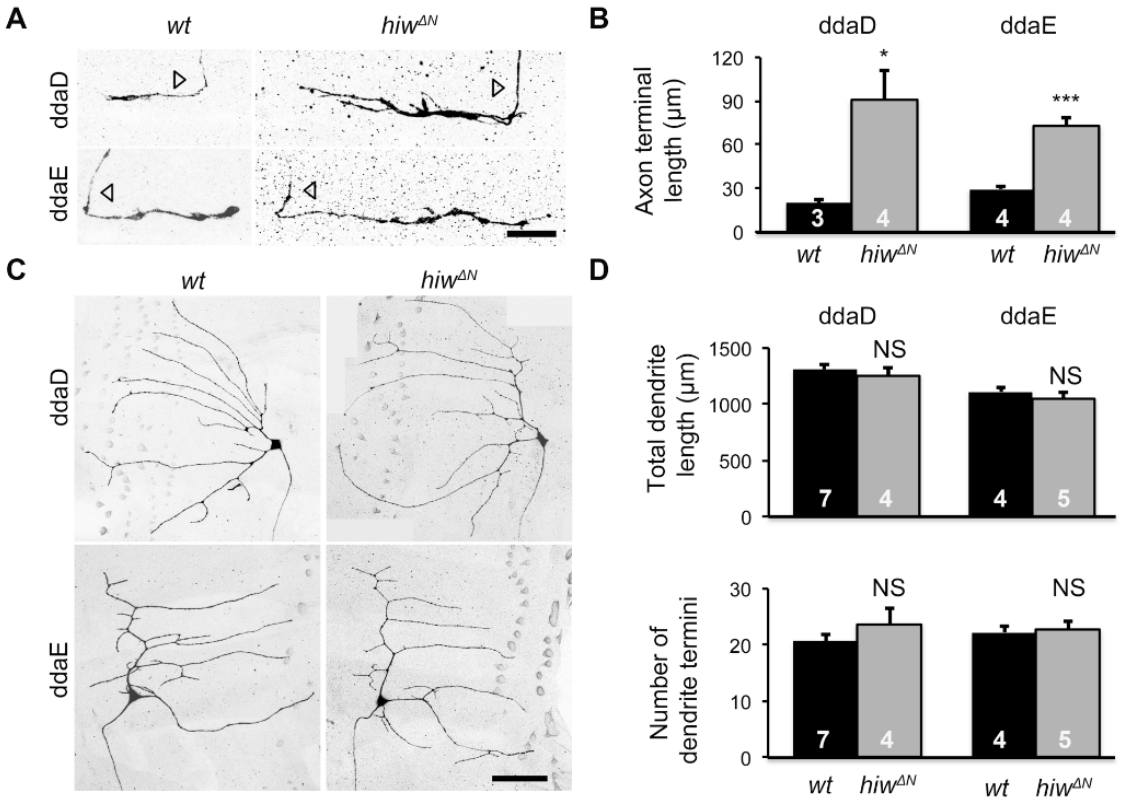

Figure 2.13 Hiw specifically restrains axonal growth in class I da neurons in a cell-autonomous manner.
(A-B) Loss of *hiw* causes axonal overgrowth in class I da (C1da) neurons. (A) Representative axon terminals of MARCM clones of the C1da neurons ddaD and ddaE are shown. Open arrowheads indicate where the axon enters the sensory neuropil. Scale bar=10µm. (B) Quantification of axon terminal length of *wt* and $hiw^{\Delta N}$ MARCM clones. (C-D) Loss of *hiw* does not alter dendritic growth in C1da neurons. Representative dendrites of MARCM clones of ddaD and ddaE are shown. (D) Quantification of total dendrite length (top) and number of dendrite termini (bottom) of *wt* and $hiw^{\Delta N}$ MARCM clones. Scale bar=50µm.

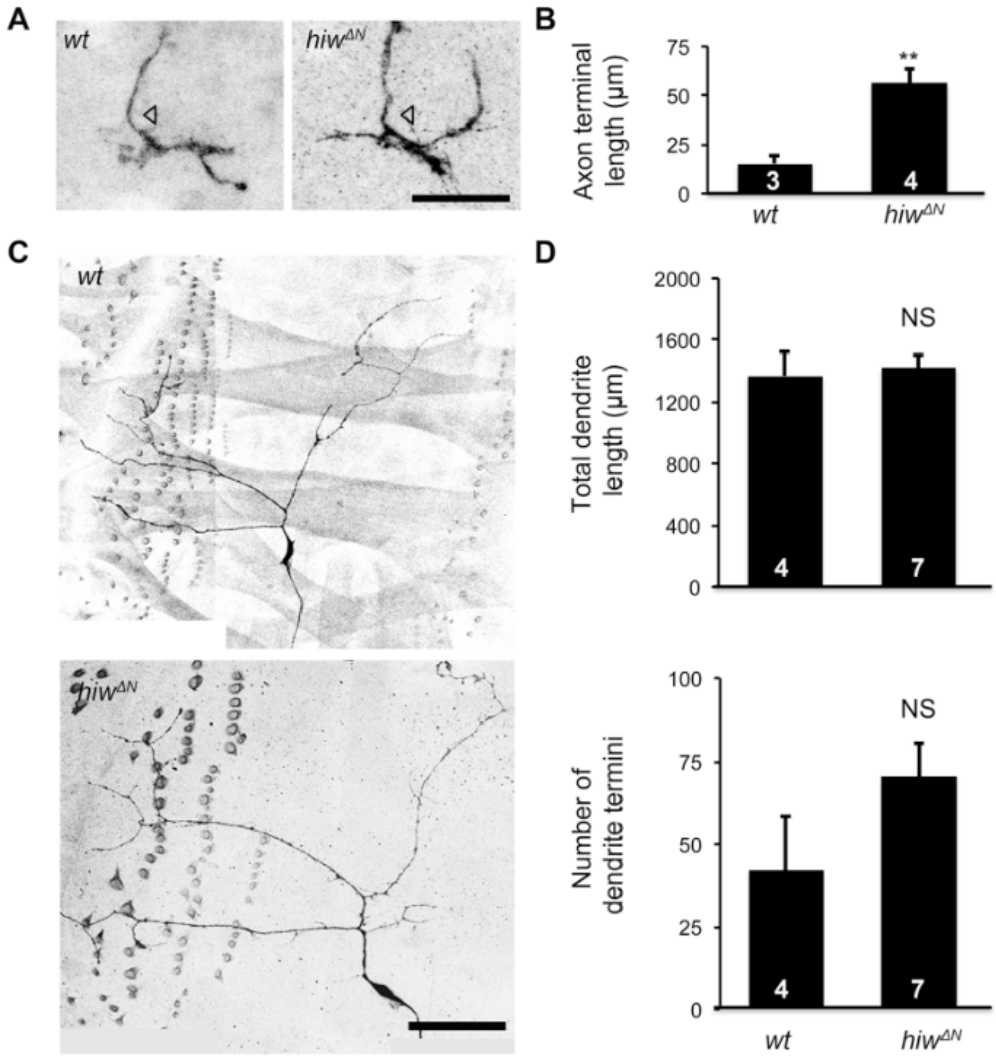

Figure 2.14 Hiw specifically restrains axon growth in class II da neurons in a cell-autonomous manner.

(A-B) Loss of *hiw* causes axonal overgrowth in class II da (C2da) neurons. (A) Representative axon terminals of MARCM clones of the C2da neurons ddaB are shown. Open arrowheads indicate where the axon enters the sensory neuropil. Scale bar=10µm. (B) Quantification of axon terminal length of *wt* and $hiw^{\Delta N}$ MARCM clones. (C-D) Loss of *hiw* does not alter dendritic growth in C2da neurons. Representative dendrites of MARCM clones of ddaB are shown. (D) Quantification of total dendrite length (top) and number of dendrite termini (bottom) of *wt* and $hiw^{\Delta N}$ MARCM clones. Scale bar=50µm.

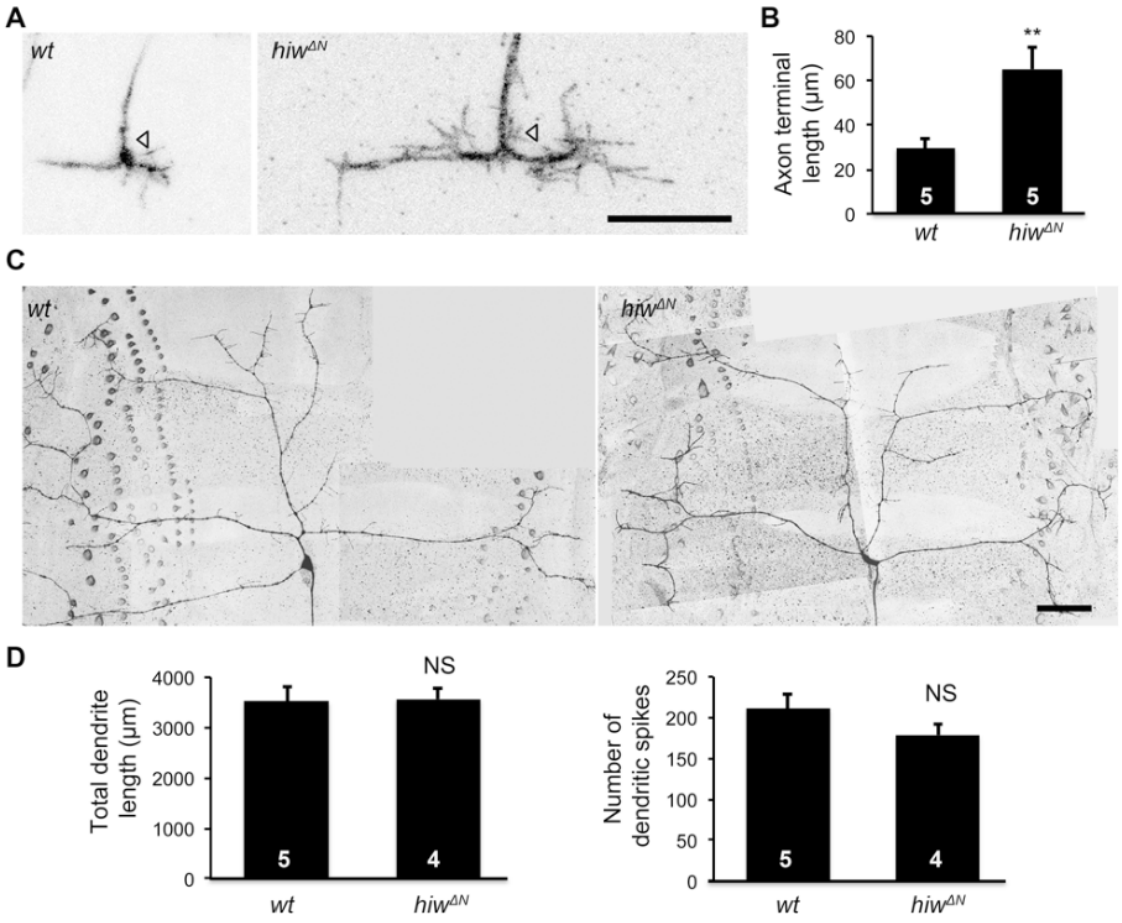

Figure 2.15 Hiw specifically restrains axon growth in class III da neurons in a cell-autonomous manner.
(A-B) Loss of *hiw* causes axonal overgrowth in class III da (C3da) neurons. (A) Representative axon terminals of MARCM clones of the C3da neurons ddaF are shown. Open arrowheads indicate where the axon enters the sensory neuropil. Scale bar=10μm. (B) Quantification of axon terminal length of *wt* and $hiw^{\Delta N}$ MARCM clones. (C-D) Loss of *hiw* does not alter dendritic growth in C3da neurons. Representative dendrites of MARCM clones of ddaF are shown. (D) Quantification of total dendrite length (top) and number of dendritic spikes (bottom) of *wt* and $hiw^{\Delta N}$ MARCM clones. Scale bar=50μm.

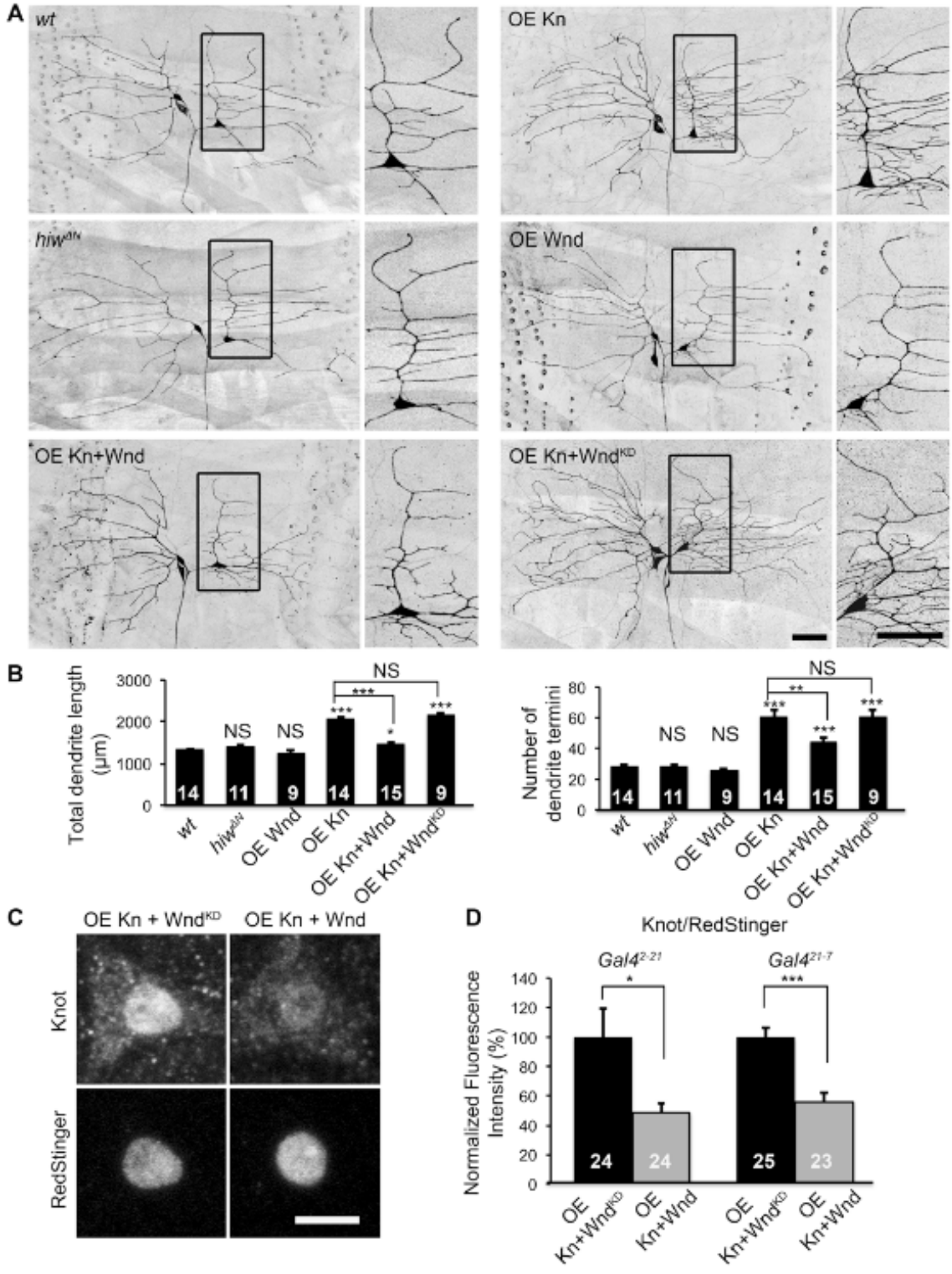

Figure 2.16 Wnd kinase inhibits dendrite growth in C1da neurons expressing ectopic Kn.

(A) Wnd overexpression does not alter dendrite morphology in wild-type C1da neurons, but restrains the dendritic overgrowth caused by ectopic Kn in these neurons. Shown are

representative dendrites of C1da neurons ddaD (left) and ddaE (right), labeled by *Gal4*$^{2\text{-}21}$*/UAS-mCD8::GFP,* of the following genotypes: (1) *wt*; (2) overexpressing Kn by *Gal4*$^{2\text{-}21}$(OE Kn); (3) *hiw*$^{\Delta N}$ homozygotes (*hiw*); (4) overexpressing Wnd by *Gal4*$^{2\text{-}21}$ (OE Wnd); (5) overexpressing Kn and Wnd by *Gal4*$^{2\text{-}21}$ (OE Kn + Wnd); (6) overexpressing Kn and a kinase-dead form of Wnd by *Gal4*$^{2\text{-}21}$(OE Kn + Wnd^{KD}). Scale bar=50μm. Magnified views of the boxed areas are shown on the right for each genotype. (B) Quantification of total dendrite length (left) and number of dendrite termini (right) of ddaEs of denoted genotypes. (C) Wnd kinase specifically down-regulates the expression of *UAS-Kn*, but not *UAS-RedStinger* (a nuclear red fluorescent protein) (103) in a post-transcriptional manner. Representative images of ddaEs labeled with antibodies against Kn (top) and RedStinger (bottom) in "OE Kn + Wnd" and "OE Kn + Wnd^{KD}" using *Gal4*$^{2\text{-}21}$. Scale bar=5 μm. (D) Quantification of immunofluorescence intensity of nuclear Kn normalized to that of RedStinger. Two different *Gal4* lines, *Gal4*$^{2\text{-}21}$ (left) and *Gal4*$^{21\text{-}7}$ (right), were tested in this experiment.

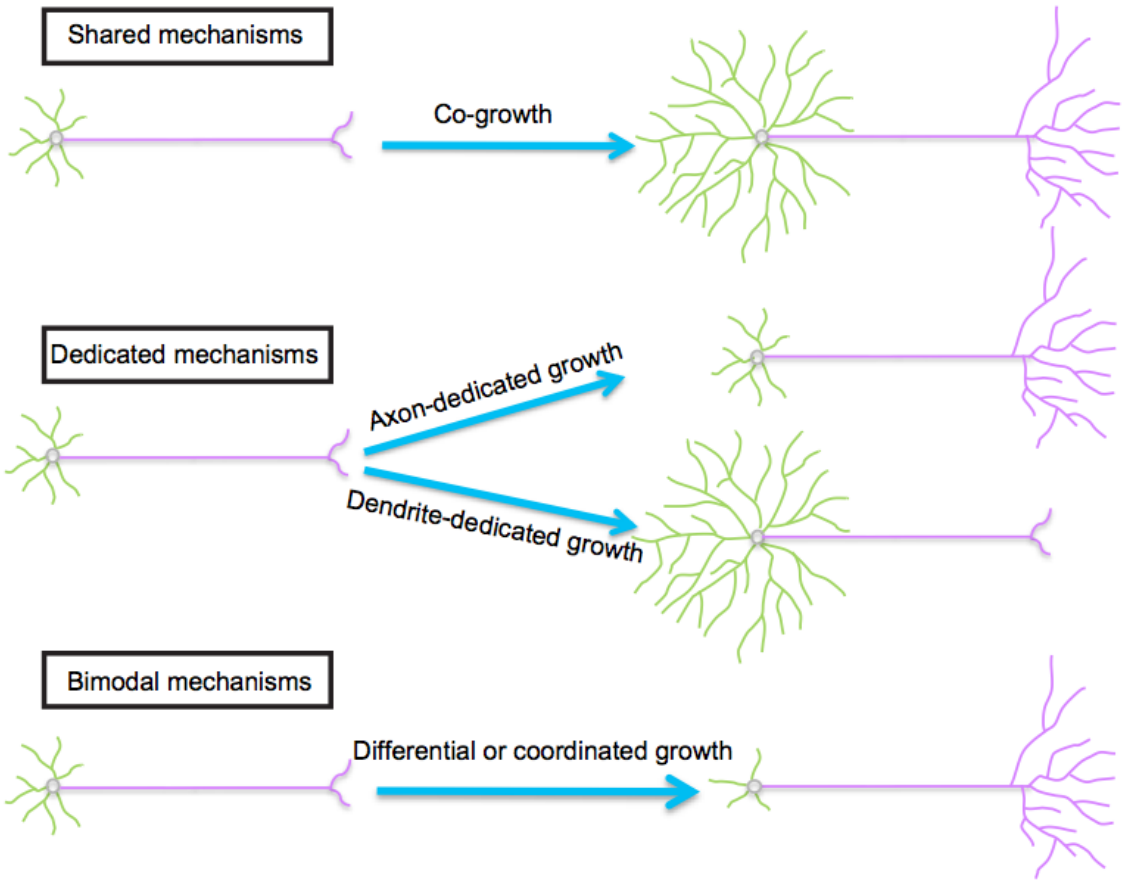

Figure 2.17 Three distinct mechanisms regulating dendritic and axonal growth. Shared mechanisms control dendrite and axon co-growth. Dedicated mechanisms direct compartment-specific growth. Bimodal mechanisms differentially regulate dendritic and axonal growth.

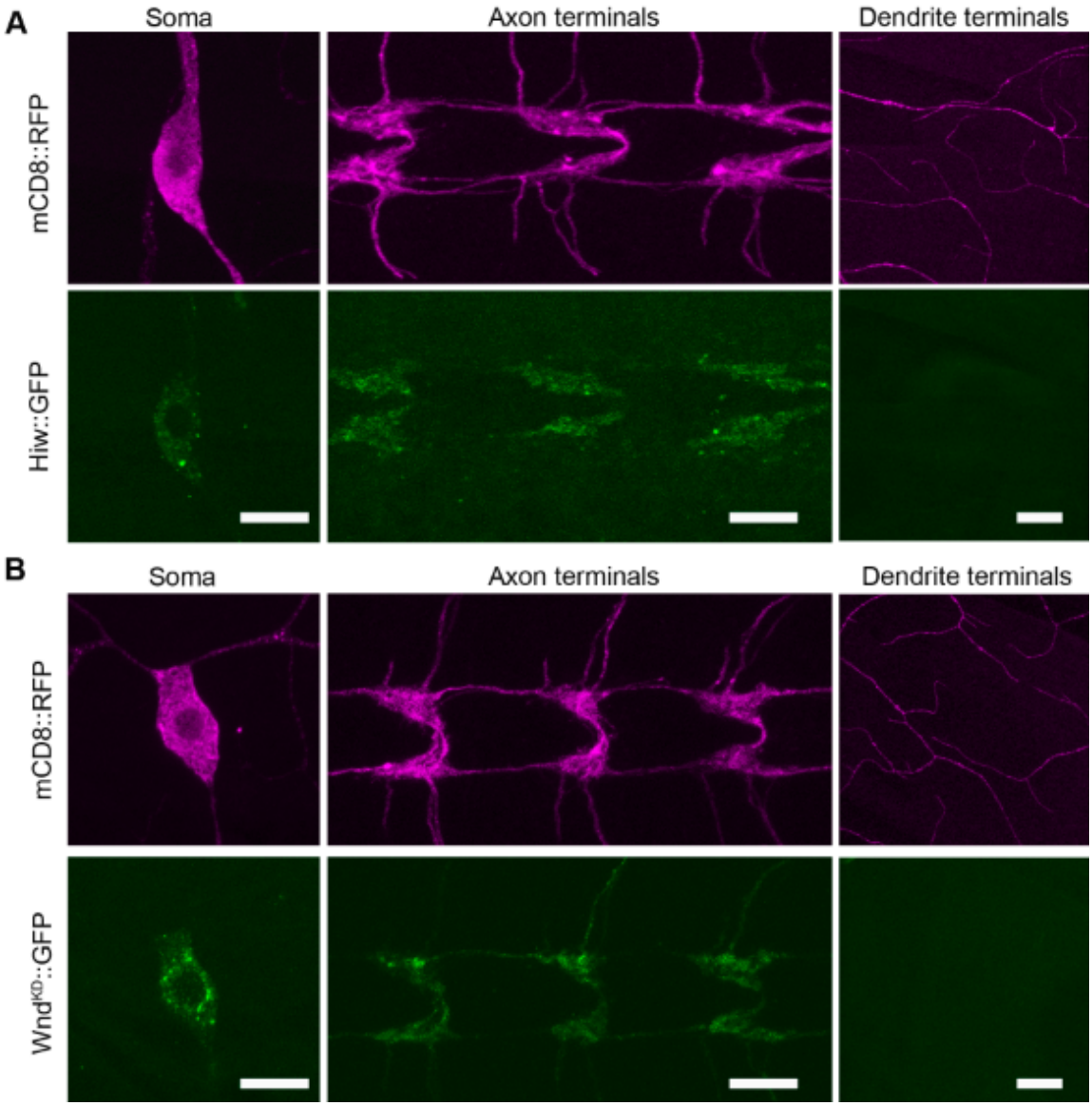

Figure 2.18 Hiw and Wnd are localized to the soma and axon terminals but not the dendrites of C4da neurons.
(A) Localization of mCD8::RFP (top) and Hiw::GFP (bottom) in the cell body (left), axon terminals (middle) and dendrites (right) of ddaC neurons that overexpress Hiw:GFP in *hiw*$^{\Delta N}$ homozygous mutants. (B) Localization of mCD8::RFP (top) and Wnd^{KD}::GFP (bottom) in the cell body (left), axon terminals (middle) and dendrites (right) of ddaC neurons. Scale bar: 10μm.

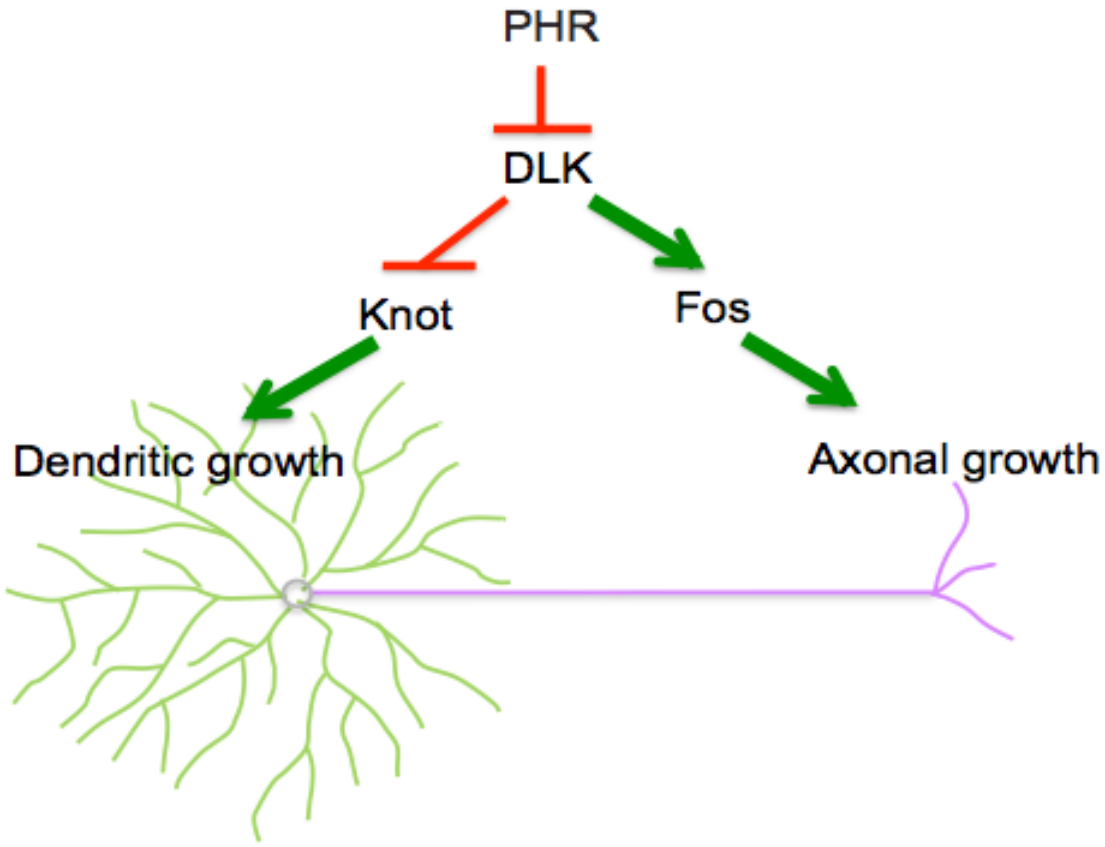

Figure 2.19 A model that postulates the differential control of dendritic and axonal growth by the DLK pathway, which is based on the present study.
In this model, DLK plays a dual role in neuron morphogenesis. Up-regulated DLK, caused either by *PHR* mutations or DLK over-activation, promotes the growth of axon terminals but restricts that of high-order dendritic branches. Such a dichotomous function is the result of signaling divergence into two transcriptional programs that are each dedicated to either dendritic or axonal growth. Fos serves a permissive role in the axonal regulation by DLK, whereas Kn specifically mediates the dendritic regulation by DLK.

Chapter 3

Independent pathways downstream of the Wnd/DLK MAPKKK regulate synaptic structure, axonal transport, and injury signaling[2]

In Chapter 2, we found that the conserved MAPKKK, named Wallenda (Wnd) in *Drosophila*, DLK in vertebrates and *C. elegans*, serves as a bimodal regulator in differentiating dendritic and axonal growth. Gain of function of Wnd caused dendritic reduction but axonal overgrowth in *Drosophila* C4da neurons (Figure 2.7). In contrast, loss of function of *wnd* did not cause noticeable defects in overall neuronal morphology (Figures 2.1 and 2.5). Thus, the function of endogenous Wnd in dendritic and axonal development remains to be further characterized. Furthermore, Wnd is specifically localized in soma and axonal terminals but undetectable in dendrites (Figure 2.18), suggesting that endogenous Wnd likely functions in axon terminals but not in dendrites. In this chapter, we uncovered a novel role of endogenous Wnd in presynaptic structures at axon terminals and dissected the independent downstream pathways that separately mediate Wnd's functions in presynaptic growth and axonal regeneration.

3.1 Abstract

MAP Kinase signaling cascades orchestrate diverse cellular activities with common molecular players. To achieve specific cellular outcomes in response to specific signals, scaffolding proteins play an important role. Here we investigate the role of the scaffolding protein JIP1 in neuronal signaling by a conserved axonal MAP Kinase Kinase Kinase (MAPKKK), known as Wallenda (Wnd) in *Drosophila,* DLK in vertebrates and

[2] Modified after the research article originally published in *J Neurosci*. (2013; 33(31): 12764 –12778) with authors listed as Susan Klinedinst, Xin Wang, Xin Xiong, Jill Haenfler, and Catherine A. Collins.

C. elegans. Recent studies in multiple model organisms suggest that Wnd/DLK regulates both regenerative and degenerative responses to axonal injury. Here we report a new role for Wnd in regulating synaptic structure during development, which implies that Wnd is also active in uninjured neurons. This synaptic role of Wnd can be functionally separated from Wnd's role in axonal regeneration and injury signaling by the requirement for the JIP1 scaffold and the p38b MAP kinase. JIP1 mediates the synaptic function of Wnd via p38, which is not required for injury signaling or new axonal growth after injury. Our results indicate that Wnd regulates multiple independent pathways in *Drosophila* motoneurons, and that JIP1 scaffolds a specific downstream cascade required for the organization of presynaptic microtubules during synaptic development.

3.2 Introduction

Neurons utilize MAPK signaling cascades to regulate many different processes, including synaptic development and plasticity, axonal growth, and survival. Wnd/DLK signaling received much recent attention for its roles in regulating neuronal responses to axonal injury. This kinase becomes activated by axonal injury and mediates different downstream responses depending upon the cell type and context: regenerative axonal growth, cell death, axonal degeneration and protection from degeneration (reviewed in(49).

In contrast to these post-developmental roles, earlier studies have suggested that Wnd/DLK is highly regulated during development, and that this regulation is important for neuronal migration, axon termination, apoptosis, and synaptic development (45, 69, 72, 77, 105, 106).

How can a single kinase mediate such diverse and dichotomous functions in neurons? Wnd is a member of the mixed lineage family of kinases, which has been shown to function as upstream regulators of the stress activated MAPKs, c-Jun NH_2-terminal kinase (JNK) and p38 (107). Towards understanding the mechanism for Wnd's multiple functions, we investigated the role of scaffolding proteins. By coordinating interactions between specific MAPKs and their activators, inactivators or substrates, scaffolding proteins can influence when and where MAPKs become activated, as well as the downstream consequences of their activation (108, 109).

We focused our study on the JNK interacting proteins (JIPs), which have been implicated in a number of JNK regulated processes in neurons (110, 111). The *Drosophila* genome encodes two JIP proteins: JIP1 (APLIP1) and JIP3, also known as Sunday Driver (Syd). In both vertebrate and *Drosophila* cells it has been shown that JIP1 mediates the activation of JNK by Wnd/DLK(110, 112-114). Both JIP1 and JIP3/Syd are carried by kinesin motors in axons (115) and influence the process of axonal transport (116-119). Since functional axonal transport machinery is required for injury signaling (51, 120), we needed to consider the relationship between JIP1 and Wnd's roles in axonal transport and signaling.

Our findings suggest that these processes can be functionally separated. Characterization of *jip1* null mutants has revealed a new role for Wnd in regulating the structure of synaptic microtubules during development of the *Drosophila* neuromuscular junction (NMJ). This developmental role, which requires JIP1 and the downstream p38b MAPK, is distinct from Wnd's roles in axonal transport and injury signaling, which do not require p38. Hence the JIP1 scaffold promotes a specific synaptic function for Wnd and MAPK signaling.

3.3 Results

3.3.1 Comparison of JIP1 and JIP3 in axonal transport and injury signaling

In order to study the role of JIP1/APLIP1 in Wnd signaling, we generated a null allele via imprecise excision of the *P-Aplip1*^{DG20707} transposon. *jip1*^{ex} removes the entire *jip1* coding region leaving the flanking genes, *LysX* and *mwh* intact (Figure 3.1A). Unlike the larval lethality observed for mutations in the JIP3 homologue *Syd* (116), *jip1*^{ex}/*jip1*^{ex} and *jip1*^{ex}/*Df* mutants develop into fully viable adults. Defects in axonal transport, as measured by accumulations of the synaptic vesicle marker DVGLUT in segmental nerves, were also less severe for *jip1*^{ex} mutants as compared to *jip3* mutants (Figure 3.1B,C). The axonal transport defect of *jip1*^{ex} can be rescued by the presence of a transgene containing one copy of genomic *jip1* (Figure 3.1C).

Wnd regulates a transcriptional response to axonal injury, which can be measured by the induction of the *puc*-lacZ reporter (87) in response to a larval segmental nerve crush (51). Injury signaling in *jip1*^{ex} mutant animals is slightly reduced at 8 hours, but

reaches levels similar to wild-type animals within 24 hours after injury (Figure 3.1D). In contrast, injury signaling was dramatically inhibited in the *jip3* mutant animals at both 8 and 24 hours post injury (Figure 3.1D). These results suggest that JIP3/Syd plays an essential role in the injury signaling mechanism, while JIP1 is dispensable. It has been shown previously that general inhibition of axonal transport can diminish the induction of *puc*-lacZ (51), therefore the divergent phenotypes for *jip1* and *jip3* in injury signaling may be an indirect consequence of their different effects upon axonal transport (Figure 3.1B,C). Since axonal transport plays a fundamental role in neurons and its disruption would affect many cellular pathways, this was an important concern in understanding the function of JIP1. We therefore asked whether JIP1 played other roles in neurons that could be functionally or phenotypically separated from its role in axonal transport.

3.3.2 JIP1 promotes the development of presynaptic boutons

The most striking phenotype observed for $jip1^{ex}$ mutants was the enlargement of the synaptic boutons at the larval NMJ (Figure 3.2A,B). The most proximal boutons were particularly enlarged, showing an approximately two-fold increase in diameter compared to wild-type synapses (Figure 3.2B). We also measured a greater than two fold increase in the total number of boutons that exceeded 5 μm per NMJ: wild-type animals averaged 1 bouton per NMJ which reached this size, however *jip1* mutants had an average of 3 boutons per NMJ that were greater than 5 μm (SEM=0.54, p=0.03) (data not shown). In contrast to the enlarged bouton sizes, we observed no differences in the overall number of boutons or branches (Figure 3.6B).

Surprisingly, $jip1^{ek4}$ mutants, which carry a point mutation within the kinesin binding domain (118) and displayed comparable defects in axonal transport as $jip1^{ex}$ (Figure 3.1B,C), did not affect bouton morphology (Figure 3. 2B). This observation suggested that the role of JIP1 in controlling synaptic morphology may be separable from its role in axonal transport. Similarly, neuronal expression of a JIP1 transgene lacking the kinesin binding domain (UAS-*JIP1*ΔKBD) also had no effect upon bouton morphology (Figure 3.2B,C) even though these animals display strong defects in axonal transport (118). In *jip3* mutants, which exhibit the strongest defect in axonal transport, the bouton diameter was actually slightly decreased compared to control synapses (Figure 3.2A, B).

Since the synaptic phenotypes did not correlate with the axonal transport phenotypes, they suggest an independent function for JIP1 in the regulation of synaptic structure.

To verify that the enlarged bouton phenotype was specific for JIP1, we used the UAS/Gal4 system to drive expression of a UAS-*JIP1* transgene using the neuronal *BG380*-Gal4 driver in a $jip1^{ex}$ mutant background. This rescued the enlarged bouton phenotype (Figure 3.2A,C). Expression of the *JIP1* transgene alone in a wild-type background also resulted in a slight but significant increase in the maximum bouton diameter (Figure 3.2C). The similarity between *gain-of-function* and *loss-of-function* phenotypes for *jip1* was previously observed for defects in axonal transport (118), and given JIP1's hypothesized role as a scaffolding protein (112, 121), these results are not unexpected.

In order to determine whether the enlarged boutons in *jip1* mutant animals resulted from either a failure to maintain synaptic structure or whether Jip1 played a role in synaptic development, we examined the synaptic morphology of *jip1* mutant synapses in younger animals. We found that 2nd instar animals, similar to 3rd instar animals, had an average of 2.5 enlarged boutons ($\geq$ 5 μm) per NMJ, however these enlarged boutons were slightly smaller in diameter (Figure 3.2D and data not shown) than in 3rd instar larvae (Figure 3.2B). We interpret that the abnormal boutons form early in NMJ development and become larger with time. These observations implicate a role for JIP1 in regulating the development of synaptic boutons at the NMJ.

3.3.3 JIP1 is required for microtubule organization in synaptic boutons

It is well established that synaptic morphology depends on cytoskeletal organization (122, 123) and that vertebrate JIP1 participates in controlling microtubule dynamics in neurons (124, 125). We therefore wanted to determine whether the increased bouton size reflected changes in the synaptic microtubules. A particularly useful marker for synaptic microtubules is the neuronal specific microtubule binding protein Futsch (homologous to MAP1B), which plays a critical role in microtubule organization at the *Drosophila* NMJ (88, 126). Another indicator of microtubule stability is the presence of post-translational modifications such as acetylated tubulin (62, 127). At the larval NMJ, both Futsch and acetylated tubulin form a tightly bundled cable that

runs through most of the NMJ (128) and Figure 3.3A,B). In *jip1* mutants this cable is disorganized (for Futsch) and broken (for acetylated tubulin), particularly in the largest boutons. Futsch staining becomes splayed and unbundled, while acetylated tubulin accumulated in a punctate, fragmented pattern, suggesting a break-down or misregulation of the microtubule cytoskeleton (Figure 3.3A,B). This disruption of the microtubule cytoskeleton is not observed in either $jip1^{ek4}$ mutants or animals neuronally expressing the JIP1 transgene lacking the kinesin binding domain (UAS-*JIP1*ΔKBD), hence is not simply a consequence of defects in axonal transport (Figure 3.3C). Importantly, both the unbundling of Futsch and the fragmentation of acetylated tubulin are rescued by the presence of a transgene containing one copy of genomic *jip1* (Figure 3.3A-C).

Mutations in *futsch* give rise to enlarged boutons (126) hence the enlarged boutons in *jip1* mutants may be the result of misregulated microtubules. We tested whether the enlarged bouton phenotype in *jip1* mutants could be suppressed by increasing the expression of Futsch. While over-expression of Futsch (using the *BG380*-Gal4 driver) did not significantly alter NMJ morphology in the wild-type background, it led to a full rescue of the enlarged bouton phenotype in *jip1* mutants (Figure 3.4A, B). These observations suggest that the bouton morphology defect in *jip1* mutants reflects a role for JIP1 in the organization of synaptic microtubules.

In contrast to the synaptic phenotype, overexpression of Futsch failed to rescue the axonal transport defect of *jip1* mutants (Figure 3.4C,D). These observations further suggest that JIP1 plays at least two independent roles in motoneurons: one in the regulation of synaptic structure, and another in axonal transport.

3.3.4 The Wnd MAPKKK regulates synaptic morphology

To understand the mechanism for JIP1's synaptic function, we considered the possible role of the Wnd MAPKKK in regulating synaptic morphology. Studies in vertebrate and *Drosophila* cells suggest that JIP1 functions as a scaffolding protein for Wnd/DLK signaling (110, 113, 118, 121), and that Wnd/DLK signaling can influence microtubule structure (129-132). Previous characterization of *wnd* mutants found no obvious defects in synaptic morphology (45), however closer examination of *wnd* mutant genotypes (wnd^1/wnd^2, wnd^1/Df and wnd^3/Df, Figure 3.5A,B) as well as neuronal specific

RNAi knockdown (Figure 3.5D,E), revealed an enlarged bouton phenotype similar to *jip1* mutants. This enlarged bouton phenotype for *wnd*, which is not as strong as the *jip1* phenotype, may not have been noticed in an earlier study (45) due to differences in the measurement method (see Materials and Methods). The larger boutons in *wnd* mutants also displayed Futsch unbundling (Figure 3.5A) similar to *jip1* mutants. These observations suggest that JIP1 and Wnd may function together, and suggest a new role for Wnd in regulating microtubule structure at synapses.

3.3.5 The p38b MAP Kinase regulates synaptic morphology

Previously characterized roles for Wnd, which include the promotion of synaptic overgrowth and injury signaling (45, 51), involve downstream activation of the JNK MAP Kinase and transcription factor Fos. We tested whether Wnd's role in regulating the synaptic cytoskeleton could also signal through these same downstream components. Inhibition of JNK and Fos, either by strong expression of dominant-negative transgenes (JNK^{DN} and Fos^{DN}) or RNAi targeted knockdown, did not result in any changes to bouton morphology (Figure 3.5F), suggesting that other factors may function downstream of Wnd and JIP1 at synapses.

We therefore tested the role of the p38 MAPKs, since it has been previously reported that Wnd/DLK signals through this MAPK in *C. elegans* (46, 133). Also, JIP family members have been shown to scaffold p38 MAPKs as well as JNK MAPKs in vertebrate cells (134-137). In *Drosophila*, the two p38 MAPK genes, *p38a* and *p38b* (138-141) have been extensively studied in relation to stress (142-146) and the fly immune system (147-150). p38 has also been shown to participate in developmental processes including axial polarity during oogenesis, intestinal stem cell proliferation and differentiation, and *dpp* regulated stem cell morphogenesis (139, 140, 151).

Using a null mutation of *p38a* ($p38a^{\Delta}$), which is deleted for the entire *p38a* locus (143), we found no significant role for p38a in the regulation of bouton size (Figure 3. 5B). However further genetic interactions with Wnd (Figure 3. 6) still imply a function for p38a at the synapse (discussed further below). To examine the role of p38b we utilized two different alleles, a null allele that removes most of the coding region ($p38b^{\Delta}$) (146) and a transposon insertion allele ($p38b^{KG01337}$). In contrast to *p38a*, *p38b* mutants

displayed a prominent bouton morphology defect, which resembled both *jip1* and *wnd* mutants in the increase in maximum bouton size (Figure 3.5A,B), as well as the number of boutons exceeding 5μm (Figure 3.5A and data not shown). Double mutants for $p38a^{\Delta}$ and $p38b^{\Delta}$ did not enhance this phenotype. Inhibition of p38b, either by RNAi knockdown (Figure 3.5D,E) or the expression of a dominant negative allele ($p38b^{DN}$), specifically in neurons also resulted in enlarged boutons (Figure 3.5F), indicating a cell autonomous role for p38b in regulating bouton morphology. The loss of *p38b* also resulted in an increase in the overall percentage of unbundled Futsch (Figure 3.5A,G), similar to what was observed in *jip1* mutants (Figure 3.3C). These findings signify a new role for p38b in regulating bouton morphology and microtubule structure at *Drosophila* synapses.

To further probe the hypothesis that Wnd and p38 regulate synaptic boutons through a common pathway, we asked whether *wnd* and *p38b* genetically interact. Figure 3.5C shows that while animals missing one copy of either *wnd* or *p38b* have no phenotype, animals missing one copy of both *wnd* and *p38b* display enlarged boutons (and, not shown, misregulated cytoskeleton) similar to complete *loss-of-function* mutations in *wnd* and *p38b*. Additional genetic interactions are described further below.

3.3.6 JIP1 and p38 mediate synaptic growth and nuclear signaling downstream of Hiw

One of the most striking documented regulators of synaptic growth is Hiw, a conserved E3 ubiquitin ligase (55-57). At the *Drosophila* NMJ, mutations in *hiw* cause a dramatic increase in the number of synaptic boutons and branches at the larval NMJ ((45, 57) and Figure 3.6A,B). This synaptic overgrowth phenotype is caused by an increased activity of Wnd, whose levels in axons and synapses is regulated by Hiw (45). We found that this synaptic *gain-of-function* phenotype for *wnd* could be suppressed by mutations in either *jip1* or *p38b* (Figure 3.6A,B). In addition, *p38a* mutants, which did not have a *loss-of-function* phenotype on their own at the NMJ (Figure 3.5B) suppressed the *hiw* synaptic overgrowth phenotype (Figure 3.6B). These observations revise a previous conclusion based on dominant negative constructs for p38 (45) and imply a role for both p38a and p38b in synaptic growth. This role may function independently of the regulation

of microtubules and bouton size. Alternatively, the function of p38a may be specific to situations when Wnd signaling levels are high. These findings further support the model that JIP1 and the p38 MAP Kinase function together with Wnd to regulate the morphology of the presynaptic axon terminus.

Of note, the genetic interactions revealed reciprocal suppression of phenotypes for *hiw*, *jip1* and *p38*: not only did mutations in either *jip1* or *p38* suppress the *hiw* synaptic overgrowth phenotype (Figure 3.6A,B), mutations in *hiw* also suppressed the enlarged bouton (Figure 3.6A,C) and Futsch unbundling (not shown) phenotypes of *jip1* and *p38* mutants. Similarly, overexpression of Wnd also suppressed the bouton morphology phenotype of *jip1* mutants (Figure 3.6D). This suppression interaction is consistent with the hypothesized role of JIP1 as a scaffold for Wnd signaling: its function in assisting the activation of Wnd can be overcome if Wnd levels are increased. However the suppression of *p38b* by *hiw* suggests that the relationships are more complex than a simple linear pathway. One possibility is that when Wnd levels are high then p38a can substitute for p38b. Overall, these genetic interactions suggest that Wnd, JIP1 and p38 function together to regulate synaptic morphology.

Previous studies of Hiw indicate that the synaptic overgrowth phenotype is mediated by a Wnd-regulated nuclear signaling cascade, which is overactive in *hiw* mutants. This leads to a strong induction of the *puc*-lacZ reporter ((51) and Figure 3.6E), which also becomes induced after axonal injury (51) and Figure 3.1D). In both injured neurons and *hiw* mutants, the induction of *puc*-lacZ is mediated by Wnd (51). While *jip1* is not required for the induction of *puc*-lacZ after injury (Figure 3.1D), we found that it is partially required for the induction of *puc*-lacZ in *hiw* mutants (Figure 3.6E). The differences in requirement for JIP1 suggest that there may be multiple mechanisms for activating Wnd in neurons. Axonal injury activates Wnd signaling through a mechanism that does not require JIP1 (Figure 3.1D). In contrast, in uninjured neurons, Wnd regulates a signaling pathway that controls the structure of synaptic boutons, and this pathway is significantly diminished in the absence of JIP1 (Figure 3.6E).

3.3.7 Wnd regulates synaptic structure and injury responses through independent signaling mechanisms

Our findings support the model that Wnd regulates multiple functions in neurons via independent downstream signaling pathways. To further test this model, we asked whether p38a and p38b, which are required for Wnd's synaptic roles (Figure 3.6), are required for axonal transport, injury signaling and axonal regeneration after injury. In contrast to *wnd*, $p38a^{D}$ and $p38b^{D}$, as well as $p38a^{D}$, $p38b^{D}$ double mutants, displayed only mild defects in axonal transport (Figure 3.7A). Also in contrast to Wnd, neither p38a nor p38b are required for the induction of *puc*-lacZ after injury (Figure 3.7B). Similarly, mutations in *p38a* or *p38b* did not impair the ability of injured axons to form new axonal branches after injury (Figure 3.7C,D). This contrasts to the essential roles for Wnd and JNK in controlling this regenerative sprouting response to injury (51). These findings imply that different downstream functions of Wnd depend upon different and functionally separable downstream mechanisms.

3.4 Discussion

Requirement for the JIP1 scaffold reveals independent pathways downstream of Wnd

Wnd/DLK signaling regulates multiple processes in neurons, including axonal transport, neuronal migration, developmental apoptosis, axonal regeneration, axonal degeneration, and cell death after injury (46, 50-53, 69, 71, 72, 106, 114, 152-154). Our data suggest the existence of a new role for Wnd in regulating the structure of synaptic microtubules. With these different and often dichotomous functions that are attributed to Wnd/DLK signaling in both neuronal development and maintenance, a major question is how this single MAPKKK can impart the specificity required to achieve these diverse outcomes. We find that Wnd's role in synaptic development can be functionally separated from its role in responding to axonal injury. Wnd's regulation of synaptic development requires both the scaffolding protein JIP1 as well as the downstream MAPK p38. In contrast, p38 is not required for Wnd's role in injury signaling and the promotion of new axonal growth after injury. Therefore, in *Drosophila* motoneurons Wnd regulates at least two independent pathways, one that promotes responses to axonal damage, and another which regulates synaptic morphology in uninjured neurons. JIP1 plays an essential role in the second pathway, but not the first (Figure 3.7E).

It is intriguing to note that *jip3/Syd* mutants have a complementary phenotype to *jip1* mutants: JIP3 is required for injury signaling, but not for regulating synaptic microtubules. The model that JIP3 scaffolds the injury signaling pathway is supported by studies of vertebrate JIP3/Syd, which interacts with phosphorylated JNK in axons, and is retrogradely transported in response to axonal injury (155). The JIP1 and JIP3 scaffolds can therefore mediate independent roles for Wnd, through distinct downstream signaling mechanisms.

Wnd/DLK regulates synaptic microtubules via p38

A number of studies of Wnd/DLK homologues in both *C. elegans* and vertebrate neurons suggest that this kinase may regulate the microtubule cytoskeleton via both JNK (129, 131, 156) and p38 (48, 130, 132) signaling, both of which are known to have microtubule-associated substrates, including Tau, MAP1B, MAP2B, and stathmin (157, 158). Moreover, the JIP1 scaffold is known to play an important role in the regulation of microtubules by MAP Kinase signaling (124, 125, 159-162). While the direct downstream effectors of Wnd/DLKs actions upon synaptic microtubules remains to be fully characterized, important functional consequences may include the facilitation of axon formation during the early stages of neuronal polarization (129, 131), regulation of a transcriptional response to depolymerized microtubules (130), and regulation of microtubule dynamics within injured axons (132), which are important for an injured axon to initiate regenerative growth (93, 163-166).

In *C. elegans* p38 appears to play a role in all the known functions of DLK, including both synapse formation (47, 77) and regeneration after injury (46, 52, 133). In contrast, we observed that in *Drosophila,* p38b mediates a synaptic role for Wnd, but p38a and p38b are not required for injury signaling and axonal sprouting after injury. While downstream signaling pathways and the mechanisms of activation may diverge in evolution, we acknowledge that the assay for the requirement of p38 in axonal regeneration is more stringent in *C. elegans* than in our sprouting assay after nerve crush in *Drosophila*, since the sprouting axons in *Drosophila* nerves fail to reach their final target (51). It therefore remains possible that p38 will be required for steps in axonal regeneration that could not be addressed in our current assay. The *puc*-lacZ induction

likely reports a specific aspect of Wnd pathway activation, and this is useful for teasing apart multiple downstream events.

In *C. elegans*, an additional MAPKKK, MLK-1, functions in parallel to DLK to promote axonal regeneration (133). The *Drosophila* homologue of MLK-1, *Slpr* (167, 168), is not required for the induction of *puc*-lacZ after injury (51), however this does not rule out other potential functions for *Slpr* in neurons. Since the synaptic phenotype of *jip1* mutants is more severe than the phenotype of *wnd* mutants, a potential role for additional MAP Kinase regulators such as *Slpr* in the regulation of synaptic microtubules should also be considered.

Separating roles in signaling from roles in axonal transport

The JIP scaffolding proteins interact with both the kinesin-I and dynein motors (115, 118, 137, 155, 169-171) and may play a role in mediating the regulation of these motors by MAP Kinase signaling (114, 172-174). Indeed, *loss-of-function* studies of JIP1/APLIP1 and JIP3/Syd suggest that both play roles in axonal transport (116-119). Since JIPs are physically carried by kinesin and dynein motors, the converse relationship may also be true: motor proteins may regulate the signaling complexes that are scaffolded by JIPs, by delivering the signaling complexes to specific subcellular locations. This appears to be the case for Wnd signaling, since the downstream cascades for both injury signaling and synaptic growth appear to depend upon functional axonal transport machinery. The localization of JIP1 to the axon terminus requires Kinesin-1 (115, 175) and we propose that this localization mediates a specific role for Wnd signaling at the synapse. Conversely, the interaction of JIP3/Syd with dynein is thought to mediate retrograde signaling in response to axonal injury (155).

An essential role for the axonal transport machinery within neurons makes it difficult to delineate the precise function for any individual molecule involved in this process. A mutant that exhibits axonal transport defects may impact multiple signaling pathways, which may rely either directly or indirectly upon the axonal transport machinery. It is therefore remarkable that the *jip1* mutants exhibit such a specific synaptic phenotype given their axonal transport impairment. Of the many other known mutations in *Drosophila* that inhibit axonal transport in motoneurons, including subunits

of kinesin-1, kinesin-3, dynactin and dynein, as well as *jip3/Syd*, none display the enlarged bouton phenotype observed for *jip1* mutants (Figure 3. 2A,B)(176-178). We were further able to dissociate a role for JIP1 signaling in synaptic development from axonal transport, because the enlarged bouton phenotype of *jip1* mutants could be suppressed independently of the axonal transport defect. While we expect that the roles of JIP1 in both axonal transport and synaptic development are intimately linked, however they can nevertheless be genetically separated.

A role for Wnd/DLK in uninjured synapses

Our studies of JIP1 have led to the discovery of a new role for Wnd signaling in regulating synaptic development via JIP1 and p38b. Previous studies in *Drosophila* and *C. elegans* have failed to detect such a function for Wnd/DLK. Instead, the previously described synaptic phenotypes were *gain-of-function*, due to the loss of regulation by the Hiw ubiquitin ligase. Since the discovery of Wnd/DLK's role in axonal regeneration (46, 51-53, 59, 133, 179), it has been hypothesized that its main function in neurons is to detect axonal injury. The current data now suggest otherwise. JIP1 promotes the activation of a signaling cascade that specifically regulates the structure of presynaptic boutons. This further suggests that Wnd becomes activated in *uninjured* neurons by unknown upstream factors. Since Wnd and JIP1 can localize to presynaptic boutons ((45, 115, 180) and data not shown), they may potentially act locally to regulate presynaptic events during synaptic development and/or plasticity. Consistent with a synaptic function for Wnd, recent behavioral studies of *hiw* mutants imply that the regulation of Wnd in mushroom body neurons is important for constraining the formation of long term memories (181). An important future direction will be to identify the mechanisms that mediate and regulate the function of Wnd/JIP1/p38b signaling at synapses.

3.5 Materials and Methods

3.5.1 Generation of *jip1* mutant

The $jip1^{ex}$ allele was created by the imprecise excision of the P element insertion $P\text{-}Aplip1^{DG20707}$, which lies in the 3'UTR of *JIP1*/*Aplip1*. Approximately 260

independent lines were screened by PCR to uncover one deletion that removed the entire *JIP1*/*Aplip1* locus.

3.5.2 Genetics

The following strains were used in this study: Canton S (WT), *puc*-lacZ^{E69} (87), *BG380*-Gal4 (182), *m12*-Gal4 (P(Gal4)^{5053A}) (183), *RRa(eve)*-Gal4 (184), *OK6*-Gal4 (185), *wnd*^{1}, *wnd*^{2}, *wnd*^{3} (45) , *hiw*^{ND8} (57), *hiw*$^{\Delta N}$ (58), UAS-Fos^{DN} (186), UAS-Bsk(Jnk)^{DN} (187), *Δp38a* (143), *p38b*$^{\Delta 45}$, *p38b*$^{\Delta 25}$*;Δp38a* (146) , UAS-p38b^{DN} (139), *syd*^{Z4}, *syd*^{2H} (116), *jip1*^{ek4}, UAS-*JIP1*ΔKBD, genomic *JIP1* (118). *Df(3L)ED229* (*wnd*), *Df(3L)Fpa2* (*jip1*), *Df(2L)b80e3* (*p38b*), UAS-*bsk-RNAi* (TRiP-JF01275), UAS-*p38b-RNAi* (TRiP-JF03341), UAS-*wnd-RNAi* (TRiP-JF02675), *p38b*^{KG01337}, *P-Aplip1*^{DG20707}, and Futsch$^{EP(x)1419}$ were obtained from the Bloomington Stock Center. UAS-*wnd-RNAi* (26910) was acquired from the Vienna RNAi Center (188). UAS-*Dcr2* was a gift from Stefan Thor. GeneSwitch *elav*-Gal4 driver (*GSelav*) was used to control temporal expression of UAS transgenes in neurons (189). In order to activate the *GSelav* driver, flies were reared on standard food that contained 20μg/ml RU-486, a non-lethal dose of the drug. Male larvae were used for all experiments using the *BG380*-Gal4 driver. For other experiments larvae of both sexes were used.

3.5.3 Immunocytochemistry

Larvae were dissected in PBS and fixed in either 4% paraformaldehyde in PBS or Bouin's fixative for 15-30 minutes, depending on the antibodies used. Antibodies were used at the following dilutions in PBS with 0.3% Triton X-100 and 5% normal goat serum: mouse anti-Futsch, 1:100 (22c10; Developmental Studies Hybridoma Bank); rabbit anti-DVGLUT (190), 1:5000; rat anti-elav 1:50 (7E8A10; Developmental Studies Hybridoma Bank); mouse anti-acetylated tubulin (Sigma-Aldrich), 1:100; Cy3-goat anti-HRP (Jackson ImmunoResearch), 1:500, Cy5-goat anti-HRP (Jackson ImmunoResearch) 1:100; A488-rabbit anti-GFP (Invitrogen), 1:1000. For secondary antibodies, Cy3 and A488-conjugated goat anti-rabbit, anti-mouse and anti-rat (Invitrogen) were used at 1:1000.

3.5.4 Imaging and Quantification

Confocal images were collected at room temperature on an Improvision spinning disk confocal system (PerkinElmer). All imaging and quantification were conducted with Volocity software (PerkinElmer). Similar settings were used to collect all compared genotypes and conditions.

To quantify the mean intensity of *puc*-lacZ expression we used the protocol previously described (51).

Futsch bundling was quantified as described previously (191). Briefly, larvae were stained with Futsch and DVGLUT antibodies to label both the cytoskeleton and the synaptic terminal, respectively. Futsch staining that co-localized with DVGLUT was classified as either unbundled (looped, splayed, punctate or missing) or bundled Futsch (tightly wound filamentous Futsch staining). The synaptic area of unbundled and bundled Futsch were measured and the area of unbundled Futsch was divided by the total Futsch area.

The axonal transport severity index was ranked by qualitative assessment of the number and size of axonal accumulations for the synaptic vesicle marker DVGLUT, while blind to genotype. Individual nerves were given a score between 0 and 4 depending on severity, with 4 being the greatest amount of clogs.

The regeneration ratio was quantified as the fraction of injured axons that exhibited sprouting (at least 5 branches) per genotype, while blind to the genotype, as described in (51).

3.5.5 Nerve crush assay

The segmental nerves of third instar larvae were subjected to nerve crush injury as previously described (51).

3.6 Acknowledgements

This work was supported by the National Science Foundation (grant IOS-0842701) and the National Institute of Health (grant NS069844). We thank Pavan Bhat, Ronny Ewanek, Mary Sprader, Jennifer Diep, Travis Washington, Nicolette Ognjanovski, Dhwani Joshi and Dayna Menken for technical assistance, and Aaron DiAntonio for

logistical support in the early stages of this project. We thank Bill Saxton and Subhabrata Sanyal for *Drosophila* lines. Additionally, we thank the Bloomington Stock Center (Indiana University), the Vienna *Drosophila* RNAi Center, and the Developmental Studies Hybridoma Bank (University of Iowa).

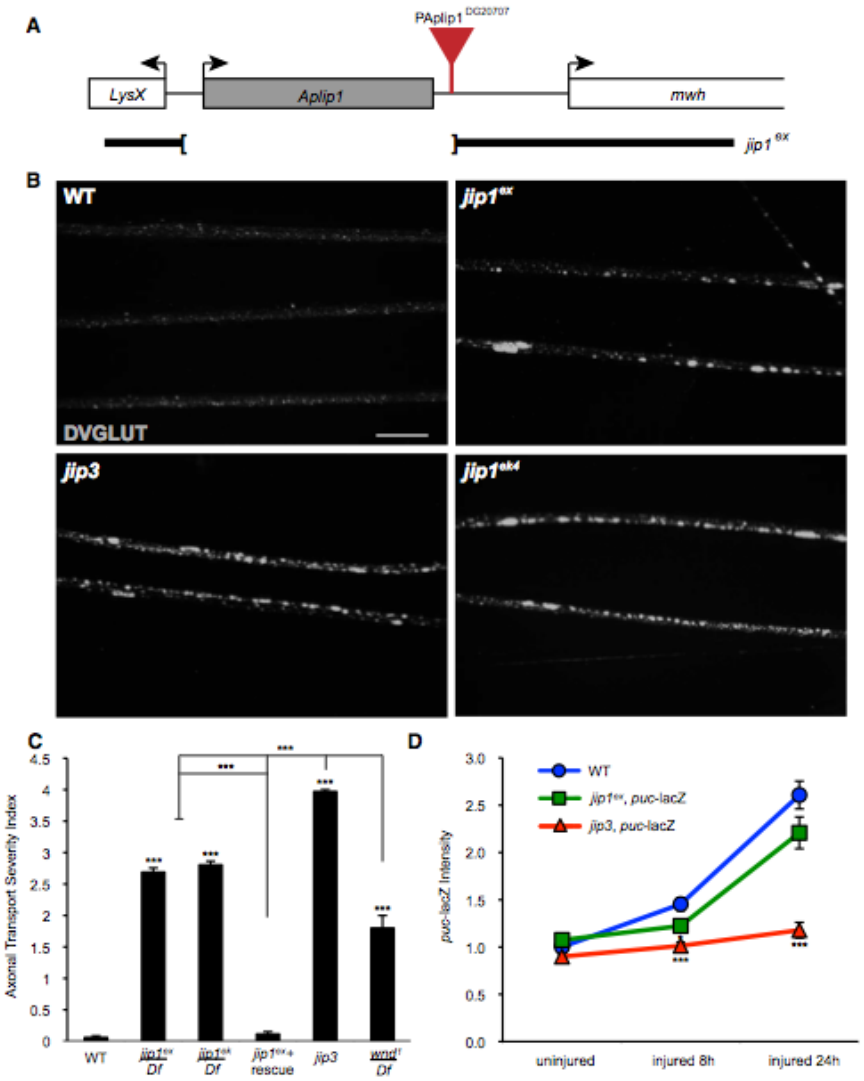

Figure 3.1 Comparison of JIP1 and JIP3 in injury signaling and axonal transport. A) Schematic of the JIP1/APLIP1 genomic region depicting the *jip1*^{ex} excision deletion mutation. The *jip1*/*Aplip1* locus with flanking genes *LysX* and *mwh*. The *jip1*^{ex} null allele was created by imprecise excision of *P-Aplip1*^{DG20707}. B) Segmental nerves from 3rd instar larvae immunostained with DVGLUT. Small punctae of DVGLUT are observed in wild-type (WT) nerves. *jip1*^{ex} null mutation caused an accumulation of DVGLUT in nerves consistent with defective axonal transport. A similar amount of accumulations were observed in the *jip1*^{ek4} hypomorphic allele. JIP3 transheterozygotes (*syd*^{Z4}/*syd*^{2H}) displayed an increase in the number of DVGLUT accumulations compared to *jip1* mutants. C) Quantification of the axonal transport severity index. The severity of the DVGLUT accumulation phenotype was ranked by qualitative assessment of the number and size of axonal accumulations (see Materials and Methods). Note that defects in *jip1* and *jip3* mutants are stronger than the strongest observed phenotype in *wnd* mutants. D) Quantification of *puc*-lacZ. The mean intensity of *puc*-lacZ is measured as described in Materials and Methods for the dorsal midline neurons. At 8 hours after injury, *puc*-lacZ intensity is increased in wild-type animals. *puc*-lacZ intensity for *jip1* (*jip1*^{ex}/*jip1Df*) and

jip3 (*syd*^{Z4}/*syd*^{2H}) mutants is significantly decreased compared to control animals. By 24 hours after injury *jip1*^{ex}, *puc*-lacZ intensity increases to near wild-type levels, however *puc*-lacZ intensity in *jip3* mutants is comparable to uninjured control animals. Error bars indicate mean ± SEM. * p≤0.01, ** p≤0.001, ***p≤0.0001. Scale bars, 10μm.

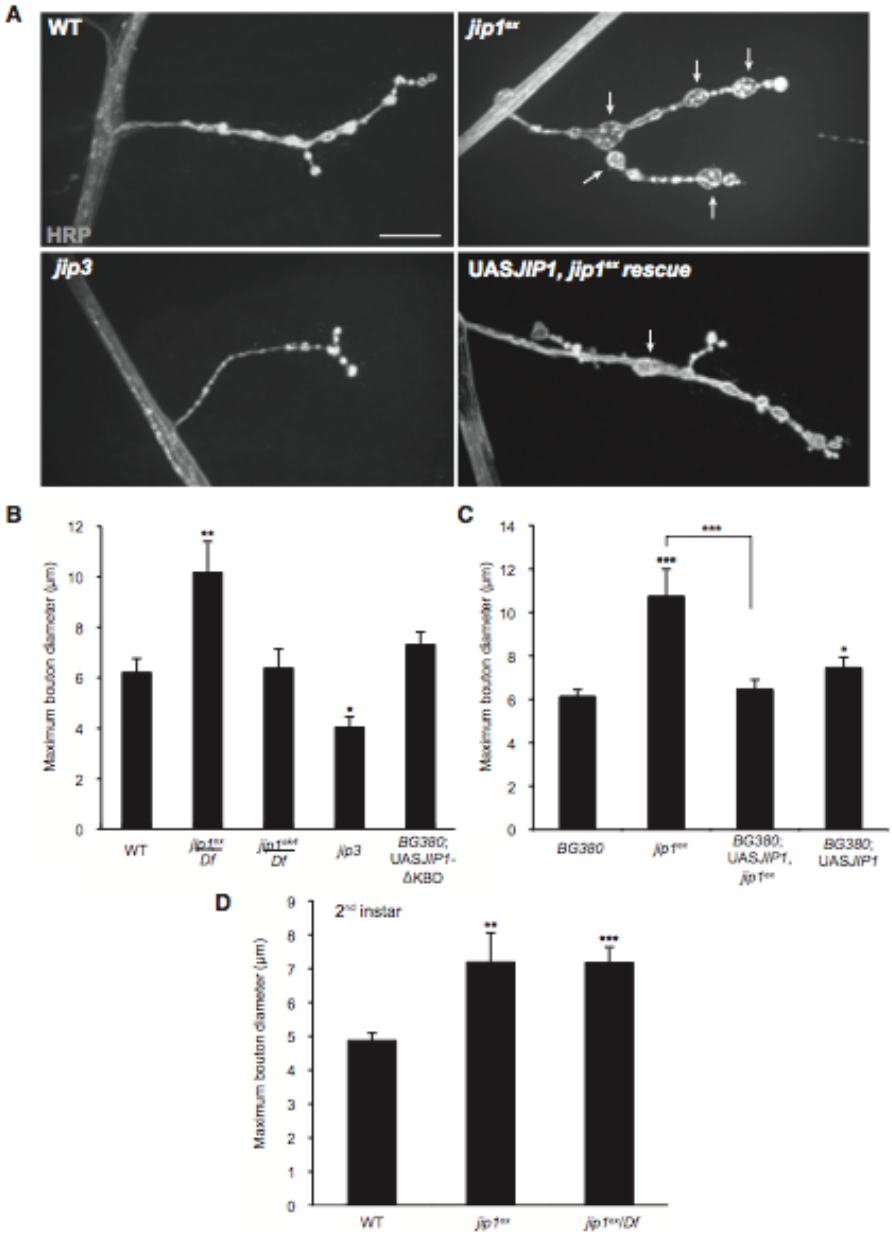

Figure 3.2 *jip1* mutants have a synaptic NMJ phenotype.
A) The axonal membrane at muscle 4 NMJ synapses is labeled by immunostaining with anti-HRP antibodies for wild-type (WT), *jip1* mutants ($jip1^{ex}/jip1^{ex}$), *jip3* mutants (syd^{Z4}/syd^{2H}) and *jip1* rescue animals (*BG380*-Gal4; UAS-*JIP1*/+; $jip1^{ex}/jip1^{ex}$). $jip1^{ex}$ mutants display enlarged boutons and this phenotype can be rescued by neuronal expression of a *JIP1* transgene. Arrows indicate the enlarged boutons ≥ 5µm. B,C) Quantification of maximum bouton diameter. B) $jip1^{ex}$ mutants have larger (and, not shown, a greater number of oversized) boutons compared to control animals. $jip1^{ek4}$ synapses look similar to wild-type animals. *jip3* synapses display smaller boutons compared to controls. Expression of the *jip1ΔKBD* transgene lacking the kinesin binding domain (UAS-*JIP1*ΔKBD) did not result in an enlarged bouton phenotype. C) The enlarged bouton phenotype observed in $jip1^{ex}$ mutants is specific for *jip1*. Neuronal

expression of a *JIP1* transgene results in synapses with slightly larger boutons compared to wild-type animals. D) Quantification of maximum bouton diameter in 2nd instar larvae. Boutons are enlarged in *jip1*^{ex} and *jip1*^{ex}/*Df* mutants even at this earlier developmental stage. Error bars indicate mean ± SEM. * $p \leq 0.01$, ** $p \leq 0.001$, ***$p \leq 0.0001$. Scale bars, 10μm.

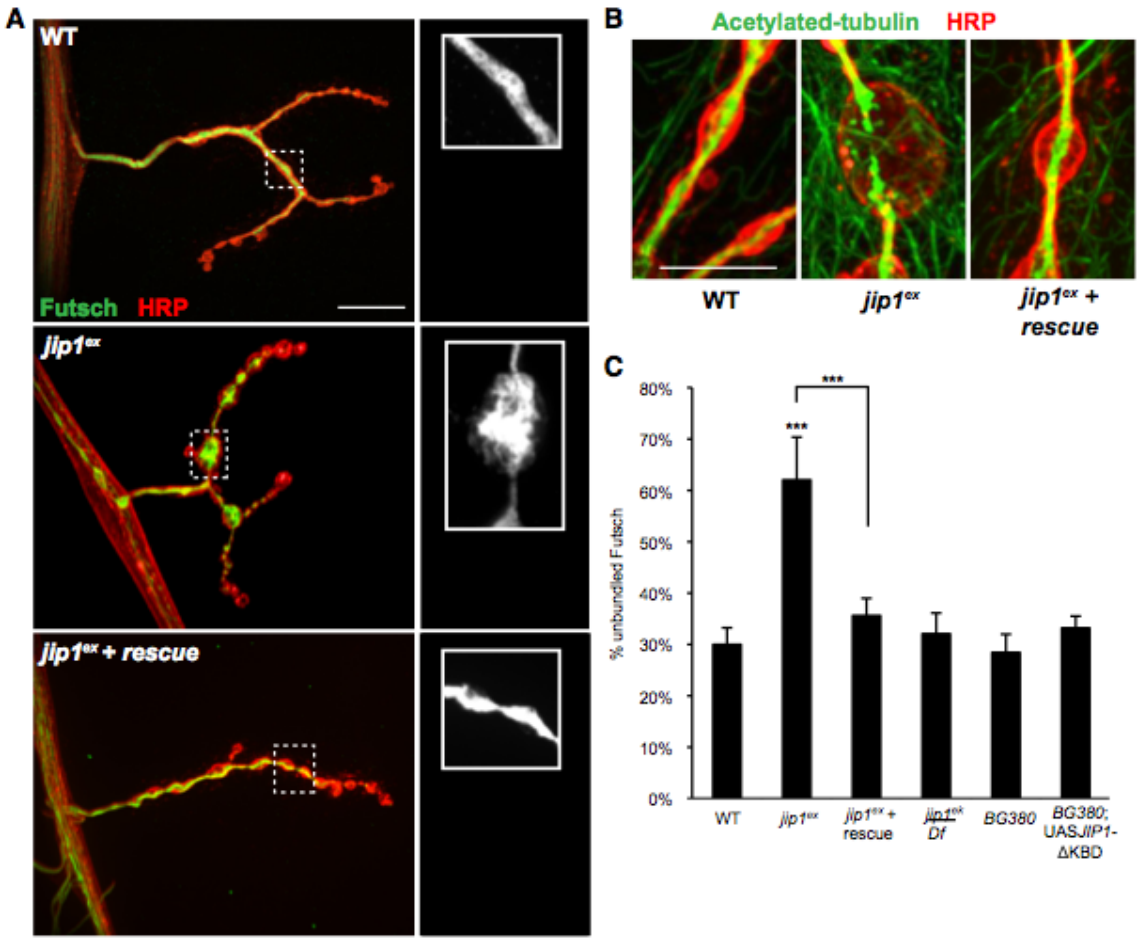

Figure 3.3 JIP1 is required for microtubule organization and stability.
A) Wild-type (WT), *jip1*^{ex}/*jip1*^{ex} and *jip1*^{ex} genomic rescue synapses immunostained with HRP (red) and Futsch (green). Although microtubules normally appear bundled within wild-type boutons, in the enlarged boutons (≥5μm) of *jip1* mutants, splaying of the microtubules is observed. This unbundling of the microtubules can be rescued with the expression of one copy of a genomic *JIP1* transgene. B) Acteylated tubulin (green) is localized in a tightly bundled cable that extends through the NMJ synapse of wild-type animals. Within enlarged boutons of *jip1* mutants, acetylated tubulin has a discontinuous, punctate pattern, which can be rescued with one copy of a genomic *JIP1* transgene. C) Quantification of the percent of unbundled Futsch for different genotypes (see Materials and Methods). C) Error bars indicate mean ± SEM. * p≤0.01, ** p≤0.001, ***p≤0.0001. Scale bars, 10μm.

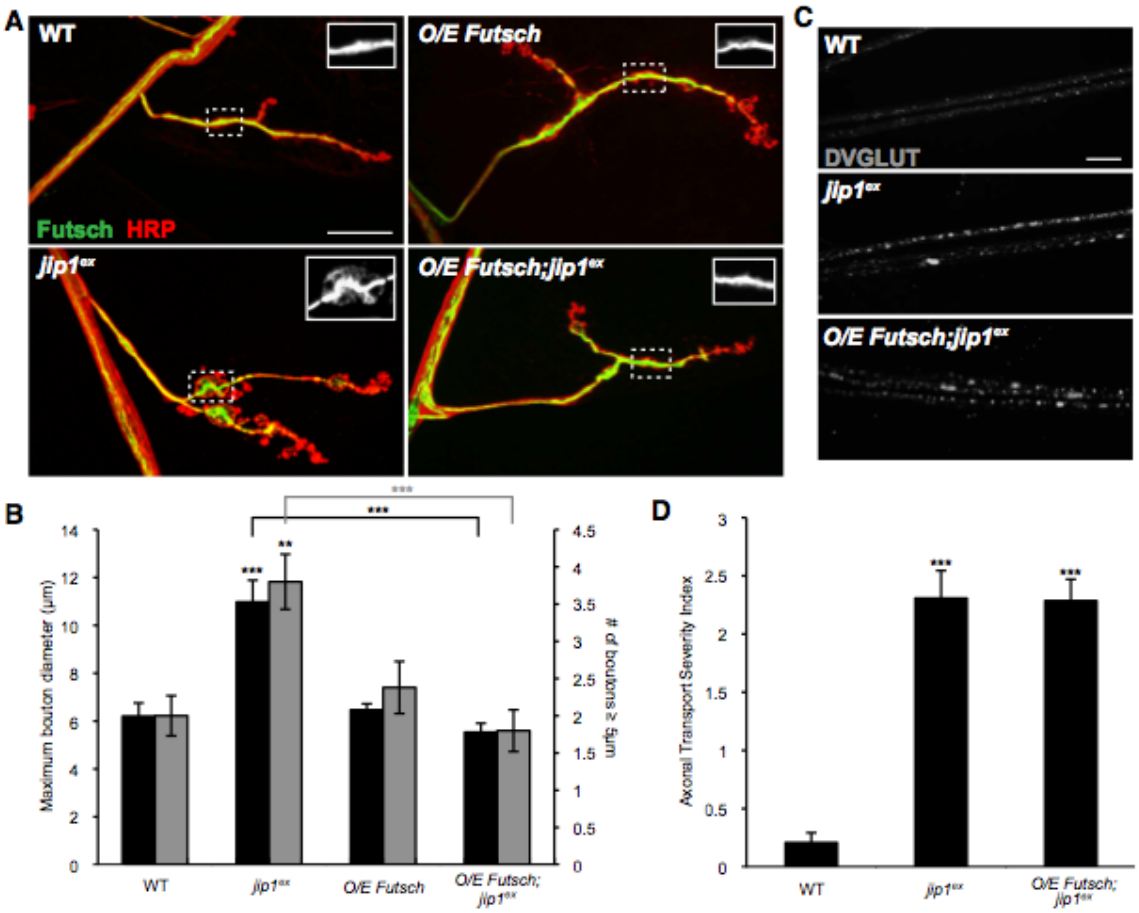

Figure 3.4 Overexpression of Futsch rescues the *jip1* synaptic defect but not the axonal transport defect.

A) Representative muscle 4 NMJs were costained with anti-HRP (red) and anti-Futsch (green) for wild-type (Canton S), *jip1* mutants ($jip1^{ex}/jip1^{ex}$), neuronally expressed Futsch (*BG380*-Gal4, $Futsch^{EP}$/+) and neuronally expressed Futsch in a *jip1* mutant background (*BG380*-Gal4, $Futsch^{EP}$/+; $jip1^{ex}/jip1^{ex}$). B) Quantification of maximum bouton diameter and number of boutons ≥ 5µm. Neuronal expression of Futsch in a *jip1* mutant background can rescue the enlarged bouton phenotype. Neuronal expression of Futsch alone does not alter the synaptic bouton size. C) Peripheral nerves from 3rd instar larvae immunostained with DVGLUT. Overexpression of Futsch in a *jip1* mutant background is unable to rescue the axonal transport defect. D) Quantification of the axonal transport severity index. There is no difference in axonal trafficking defects between *jip1* mutants and *jip1* mutants with Futsch overexpressed in neurons. Error bars indicate mean ± SEM. * p≤0.01, ** p≤0.001, ***p≤0.0001. Scale bars, 10µm.

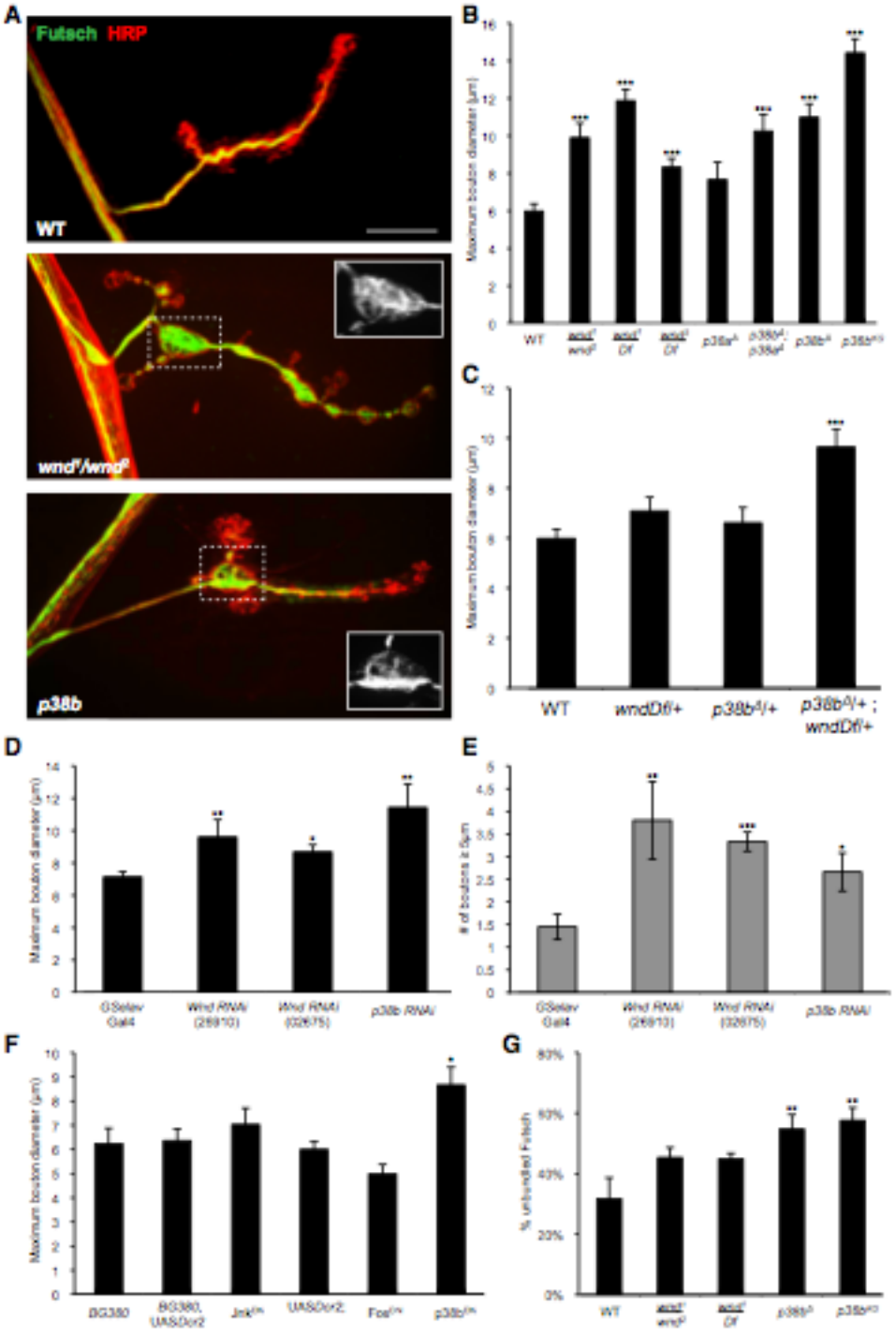

Figure 3.5 Regulation of synaptic morphology and cytoskeleton by the Wnd/DLK MAPKKK and p38b MAPK.

A) Wild-type (Canton S), *wnd* mutant (wnd^1/wnd^2) and *p38b* mutant ($p38b^{\Delta}$) muscle 4 synapses immunostained with HRP (red) and Futsch (green). Both *wnd* and *p38b* mutants display enlarged boutons compared to wild-type animals. In the large boutons, Futsch staining becomes unbundled (see inset). B-F) Quantification of maximum bouton diameter and number of boutons ≥ 5µm. B) Three different allelic combinations for *wnd*

display an increase in maximum bouton diameter and the number of boutons ≥5μm (data not shown). *p38a* null mutants do not have a synaptic morphology defect. *p38b* mutants have an enlarged bouton phenotype that is similar to both *wnd* and *jip1* mutants. *p38a* and *p38b* double mutants display enlarged boutons similar to the *p38b* null mutant alone. C) Trans-heterozygous genetic interaction between *wndDf*/+ and $p38b^{\Delta}$/+. D,E) Pan-neuronal expression of either *wnd* or *p38b* RNAi knockdown constructs resulted in animals with significantly larger boutons compared to control animals (*GSelav*-Gal4/+). F) Neuronal expression of either dominant negative transgenes or RNAi knockdown of JNK or Fos does not result in animals that have larger boutons. Expression of a dominant negative transgene for *p38b* resulted in animals with enlarged boutons. G) Quantification of the percentage of unbundled Futsch. Both *p38b* null and $p38b^{KG}$ insertion animals have a significant increase in the amount of unbundled Futsch. *wnd* mutants display unbundled Futsch in large boutons, however the total amount of unbundled Futsch is unchanged compared to controls. Error bars indicate mean ± SEM. * $p \leq 0.01$, ** $p \leq 0.001$, *** $p \leq 0.0001$. Scale bars, 10μm.

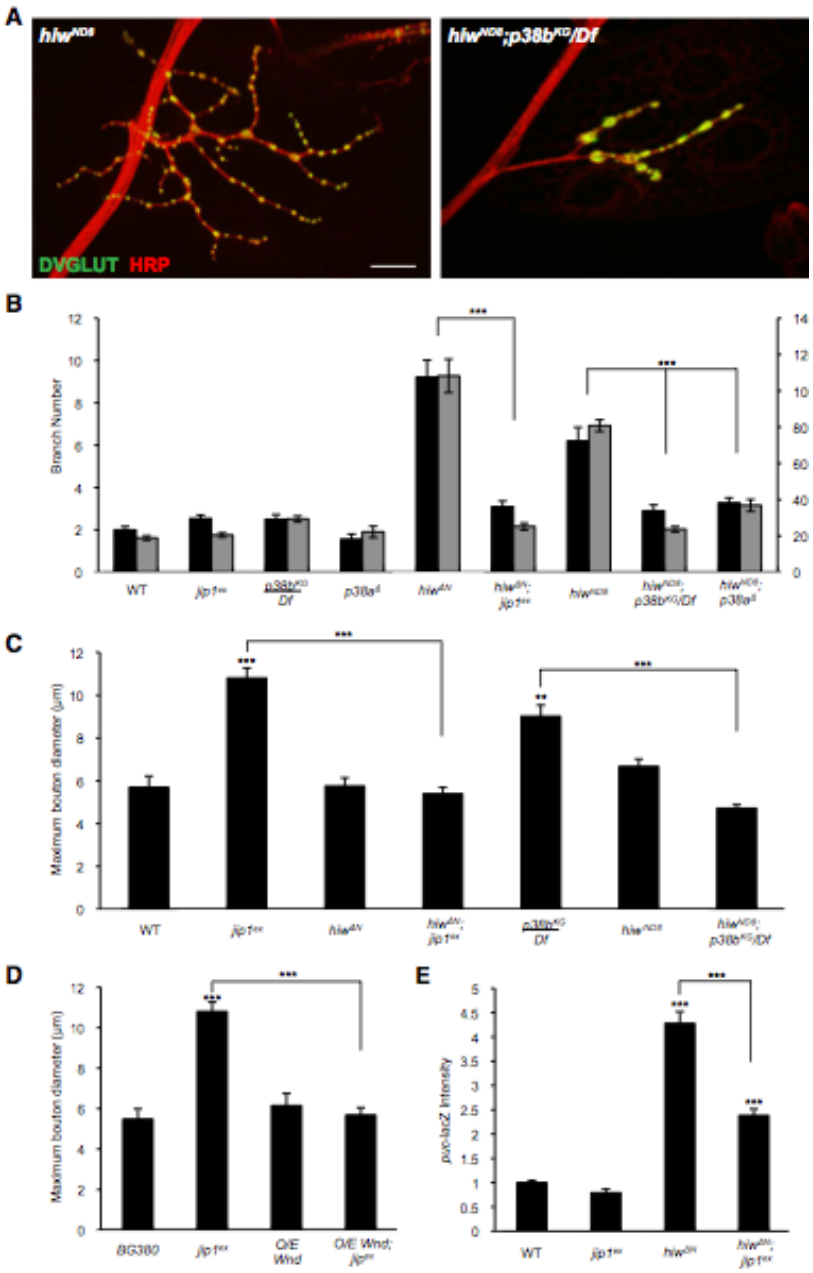

Figure 3.6 Wnd regulates synaptic structure via the p38 MAPK and JIP1 scaffold. A) NMJ synapses at muscle 4 stained with the neuronal membrane marker HRP (red) and synaptic vesicle marker DVGLUT (green) of *hiw* (*hiw*^{ND8}) mutants, and double mutants for *hiw* and *p38b* (*hiw*^{ND8}; *p38b*^{KG}/*Df*). B) Quantification of suppression of the *hiw* synaptic morphology phenotype including branch number (black bars) and bouton number (gray bars). *p38a*, *p38b* and *jip1* can all rescue the synaptic overgrowth phenotype of *hiw* mutants. C,D) Quantification of suppression of maximum bouton diameter. *hiw* and neuronally expressed Wnd (*BG380*-Gal4;UAS-*wnd*/+) can rescue the enlarged bouton phenotype in *jip1* and *p38b* (*p38b*^{KG}/*Df*) mutants. E) Quantification of *puc*-lacZ. *jip1* is required for the induction of *puc*-lacZ in *hiw* mutants. Error bars indicate mean ± SEM. * p≤0.01, ** p≤0.001, ***p≤0.0001. Scale bars, 10µm.

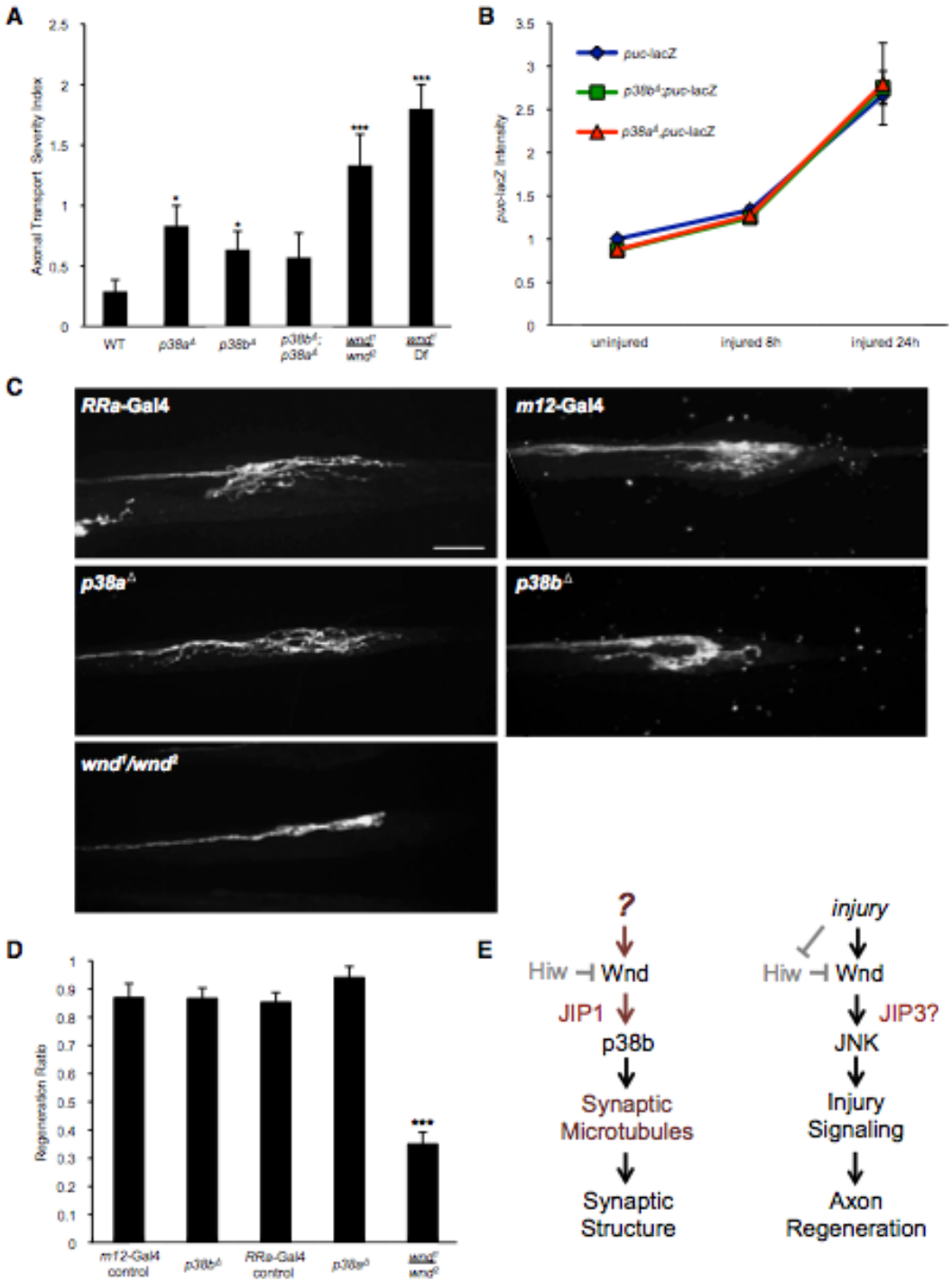

Figure 3.7 Different downstream actions of Wnd require different downstream signaling components.

A) Quantification of axonal transport severity index. *p38a* and *p38b* null mutants display very minor, however statistically significant, defects in axonal transport. B) Quantification of *puc*-lacZ intensity after injury. Both *p38a* and *p38b* mutants show increased levels of *puc*-lacZ intensity similar to controls. C) Axons are labeled by driving expression of UAS-mCD8-RFP with *RRa(eve)*-Gal4 or UAS-mCD8-GFP with *m12*-Gal4. In wild-type animals the proximal stump forms extensive new branches by 15 hours after

injury. Sprouting after injury is inhibited in a *wnd* mutant background (wnd^1/wnd^2). New sprouting forms at the proximal stumps in both *p38b* and *p38a* mutants similar to control axons. D) Quantification of regeneration ratio 15 hours after injury. The fraction of injured axons that displayed sprouting was measured while blinded to the genotype. E) Model: Wnd promotes the development of synaptic structure and injury signaling through separate pathways which differ in their requirement for p38b and the JIP1 scaffolding protein. Error bars indicate mean ± SEM. * $p \leq 0.01$, ** $p \leq 0.001$, *** $p \leq 0.0001$. Scale bars, 10μm.

Chapter 4

Dscam expression levels determine presynaptic arbor sizes in *Drosophila* sensory neurons[3]

In Chapters 2-3, we found that DLK/Wnd oppositely regulates dendritic and axonal growth and is required for presynaptic strucutres. In this Chapter, we identified the cell adhesion molecule Dscam acts downstram of DLK/Wnd for its axonal regulation. Loss of *Dscam* dramatically reduced axon presynaptic length, whereas overexpressing Dscam induced overgrown axon terminals in C4 da neurons. In contrast, the dendritic length was not affected by changes in *Dscam* expression level, suggesting that Dscam functions as an axon-dedicated regulator in C4 da neurons.

4.1 Abstract

Expression of the Down syndrome cell-adhesion molecule (Dscam) is increased in the brains of patients with several neurological disorders. Although Dscam is critically involved in many aspects of neuronal development, little is known about either the mechanism that regulates its expression or the functional consequences of dysregulated Dscam expression. Here, we show that Dscam expression levels serve as an instructive code for the size control of presynaptic arbor. Two convergent pathways, involving dual leucine zipper kinase (DLK) and fragile X mental retardation protein (FMRP), control Dscam expression through protein translation. Defects in this regulation of Dscam translation lead to exuberant presynaptic arbor growth in *Drosophila* somatosensory neurons. Our findings demonstrate a previously unknown aspect of Dscam function and

[3] Modified after the research article originally published in *Neuron.* (2013; 78: 827-838) with authors listed as Jung Hwan Kim*, Xin Wang *, Rosemary Coolon and Bing Ye (* denotes equal contribution).

provide insights into how dysregulated Dscam may contribute to the pathogenesis of neurological disorders.

4.2 Introduction

The Down syndrome cell-adhesion molecule (Dscam) is important for the development of neural circuits in both invertebrates and vertebrates (192-195) (196). In *Drosophila*, *Dscam* undergoes extensive alternative splicing to generate as many as 38,016 different isoforms (197). This diversity is critical for neurite self-recognition (198-200). For example, loss of *Dscam* function results in a dramatic increase in intraneuronal dendritic crossings in the dendritic arborization (da) neurons (40, 201, 202) and a failure in sister branch segregation of the axons of mushroom body neurons (198, 203).

In addition to self-recognition, *Drosophila* Dscam regulates synaptic target selection and axon guidance in several types of neurons (203-207). For instance, in mechanosensory neurons of the adult fly, *Dscam* mutants exhibit profound loss of axon terminal branches as a result of defective branch extension and target selection (204).

Despite the absence of the remarkable molecular diversity seen in insects, vertebrate Dscam is also essential for neurite self-avoidance and synaptic target selection (192, 193, 196, 208), suggesting that the functions of Dscam in neuron morphogenesis and circuit assembly are evolutionarily conserved.

Little is known about how Dscam is regulated, but several observations suggest that its expression must be tightly controlled. Dscam expression is dynamically regulated in developing brains (209, 210). In mouse, Dscam protein levels peak at postnatal day 7 to 10 in the cerebral cortex, coinciding with a period of extensive axonal branching (211), and decreases after postnatal day10 (209). Moreover, Dscam expression is elevated in several brain disorders, including Down Syndrome (DS) (210), intractable epilepsy (212), and bipolar disorder (213). These findings suggest that appropriate regulation of Dscam expression may be important for development, and that inappropriate or dysregulated Dscam expression may lead to developmental abnormalities and disease. However, the mechanisms that regulate Dscam expression and the function of such regulations are thus far unknown.

In the present study, we describe an important role for the regulation of Dscam expression in determining the size of the presynaptic arbor. We found that while isoform diversity of Dscam is critical for presynaptic arbor targeting, Dscam expression level determines the size of the presynaptic arbor. We further define novel regulatory mechanisms that control the size of the presynaptic arbor by regulating the translation of Dscam protein. These findings emphasize the importance of the regulation of Dscam expression during development, and the potential consequences of dysregulated Dscam expression in disease.

4.3 Results

4.3.1 Dscam instructs presynaptic arbor growth

We studied the role of *Dscam* in presynaptic arbor development in *Drosophila* larval class IV dendritic arborization (C4da) neurons (86) (Figure 2.1 A and A'), a system that was used to establish the function of *Dscam* in dendritic self-recognition (40, 201, 202). These axon terminals are presynaptic arbors, as shown by enrichment of the presynaptic marker synaptotagmin::GFP (syt::GFP) (Figure 4.2A).

We investigated the requirement of *Dscam* in presynaptic arbor development by using the Mosaic Analysis with a Repressible Cell Marker (MARCM) (33). Single C4da neurons homozygous for *Dscam* null mutations, $Dscam^{P1}$ (197) or $Dscam^{18}$ (203), exhibited markedly reduced presynaptic arbor growth (Figure 4.1). These dramatic defects in presynaptic arbor growth were completely restored by the introduction of a transgene harboring *Dscam* genomic DNA (Figure 4.1, *Rescue*), confirming that loss of *Dscam* function led to the observed defects.

Conversely, we found that gain of *Dscam* function promoted presynaptic terminal growth. Alternative splicing of *Dscam* mRNA generates two transmembrane domain (TM) isoforms that differ in their subcellular distribution (214). The TM1 isoform is preferentially localized in dendrites, while the TM2 isoform is preferentially localized in the axon (214). Overexpression of a *Dscam* transgene containing TM2 caused abnormally long presynaptic arbors, resulting in a 2.7-fold increase in presynaptic terminal length (Figure 4.1, OE Dscam[TM2]::GFP and Figure 4.2A). In contrast, overexpression of a *Dscam* transgene containing TM1 caused only a 24% increase in presynaptic growth

(Figure 4.1, OE Dscam[TM1]::GFP). These results demonstrate that Dscam plays an instructive role in the presynaptic arbor growth of C4da neurons.

4.3.2 The role of dscam in presynaptic arbor growth is independent of the ectodomain diversity of Dscam

In *Drosophila*, *Dscam* mRNA undergoes extensive alternative splicing in ectodomain-encoding exons 4, 6, and 9, resulting 19,008 potential isoforms of the ectodomain (197). This ectodomain diversity is essential for Dscam's known functions in neurite self-avoidance (198-200) and axon targeting (204, 215). We wondered whether the reduced presynaptic arbor size in *Dscam* null mutant neurons is secondary to self-avoidance or targeting defects caused by loss of ectodomain diversity.

To address this, we first used a *Dscam* allele with a 75% reduction in isoform diversity (214) to assess the effect of reduced diversity on presynaptic arbor development. Reducing *Dscam* diversity by 75% did not affect the development of presynaptic terminals in C4da neurons (Figure 4.3). Furthermore, we employed the intragenic MARCM technique to examine presynaptic arbor development of neurons expressing a single ectodomain isoform from the endogenous locus (198). Importantly, Dscam expression levels in these mutants are comparable to those of wild-type (198). C4da neurons expressing the single Dscam isoform containing exons 4.10, 6.27, and 9.25 (referred to as $Dscam^{10.27.25}$) exhibited defective targeting of the synaptic terminals (Figure 4.4 A and B). 47% of the $Dscam^{10.27.25}$ ddaC neurons completely lost their anterior branches and 29.4% lost their contralateral branches, while 100% of wild-type control clones (referred as $Dscam^{FRT}$) had both branches (Figure 2A and 2B). Similar targeting defects were observed in C4da neurons homozygous of a second allele, $Dscam^{3.31.8}$ (Figure 4.4B). Strikingly, the presynaptic arbor sizes of $Dscam^{10.27.25}$ and $Dscam^{3.31.8}$ neurons were indistinguishable from those of wild-type neurons (Figure 4.4C). These results strongly suggest that the ectodomain diversity is dispensable for Dscam-mediated control of presynaptic arbor size and that the reduced growth seen in *Dscam* mutant presynaptic arbors is not due to defective synaptic targeting.

Consistently, overexpression of two independent Dscam[TM2] transgenes containing different and randomly chosen ectodomains: $Dscam^{11.31.25}$ (216)and

Dscam$^{3.36.25}$ (214), were both sufficient to induce exuberant presynaptic overgrowth (Figure 4.4D).

Collectively, these results demonstrate two separable functions of *Dscam* in the development of presynaptic terminals: an ectodomain diversity-dependent role in directing presynaptic terminal targeting, and an ectodomain diversity-independent role in controlling presynaptic arbor size.

4.3.3 The DLK signaling pathway controls presynaptic arbor growth by regulating Dscam expression

The instructive role of Dscam in presynaptic arbor growth led us to hypothesize that expression level of Dscam determines the size of the presynaptic arbor. To test this hypothesis, we sought to identify the molecular mechanisms that regulate Dscam expression. We screened a number of signaling pathways known to regulate synaptic and axonal growth and found that loss of *highwire* (*hiw*) caused dramatic presynaptic overgrowth in C4da neurons (see Chapter 2, Figure 2.2D), which resembled the phenotype of Dscam[TM2]-overexpressing neurons (Figures 4.1 and 4.2).

Hiw encodes the *Drosophila* homolog of the evolutionarily conserved E3 ubiquitin ligase PAM/Hiw/RPM-1 (PHR) (48, 55, 56, 217). The PHR proteins downregulate the dual leucine zipper kinase (DLK) to restrict synaptic growth (45, 47, 48). Consistently, we found that this signaling module, consisting of Hiw and the *Drosophila* DLK, Wallenda (Wnd), operates in C4da neurons to regulate presynaptic arbor size (see Chapter 2).

To determine whether the *Drosophila* DLK pathway and Dscam genetically interact to control presynaptic arbor growth, we did epistasis analysis by generating *Dscam* null mutant (*Dscam*^{18}) MARCM clones in either a *hiw* mutant (*hiw*$^{\Delta N}$) background or in C4da neurons overexpressing Wnd (OE Wnd). Both *hiw* mutant and Wnd-overexpressing C4da neurons exhibited dramatically overgrown presynaptic arbors (Figure 4.5A). Notably, such overgrowth was completely abolished in both conditions in *Dscam* mutant clones. The presynaptic arbors of *hiw* and *Dscam* (*hiw*$^{\Delta N}$;*Dscam*^{18}) double-mutant clones, and *Dscam* clones with Wnd-overexpression (*Dscam*^{18} + OE Wnd) were morphologically indistinguishable from those of *Dscam* MARCM clones (Figure 4.5A),

suggesting that *Dscam* is essential for presynaptic arbor regulation by the Hiw-Wnd pathway.

This epistasis also raised the possibility that the Hiw-Wnd pathway regulates Dscam expression to control presynaptic arbor size. We examined Dscam protein levels in the brains of *hiw* mutant larvae by Western analysis. Compared to wild-type, Dscam protein levels were increased by 2.5-fold in *hiw* mutant brains (Figure 4.5B). Consistently, overexpressing Wnd in a subset of neurons significantly increased Dscam expression in larval brains (Figure 4.5C). Taken together, these results suggest that the *Drosophila* DLK pathway controls presynaptic arbor growth by regulating Dscam expression. They also underscore the importance of regulating Dscam expression for proper presynaptic arbor size.

4.3.4 The DLK pathway regulates Dscam expression through the 3'UTR of *Dscam*

We next asked how the DLK pathway regulates Dscam expression. The DLK pathway has been shown to regulate axon growth and regeneration through transcription or mRNA stability (45, 50, 52). We therefore tested whether the Hiw-Wnd pathway regulates *Dscam* mRNA levels with quantitative real-time PCR on wild-type and *hiw* larval brains. Using two independent primer sets against the invariant exon 24 of *Dscam* mRNA, we did not detect any significant difference in *Dscam* transcript amounts (Figure 4.5D). As a positive control, *hiw* mutations caused an increase in the transcripts of *Puckered*, which is known to be up-regulated by loss of *hiw* in motoneurons (51). Moreover, the Hiw-Wnd pathway does not regulate *Dscam* promoter activity, because the expression of a Dscam[TM2]::GFP transgene, under the control of the *Dscam* promoter, was not significantly different between wild-type and *hiw* mutant brains (Figure 4.6).

These results suggest that Hiw-Wnd pathway regulates Dscam expression through a previously unknown mechanism, possibly at the level of protein translation. The untranslated regions (UTRs) of mRNAs are key components of protein translational control (218). In order to determine the requirement of the UTRs in Dscam expressional control, we generated *Dscam* transgenes fused to GFP with or without *Dscam* 5' and/or 3' UTRs (Figure 4.7). The expression of a *Dscam* transgene lacking both UTRs (Dscam::GFP) was not affected by *hiw* mutations (Figure 4.7A). Similarly, expression of

a transgene with only the 5' UTR(5'-Dscam::GFP) was also unaffected by *hiw* function (Figure 4.7B). In contrast, the expression levels of a transgene with both the 5' and 3' UTRs (5'-Dscam::GFP-3') and those of the transgene with only the 3'UTR (Dscam::GFP-3') were significantly elevated in *hiw* mutant neurons (Figure 4.7 C and D). Consistently, overexpressing Wnd enhanced the expression of the *Dscam* transgene with only 3'UTR in C4da neurons (Figure 4.7E) as well as *Drosophila* Schneider 2 (S2) cells in culture (Figure 4.7F). These results denote that Hiw-Wnd pathway controls Dscam expression through the 3'UTR of *Dscam* mRNA.

Next, we tested whether the *Dscam* 3'UTR is sufficient for translational control by the Hiw-Wnd pathway. We generated reporter transgenes by fusing EGFP cDNA with either the 3'UTR of *Dscam* mRNA or that of SV40 as a control (Figure 4.8A and B). *Hiw* mutations specifically enhanced the expression of the *Dscam* 3'UTR reporter in C4da neurons (Figure 4.8 A and B). Consistently, expression of Wnd in cultured S2 cells markedly increased expression of the *Dscam* 3'UTR reporter (Figure 4.8 C). We further found that the first 202 nucleotides of *Dscam* 3'UTR are sufficient for the Wnd-regulation (Figure 4.8 D). Taken together, these results suggest that the *Dscam* 3'UTR is necessary and sufficient for translational regulation by the *Drosophila* DLK pathway.

4.3.5 FMRP suppresses Dscam expression to restrict presynaptic arbor growth

The RNA-binding protein fragile X mental retardation protein (*FMRP*) is involved in the post-transcriptional regulation of a number of target mRNAs (219). FMRP has been reported to bind to *Dscam* mRNA in mammalian neurons (220, 221), but the functional relevance of this binding is unknown. We wondered whether FMRP might also regulate Dscam protein translation. We tested the association between *Drosophila* FMRP (dFMRP) and *Dscam* mRNA in larval brain lysates by RNA-immunoprecipitation. Compared to a control antibody, anti-dFMRP antibody pulled down more *Dscam* mRNA as assessed by real-time PCR (Figure 4.9A). The difference in cycle number (DCt) between dFMRP- and control immunoprecipitates translates into a 5.8-fold more association of *Dscam* mRNA to dFMRP immunoprecipitates, suggesting that dFMRP binds to *Dscam* mRNA in *Drosophila*. We then examined whether FMRP regulates Dscam expression. Western blot analysis of larval brain lysates showed that

dFMRP null mutations led to a 49% increase in Dscam protein levels (Figure 4.9B), which is consistent with the role of FMRP as a translational repressor (222). Furthermore, in keeping with a previous study of the *Drosophila* neuromuscular junction (NMJ) (223), *dFMRP* mutations in C4da neurons caused mild but significant overgrowth of presynaptic terminals that was completely abolished by *Dscam* null mutations (Figure 4.9 C and D).

Taken together, these results suggest that dFMRP regulates Dscam expression to restrain presynaptic arbor growth.

4.3.6 FMRP suppresses Dscam expression through the coding region

While Wnd expression greatly enhanced the expression levels of the EGFP reporter containing *Dscam* 3'UTR in S2 cells (Figure 4.8 C), dFMRP overexpression did not change the expression levels of the same reporter (Figure 4.10), suggesting that the regulation by dFMRP is independent of Hiw-Wnd pathway.

Recent studies have uncovered that FMRP acts on the coding regions of some mRNAs to control translation (221, 224). We thus tested the involvement of *Dscam* coding region in the regulation by FMRP. Overexpressing dFMRP in S2 cells strongly inhibited the expression of both *Dscam* transgenes either with or without UTRs (Figure 4.9D), suggesting that dFMRP suppresses Dscam translation via *Dscam* coding region. Similarly, dFMRP overexpression in C4da neurons reduced the expression of a Dscam[TM2]::GFP transgene that does not contain *Dscam* UTRs (Figure 4.9E).

Consistent with the change in expression, dFMRP overexpression reduced presynaptic arbor overgrowth caused by Dscam[TM2]::GFP overexpression (Figure 4.10B). Moreover, *dFMRP* mutations increased presynaptic arbor sizes in C4da neurons overexpressing Dscam (with both 5' and 3'UTRs) (43.0 ± 15.3 % increase) proportionally to those without Dscam overexpression (38.2 ± 7.1 % increase) (Figure 4.10 C-E). Consistent with the notion that dFMRP suppresses Dscam translation by acting on the coding region, *dFMRP* null mutations led to similar percentage of increase in presynaptic arbors between neurons expressing Dscam transgene with *Dscam* UTRs, and those without *Dscam* UTRs (Figure 4.10 C-E). Taken together, these results demonstrate that FMRP regulates Dscam expression through the coding region.

4.3.7 The DLK Pathway and FMRP converge on translational control of Dscam to regulate presynaptic arbor growth

Although both the DLK pathway and FMRP regulate Dscam translation, they exert their influences on different parts of *Dscam* mRNA. The *Dscam* 3'UTR was sufficient to mediate regulation by Wnd (Figure 4.8 C), but not by dFMRP (Figure 4.10A). Moreover, the *Dscam* coding region does not respond to the regulation by the Hiw-Wnd pathway (Figure 4.7 A), but it mediates the suppression by dFMRP (Figure 4.9 D-E). Thus, these two regulatory mechanisms appear to operate in parallel (Figure 4.12B). If these two pathways converge on Dscam expression to direct presynaptic arbor growth, the suppression of Dscam function by dFMRP would counteract the enhanced Dscam function in *hiw* mutants. Indeed, overexpressing dFMRP significantly suppressed the presynaptic arbor overgrowth caused by either *hiw* mutations (Figure 4.11) or Wnd overexpression (Figure 4.11).

Having established the importance of Dscam expression regulation for presynaptic arbor growth, we sought to determine the degree of correlation between presynaptic arbor sizes and Dscam protein levels. We plotted relative Dscam expression levels, as assayed by Western analysis (Figures 4.5 B, and 4.9 B), against relative presynaptic arbor sizes of single C4da neurons (Figures 4.1B, 4.5A, and 4.9C) in different genetic backgrounds. The statistical analysis showed a striking linear correlation, with a coefficient of determination (R^2) of 0.997 between Dscam levels and presynaptic arbor sizes (Figure 4.12A). This not only suggests that Dscam expression levels are tightly controlled for precise presynaptic arbor growth, but also emphasizes the function of Dscam expression levels in determining presynaptic arbor sizes.

4.4 Discussion

In this study, we found that in addition to the ectodomain diversity, the expression level of Dscam serves as a code for neuronal development. We identified two regulatory mechanisms, one involving the kinase DLK and another involving the RNA-binding protein FMRP, which control Dscam expression at the level of protein translation. Defects in either of these regulatory pathways lead to aberrant growth of presynaptic

arbors. The importance of this regulation is underscored by the strong correlation between the expression levels of Dscam and the sizes of presynaptic arbors.

An instructive role of Dscam in presynaptic arbor growth

After reaching their target regions, axons branch and extend to form presynaptic arbors. A presynaptic arbor of a given neuron type typically develops a specific pattern and size, which is critical for establishing appropriate number of synaptic connections with specific targets. How the patterning mechanism relates to the ultimate size that each presynaptic arbor assumes is unknown. Here, we propose that both the patterning and size control of presynaptic terminals can be instructed by a common regulator, such as Dscam. The isoform diversity of Dscam determines the pattern of presynaptic terminals, whereas the expression levels of Dscam instruct the sizes of these terminals (Figure 4.12B).

Is the function of Dscam in presynaptic arbor size control a consequence of its dendritic functions? Several lines of evidence argue against this possibility. First, while expressing the axon-enriched TM2 isoforms caused dramatic increase of presynaptic arbor growth, expressing the dendrite-enriched TM1 isoforms led to only a minimal increase in presynaptic arbor growth (Figure 4.1), suggesting that axonal Dscam regulates presynaptic growth. Second, overexpressing TM2 isoforms did not elicit any significant change in dendrite growth but caused dramatic increase in presynaptic arbor growth (Figure 4.2 B and C), demonstrating that the axonal function of Dscam is separable from its dendritic functions. Third, whereas Dscam ectodomain diversity is required for dendritic self-avoidance, it is dispensable for presynaptic arbor growth (Figure 4.4). Therefore, the instructive role of Dscam levels in presynaptic arbor growth is independent of the dendritic functions of Dscam.

How might Dscam instruct presynaptic arbor growth? Dscam is a type I transmembrane protein with a cytoplasmic domain that is heavily tyrosine-phosphorylated (197). The cytoplasmic domain of Dscam interacts with the signaling molecule Pak1 (195, 225), which is important for the guidance of embryonic Bolwig's nerve (197). However, we observed no defect in C4da presynaptic arbor growth in either loss-of-function or gain-of-function of *Pak1* (data not shown), indicating that Dscam does not act through Pak1 to instruct presynaptic arbor growth in C4da neurons. It remains to

be determined how expression levels of Dscam instruct intracellular signaling and organelles to control the sizes of presynaptic arbors.

A novel regulatory mechanism by the DLK signaling pathway

Given the strong correlation between Dscam expression level and presynaptic arbor size (Figure 4.12A), Dscam expression seems to be tightly controlled to ensure proper neural connectivity. Here we provide evidence for the translational control of Dscam by the DLK pathway. In *Drosophila* and *C. elegans*, respectively, Hiw orthologs regulate the turnover of Wnd and DLK1 (45, 47). Studies in *C. elegans*, *Drosophila* and mammals have demonstrated that DLK regulates axon growth and regeneration through either transcription programs or mRNA stabilization (45, 47, 50). However, our findings indicate that the regulation of Dscam expression by the DLK pathway does not occur through transcription or mRNA stability (Figure 4.5D). We thus propose that DLK has the novel function of enhancing protein translation through the 3'UTR of target mRNAs. How might Wnd enhance Dscam translation? Wnd, as a kinase, is likely to require downstream effecter(s) to regulate mRNA translation. It has been reported that *Dscam* mRNAs are translated in the dendrites of hippocampal neurons in culture, possibly through CPEB1 (226). In the future, it will be interesting to test if Wnd acts on CPEB1 to regulate Dscam translation.

Relevance to neurological disorders

Our findings on the function of Dscam in presynaptic arbor growth are relevant to neurological disorders not only because Dscam expression is elevated in several of these disorders, but also because growth of presynaptic arbors is involved in epilepsy and axon regeneration (63, 227-229). Dscam protein level is elevated in intractable epilepsy (212), which involves aberrant mossy fiber sprouting (229). Of note, increased occurrence of epileptic seizures is often associated with DS as well as fragile X syndrome (FXS) (230, 231), which is caused by loss of FMRP function (232). Our study suggests that elevated Dscam levels may contribute to the pathogenesis of these disorders by causing excessive presynaptic arbor growth. It also establishes a functional link between Dscam and FMRP,

raising the intriguing possibility that Dscam might be a mechanistic link between DS and FXS, the two most prevalent genetic causes of mental retardation.

Recent studies have shown that axon injury activates the DLK pathway, which is essential for subsequent axon regeneration (46, 50-52, 59). In light of the present study, it will be interesting to determine whether the DLK pathway requires Dscam to instruct axon regeneration.

In summary, this study demonstrates that Dscam expression levels, regulated by the DLK pathway and FMRP, determine presynaptic arbor size. It further shows the functional significance of dysregulated Dscam expression in neuronal development and provides a model for studying the pathogenesis of neurological disorders with dysregulated Dscam expression.

4.5 Experimental procedures

4.5.1 Fly strains

hiw$^{\Delta N}$,*UAS-Hiw::GFP (58)*; *wnd*^{1}, *wnd*^{3}, and *UAS-Wnd (45)*; *Dscam*^{P1} (197); *Dscam*^{18} (203); *UAS-Dscam[TM2]::GFP (3.36.25)*, *UAS-Dscam[TM1]::GFP (3.36.25)*, and *DscamP-Dscam[TM2]::GFP (3.36.25)* (214); *UAS-Dscam[TM2] (11.31.25)* (216); *Dscam*$^{10.27.25}$, *Dscam*$^{3.31.8}$ and *Dscam*^{FRT} (198); *dFMRP*^{50M} , *UAS-dFMRP* (223);(102); *ppk-CD4::tdTomato* (75); and *UAS-Syt::eGFP* (233).

4.5.2 DNA constructs for generating transgenic flies and S2 cell transfection

cDNA constructs of EGFP expression reporters and *dFMRP* were subcloned into the pUAST vector. *Dscam* cDNA containing variable exons 4.3-6.36-9.25-17.2 (214) were used to generate Dscam[TM2]::GFP constructs with or without the 5' and/or 3'UTR of *Dscam* mRNA in the pUASTattB vector. Using standard methods (234), UAS-Dscam[TM2]::GFP (3.36.25) transgenic lines were generated using PhiC31 integrase-mediated site-specific insertion at the attP40 landing site. As such, there is no position-effect on the transcription of these transgenes. The UAS-EGFP construct containing the *Dscam* 3'UTR was used to generate serial deletion constructs of the *Dscam* 3'UTR for mapping the required sequence for Wnd regulation. The genomic *Dscam* transgene used for rescue experiments and the *wnd* cDNA construct were, respectively, generous gifts

from Dr. Tzumin Lee (Howard Hughes Medical Institute) and Dr. Catherine Collins (University of Michigan).

4.5.3 Labeling of the presynaptic arbors with genetic mosaic techniques

The single C4da presynaptic arbors in Figure 1A were labeled by the flip-out technique with CD2 flanked by two FRT sequences sandwiched between UAS and mCD8::GFP. Excision of CD2 was achieved by heat-shock-induced flippase expression. The resulting C4da clones expressed mCD8::GFP; the rest of the C4da neurons expressed CD2. A modified flip-out technique with an excisable GAL80 (235) was used to express the membrane marker mCD8::mRFP and the presynaptic marker synaptotagmin::GFP under the control of *ppk* promoter in Figure S1A.

The MARCM technique (33) was used to generate and label homozygous $Dscam^{18}$, $Dscam^{P1}$, and $dFMRP^{50m}$ C4da neurons, and to overexpress Dscam[TM2]::GFP and Wnd. MARCM clones were induced as previously described (36). The same MARCM technique was also used to label presynaptic arbors of single ddaC neurons in $hiw^{\Delta N}$ hemizygous third-instar larvae.

To generate single C4da neurons expressing a single isoform of the ectodomain ($Dscam^{10.27.25}$, $Dscam^{3.31.8}$), we applied the intragenic MARCM technique (198), A wild-type *Dscam* allele containing an *FRT* at the same genomic location as $Dscam^{Single}$ was used as control ($Dscam^{FRT}$).

4.5.4 Immunostaining and imaging

Third instar larvae were immunostained as described (36). The primary antibodies used were mouse anti-GFP (Invitrogen) and rabbit anti-RFP (Rockland). Confocal imaging was done with a Leica SP5 confocal system equipped with 63x immersion oil lenses. To minimize the variation in presynaptic arbor sizes among C4da neurons in different body segments, only neurons in abdominal segments 4, 5, and 6 were imaged. Images were collected with z-stacks of 0.3-mm step size. The resulting 3D images were projected into 2D images using a maximum projection method. To ensure that fluorescence intensities reflected protein levels, image acquisition was adjusted to minimum signal saturation. The same imaging setting was applied throughout the

imaging process. After image transformation into 2D images, the mean fluorescence intensity of the region of interest was measured with NIH ImageJ software.

4.5.5 Quantification of Presynaptic Arbor Size

The Neurolucida software was used to trace and measure the length between an axon's entry point into the C4da neuropil and the axon endings. Branches shorter than 5 μm were excluded from analysis.

4.5.6 Western Blots

To analyze reporter expression in cultured cells, S2 cells maintained in Schneider's medium with 10% fetal bovine serum were transfected with Lipofectamine 2000^{TM} (Invitrogen). A construct containing the tubulin promoter fused to the cDNA of GAL4 was co-transfected with pUAST constructs. Two days after transfection, cells were harvested by centrifugation, homogenized in SDS sample buffer, separated by SDS-PAGE, and analyzed by Western blot.

To analyze Dscam protein levels in vivo, brains were removed from wandering third instar larvae and homogenized in SDS sample buffer. Homogenates of equal numbers of brains (3–5) from control and experimental groups were separated by SDS-PAGE and analyzed by Western blot. The primary antibodies used were mouse monoclonal anti-Dscam (236), rabbit polyclonal anti-GFP (Invitrogen), mouse monoclonal anti-tubulin (Sigma), mouse monoclonal anti-dFMRP (Developmental Studies Hybridoma Bank), rat monoclonal anti-Elav (Developmental Studies Hybridoma Bank), and mouse monoclonal anti-βGal (Developmental Studies Hybridoma Bank).

4.5.7 RNA-Immunoprecipitation

Larval brains (~150) were dissected from wandering third instars in PBS and washed two times with PBS. Crude homogenates were generated by homogenizing brains in lysis buffer (50 mM Tris/HCl, pH 7.5; 150 mM KCl; 1 mM EDTA; 0.5% TX100) in the presence of RNase inhibitor and protease inhibitor and centrifuged for 30 min at 20,000 x g, 4˚C. The equal amount of supernatant was incubated for 1hr at 4˚C with Dynabeads Protein-G (Life Technologies) precoupled with same amount of monoclonal

anti-dFMRP antibody 5B6 (Developmental Studies Hybridoma Bank) or normal mouse IgG as a negative control. Beads were washed 5 times with lysis buffer, supplemented with 10 mg glycogen (Invitrogen) and 10 pg of firefly luciferase mRNA (Promega), then processed for RNA extraction.

4.5.8 Real-Time PCR

Total RNA was extracted from brains of third instar larvae, using a standard Trizol protocol (Invitrogen). First-strand cDNA was synthesized with Invitrogen SuperScript III First-Strand Synthesis SuperMix (Invitrogen). cDNA from 10 ng RNA was used for each real-time PCR reaction (15 μl), using the Absolute QPCR SYBR Green mix (Thermo Scientific) with Applied Biosystems 7300. After the cycle number at the threshold level of log-based fluorescence (Ct) had been collected for each sample, ΔCt for each test gene was calculated by subtracting the Ct number of the reference gene (*elav*) from that of the test gene (Ct_{test}-Ct_{elav}) (237). This normalizes transcript levels of test genes to *elav*. Our extensive tests showed that *hiw* mutations do not alter *elav* or *Chmp1* transcript levels. The ΔCt of each test gene was statistically compared between wild-type and *hiw,* and then converted to fold change. The Mann-Whitney test was used to determine the statistical significance of changes in different transcripts.

For RNA-immunoprecipitation, ΔCt for *Dscam* mRNA was calculated by subtracting the Ct number of the reference mRNA (*a-tubulin*) from that of *Dscam* mRNA. We used *a-tubulin* mRNA as the reference because mammalian *a-tubulin* mRNA does not bind to FMRP (221). Three independent RNA-immunoprecipitation experiments were done and the values of ΔCt were compared between control antibody and anti-dFMRP antibody by using two-tailed paired Student *t*-test.

Primer sets used were: *elav*, 5'-CTGCCAAAGACGATGACC-3' and 5'-TAAAG CCTACTCCTTTCGTC-3'; *Chmp1*, 5'-AAAGGCCAAGAAGGCGATTC-3' and 5'-GGGCAC TCATCCTGAGGTAGTT-3'; *Puckered*, 5'-AAAGTCCCAATGAGAGCC-3' and 5'-CGTGCA TCTTCGATAAAGTC-3'; *Dscam* #1, 5'-CTTACGATTGTGCTCATTACTC-3' and 5'-CAGTT TCGATTTGTTCTGTTGG-3'; *Dscam* #2, 5'-ATCGAAACTGTTCAATGCAC-3' and 5'-CTT GAGTGTATCTGTGTTTCGG-3'; *firefly luciferase*, 5'-

CTCACTGAGACTACATCAGC-3' and 5'- TCCAGATCCACAACCT TCGC-3'; *a-tubulin*, 5'-GCCAATTAGGCGATTGAGATTC-3' and 5'-AGCACTCGGACTGTGCGTTT-3'.

4.5.9 Statistical Analysis

A two-tailed unpaired Student *t*-test was used for presynaptic arbor size analysis and Western blot analysis unless otherwise noted. The Mann-Whitney test was used for real-time PCR experiments. P-values smaller than 0.05 were considered statistically significant. All p values are indicated as: *: $p < 0.05$, **: $p < 0.01$, and ***: $p < 0.001$. Data are presented as mean ± SEM.

4.6 Acknowledgements

We thank Drs. Tzumin Lee, Larry Zipursky, Catherine Collins, Chunlai Wu, Kendal Broadie, Chun Han, Liqun Luo, and Yuh Nung Jan generously for sharing reagents, Drs. Ting Han and John Kim for their help on the RNA-IP experiments, the members of Dr. Jiandie Lin's lab for helping us to set up the real-time PCR experiments. We also thank Dr. Catherine Collins, Dr. Tzumin Lee, Dr. Hisashi Umemori, and Gabriella Sterne for critical comments on earlier versions of the manuscript. This work was supported by grants from NIH (R00MH080599 and R01MH091186), the Whitehall Foundation, and the Pew Scholars Program in the Biological Sciences to B.Y.

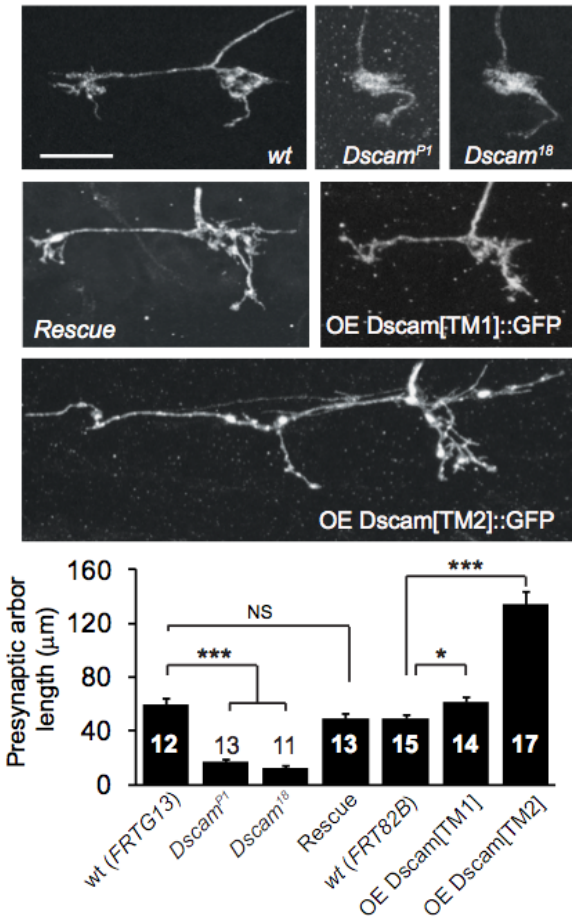

Figure 4.1 Dscam instructs presynaptic arbor growth.
Representative images and quantification of the presynaptic arbors of single C4da neurons that are *wild-type* (*wt*), null mutants of *Dscam* (*Dscam*^{P1} or *Dscam*^{18}), null mutants rescued by one copy of a transgene harboring the *Dscam* genomic DNA (*Rescue*), overexpressing the dendritic (OE Dscam[TM1]::GFP) or overexpressing the axonal (OE Dscam[TM2]::GFP) isoform. The MARCM technique was used in these experiments, and the arbors of single ddaC neurons are shown. Sample numbers are indicated in each bar. Scale bars: 10 μm.

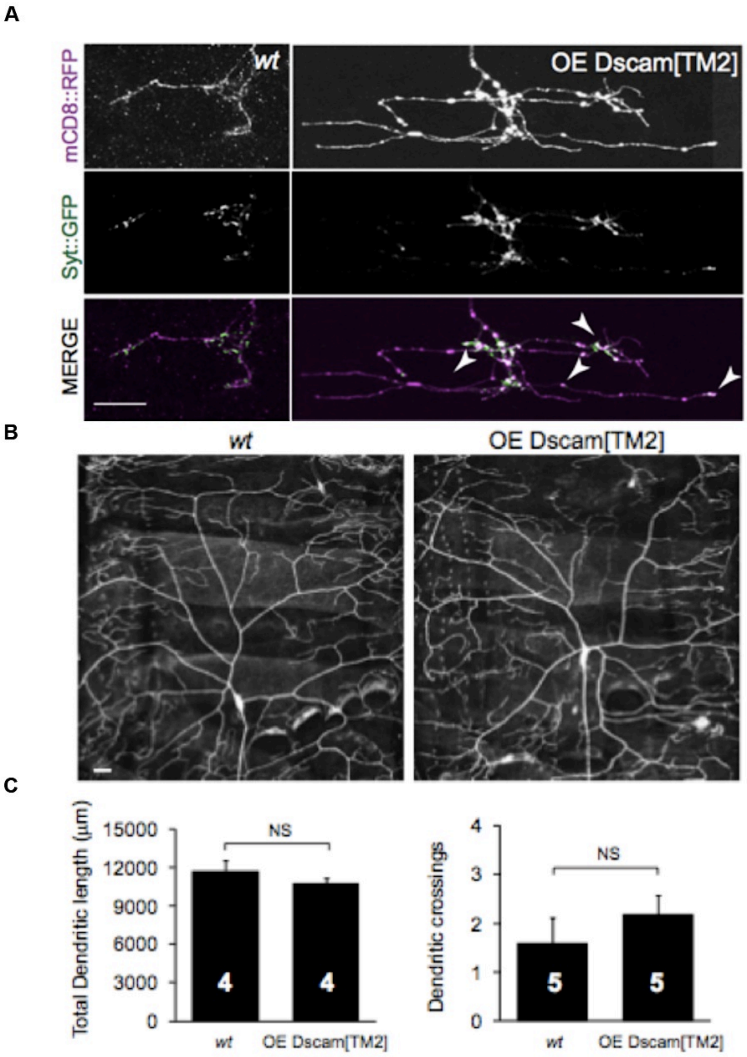

Figure 4.2 Overexpression of Dscam[TM2] promotes presynaptic arbor growth but does not change dendritic patterning in C4da neurons.
(A) Axon terminal arbors of single ddaC neurons labeled with the presynaptic marker synaptotagmin::GFP (Syt::GFP). The flip-out technique with an excisable GAL80 (235) was used to express the membrane marker mCD8::mRFP (magenta) and the presynaptic marker Syt::GFP (green) in wild-type (*wt*) and in Dscam[TM2]-overexpressing C4da neurons. Arrowheads point to ectopic synaptic regions formed in overgrown axon terminals. Scale bar: 10 µm. (B) *Dscam[TM2]* transgene was expressed by *ppk-Gal4* driver in C4da neurons. Dendritic arbors were visualized with mCD8::GFP. Scale bar: 10 mm. (C) Quantification of total dendritic length and branch crossings. Sample numbers are shown in the bars.

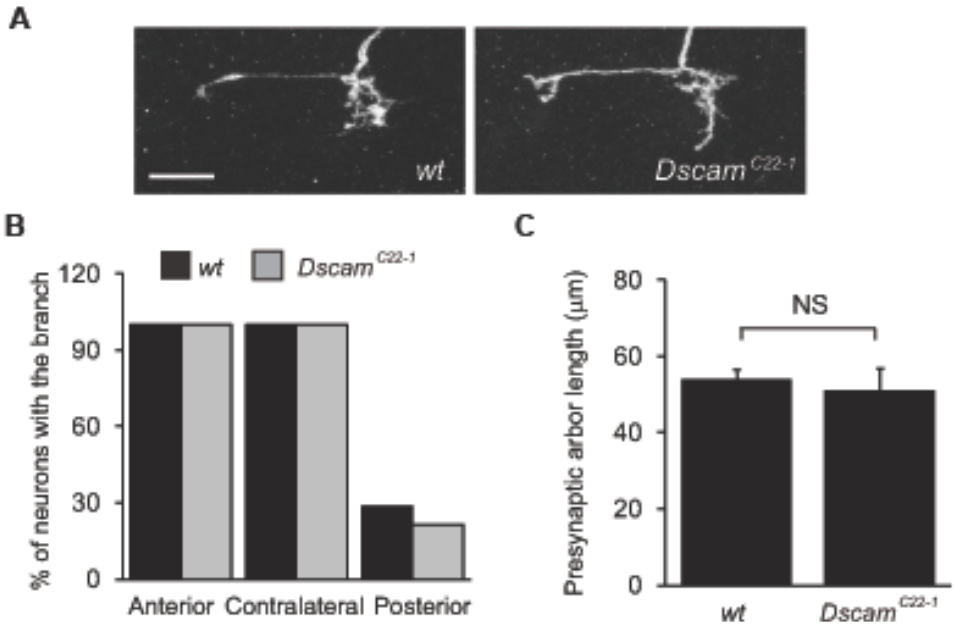

Figure 4.3 Reducing the diversity of Dscam ectodomain does not affect either the targeting or the growth of C4da presynaptic arbors.
(A) Shown are representative images and of single C4da neurons that are *wild-type* (*wt*), homozygous for a *Dscam* allele with reduced diversity ($Dscam^{C22\text{-}1}$). $Dscam^{C22\text{-}1}$ is a partial deletion of the exon 4 cluster, resulting in 75% reduction of alternative exon 4 (214). (B-C) quantification of presynaptic targeting (B) and the presynaptic arbors length (C). Scale bar: 10 µm. *wt*, n = 14; $Dscam^{C22\text{-}1}$, n = 14.

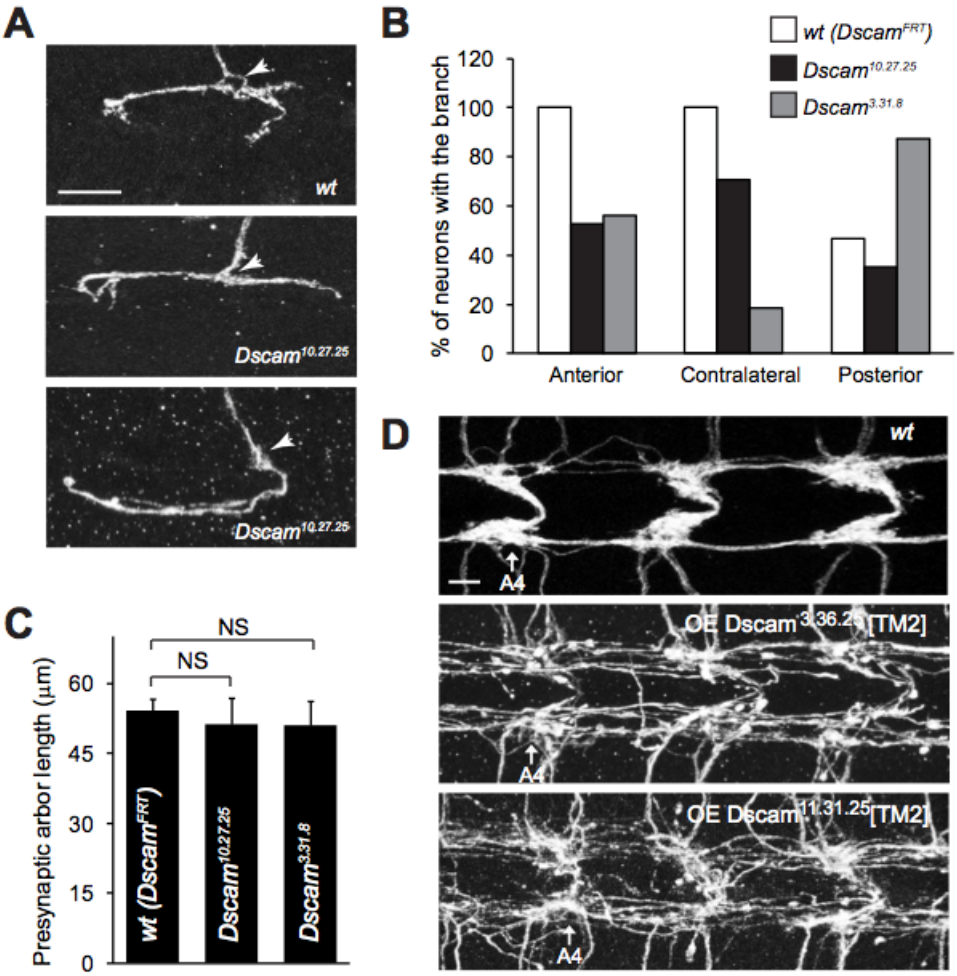

Figure 4.4 Dscam instruction of presynaptic arbor growth is independent of ectodomain diversity.
(A) Presynaptic arbors of a wild-type (*Dscam*^{FRT}) and two *Dscam*$^{10.27.25}$ intragenic MARCM clones (ddaC). Arrows point to the entry points into the C4da neuropil. The middle panel shows a *Dscam*$^{10.27.25}$ ddaC clone that lacks a contralateral branch but extends an unusually long posterior branch. The bottom panel shows a clone that lacks the anterior projection but forms an abnormally long contralateral projection. Scale bar: 10 mm. (B) Summary of the presynaptic arbor patterns of *wt* (*Dscam*^{FRT}), *Dscam*$^{10.27.25}$, and *Dscam*$^{3.31.8}$ intragenic MARCM clones. (C) Quantification of presynaptic arbor length of intragenic MARCM clones. Sample numbers: *wt* (*Dscam*^{FRT}), n = 15; *Dscam*$^{10.27.25}$, n = 17; *Dscam*$^{3.31.8}$, n = 16. (D) Presynaptic arbor overgrowth caused by expressing Dscam[TM2] transgenes are independent of ectodomain diversity. Two independent Dscam[TM2] transgenes containing different and randomly chosen ectodomains, Dscam$^{3.36.25}$ and Dscam$^{11.31.25}$, were overexpressed in C4da neurons using the *ppk-Gal4* driver. Presynaptic arbors of all C4da neurons were collectively visualized with *ppk*-CD4::tdTomato. C4da presynaptic arbors in abdominal segments 4 (A4) through 6 are shown. Scale bar: 5 µm.

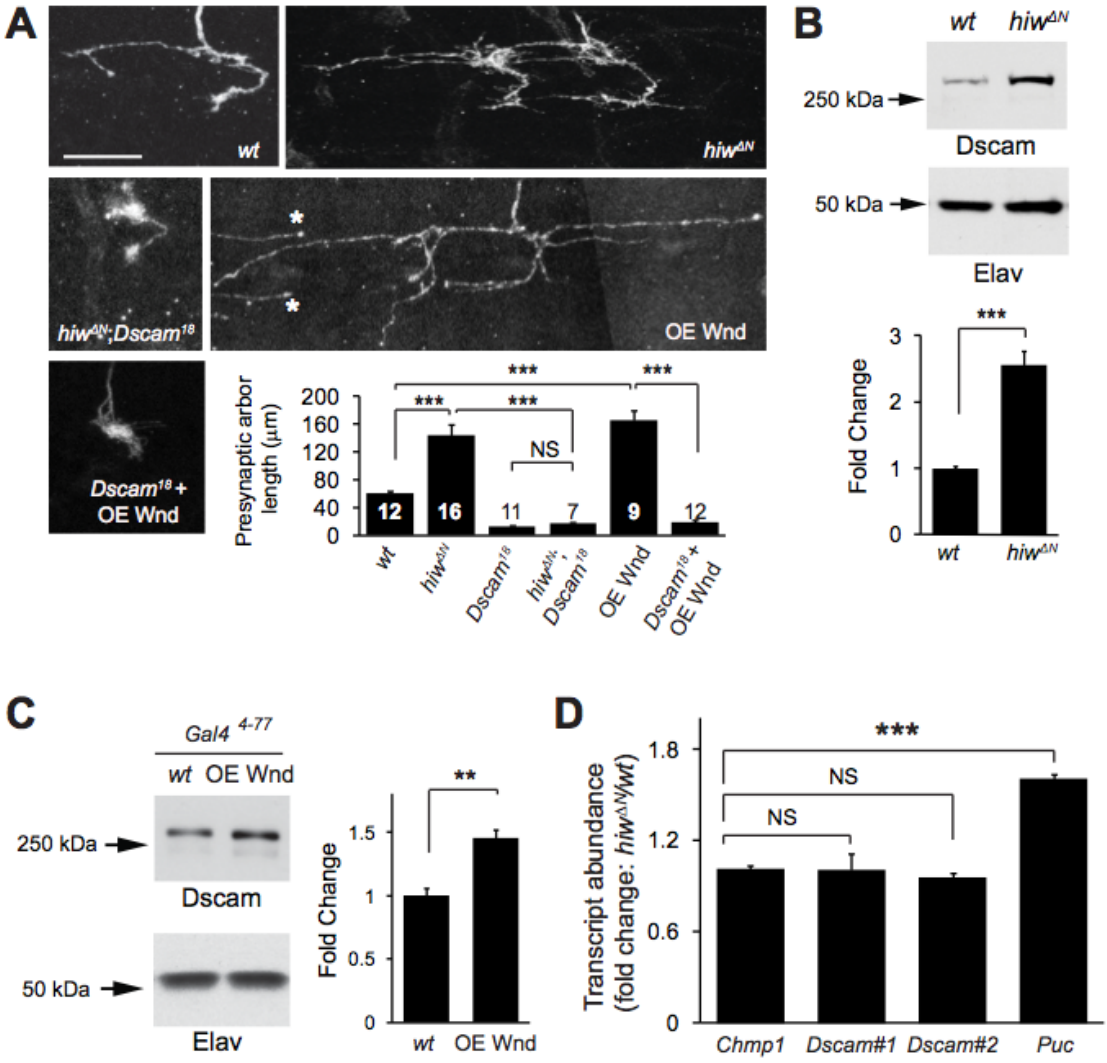

Figure 4.5 Hiw and Wnd control presynaptic arbor growth by regulating Dscam expression.

(A) *Dscam* is required for the overgrowth of presynaptic arbors in *hiw* mutant neurons and Wnd- overexpressing neurons. Shown are representative presynaptic arbors of single ddaC neurons generated by MARCM in wild-type (*wt*), $hiw^{\Delta N}$ hemizygote ($hiw^{\Delta N}$), $hiw^{\Delta N}$ and $Dscam^{18}$ double mutant ($hiw^{\Delta N}$;$Dscam^{18}$), Wnd overexpression (OE Wnd)(* marks two presynaptic terminals from adjacent neurons), and overexpressing Wnd in $Dscam^{18}$ mutant ($Dscam^{18}$ + OE Wnd). Scale bar: 10 mm. Quantification of presynaptic arbor length for each genotype is shown. Data for wild-type (FRT^{G13}) and $Dscam^{18}$ are the same as that shown Figure 1B. Sample numbers for each condition are shown in the bars. (B) Dscam expression is elevated in $hiw^{\Delta N}$ mutants. Top: Western blots from brains of wild-type (w^{1118}) and $hiw^{\Delta N}$ mutant third instar larvae. Bottom: Quantification of Western blots (n = 5). The intensities of Dscam bands were normalized to those of the neuron-specific protein Elav and presented as fold change. (C) Dscam expression is elevated in neurons overexpressing Wnd. Top: Western blots of brain lysates from third instar larvae overexpressing Wnd under the control of $Gal4^{4-77}$ (OE Wnd). For consistency, only one

copy of *Gal4*$^{4\text{-}77}$ was used as a wild-type control (*wt*). Bottom: Quantification of Western blots (n = 4). (D) *hiw*$^{\Delta N}$ does not affect the levels of *Dscam* transcripts. The relative transcript levels of *Chmp1* (n = 8), *Dscam* (two independent sets of primers, #1 and #2, against the invariant exon 24 of *Dscam* mRNA) (n = 4 and 8, respectively), and *Puckered* (*Puc*) (n = 4) from *wt* and *hiw* mutant larval brains were measured by real-time PCR.

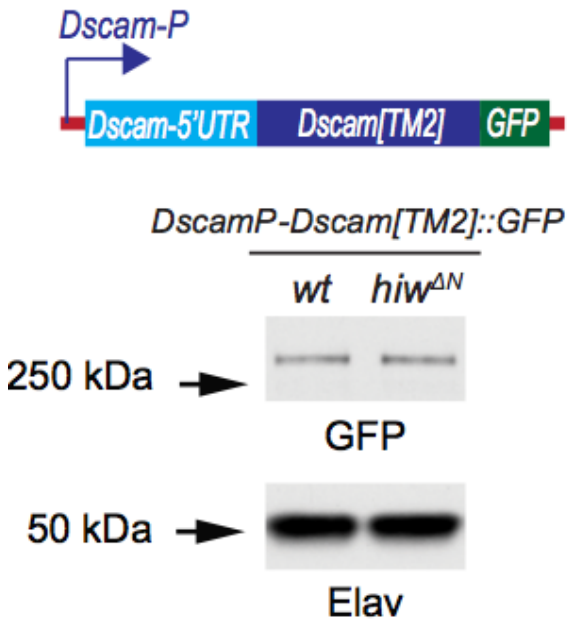

Figure 4.6 Hiw-Wnd pathway does not regulate Dscam promoter activity.
Dscam[TM2]::GFP is expressed under the control of the Dscam promoter (Dscam-P) and Dscam 5'UTR in wt and hiwΔN larvae. Dscam[TM2]::GFP expression in larval brain was examined by Western blot analysis with an anti-GFP antibody and normalized to Elav (wild-type: 1.00 ± 0.08, n = 3; hiwΔN: 1.21 ± 0.14, n = 3; mean ± SEM; p = 0.18, paired t-test).

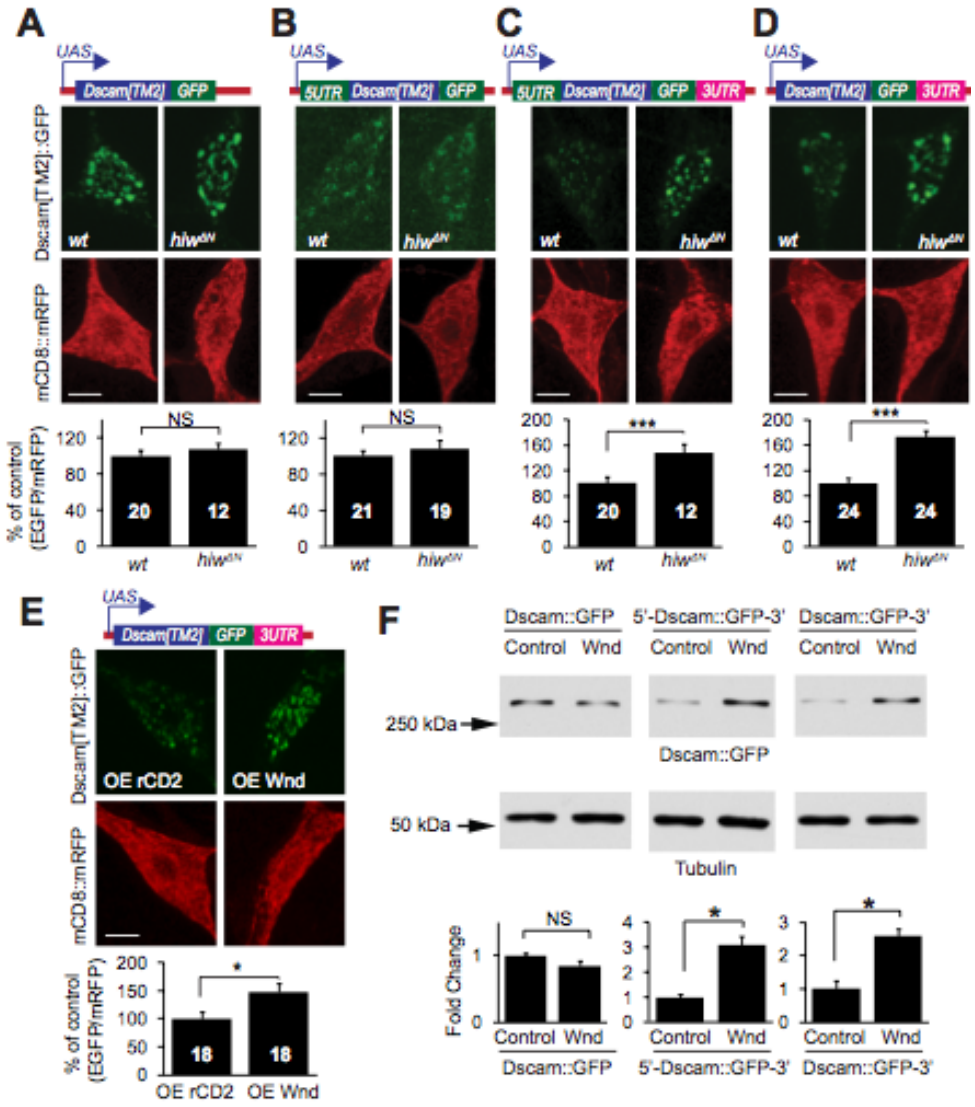

Figure 4.7 Hiw and Wnd regulate Dscam expression through *Dscam* 3'UTR.
(A-D) The *Dscam* 3'UTR is required by *hiw* to regulate Dscam expression in C4da neurons. Dscam[TM2]::GFP transgenes with or without UTRs (schematically shown at the top) were co-expressed with mCD8::mRFP in wild-type (*wt*) or $hiw^{\Delta N}$ C4da neurons using the C4da driver $Gal4^{4\text{-}77}$. Quantification of the immunofluorescence intensities is shown at the bottom. Sample numbers are shown in the bars. (E) Wnd promotes Dscam expression through the *Dscam* 3'UTR in C4da neurons. Dscam[TM2]::GFP transgene containing 3'UTR, was co-expressed with either Wnd (OE Wnd) or the membrane protein rCD2 (OE CD2) as a control, together with mCD8::mRFP, by the C4da driver $Gal4^{4\text{-}77}$. In A-E, Dscam[TM2]::GFP immunofluorescence in ddaC cell bodies were normalized to that of mCD8::mRFP and presented as % of controls. Scale bars: 5 mm. (F) Wnd promotes Dscam expression through the *Dscam* 3'UTR in cultured S2 cells. Dscam constructs were transfected into S2 cells along with either an empty vector (control) or a Wnd-expression construct (Wnd). Dscam::GFP expression was examined using Western

blotting with an anti-GFP antibody. The intensities of Dscam::GFP bands were normalized to those of tubulin and presented as fold change for statistical analysis (n = 4).

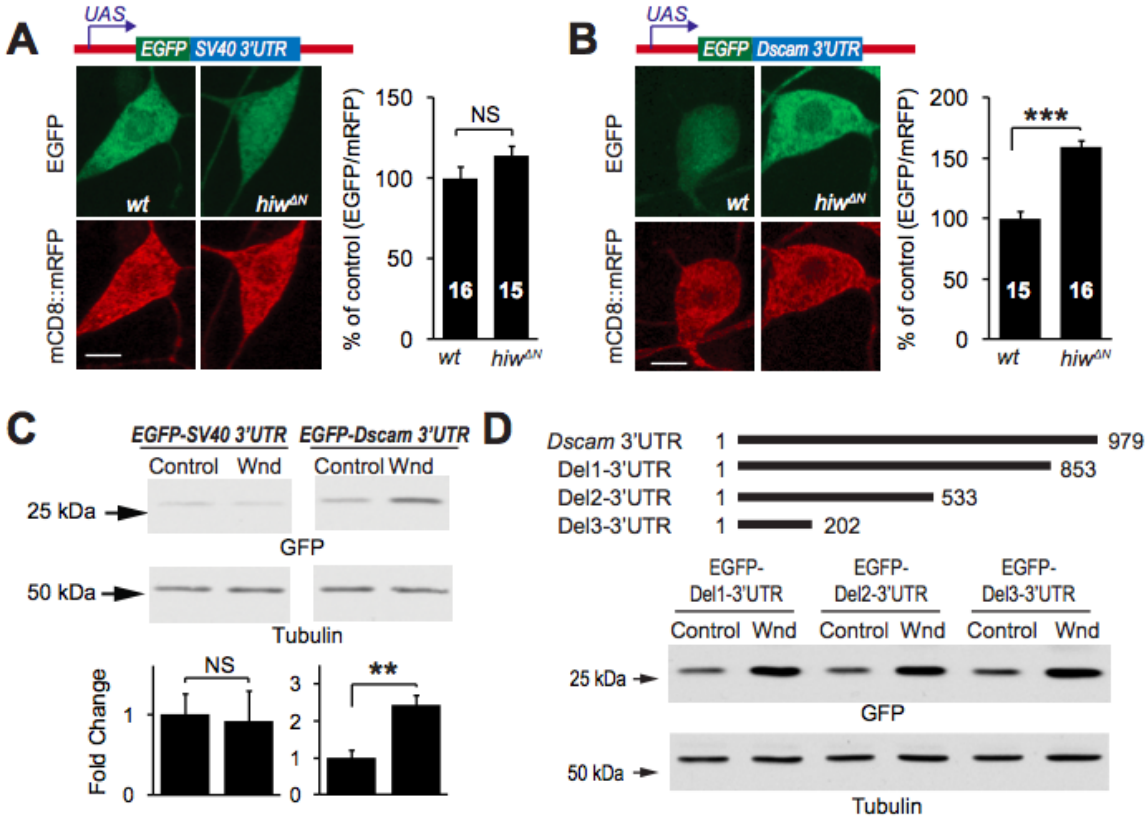

Figure 4.8 The 3'UTR of *Dscam* mRNA is sufficient for the regulation by Hiw-Wnd pathway.

(A and B) Dscam 3'UTR is sufficient to enhance expression in *hiw* loss-of-function neurons in vivo. EGFP reporter transgenes containing either SV40 3'UTR (A) or *Dscam* 3'UTR (B) were expressed in *wild-type* (*wt*) or $hiw^{\Delta N}$ C4da neurons. EGFP immunofluorescence in the cell bodies of ddaC was normalized to that of mCD8::mRFP, and presented as % of control. Sample numbers are shown in the bars. Scale bar: 5 mm. (C) Western blots of lysates from S2 cells expressing the EGFP reporters SV40 3'UTR (*EGFP-SV40 3'UTR*) or *Dscam* 3'UTR (*EGFP-Dscam 3'UTR*), along with a Wnd-expression construct (Wnd) or an empty vector (control). EGFP expression levels were normalized to tubulin levels and are presented as fold change (bottom panel, n = 4). (D) Mapping of the regions of the *Dscam* 3'UTR required for Wnd-mediated regulation. EGFP reporter constructs containing serial deletions in the *Dscam* 3'UTR (schematics shown at the top) were transfected into S2 cells along with Wnd-expression construct (Wnd) or the empty vector (control). EGFP expression levels were normalized to tubulin levels and presented as fold change (bottom panel, n = 4).

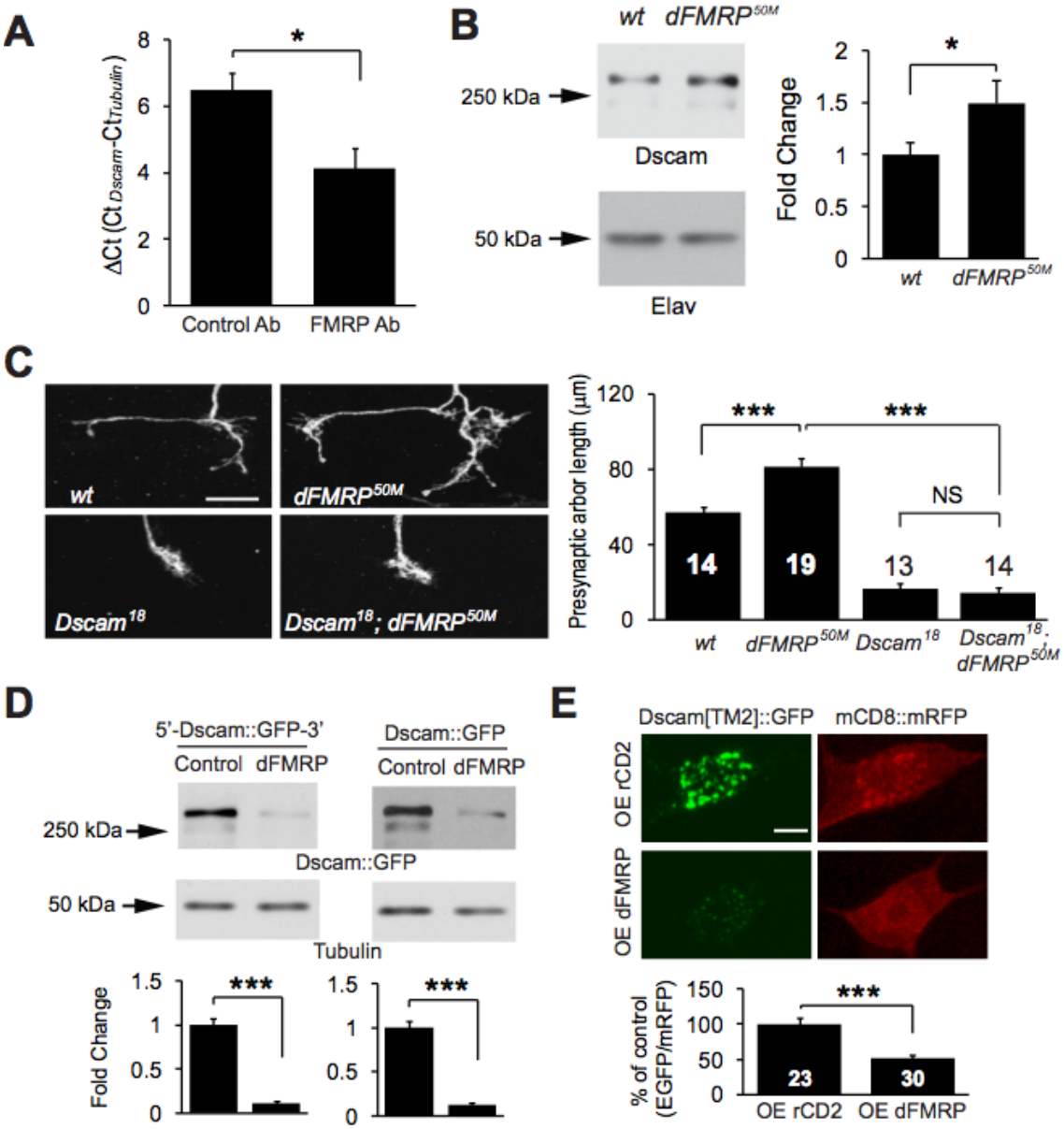

Figure 4.9 FMRP suppresses Dscam expression to restrict presynaptic arbor growth.

(A) dFMRP associates with *Dscam* mRNA in vivo. RNA-immunoprecipitation, followed by reverse transcription and real-time PCR, was done using larval brain lysates (n = 3). The difference in ΔCt between control and dFMRP-immunoprecipitates reflects a 5.8-fold binding of *Dscam* mRNA to FMRP. (B) Western analysis of Dscam expression in the brains of wild-type (w^{1118}) and $dFMRP^{50M}$ third instar larvae. The intensities of Dscam bands were normalized to those of the neuron-specific protein Elav and presented as fold change (n = 13). (C) *Dscam* is required by *dFMRP* to restrict presynaptic arbor growth. Images show the presynaptic arbors of ddaC MARCM clones of *wt*, $dFMRP^{50M}$, $Dscam^{18}$, and $Dscam^{18}/dFMRP^{50M}$ double mutant ($Dscam^{18}$; $dFMRP^{50M}$) neurons. Scale bar: 10 mm. Right: Quantification of presynaptic arbor length for each condition. Sample

numbers are shown in or above the bars. (D) dFMRP regulates Dscam expression through the coding region of *Dscam* in S2 cells. Shown are Western blots of lysates of cultured S2 cells expressing Dscam[TM2]::GFP with *Dscam* 5' and 3'UTR (5'-Dscam::GFP-3') or with SV40 3'UTR (Dscam::GFP) in the presence of a dFMRP-expression construct (dFMRP) or the empty vector (Control). Dscam[TM2]::GFP levels were normalized to tubulin levels and presented as fold change (n = 4). (E) dFMRP suppresses Dscam expression through the Dscam coding region in vivo. Dscam[TM2]::GFP and mCD8::RFP were expressed in C4da neurons using $Gal4^{4\text{-}77}$, along with either rCD2 (control) or dFMRP (OE dFMRP). Dscam[TM2]::GFP levels in ddaC cell bodies were normalized to mCD8::mRFP levels and presented as % of control (right panel).

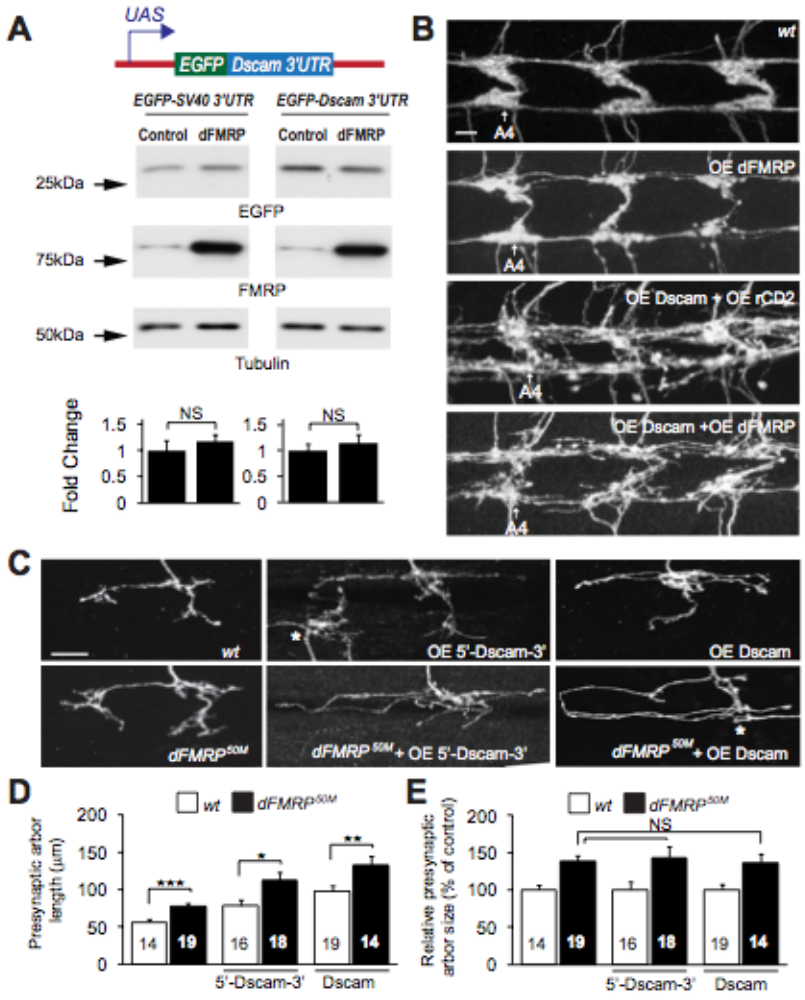

Figure 4.10 FMRP regulates Dscam expression through the coding region of *Dscam* mRNA.

(A) FMRP does not regulate Dscam expression through *Dscam* 3'UTR. Western blots of lysates of cultured S2 cells expressing EGFP reporters with SV40 3'UTR or *Dscam* 3'UTR together with dFMRP cDNA (dFMRP) or the empty vector (Control). Bar chart: quantification of the expression levels of EGFP reporter. EGFP expression levels were normalized to tubulin levels and presented as fold change for statistical analysis (n = 4). (B) FMRP is sufficient to suppress presynaptic arbor overgrowth caused by Dscam-overexpression. Shown are presynaptic arbors of larval C4da neurons labeled with *ppk*-CD4::tdTomato in C4da neurons that are wild-type (wt), overexpressing dFMRP (OE dFMRP), overexpressing a *Dscam* transgene that does not contain *Dscam* 5' and 3'UTRs together with the membrane protein rat CD2 (OE Dscam + OE rCD2), and overexpressing the Dscam transgene together with dFMRP (OE Dscam + OE dFMRP). C4da presynaptic arbors in abdominal segments 4 (A4) to 6 are shown. Scale bar: 5 mm. (C) FMRP is required to restrain presynaptic arbor overgrowth caused by Dscam-overexpression. Shown are presynaptic arbors of single ddaC MARCM clones that are wild-type (wt), $dFMRP^{50M}$ homozygotes, overexpressing Dscam coding region plus the 5' and 3'UTRs (OE 5'-Dscam-3'), overexpressing 5'-Dscam-3' in $dFMRP^{50M}$

background (*dFMRP*^{50M} + OE 5'-Dscam-3'), overexpressing Dscam coding region only (OE Dscam), overexpressing Dscam coding region in *dFMRP*^{50M} background (*dFMRP*^{50M} + OE Dscam). To avoid possible saturation of presynaptic arbor growth by Dscam-overexpression, we chose the UAS-Dscam and UAS-5'-Dscam-3' transgenes that express Dscam at a lower level than those used in Figure 1B and 2D. These two transgenes are located in the same genomic locus. (D) Quantification of presynaptic arbor length. Sample numbers are shown in the bars. (E) Quantification of relative presynaptic arbor size. Relative presynaptic arbor sizes are obtained by normalizing values from *dFMRP* mutant clones to the average values of corresponding of wild-type clones (*dFMRP*^{50M} vs *wt*; *dFMRP*^{50M} + OE 5'-Dscam-3' vs OE 5'-Dscam-3'; *dFMRP*^{50M} + OE Dscam vs OE Dscam). Sample numbers are shown in the bars.

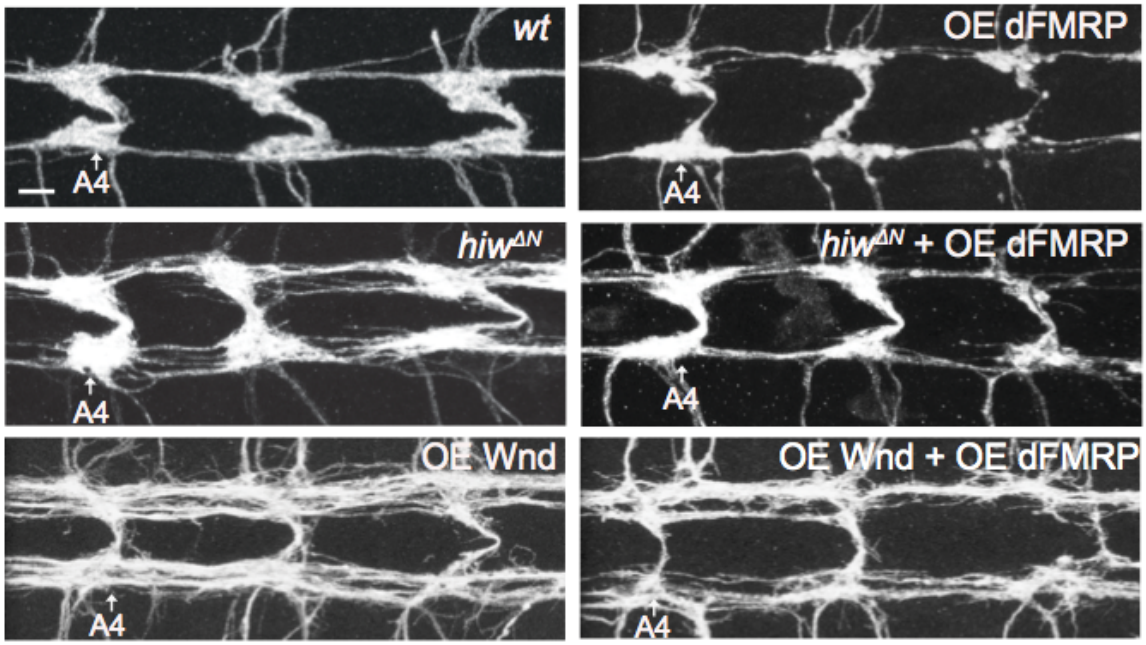

Figure 4.11 Hiw-Wnd pathway and FMRP converge to regulate presynaptic arbor growth.
dFMRP was expressed with *ppk-Gal4* either in *wild-type* (*wt*) or *hiw* mutant ($hiw^{\Delta N}$ + OE dFMRP) C4da neurons. Wnd was expressed by the driver *ppk-Gal4* with either the control transgene rCD2 (OE Wnd) or dFMRP (OE Wnd + OE dFMRP). Note that dFMRP suppresses extensive overgrowth of C4da presynaptic arbors caused by Wnd overexpression (OE Wnd) or *hiw* mutations. C4da presynaptic arbors in abdominal segments 4 (A4) to 6 are shown. Scale bar: 5 mm.

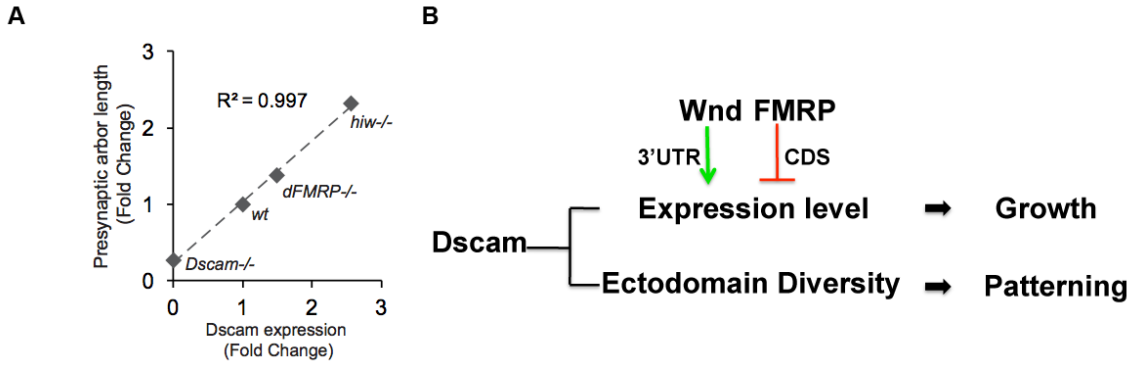

Figure 4.12 Dscam expression levels correlate with presynaptic arbor sizes.
(A) Dscam expression levels correlate with presynaptic arbor length. The relative presynaptic arbor sizes of single ddaC neurons from different genetic backgrounds were normalized to corresponding wild-type controls and denoted as fold change. Dscam expression levels from Western analyses were normalized to corresponding wild-type controls and presented as fold change. The presynaptic arbor size of *Dscam*^{18} was used for *Dscam-/-*. *Dscam*^{18} is a protein-null allele (40). R^2 value was derived from linear regression. (B) The present study suggests a model that explains how presynaptic arbor patterning and size control may be differentially controlled by a shared molecule, Dscam. The Dscam ectodomain diversity determines the pattern of presynaptic terminals, whereas its expression level instructs presynaptic terminal size. The DLK pathway and FMRP regulate Dscam expression levels to control presynaptic arbor size.

Chapter 5

The Krüppel-like factor Dar1 determines the multipolar organization of neuronal processes [4]

In Chapter 4, we found that Dscam specifically instructs axonal growth in C4 da neurons. In this Chapter, I will focus on a dendrite-dedicated regulator the Krüppel-like transcription factor Dar1 that is selectively in multipolar neurons, and determines the multipolar dendritic morphology.

5.1 Abstract

The nervous systems of different species across evolution contain unipolar, bipolar and multipolar neurons, but little is known about the molecular mechanisms that generate these morphological organizations. Among a number of molecules found to regulate dendritic growth, we identified the Krüppel-like transcription factor Dar1 as a unique instructive determinant of multipolar neuronal morphology in *Drosophila*. Dar1 is selectively expressed in multipolar, but not unipolar or bipolar, neurons. Loss of *dar1* reduced the number of primary dendrites in multipolar neurons, and transformed them into bipolar or unipolar morphologies. Conversely, ectopic expression of Dar1 or its mammalian homolog in *Drosophila* unipolar and bipolar neurons caused them to assume multipolar morphologies. We further show that Dar1 determines the multipolar morphology by regulating the dynein complex. This study offers, to our knowledge, the first post-mitotic molecular mechanism underlying the structural diversity of multipolar, bipolar, and unipolar neurons, which is fundamental for the processing of input information and the wiring of neural circuits.

[4] In preparation with authors listed as Xin Wang, Jung Hwan Kim, Gabriella Sterne, and Bing Ye.

5.2 Introduction

Ramon y Cajal described the major morphological types of neurons as unipolar, bipolar, and multipolar based on the number of primary dendrites (65) (Figure 5.1A). The multipolar organization separates the dendritic arbor into distinct fields, which have consequences not only on the passive current spread and processing of electrical signals in neurons (238), but also on the types of synaptic or sensory inputs the neuron receives. For example, the multipolar pyramidal cells in the cerebral cortex exhibit a separation of apical and basal dendrites, both of which connect to the soma but receive distinct types of inputs (239).

In addition to information processing and input types, the three fundamental morphological types are relevant to the distinct organizational principles employed in different parts of the nervous system and in the nervous systems of different animal species. Although all three types exist in different species throughout evolution, the majority of neurons in invertebrates are unipolar whereas those in vertebrates are multipolar (240-242). In insect CNS, the unipolar neurons extend a single process from the soma to a synapse-enriched neuropil, and then bifurcate into dendrites that usually stay local and an axon that typically projects to other neuropil areas or target tissues (240). Unipolar organization of neuronal processes allows forming synaptic connections away from the birthplace of the neurons, so it is likely a surrogate strategy for neuronal migration, which is absent in the insect CNS (243) but common in the vertebrate CNS (244).

Despite the importance of these fundamental morphological organizations of neuronal processes, we know very little insight about the molecular switches that lead post-mitotic neurons to develop multipolar, bipolar, or unipolar morphologies since their description about a century ago. In this study, we demonstrate that the Krüppel-like transcription factor Dar1, previously identified as a dendrite-specific regulator (36), determines multipolar dendritic structures in *Drosophila* nervous system.

5.3 Results

To investigate the molecular mechanism that defines the three major morphological types of neurons, we used the *Drosophila* nervous system to identify

genes that control the number of primary dendrites. The *Drosophila* CNS neurons are predominantly unipolar (240-242). In contrast, the PNS neurons are either bipolar or multipolar (245). For instance, the external sensory (es) and chordotonal (ch) neurons are bipolar with only a single primary dendrite in addition to the axon (245), whereas the dendritic arborization (da) neurons are multipolar with more than one primary dendrite (86, 245) (Figure 5.1B). We first asked whether the number of primary dendrites is determined by general mechanisms that govern dendritic growth by testing mutations known to cause retarded dendritic growth in the multipolar da neurons. In the neurons defective of Cut (82) and Hiw (41) (See Chapter 2), the da neurons still formed the normal number of primary dendrites, despite of simplified higher order branches (Figure 5.2). Therefore, the number of primary dendrites of a neuron – thus the multipolar versus bipolar/unipolar morphology - is determined by mechanisms that are distinct from those regulating dendritic growth.

We previously identified the *dendritic arbor reduction 1* (*dar1*) gene, which encodes a member of the Krüppel-like factor (KLF) family of transcriptional regulators, as a specific regulator for dendritic, but not axonal, growth (36). In neurons that lack *dar1* function, total length and branch number of dendrites in da neurons are reduced. Conversely, overexpressing Dar1 in these neurons increases dendrite length and branch number (36). Whether or not *dar1* plays a role in determining the number of primary dendrites remains unknown. Strikingly, Dar1 was exclusively expressed in multiple dendritic (md) neurons, and was undetectable in bipolar and unipolar neurons in the PNS and CNS in both the embryo (36) and the larva (Figure 5.1, B'-D'). As a comparison, other transcription factors known to regulate dendritic development in md neurons, such as Knot, Cut and Spineless, are expressed either in a subset of or in all PNS and CNS neurons (82-85, 246)} (Figures 5.1B' and 5.3). The unique and selective expression of Dar1 in multipolar neurons led us to hypothesize that it is not only a regulator for dendritic growth but also determines the multipolar morphology of neurons.

To test this hypothesis, we introduced *dar1* mutations into single md neurons using the mosaic analysis with a repressible cell marker (MARCM) technique (33). The wild-type class I (c1), class III (c3), and class IV (c4) da neurons typically extend two or three primary dendrites from the soma (Figures 5.1B, and 5.4A-C). In sharp contrast, the

majority of *dar1* mutant neurons became bipolar with a single primary dendrite and an axon (Figure 5.4, A-C and E). The dendrite-axon polarity was preserved in the mutant neurons (Figure 5.5). Loss of *dar1* even converted some c1da neurons into unipolar morphology (Figure 5.4A), which was never observed in wild-type neurons. Consistent with the observation that Dar1 is absent in bipolar neurons (Figure 5.1D'), es neurons carrying *dar1* mutations still projected a single primary dendrite (Figure 5.4D and E). Taken together, these results demonstrate that Dar1 is indispensable for the formation of multiple primary dendrites in the md multipolar neurons.

Next, we asked whether ectopic expression of Dar1 in unipolar or bipolar neurons induces the formation of supernumerary primary dendrites. Because inducing Dar1 expression in large numbers of CNS neurons caused lethality (data not shown), we overexpressed Dar1 in a small subset of motor neurons using the *RN2-Gal4* driver (184, 247) and then examined their morphology. The RN2 neurons are unipolar: each soma extends a single primary neurite, which branches into a few dendritic branches and a long axon (Figures 5.6, 5.7A and C). In sharp contrast, Dar1-overexpressing RN2 neurons extended ectopic neurites directly from the soma and consequently became multipolar (Figure 5.7A and B). Many of these primary neurites were also labeled by Nod::βGal, a marker that labels subsets of dendritic branches (21) (Figure 5.7C). Similarly, Dar1 expression transformed the bipolar es neurons in larval PNS (Figure 5.7D and E) and the unipolar PDF neurons in adult brain (Figure 5.7F and G) into multipolar morphology. These results suggest that Dar is sufficient to convert unipolar/bipolar into multipolar dendritic structures. We also found that overexpressing a mouse homolog of Dar1, mKLF7 led to a dramatic increase in the number of primary dendrites in unipolar neurons (Figure 5.7A-B and F-G), supporting an evolutionarily conserved mechanism underlying multipolar organizations of neuronal processes.

To investigate the mechanisms by which the Dar1 transcription factor determines multipolar organizations of neuronal processes, we used a microarray-directed RNAi screen to identify the genes that are regulated by Dar1 to determine the number of primary dendrites. The selective expression of Dar1 in the PNS multipolar neurons, which consists of only several hundreds of neurons in each animal, presented a technical challenge to the microarray-based comparison of gene expression between wild-type and

dar1 mutant neurons. To meet this challenge, we used a GAL80-based strategy to label PNS neurons with the enhanced green fluorescent protein (eGFP) in only *dar1* homozygous, but not the heterzyogous, embryos (Figure 5.8A). This approach allowed us to efficiently purify PNS neurons from large quantities of *dar1* mutant embryos using fluorescence-activated cell sorting (FACS) (Figure 5.8B). The purified wild-type and mutant neurons were used for microarray analysis. Gene ontology-based functional annotation (248) of the differentially expressed genes showed that the significantly enriched gene ontology (GO) terms of cellular component mostly related to microtubules (Table 5.1). Markedly, the expression of a number of genes involved in the dynein complex was reduced in *dar1* mutant neurons (Table 5.2), raising the possibility that the dynein complex is essential for the multipolar organization of neuronal processes.

To test this possibility, we first used RNA interference (RNAi) to knock down the dynein complex genes affected by *dar1* mutations. Knocking down the expression of several genes, namely CG9492, CG8407, CG14763, and CG6971, reduced the number of primary dendrites (Figure 5.9A and B). The number of primary dendrites was also reduced in the animals that overexpressed a dominant-negative dynactin subunit p150/Glued (Glued ^{DN}) (249) (Figure 5.9A and B). Moreover, growing larvae carrying one copy of a temperature-sensitive allele of the dynein intermediate chain (*short wing*), *sw* ^{ts}, at the non-permissive temperatures, led to the appearance of a single primary dendrite in multipolar c1da neurons (Figure 5.9A and B). We further tested whether Dar1 requires dynein complex to induce primary dendrite formation in unipolar neurons by introducing heterzygous *sw*^{ts} mutation in RN2 neurons overexpressing Dar1. In larvae raised at a non-permissive temperature, the *sw*^{ts} mutation potently reduced the supernumerary primary dendrites induced by overexpressing Dar1 (Figure 5.9C-C'), suggesting that *dar1* requires the dynein complex to determine multipolar morphology of neurons.

Quantitative real-time PCR has shown that the expression of the microtubule severing protein Spastin (250) is increased in *dar1* mutants (36), which was confirmed in our microarray analysis (Table 5.2). We found that, although overexpressing Spastin restrained total dendritic growth (36), it did not alter the number of primary dendrites (Figure 5.10). These results suggest that Dar1 determines the number of primary

dendrites by regulating microtubule-based transport but promotes dendritic growth by regulating microtubule severing.

5.4 Discussion

Dar1 functions post-mitoticly to determine multipolar neuron mophorlogy

Taken together, these results uncover a novel, instructive role of Dar1 in determining the multipolar organization of neuronal processes. The transcription factor Hamlet is previously reported to be critical for the es cell lineage, and loss of *hamlet* leads to a cell-fate switch from es neurons to md neurons (251). Hamlet is expressed in neural progenitor cells and post-mitotic es neurons, and is absent in multipolar neurons at the time when dendrites extend from the soma. Different from Hamlet, several lines of evidence suggest that Dar1 determines the multipolar morphology in post-mitotic neurons without changing the cell fates. First, in contrast to the defects seen in the dendrites, axon morphology (36) and targeting (Figure 5.4C') were unchanged in *dar1* mutant neurons. Second, ectopic expression in post-mitotic neurons led to supernumerary primary dendrites (Figure 5.3). Third, in the neurons carrying *dar1* mutations, the remaining dendrites still followed the branching pattern that wild-type neurons assume (36)(Figure 5.4). Therefore, our results reveal the first molecular mechanism that determines the multipolar morphology after neuronal fate is established (Figure 5.11).

The role of dynein in determing multipolar neuron morphology

The microtubule motor dynein performs diverse functions during neuron development. It is indispensable for retrograde transport of cargos, establishing microtubule orientation and neuron polarity (21). Loss of *dynein light intermediate chain 2 (dlic2)* caused pleiotropic phenotypes in *Drosophila* da neurons, including switched molecular identities in dendrites and the axon, a proximal shift of dendritic branches, and reduced dendritic growth (21). In this study, we found that milder disruptions of dynein function, such as knock down or sw^{ts} heterozygosity, altered the number of primary dendrites (Figure 5.9). Our results revealed a novel function of dynein, which might be masked by the severe defects in establishing neuronal polarity in *dlic2* mutants (21).

How might dynein affect the number of primary dendrites? First, microtubules in the dendrites of *Drosophila* multipolar neuron are mostly minus-end out, especially in the proximal dendrites where over 90% microtubules are minus-end out (20, 22). The minus-end directed dynein would be important to transport microtubules and membraneous supplies into outgrowing primary dendrites at early developmental events and stablize the newly formed primary dendrites. In addition, in migrating cortical neurons in mammalian CNS, the soma, especially the nucleus, translocates with the leading dendrite process, which is an important step for neurons to assume the multipolar morphology by the end of migration (252). The coupling the soma/nucleus with the dendrites requires dynein (252, 253). We speculate that dynein might determine the number of primary dendrites by coordiating the positions between the soma/nucleus and the dendrites. To test these possibilities, it will be informative to characterize how primary dendrites are initially extended in relation to the soma, and to determine the temporal requirement of dynein function in primary dendrite formation.

Distinct regulatory mechanisms of primary dendrite formation and higher-order dendrite branching

In this study, we examined the involvement of several known dendritic regulators in determining the three basic morphological types. Our results revealed that some dendritic regulators, such as Ct (82) and Hiw (41), are specifically required for dendritic branching of second-order or above (Figure 5.2). In contrast, Dar1 controls both primary dendrite formation and the growth of higher order dendrites. Dynein and Spastin respectively mediate these two actions of Dar1 (Figure 5.11). These results suggest that neurons employ distinct regulators for branching out primary dendrites and higher-order dendrites. Moreover, in early development, we observed that primary and higher-order dendrites grow concurrently (Figure 6.2 B-D), suggesting that these distinct regulatory mechanisms may operate at the same time during neuronal development.

The functional significance of switching morphological types

It has been hypothesized in neuron doctrine that dendritic and axonal structures are linked with neuronal specialized functions. Several functional significances in regard

to these three morphological types have been speculated. First, the conduction time of information transmission might differ. For instance, signals might be directly transmitted from dendrites into the axon bypassing the soma in unipolar neurons, resulting a shorter conduction time than in bipolar or multipolar neurons. In addition, switching unipolar into bipolar or multipolar neuron morphology with more primary dendrites likely causes ectopic postsynapses and mispairing of pre-and post-synaptic partners. On the contrary, loss of primary dendrites would result in a reduction in receptive field and number of postsynapses (Figure 5.4). Either excessive or comprised number of synaptic connections would introduce errors in the wiring of neural circuits.

The universal morphological organization of neuronal dendrites and axons – the unipolar, bipolar and multipolar morphologies – is both a denominator of the information processing of neurons as well as a factor in the wiring scheme of neural circuits. Experimental investigations on the roles of these fundamental neuronal organizations have not been approachable; as such investigations require manipulations that alter the unipolar, bipolar or multipolar organizations without affecting the cell fates that affect aspects such as axon targeting and the selection of synaptic partners. Thus, the molecular and cellular mechanisms, as reported in this study, are crucial for understanding the roles of structural organizations of neuronal processes in the function and assembly of neural circuits. Moreover, this study opens door for a unifying theory of basic structural organization of neuronal processes across species.

5.5 Materials and Methods

5.5.1 Fly stocks and cDNA constructs

Fly stocks include: *dar1* ^{3232}, FRT^{2A} (36); *Ct* ^{C145}, FRT^{19A} (82); *hiw* $^{\Delta N}$, FRT^{19A} (41); *UAS-Dar1* (36); *UAS-Nod::βGal* (76), *ppk-CD4::tdTomato* (75); *RN2-Gal4* (184); *PDF-Gal4* (254); *UAS-Glued* ^{DN}(249); *sw* ^{ts}(255); *UAS-Spas* (the EP insertion T32) (250). The following RNAi lines were obtained from the Vienna Drosophila RNAi Center: v105898(CG9492); v23504 (CG8407); v8737 (CG14763); v35154 (CG6971).

The DNA construct for making the UAS-mKLF transgenic lines was generated by inserting the mouse KLF7 cDNA (tagged with a V5-epitope at the C-terminus) into the pUAST vector.

5.5.2 MARCM and Flip-out Analyses

The MACRM experiments were performed as previously described (36). For MARCM analyses of *dar1* mutations in different classes of da neurons and es neurons, the hs-flp; *Gal4*$^{21\text{-}7}$, UAS-mCD8::GFP; tubP-Gal80, FRT^{2A} virgins were mated with males of *dar1* ^{3232},FRT^{2A}.

For MARCM analyses of *dar1* mutations with the Golgi marker ManII::RFP in C4da neurons, the hs-flp; *ppk-Gal4*, UAS-mCD8::GFP; tubP-Gal80, FRT^{2A} virgins were mated with males of *UAS-ManII::TagRFPt*; *dar1* ^{3232},FRT^{2A}.

For MARCM analyses of *dar1* mutations with the c4da neuropil marker *ppk-CD4::tdTomato*, the hs-flp; *ppk-Gal4*, UAS-mCD8::GFP; tubP-Gal80, FRT^{2A} virgins were mated with males of *ppk-CD4::tdTomato*; *dar1* ^{3232},FRT^{2A}.

For Flip-out analysis of overexpressing Dar1 in es neurons, the UAS-Dar1 virgins were mated with males of hs-flp; *Gal4*$^{21\text{-}7}$; UAS-FRT-CD2stop-FRT-CD8::GFP.

5.5.3 Immunostaining and confocal imaging

Third instar larvae were dissected and immunostained as previously described (36). The primary antibodies include: mouse anti-GFP (Invitrogen, 1:1,000), chick anti-GFP (1: 1,000), rabbit anti-RFP (Rockland, 1:1,000), rat anti-Elav (DSHB, 1:500), guinea pig anti-Dar1 (1:1,000) (36), guinea pig anti-Knot (gift from Adrian Moore, 1:1,000), rat anti-Cut (1:1,000) (82), mouse anti-βGAL (DSHB, 1:100).

Confocal imaging was performed with a Leica TCS SP5 confocal microscope (Leica Microsystems).

5.5.4 Quantifications, statistical analysis

The number of primary dendrites was counted in three-dimensional z-stacks. Neurons in which primary dendrites overlapped with neurites of neighboring neurons were unquantifiable and were excluded. For PDF neurons, neurites shorter than 10μm

were excluded. In all bar charts of quantification: values and error bars indicate mean ±SEM. Sample numbers were indicated. Two-tailed unpaired student t-test was used unless otherwise noted. p values were indicated as: not significant (NS) $p>0.05$, * $p<0.05$, ** $p<0.01$, *** $p<0.001$.

5.5.6 Microarray with purified *Drosophila* PNS neurons and microarray analysis

PNS neurons were labeled with $Gal4^{21\text{-}7}$, UAS-mCD8::GFP and were purified with FACS as previously described (36). For each microarray sample (n=3 for wild-type or *dar1* mutant), total RNA was extracted from approximately 20,000 GFP-positive cells using Trizol (Invitrogen) followed by purification with the RNeasy Micro Kit (Qiagen). cDNA was synthesized and amplified with WT-Ovation Pico RNA amplification System (NuGEN Technologies), followed by biotin-labeling with the Encore Biotin Module (NuGEN Technologies). The biotin-labeled cDNA were hybridized to *Drosophila* Genome 2.0 Array (Affymetrix).

To detect differential expressed genes, Bayesian tests were used and implemented in the limma R package (256). Genes with FDR<0.05 were considered as differentially expressed.

For functional annotation of differential expressed genes, we used the DAVID bioinformatics resource (248). Cellular component GO Terms with Benjamini FDR<0.05 were considered as significantly enriched.

5.6 Acknowledgements

We thank Drs. Cheng-Yu Lee, Yukiko Yamashita, and Hisashi Umemori for critical comments on earlier versions of the manuscript. This work was supported by grants from NIH (R01MH091186), the Whitehall Foundation, and the Pew Scholars Program in the Biological Sciences to B.Y.

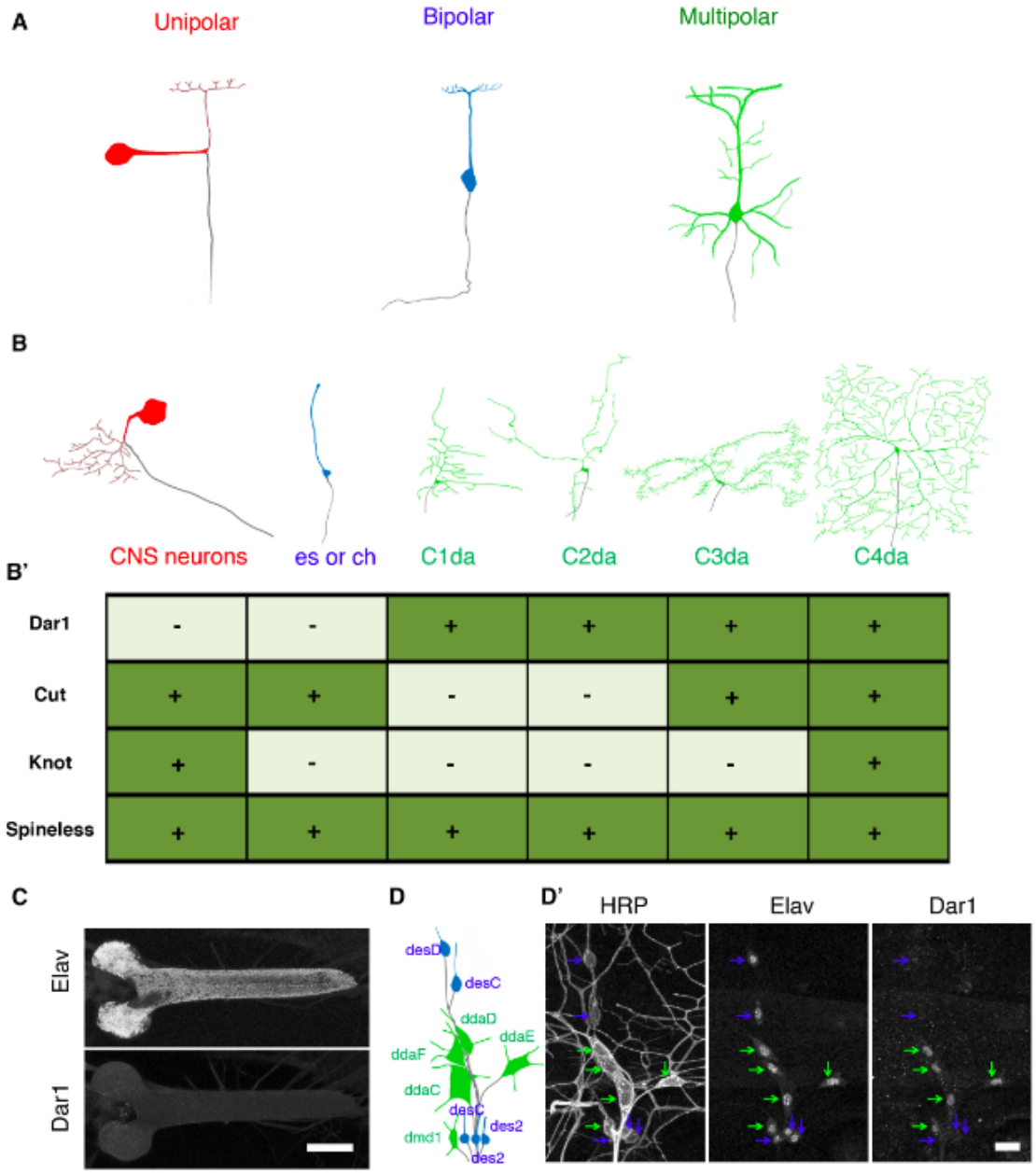

Figure 5.1 Dar1 is selectively expressed in multipolar neurons in *Drosophila* larval nervous system.

(**A**) Schematics of three classifications of neurons observed in the nervous systems across species. (**B**) Tracings of the three neuronal types in *Drosophila* nervous system: unipolar neuron (red) is the tracings of an RN2 neuron located in the ventral nerve chord; bipolar neuron (blue) is the tracings of an es neuron in PNS; multipolar neurons (green) are the tracings of c1-c4da neurons in the peripheral nervous system. (**B'**) Summary of expression patterns of different transcriptional regulators: Dar1, Cut, Knot and Spineless in the three types of neurons. (**C**) Dar1 is absent in CNS. CNS neurons labeled with antibodies against the pan-neuronal protein Elav (top) and Dar1 (bottom). Scale bar= 100 µm. (**D-D'**) Dar1 is exclusively expressed in multipolar neurons in PNS. (**D**) Schematics of the positions of multipolar neurons (green) and bipolar neurons (blue) in an

abdominal-dorsal segment. (**D'**) Dorsal cluster of PNS neurons labeled with antibodies against HRP (left), Elav (middle), and Dar1 (right). Blue arrows: es neurons; green arrows: multipolar neurons. Scale bar= 10 μm.

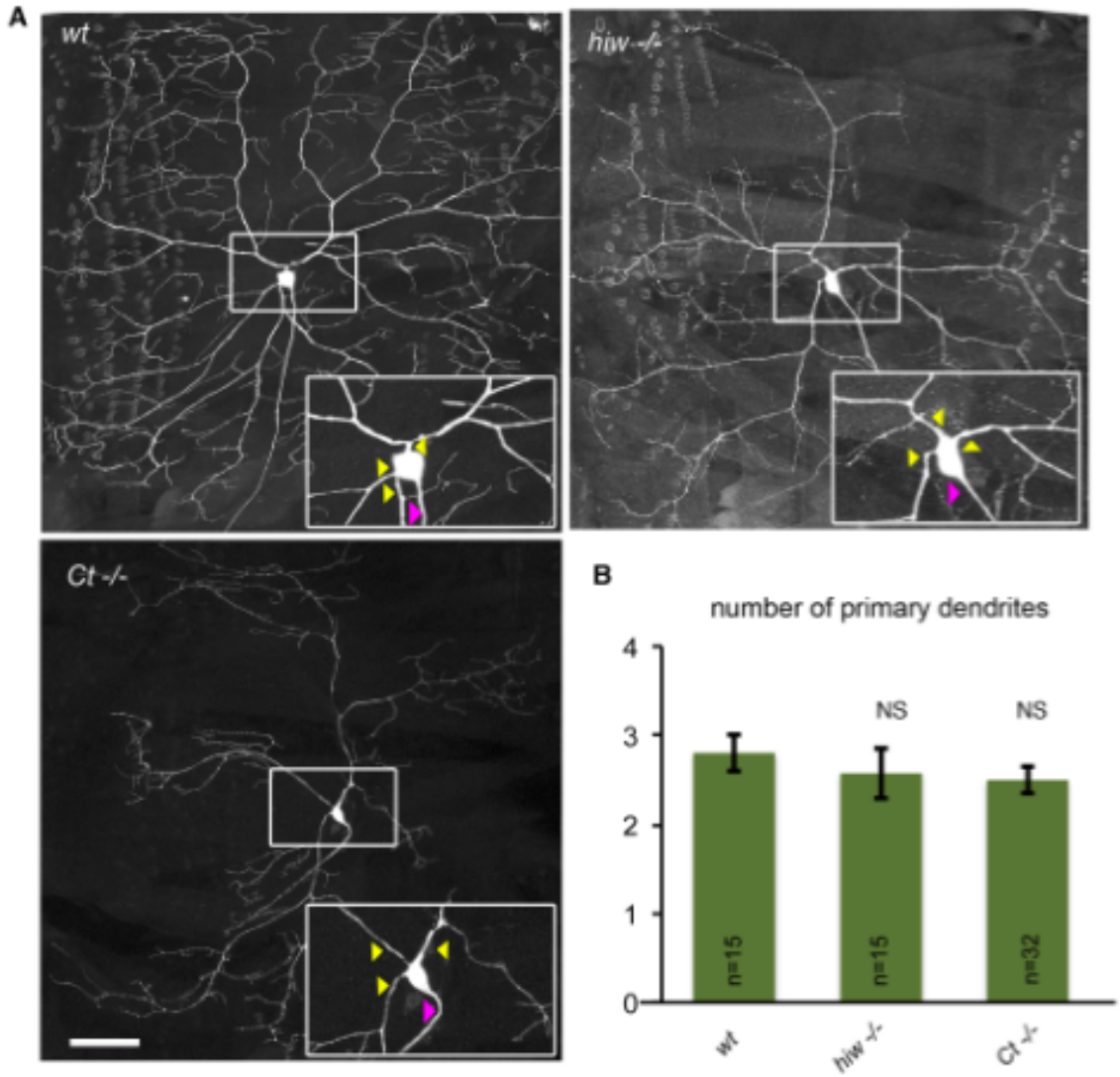

Figure 5.2 Dendritic regulators Hiw and Ct are dispensable for primary dendrites formation.
(**A**) Wild-type (FRT^{19A}), *hiw* $^{\Delta N}$, and *Ct* ^{C145} MARCM clones of c4da ddaC neurons. Scale bar= 50μm. (**B**) Bar chart of quantifications of the number of primary dendrites. Yellow triangles: primary dendrites; magenta triangles: axons.

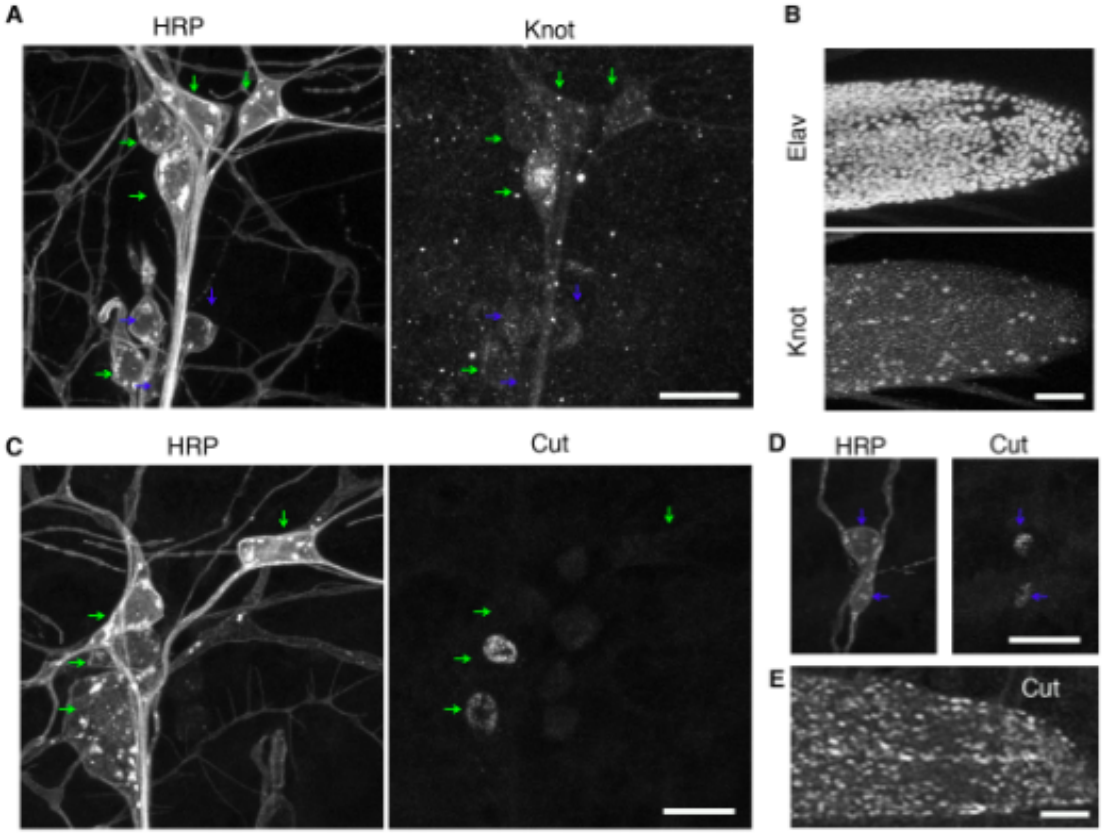

Figure 5.3 Expression patterns of Knot and Cut in *Drosophila* larval nervous system.

(**A**) Dorsal cluster of PNS neurons labeled with antibodies against HRP (left) and Knot (right). Scale bar= 10 µm. (**B**) CNS neurons in the ventral nerve chord labeled with antibodies against Elav (top) and Knot (bottom). Scale bar= 25µm. (**C**) Dorsal cluster of PNS neurons labeled with antibodies against HRP (left) and Cut (right). Scale bar= 10 µm. (**D**) es neurons labeled with antibodies against HRP (left) and Cut (right). Scale bar= 10 µm. (**E**) CNS neurons in the ventral nerve chord labeled with antibodies against Cut. Scale bar= 25µm. Blue arrows: es neurons; green arrows: multipolar neurons.

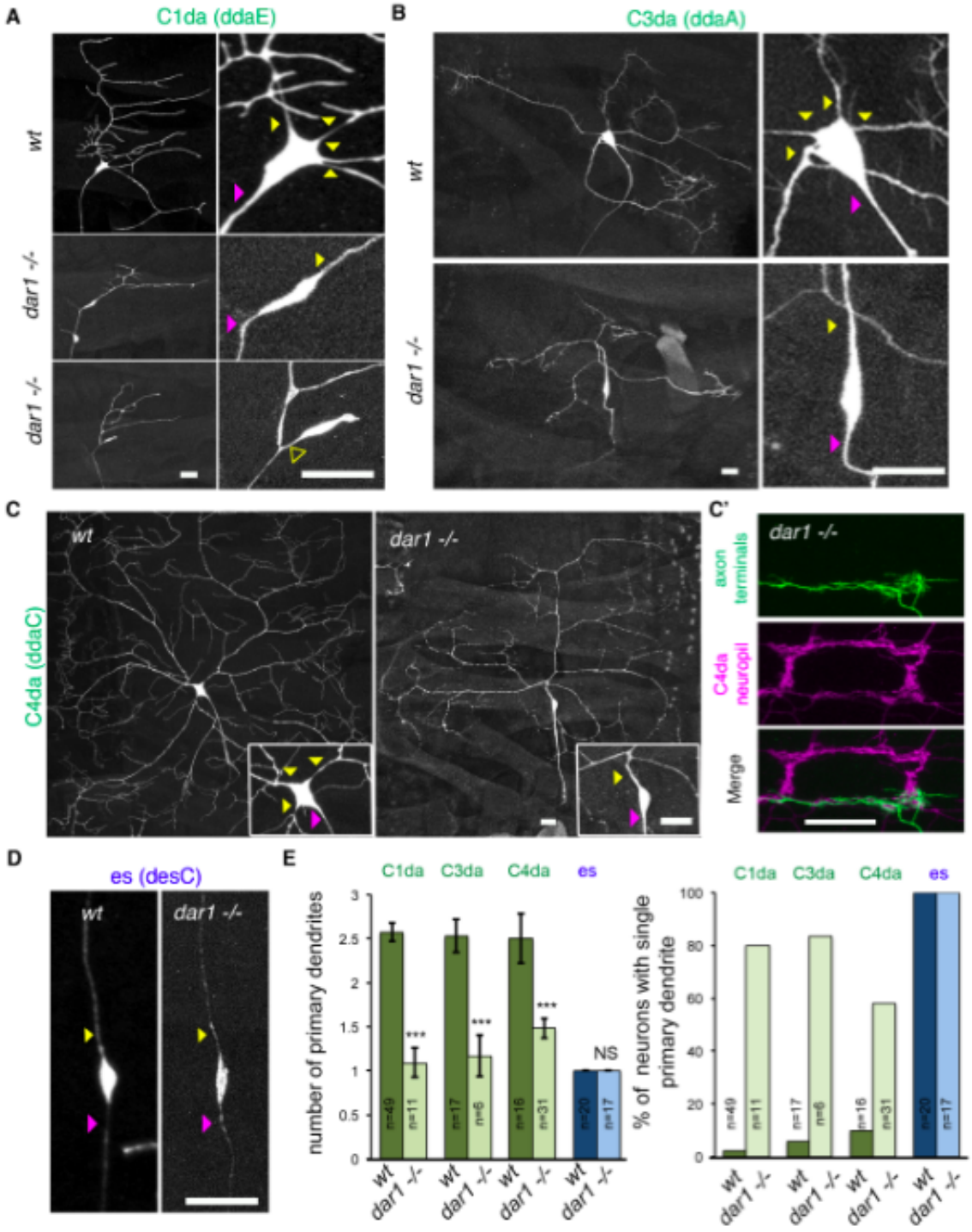

Figure 5.4 Loss of *dar1* converts multipolar to unipolar or bipolar morphology. (**A**) wild-type (top) and *dar1* ^{3232} (middle and bottom) MARCM clones of c1da ddaE neurons. *dar1* mutant ddaE neurons exhibit bipolar (middle) or unipolar (bottom) morphology. (**B**) wild-type (top) and *dar1* ^{3232} (bottom) MARCM clones of c3da ddaA neurons. (**C**) wild-type (left) and *dar1* ^{3232} (right) MARCM clones of c4da ddaC neurons. (**C'**) Representative axon terminals of a *dar1* ^{3232} MARCM clone of c4da vada neuron.

Top: axon terminals labeled with CD8::GFP; middle: C4da neuropil labeled with *ppk-CD4-tdTomato*; bottom: merged image. (**D**) wild-type (left) and *dar1* ^{3232} (right) MARCM clones of es desC neurons. (**E**) Bar charts of quantifications of the number of primary dendrites (left) and percentage of neurons with single dendrites (right) in wild-type and *dar1* ^{3232} MARCM multipolar (green) and bipolar (blue) neurons. Yellow solid triangles: primary dendrites; magenta solid triangles: axons; open triangle: the primary neurite in unipolar neurons. Scale bar= 20 μm.

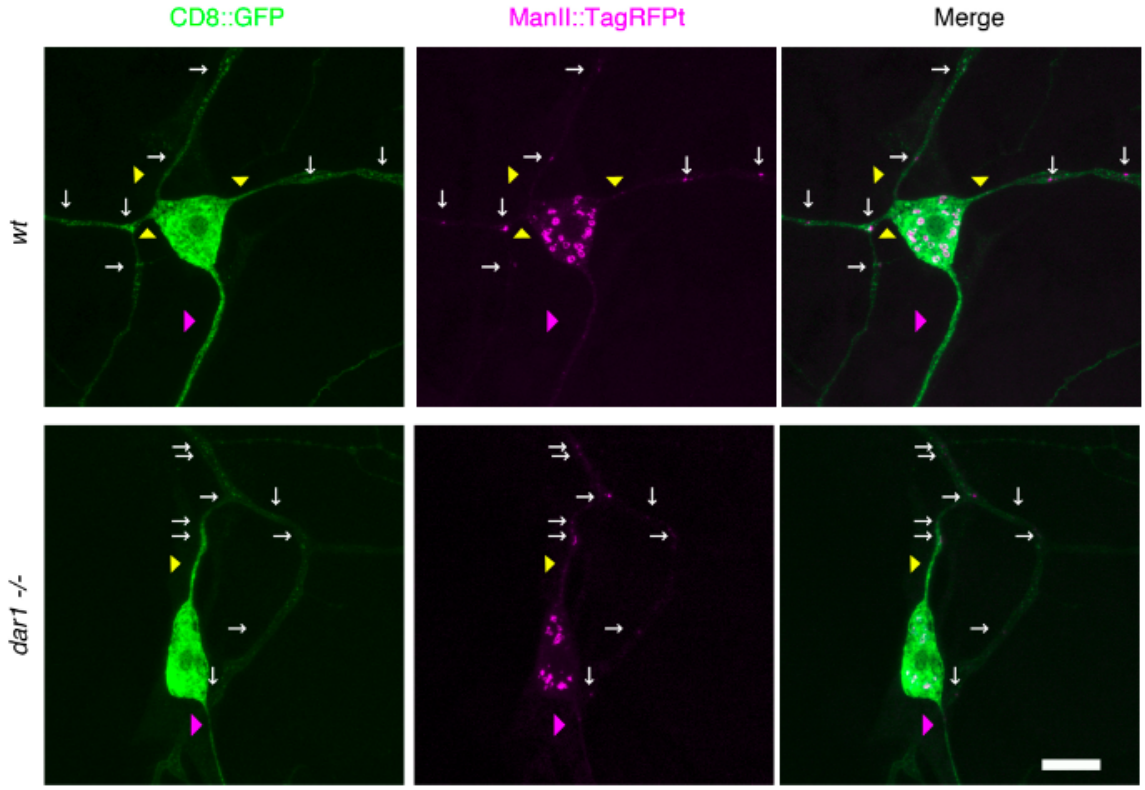

Figure 5.5 Loss of *dar1* did not alter neuronal polarity.
Wild-type (top) and *dar1* ^{3232} (bottom) MARCM clones of c4da ddaC neurons labeled with CD8::GFP (left) and ManII:: TagRFPt (middle). Puncta containing ManII: TagRFPt, which mostly labels soma Golgi and dendritic Golgi outposts are enriched in the dendritic branches but not in axons in both wild-type and *dar1* mutant neurons. Yellow triangles: primary dendrites; magenta triangles: axons; white arrows: dendritic Golgi outposts. Scale bar= 10μm.

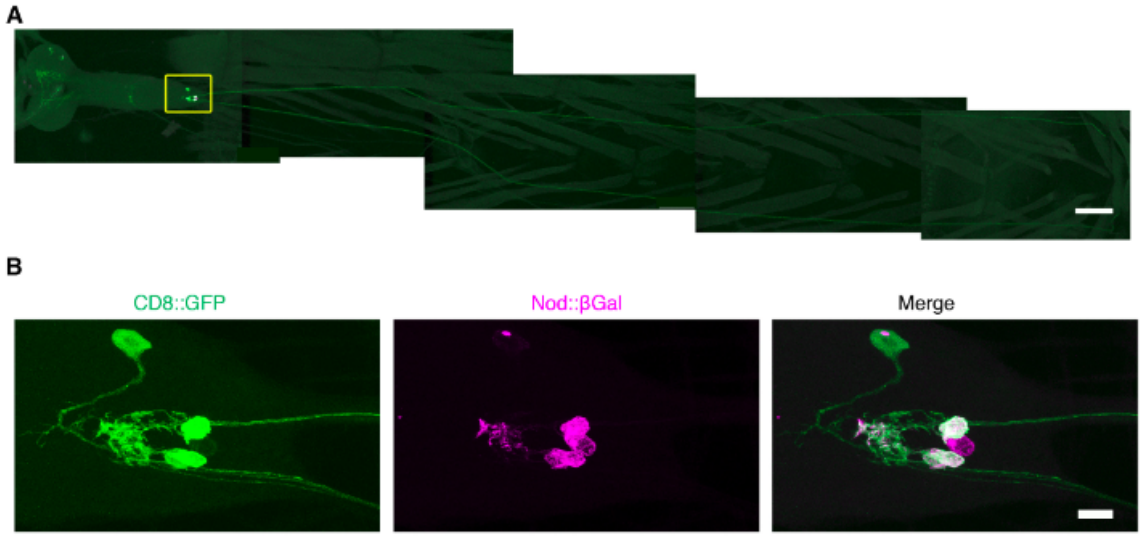

Figure 5.6 RN2 motoneuron morphology.
(A) The soma and dendrites of RN2 neurons are located in the ventral nerve chord, whereas the axons project to the posterior segment of the larva. Scale bar= 100 μm. Yellow box indicates the zoomed area in (B). (B) RN2 neurons labeled with CD8::GFP (left) and a dendritic marker: Nod:: βGal (middle). Scale bar= 10μm.

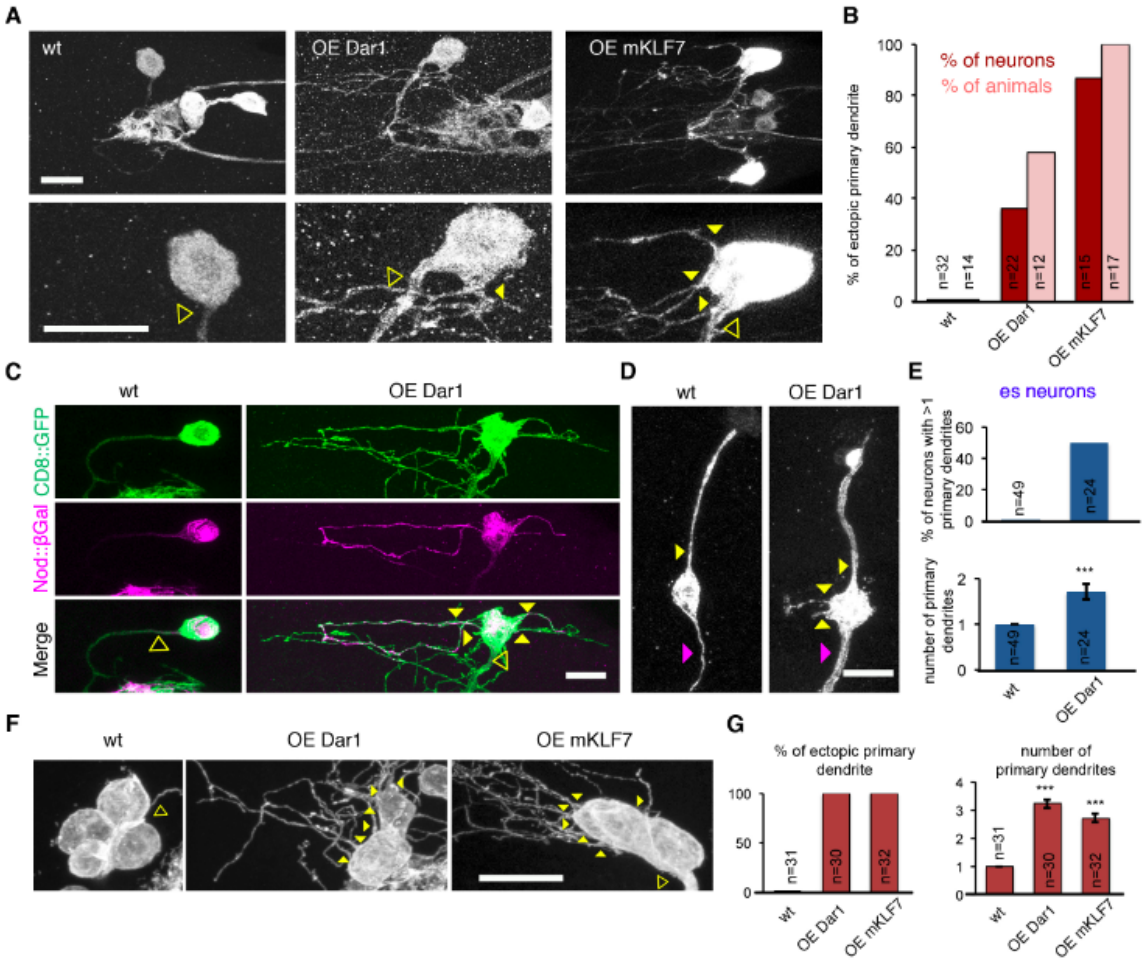

Figure 5.7 Overexpressing Dar1 switches unipolar/bipolar to multipolar morphology.

(**A**) RN2 neurons of wild-type (left), overexpressing Dar1 (middle) and overexpressing mKLF7 (right). (**B**) Bar chart of quantifications of percentage of ectopic primary dendrites in RN2 neurons. (**C**) RN2 neurons of wild-type (left), overexpressing Dar1 (right) labeled with CD8::GFP (top) and a dendritic marker Nod::βGal (middle). (**D**) es neurons of wild-type (left), overexpressing Dar1 (right). (**E**) Bar charts of quantifications of percentage of neurons with more than one primary dendrites (top) and number of primary dendrites (bottom) in es neurons. (**F**) CNS PDF neurons of wild-type (left), overexpressing Dar1 (middle) and overexpressing mKLF7 (right). (**G**) Bar charts of quantifications of percentage of ectopic primary dendrites (left) and number of primary dendrites (right) in PDF neurons. Yellow solid triangles: primary dendrites; magenta solid triangles: axons; open triangles: the primary neurites in unipolar neurons. Scale bar= 10 μm.

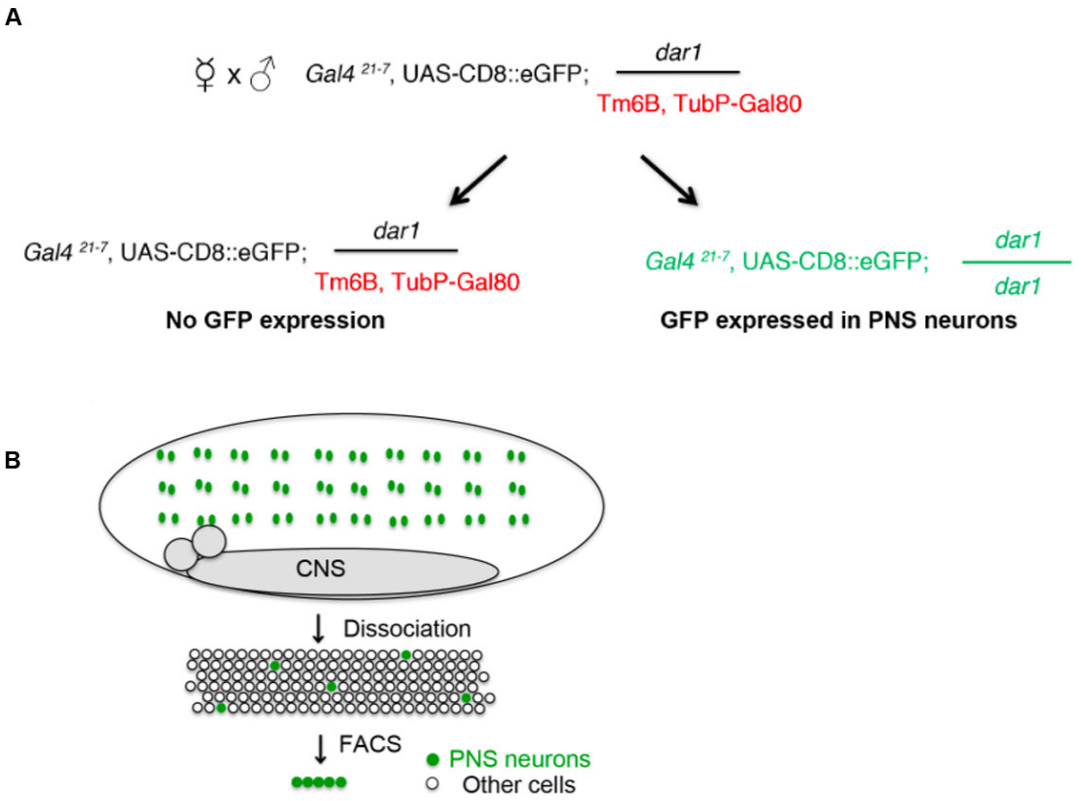

Figure 5.8 Scheme of purifying PNS neurons in *dar1* mutant *Drosophila* embryos. (**A**) Genetic scheme of generating *dar1* mutant embryos of which PNS neurons are labeled with GFP. (**B**) Schematics of purifying PNS neurons with fluorescence activating cell sorting (FACS) in *Drosophila* embryos.

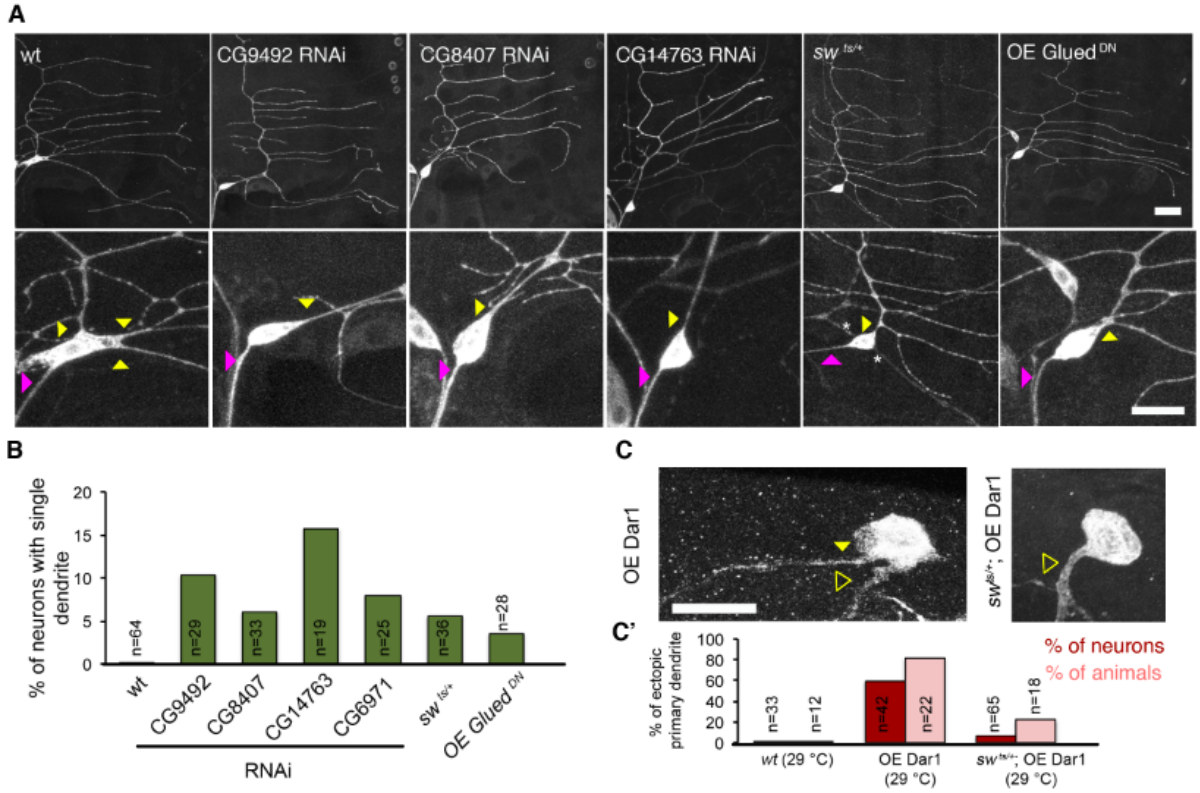

Figure 5.9 Dar1 regulates genes involved in the dynein complex to control primary dendrite formation.

(**A**) c1da ddaE neurons of the following genotypes: 1) wild-type; 2) CG9492 RNAi; 3) CG8407 RNAi; 4) CG14763 RNAi; 5) larvae carrying a temperature-sensitive allele of the dynein intermediate chain, *sw* $^{ts/+}$ at non-permissive temperature 25 °C; 6)overexpressing a dominant negative form of dynactin (OE Glued ^{DN}). The RNAi transgenes were driven by either *Elav-Gal4* or *Gal4* $^{2\text{-}21}$ along with *UAS-Dcr2*; the Glued ^{DN} transgene was driven by *Gal4* $^{2\text{-}21}$. *UAS-Dcr2* driven by *Gal4* $^{2\text{-}21}$ was used as control. Yellow triangles: primary dendrites; magenta triangles: axons; asterisks: dendrites of a neighboring ddaC neuron. Scale bar= 20 µm. (**B**) Bar chart of quantifications of percentage of neurons with single primary dendrites. (**C**) RN2 neurons of overexpressing Dar1 (left) and overexpressing Dar1 in *sw* ^{ts} heterozygous background (right). The animals were raised at non-permissive temperature 29 °C. Yellow solid triangles: primary dendrites; open triangles: primary neurites. Scale bar= 10µm. (**C'**) Bar chart of quantifications of percentage of ectopic primary dendrites in RN2 neurons of denoted genotypes.

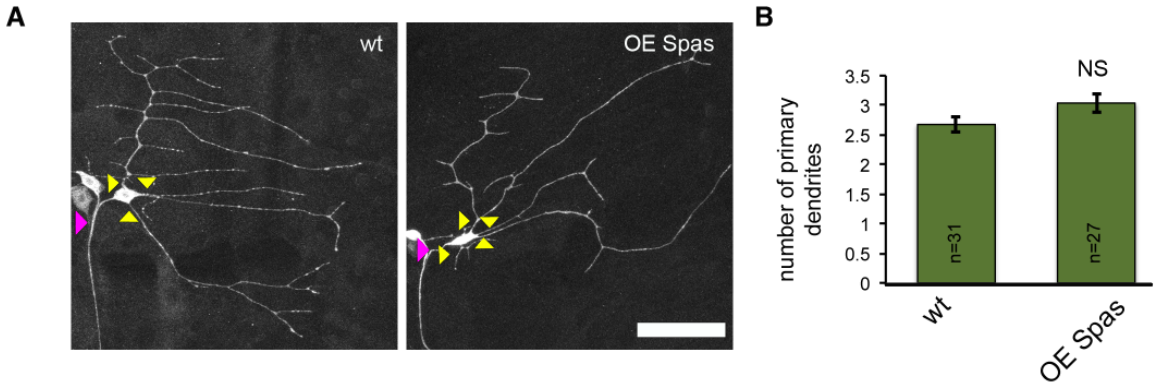

Figure 5.10 Overexpressing Spastin did not alter the number of primary dendrites. (**A**) wild-type (left) and overexpressing Spastin (right) c1da ddaE neurons. Yellow triangles: primary dendrites; magenta triangles: axons. Scale bar= 50µm. (**B**) Bar chart of quantifications of the number of primary dendrites.

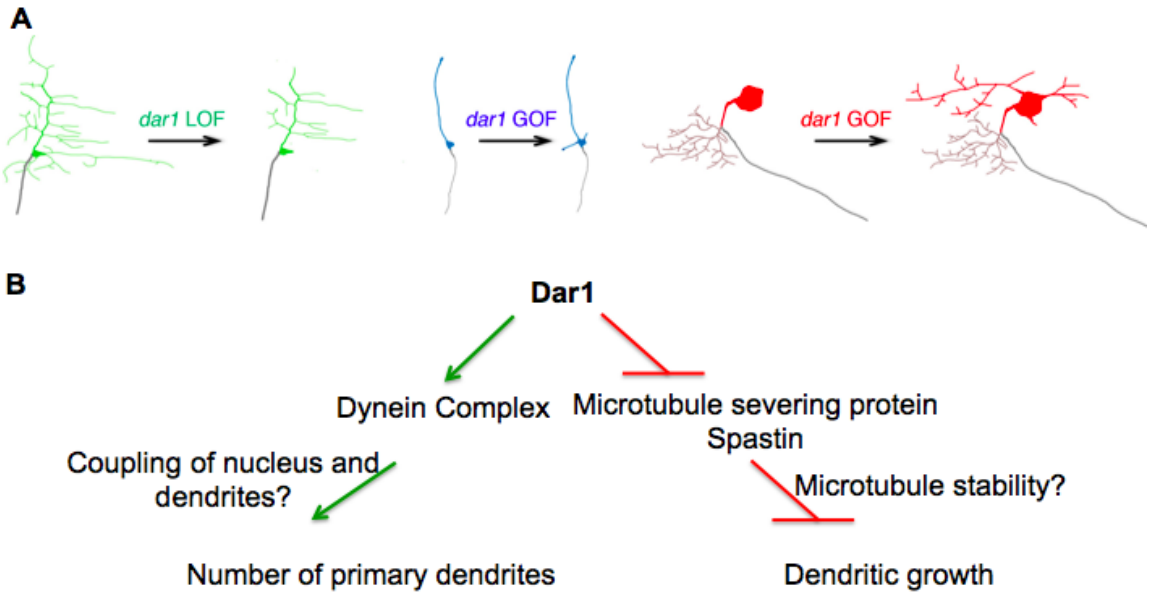

Figure 5.11 A schematic model showing Dar1 switches multipolar and unipolar or bipolar neuron morphology.
(**A**) Loss of *dar1* in multipolar neurons caused bipolar or unipolar morphology. Overexpressing Dar1 in bipolar or unipolar neurons led to multipolar morphology. Green: multipolar ddaE neurons; blue: bipolar es neurons; red: unipolar RN2 neurons.
(**B**) As a transcription factor, Dar1 regulates the transcription of several genes invovled in the dynein complex and the microtubule severing protein Spastin. Based on mammalian studies, it is speculated that dynein determines primary dendrite number by coupling nucleus-dendrite positions. In contrast, overexpressing Spastin caused impaired dendritic growth without affecting the number of primary dendrites. Collectively, Dar1 likely regulates divergent transcriptional targets for controling primary dendrites formation and dendritic growth.

GOTERM_CC	Fold enrichment	FDR
GO:0015630 microtubule cytoskeleton	2.39	0.005
GO:0030286 dynein complex	5.17	0.007
GO:0044430 cytoskeletal part	2.09	0.009
GO:0005856 cytoskeleton	1.88	0.017
GO:0005874 microtubule	3.04	0.018
GO:0005930 axoneme	8.25	0.018
GO:0044463 cell projection part	4.01	0.018
GO:0005875 microtubule associated complex	2.73	0.02
GO:0005858 axonemal dynein complex	9.63	0.029

Table 5.1 Significantly enriched Gene Ontology terms (cellular components) between wild-type and *dar1*^{3232} mutant microarrays.

Gene Symbol	Molecular Function	Fold change	FDR
Dhc36C	dynein heavy chain	-3.62	0.0006
CG6971	dynein light chain	-4.12	0.0008
CG6053	dynein complex	-2.67	0.0008
CG9068	dynein heavy chain	-2.34	0.0013
CG14838	dynein complex	-2.18	0.0035
CG9492	dynein heavy chain	-2.7	0.0041
Dhc93AB	dynein heavy chain	-3.08	0.0041
CG14763	dynein complex	-1.87	0.0114
Dhc16F	dynein heavy chain	-2.11	0.0023
robl	dynein light chain	-1.03	0.0255
CG8407	dynein light chain	-2.98	0.0008
Spas	microtubule severing protein	1.13	0.0368

Table 5.2 Summary of differentially expressed microtubule-associated genes between wild-type and *dar1*^{3232} embryonic PNS neurons

Chapter 6
Significance and implications

Dendrites and the axon are two separate compartments of the same neuron that are specialized for receiving and distributing information respectively. The discovery of molecular determinants of such two-part design provides insights into our understanding of neural circuit wiring and the pathogenesis of neurological diseases. In Chapters 2-5, I have presented three molecular mechanisms that differentially regulate dendritic and axonal growth in vivo. These studies have provided novel paradigms to be further tested in both the *Drosophila* and mammalian nervous systems. In this chapter, I will discuss the functional relevance and future directions of this thesis.

6.1 DLK/Wnd level might underlie the diversity of neuronal morphology

Different neuron types exhibit distinctive relative sizes of dendritic and axonal arbors. For instance, the cerebellar Purkinje neurons have a remarkably large dendritic arbor but a relatively small axonal arbor. In contrast, the cerebellar granule neurons have a dendritic arbor that is smaller than the axonal arbor. Such remarkable diversity was described more quantitatively by Craig et al. (1994): the ratio of dendrite and axon surface areas of a spinal motoneuron was estimated 1:13, in contrast that of a dentate granule cell was approximately 4.7:1 (2). Despite these observations, there is no unifying theory explaining how the diversity of neuron morphology is achieved in the nervous system.

The results presented in Chapter 2 show that high levels of DLK/Wnd inhibit dendritic growth but induce axonal overgrowth. We speculate that the relative sizes of the dendritic and axonal arbors of a neuron are controlled by DLK/Wnd protein abundance (Figure 6.1). This hypothesis predicts that, in neuron types with high DLK/Wnd

expression or activity, the dendritic arbor would be smaller than the axonal arbor, and vice versa (Figure 6.1).

C4da neurons have large dendritic arbors but small axonal arbors; the total dendritic length is almost 10-fold as the axonal length of C4da neurons in third instar larvae (5). Consistent with our hypothesis (Figure 6.1), we found that Wnd protein is undetectable in C4da neurons and loss of *wnd* did not elicit dramatic changes in either dendritic or axonal growth. To test the reverse scenario, the dendritic and axonal morphologies of additional neuron types need to be characterized. Wnd level is predicted to be high in the types of neurons with elaborative axonal arbors but simple dendritic branches. If so, loss of *wnd* would potentiate dendritic growth but impair axonal growth in such neuron types. Moreover, it will be informative to test this paradigm in mammalian brain. Further experiments will address whether DLK levels vary among different types of neurons, such as Purkinje neurons versus granule cells in the cerebellar, and how changes in DLK expression alter the dendritic and axonal sizes in these neurons.

6.2 DLK/Wnd might coordinate dendritic and axonal growth during development.

Dendritic and axonal growth rates vary at different stages of neuronal polarization. For instance, the axon often grows more rapidly than the dendrites in the early developmental events (2, 3, 5). In C4da neurons, we also observed different time windows for rapid dendritic growth phase and axonal growth phase. At late stage 15 or early stage 16 during embryogenesis, the axons of C4da neurons already projected into the ventral nerve chord and started to extend presynaptic terminals (Figure 6.2 A and B). At this time, few dendrites were detected (Figure 6.2 A and B). By the end of stage 16, the axon terminals finished forming the ladder-like structures (Figure 6.2C), as observed in 3rd instar larvae (Figure 2.1), and the dendrites start to grow extensively (Figure 6.2 C and D). Collectively, C4da neurons seem to first engage in axonal growth during embryogenesis, and then switch to prefer dendritic growth in larval stages (Figure 6.2E). Little is known about the temporal codes switching rapid axonal growth phase to rapid dendrite growth phase.

Interestingly, Wnd expression level is developmentally regulated. Wnd protein level decreases dramatically between stage 16 embryos and larval stages (45). The

correlation between the timing of changes in Wnd protein level and that of the changes in dendritic and axonal growth rates raised the possibility that Wnd temporally coordinates dendritic and axonal growth (Figure 6.2E). During embryogenesis when Wnd is relatively abundant, Wnd acts as a bimodal regulator (41) (See chapter 2) to promote axonal growth but restrict dendritic growth. When Wnd protein level decreases, possibly degraded by Hiw (45), the dendrites get rid of the negative regulation by Wnd and grow more rapidly than the axon.

To test this hypothesis, we need to analyze the consequences of loss of *wnd* in early embryogenesis. In the absence of Wnd, it is predicted that projection of axons into CNS and the formation of presynaptic terminals would be inhibited or delayed; whereas the dendrites would outgrow before axonal terminals are fully extended. A technical difficulty for this experiment is to remove the maternal contribution of Wnd in embryos. Because *wnd* homozygous mutant females are sterile or infertile, we need to generate *wnd* mutant germ line clones to remove the maternal contributions.

6.3 DLK/Wnd might coordinate dendritic and axonal growth after injury.

As a bimodal regulator, DLK/Wnd might coordinate dendritic and axonal growth not only during development but also in respond to axon injury. Previous studies observed an increase in DLK/Wnd protein level after nerve crush in both *Drosophila* motor neurons (51) and mouse optic nerves (50). Based on our study in Chapter 2 (41), increased DLK/Wnd level likely results in a reduction in dendritic size of injured neurons while promoting axonal regeneration (Figure 6.3). Indeed, axotomy not only triggers axon regeneration but also makes dendrites more simplified in C4da neurons (93) and mammalian neurons (94, 95). These observations suggest that neurons might engage in axonal regeneration at the expense of dendritic loss. To test the involvement of DLK/Wnd in inducing these subsequent changes in dendritic and axonal morphologies after injury, it needs further analyses of the dendritic and axonal responses to injury in *wnd* mutant neurons. To assess the direct consequences of Wnd upregulation by injury, it will be ideal to generate a temperature sensitive allele of *wnd* so that we can introduce *wnd* mutations immediately after injury.

6.4 Genetic dissection of the downstream components of DLK/Wnd in dendritic and axonal development

As a mitogen activated protein Kinase Kinase Kinase (MAPKKK), DLK/Wnd likely performs diverse functions through multiple downstream MAP Kinases. In Chapter 3, we identified independent downstream components of Wnd that mediate its roles in synaptic growth, injury response and axonal transport (54). The MAPK p38b and the scaffolding protein JIP1 act downstream to Wnd to control synaptic growth. Mutations in *p38b* or *jip1* disrupted synaptic microtubule organization and synaptic morphology, which is similar to that caused by *wnd* loss of function (54). In parallel, the MAPK JNK is required for injury responses such as axonal regeneration but not in synaptic development (54).

It remains unclear Wnd requires which MAPK(s) or scaffolding proteins in differentiating dendritic growth versus axonal growth. In Chapter 2, we found that Wnd requires the transcriptional factor Fos for axonal regulation, and the transcriptional factor Knot for dendritic regulation. We speculated that the MAPK JNK is involved in the axonal regulation, because biochemistry studies demonstrated JNK phosphorylates Fos (79). Indeed, loss of the *Drosophila* JNK homolog, *bsk* rescued the axonal overgrowth but not dendritic reduction caused by OE Wnd (data not shown), suggesting that JNK specifically mediates the axonal regulation (Figure 6.4). Further genetic and biochemistry studies will determine whether p38b, JIP1 or other MAP kinases and scaffolding proteins are required for the dendritic regulation. It is possible that MAP kinases, such as p38b, might suppress Knot level/activity by phosphorylation to restrict dendritic growth (Figure 6.4).

6.5 How DLK/Wnd regulates Dscam translation via the 3'UTR of *Dscam* mRNA

In Chapter 4, we identified a novel function of DLK/Wnd in controlling Dscam expression level through the 3'UTR of *Dscam* mRNA (257). We speculated that DLK/Wnd might require RNA binding proteins to act on the 3'UTR, and tested the involvement of an RNA binding protein: FMRP. Our results suggest FMRP acts on the coding region instead of the 3'UTR of *Dscam* mRNA, and thus functions in parallel to

DLK/Wnd. Additional RNA binding proteins will be tested in order to understand how DLK/Wnd regulates the 3'UTR of *Dscam* mRNA.

There are several hundreds of RNA binding proteins in *Drosophila* (258), which is feasible to screen in vitro. We will use EGFP-*Dscam* 3'UTR as a reporter whose expression was enhanced by DLK/Wnd in S2 cell culture (257). If knockdown of any RNA binding protein blocks the increase in reporter expression level by Wnd, we will further characterize their endogenous function in vivo. Considering the functional relevance of dysregulated Dscam expression in diseases, identifying additional regulatory components of Dscam translation will provides insights into developing treatment of neurological diseases in which Dscam expression is increased, such as Down syndrome.

6.6 The roles of mammalian KLFs in determining multipolar dendritic structures

The three morphological types of neurons exist in both invertebrate and vertebrate. Our study in Chapter 5 demonstrated that the *Drosophila* Krüppel-like factor (KLF), Dar1determines the multipolar morphology. The fact that overexpressing mouse KLF7 converted unipolar into multipolar neurons in *Drosophila* (See Chapter 5) raised the possibility that KLFs might perform conserved functions across species.

In the mammalian nervous system, the majority of CNS neurons are multipolar, such as pyramidal neurons. The retinal neurons are bipolar and the mature dorsal root ganglion (DRG) neurons usually take unipolar morphology. The molecular determinant of these three basic types is unknown in mammals. Further studies will examine the expression patterns of mKLF(s) in these different neuron types and assess the morphological changes caused by loss-of-function and gain-of-function of KLF(s). In addition, there are 17 KLF(s) in mouse (259), which likely perform diverse roles in determining dendritic structure types.

6.7 Summary

The separation of dendrites and the axon is crucial for information processing in the nervous system. The molecular understanding of dendritic and axonal development has expanded from recent decades of studies. My thesis studies have identified three intrinsic molecular mechanisms that differentiate the growth of these two compartments

in *Drosophila*; and their mammalian homologs possibly perform conserved functions. Moreover, this thesis provides insights into understanding the diversity of neuron morphologies and developing treatment for neurological diseases.

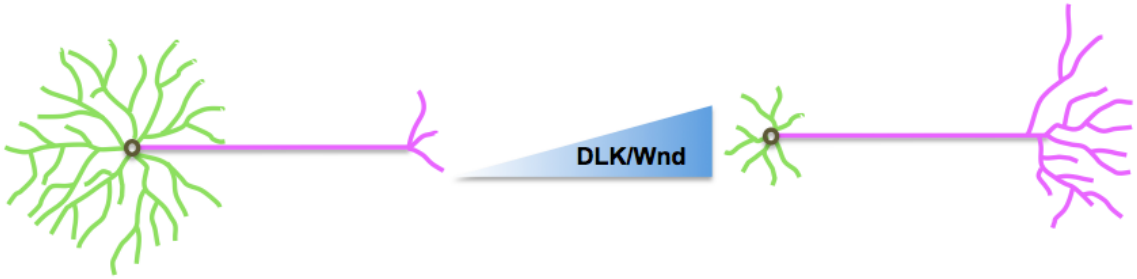

Figure 6.1 A schematic model illustrating that DLK/Wnd level underlies diversity of dendritic and axonal structures.
On the left is an illustration of types of neuron with complex dendrites and simple axonal arbor (e.g. C4da neuron in *Drosophila*, Purkinje neurons in mammals). On the right is an illustration of types of neuron with and exuberant axonal structures (e.g. mammalian cerebellar granule neurons). Different levels of DLK/Wnd may contribute to such morphological diversity. Low levels of DLK/Wnd lead to larger dendritic size than axonal size, whereas high levels of DLK/Wnd result in larger axonal size thant dendritic size. The dark circle indicates the soma; the green and magenta processes indicate the dendrites and the axon respectively. The blue gradient triangle indicates the protein level or activity of DLK/Wnd.

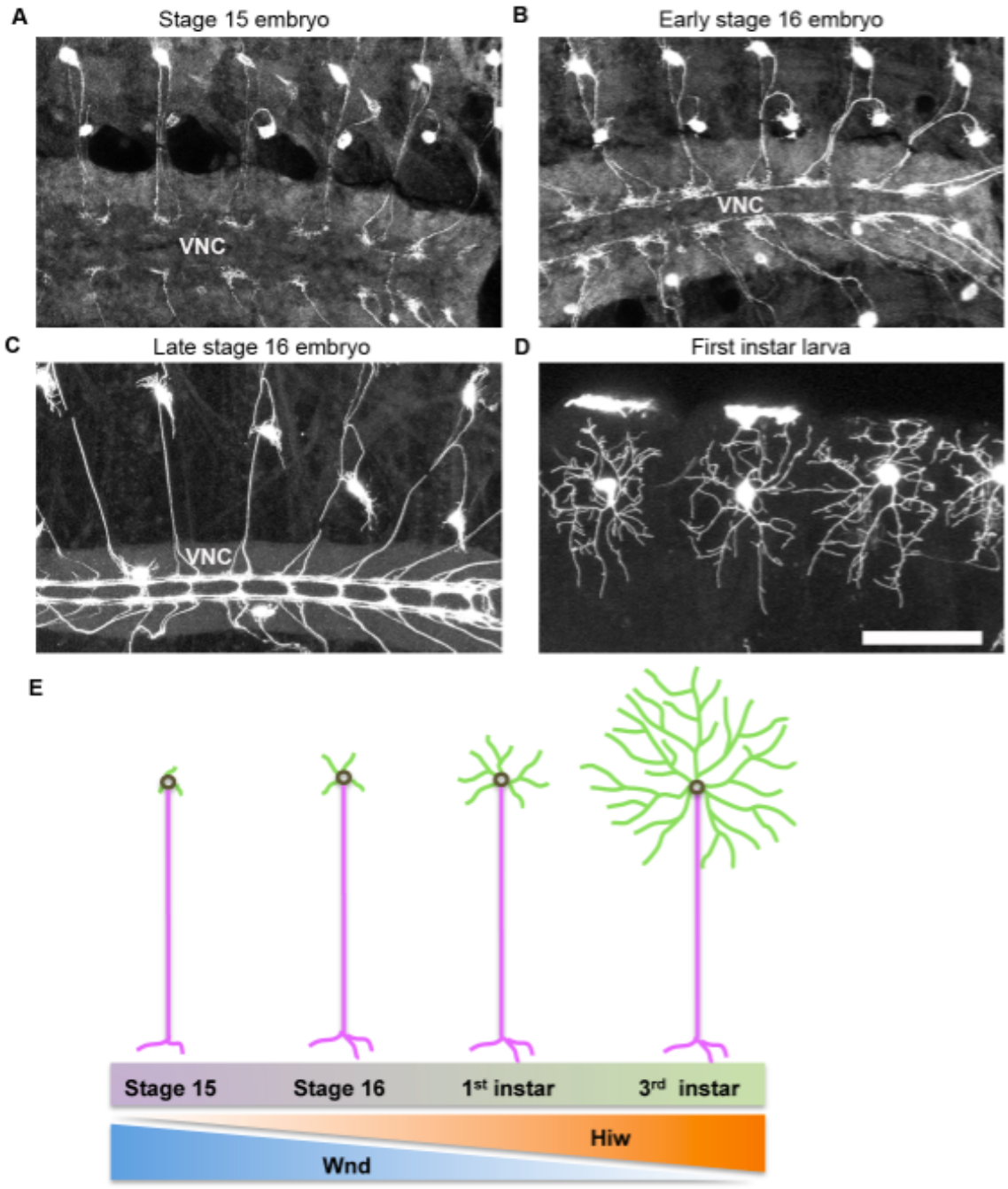

Figure 6.2 Wnd protein level might serve as a temporal code coordinating dendritic and axonal growth.
(A-C) Shown are C4da neuron morphology visualized by *ppk-CD4-tdGFP* in embryonic stages 15-16. The C4da axons grew rapidly into ventral nerve chord (vnc) and extended presynaptic arbors in this developmental stage. (D) Shown are C4da dendrites visualized by *ppk-CD4-tdGFP* in a first instar larva. Note that the dendrites were much more elaborated as compared to those in the embryos. Scale bar=50 μm. (E) A schematic model illustrating Wnd coordinates dendritic and axonal growth during development.

Axons grow more rapidly in embryos, whereas dendrites grow more extensively in larval stage. Interestingly, Wnd protein level (represented in blue triangle) is higher in embryos than larvae. It is speculated that the change in Wnd protein abundance results in a switch of preference from axonal growth into dendritic growth in C4da neurons.

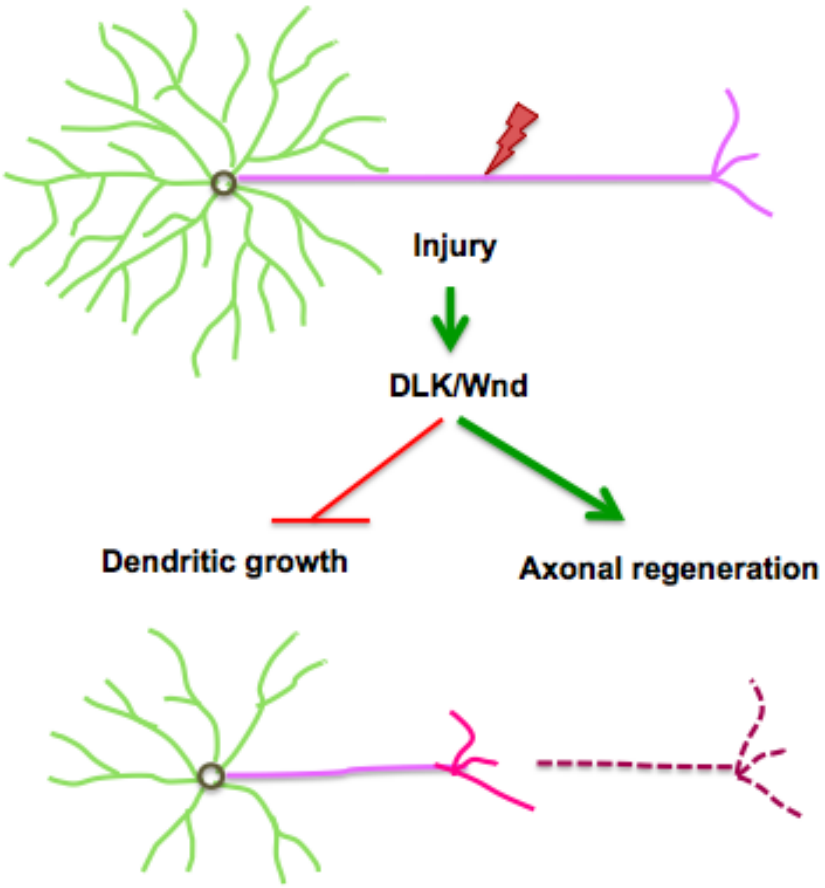

Figure 6.3 A schematic model illustrating that DLK/Wnd coordinates dendritic and axonal responses to injury.
Axonal injury resulted an increase in DLK/Wnd protein level, which consequently promotes axonal regeneration but causes dendritic retraction. The injured neuron might redistribute cytoskeleton components or membrane supplies to facilitate axonal regeneration. The dark circle indicates the soma; the green and magenta processes indicate the dendrites and the axon respectively. The dashed processes indicate degenerating axons distal to injury site, and the pink processes indicate newly regenerated axonal branches.

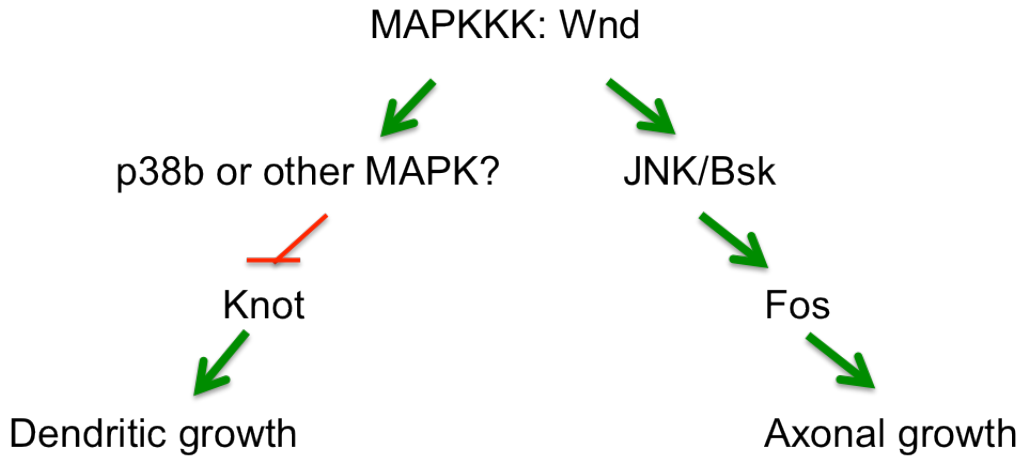

Figure 6.4 Independent downstream pathways of Wnd in regulating dendritic and axonal growth.
Wnd plays diverse roles in neuronal development and neuronal responses to injury. Chapter 3 has found that MAP Kinases p38b and JNK mediate Wnd functions in synaptic growth and axonal regeneration respectively. It remains unclear whether different MAPKs are also involved in the bimodal control of Wnd in differentiating dendritic and axonal growth. We hypothesize that the MAPK JNK specifically mediates the axonal regulation, whereas another MAPK, such as p38b, might regulate dendritic growth via phosphorylating the transcription factor Knot.

BIBLIOGRAPHY

1. Caceres A, Ye B, & Dotti CG (2012) Neuronal polarity: demarcation, growth and commitment. *Curr Opin Cell Biol* 24(4):547-553.
2. Craig AM & Banker G (1994) Neuronal polarity. *Annu Rev Neurosci* 17:267-310.
3. Dotti CG, Sullivan CA, & Banker GA (1988) The establishment of polarity by hippocampal neurons in culture. *J Neurosci* 8(4):1454-1468.
4. Pollarolo G, Schulz JG, Munck S, & Dotti CG (2011) Cytokinesis remnants define first neuronal asymmetry in vivo. *Nat Neurosci* 14(12):1525-1533.
5. Ye B*, et al.* (2007) Growing dendrites and axons differ in their reliance on the secretory pathway. *Cell* 130(4):717-729.
6. de Anda FC*, et al.* (2005) Centrosome localization determines neuronal polarity. *Nature* 436(7051):704-708.
7. Basto R*, et al.* (2006) Flies without centrioles. *Cell* 125(7):1375-1386.
8. Zolessi FR, Poggi L, Wilkinson CJ, Chien CB, & Harris WA (2006) Polarization and orientation of retinal ganglion cells in vivo. *Neural Dev* 1:2.
9. Stiess M*, et al.* (2010) Axon extension occurs independently of centrosomal microtubule nucleation. *Science* 327(5966):704-707.
10. Distel M, Hocking JC, Volkmann K, & Koster RW (2010) The centrosome neither persistently leads migration nor determines the site of axonogenesis in migrating neurons in vivo. *J Cell Biol* 191(4):875-890.
11. Oliva AA, Jr., Atkins CM, Copenagle L, & Banker GA (2006) Activated c-Jun N-terminal kinase is required for axon formation. *J Neurosci* 26(37):9462-9470.
12. Shi SH, Jan LY, & Jan YN (2003) Hippocampal neuronal polarity specified by spatially localized mPar3/mPar6 and PI 3-kinase activity. *Cell* 112(1):63-75.
13. Menager C, Arimura N, Fukata Y, & Kaibuchi K (2004) PIP3 is involved in neuronal polarization and axon formation. *J Neurochem* 89(1):109-118.
14. Shi SH, Cheng T, Jan LY, & Jan YN (2004) APC and GSK-3beta are involved in mPar3 targeting to the nascent axon and establishment of neuronal polarity. *Curr Biol* 14(22):2025-2032.
15. Shelly M, Cancedda L, Heilshorn S, Sumbre G, & Poo MM (2007) LKB1/STRAD promotes axon initiation during neuronal polarization. *Cell* 129(3):565-577.
16. Shelly M*, et al.* (2010) Local and long-range reciprocal regulation of cAMP and cGMP in axon/dendrite formation. *Science* 327(5965):547-552.
17. Shelly M*, et al.* (2011) Semaphorin3A regulates neuronal polarization by suppressing axon formation and promoting dendrite growth. *Neuron* 71(3):433-446.
18. Barnes AP*, et al.* (2007) LKB1 and SAD kinases define a pathway required for the polarization of cortical neurons. *Cell* 129(3):549-563.

19. Kishi M, Pan YA, Crump JG, & Sanes JR (2005) Mammalian SAD kinases are required for neuronal polarization. *Science* 307(5711):929-932.
20. Ori-McKenney KM, Jan LY, & Jan YN (2012) Golgi outposts shape dendrite morphology by functioning as sites of acentrosomal microtubule nucleation in neurons. *Neuron* 76(5):921-930.
21. Zheng Y*, et al.* (2008) Dynein is required for polarized dendritic transport and uniform microtubule orientation in axons. *Nat Cell Biol* 10(10):1172-1180.
22. Stone MC, Roegiers F, & Rolls MM (2008) Microtubules have opposite orientation in axons and dendrites of Drosophila neurons. *Mol Biol Cell* 19(10):4122-4129.
23. Yan J*, et al.* (2013) Kinesin-1 regulates dendrite microtubule polarity in Caenorhabditis elegans. *Elife* 2:e00133.
24. Goldberg JL (2004) Intrinsic neuronal regulation of axon and dendrite growth. *Current opinion in neurobiology* 14(5):551-557.
25. Jan Y-N & Jan LY (2010) Branching out: mechanisms of dendritic arborization. *Nat Rev Neurosci* 11(5):316-328.
26. Wang X & Ye B (2012) Transcriptional regulators that differentially control dendrite and axon development. *Front Biol* 7(4):292-296.
27. Gaudillière B, Konishi Y, de la Iglesia N, Yao Gl, & Bonni A (2004) A CaMKII-NeuroD signaling pathway specifies dendritic morphogenesis. *Neuron* 41(2):229-241.
28. Lein P, Johnson M, Guo X, Rueger D, & Higgins D (1995) Osteogenic protein-1 induces dendritic growth in rat sympathetic neurons. *Neuron* 15(3):597-605.
29. Withers GS, Higgins D, Charette M, & Banker G (2000) Bone morphogenetic protein-7 enhances dendritic growth and receptivity to innervation in cultured hippocampal neurons. *Eur J Neurosci* 12(1):106-116.
30. Ikeuchi Y*, et al.* (2009) A SnoN-Ccd1 pathway promotes axonal morphogenesis in the mammalian brain. *J Neurosci* 29(13):4312-4321.
31. Golic KG & Lindquist S (1989) The FLP recombinase of yeast catalyzes site-specific recombination in the Drosophila genome. *Cell* 59(3):499-509.
32. Xu T & Rubin GM (1993) Analysis of genetic mosaics in developing and adult Drosophila tissues. *Development* 117(4):1223-1237.
33. Lee T & Luo L (1999) Mosaic analysis with a repressible cell marker for studies of gene function in neuronal morphogenesis. *Neuron* 22(3):451-461.
34. Grueber WB, Ye B, Moore AW, Jan LY, & Jan YN (2003) Dendrites of distinct classes of Drosophila sensory neurons show different capacities for homotypic repulsion. *Curr Biol* 13(8):618-626.
35. Lee MC, Miller EA, Goldberg J, Orci L, & Schekman R (2004) Bi-directional protein transport between the ER and Golgi. *Annu Rev Cell Dev Biol* 20:87-123.
36. Ye B*, et al.* (2011) Differential regulation of dendritic and axonal development by the novel Krüppel-like factor Dar1. *J Neurosci* 31(9):3309-3319.
37. Luo L, Liao YJ, Jan LY, & Jan YN (1994) Distinct morphogenetic functions of similar small GTPases: Drosophila Drac1 is involved in axonal outgrowth and myoblast fusion. *Genes Dev* 8(15):1787-1802.
38. Hall A (1994) Small GTP-binding proteins and the regulation of the actin cytoskeleton. *Annu Rev Cell Biol* 10:31-54.

39. Luo L*, et al.* (1996) Differential effects of the Rac GTPase on Purkinje cell axons and dendritic trunks and spines. *Nature* 379(6568):837-840.
40. Soba P*, et al.* (2007) Drosophila sensory neurons require Dscam for dendritic self-avoidance and proper dendritic field organization. *Neuron* 54(3):403-416.
41. Wang X*, et al.* (2013) Bimodal control of dendritic and axonal growth by the dual leucine zipper kinase pathway. *PLoS Biol* 11(6):e1001572.
42. Polleux F, Morrow T, & Ghosh A (2000) Semaphorin 3A is a chemoattractant for cortical apical dendrites. *Nature* 404(6778):567-573.
43. Hur EM*, et al.* (2011) GSK3 controls axon growth via CLASP-mediated regulation of growth cone microtubules. *Genes Dev* 25(18):1968-1981.
44. Lein PJ*, et al.* (2007) The novel GTPase Rit differentially regulates axonal and dendritic growth. *J Neurosci* 27(17):4725-4736.
45. Collins CA, Wairkar YP, Johnson SL, & DiAntonio A (2006) Highwire restrains synaptic growth by attenuating a MAP kinase signal. *Neuron* 51(1):57-69.
46. Hammarlund M, Nix P, Hauth L, Jorgensen EM, & Bastiani M (2009) Axon regeneration requires a conserved MAP kinase pathway. *Science* 323(5915):802-806.
47. Nakata K*, et al.* (2005) Regulation of a DLK-1 and p38 MAP kinase pathway by the ubiquitin ligase RPM-1 is required for presynaptic development. *Cell* 120(3):407-420.
48. Lewcock JW, Genoud N, Lettieri K, & Pfaff SL (2007) The ubiquitin ligase Phr1 regulates axon outgrowth through modulation of microtubule dynamics. *Neuron* 56(4):604-620.
49. Tedeschi A & Bradke F (2013) The DLK signalling pathway--a double-edged sword in neural development and regeneration. *EMBO Rep* 14(7):605-614.
50. Watkins TA*, et al.* (2013) DLK initiates a transcriptional program that couples apoptotic and regenerative responses to axonal injury. *Proc Natl Acad Sci U S A* 110(10):4039-4044.
51. Xiong X*, et al.* (2010) Protein turnover of the Wallenda/DLK kinase regulates a retrograde response to axonal injury. *J Cell Biol* 191(1):211-223.
52. Yan D, Wu Z, Chisholm AD, & Jin Y (2009) The DLK-1 kinase promotes mRNA stability and local translation in C. elegans synapses and axon regeneration. *Cell* 138(5):1005-1018.
53. Xiong X & Collins CA (2012) A conditioning lesion protects axons from degeneration via the Wallenda/DLK MAP kinase signaling cascade. *J Neurosci* 32(2):610-615.
54. Klinedinst S, Wang X, Xiong X, Haenfler JM, & Collins CA (2013) Independent pathways downstream of the Wnd/DLK MAPKKK regulate synaptic structure, axonal transport, and injury signaling. *J Neurosci* 33(31):12764-12778.
55. Zhen M, Huang X, Bamber B, & Jin Y (2000) Regulation of presynaptic terminal organization by C. elegans RPM-1, a putative guanine nucleotide exchanger with a RING-H2 finger domain. *Neuron* 26(2):331-343.
56. Schaefer AM, Hadwiger GD, & Nonet ML (2000) rpm-1, a conserved neuronal gene that regulates targeting and synaptogenesis in C. elegans. *Neuron* 26(2):345-356.

57. Wan HI, *et al.* (2000) Highwire regulates synaptic growth in Drosophila. *Neuron* 26(2):313-329.
58. Wu C, Wairkar YP, Collins CA, & DiAntonio A (2005) Highwire function at the Drosophila neuromuscular junction: spatial, structural, and temporal requirements. *J Neurosci* 25(42):9557-9566.
59. Shin Jung E, *et al.* (2012) Dual leucine zipper kinase is required for retrograde injury signaling and axonal regeneration. *Neuron* 74(6):1015-1022.
60. Wittmann T & Waterman-Storer CM (2005) Spatial regulation of CLASP affinity for microtubules by Rac1 and GSK3beta in migrating epithelial cells. *J Cell Biol* 169(6):929-939.
61. Galjart N (2005) CLIPs and CLASPs and cellular dynamics. *Nat Rev Mol Cell Biol* 6(6):487-498.
62. Conde C & Caceres A (2009) Microtubule assembly, organization and dynamics in axons and dendrites. *Nat Rev Neurosci* 10(5):319-332.
63. Cavazos JE, Golarai G, & Sutula TP (1991) Mossy fiber synaptic reorganization induced by kindling: time course of development, progression, and permanence. *J Neurosci* 11(9):2795-2803.
64. Shelly M & Poo MM (2011) Role of LKB1-SAD/MARK pathway in neuronal polarization. *Dev Neurobiol* 71(6):508-527.
65. Cajal R (1995) *Histology of the nervous system of man and vertebrates* (Oxford University Press, USA).
66. D'Souza J, *et al.* (2005) Formation of the retinotectal projection requires Esrom, an ortholog of PAM (protein associated with Myc). *Development* 132(2):247-256.
67. Hendricks M, *et al.* (2008) Disruption of Esrom and Ryk identifies the roof plate boundary as an intermediate target for commissure formation. *Mol Cell Neurosci* 37(2):271-283.
68. Burgess RW, *et al.* (2004) Evidence for a conserved function in synapse formation reveals Phr1 as a candidate gene for respiratory failure in newborn mice. *Mol Cell Biol* 24(3):1096-1105.
69. Bloom AJ, Miller BR, Sanes JR, & DiAntonio A (2007) The requirement for Phr1 in CNS axon tract formation reveals the corticostriatal boundary as a choice point for cortical axons. *Genes Dev* 21(20):2593-2606.
70. Shin JE & DiAntonio A (2011) Highwire regulates guidance of sister axons in the Drosophila mushroom body. *J Neurosci* 31(48):17689-17700.
71. Miller BR, *et al.* (2009) A dual leucine kinase-dependent axon self-destruction program promotes Wallerian degeneration. *Nat Neurosci* 12(4):387-389.
72. Ghosh AS, *et al.* (2011) DLK induces developmental neuronal degeneration via selective regulation of proapoptotic JNK activity. *J Cell Biol* 194(5):751-764.
73. Xiong X, *et al.* (2012) The highwire ubiquitin ligase promotes axonal degeneration by tuning levels of nmnat protein. *PLoS Biol* 10(12):e1001440.
74. Grueber WB, *et al.* (2007) Projections of Drosophila multidendritic neurons in the central nervous system: links with peripheral dendrite morphology. *Development* 134(1):55-64.
75. Han C, Jan LY, & Jan YN (2011) Enhancer-driven membrane markers for analysis of nonautonomous mechanisms reveal neuron-glia interactions in Drosophila. *Proc Natl Acad Sci U S A* 108(23):9673-9678.

76. Clark I, Giniger E, Ruohola-Baker H, Jan LY, & Jan YN (1994) Transient posterior localization of a kinesin fusion protein reflects anteroposterior polarity of the Drosophila oocyte. *Curr Biol* 4(4):289-300.
77. Grill B*, et al.* (2007) C. elegans RPM-1 regulates axon termination and synaptogenesis through the Rab GEF GLO-4 and the Rab GTPase GLO-1. *Neuron* 55(4):587-601.
78. Ma J, Plesken H, Treisman JE, Edelman-Novemsky I, & Ren M (2004) Lightoid and Claret: a rab GTPase and its putative guanine nucleotide exchange factor in biogenesis of Drosophila eye pigment granules. *Proc Natl Acad Sci U S A* 101(32):11652-11657.
79. Ciapponi L, Jackson DB, Mlodzik M, & Bohmann D (2001) Drosophila Fos mediates ERK and JNK signals via distinct phosphorylation sites. *Genes Dev* 15(12):1540-1553.
80. Zeitlinger J*, et al.* (1997) Defective dorsal closure and loss of epidermal decapentaplegic expression in Drosophila fos mutants. *Embo J* 16(24):7393-7401.
81. Kockel L, Zeitlinger J, Staszewski LM, Mlodzik M, & Bohmann D (1997) Jun in Drosophila development: redundant and nonredundant functions and regulation by two MAPK signal transduction pathways. *Genes Dev* 11(13):1748-1758.
82. Grueber WB, Jan LY, & Jan YN (2003) Different levels of the homeodomain protein cut regulate distinct dendrite branching patterns of Drosophila multidendritic neurons. *Cell* 112(6):805-818.
83. Crozatier M & Vincent A (2008) Control of multidendritic neuron differentiation in Drosophila: the role of Collier. *Dev Biol* 315(1):232-242.
84. Hattori Y, Sugimura K, & Uemura T (2007) Selective expression of Knot/Collier, a transcriptional regulator of the EBF/Olf-1 family, endows the Drosophila sensory system with neuronal class-specific elaborated dendritic patterns. *Genes Cells* 12(9):1011-1022.
85. Jinushi-Nakao S*, et al.* (2007) Knot/Collier and cut control different aspects of dendrite cytoskeleton and synergize to define final arbor shape. *Neuron* 56(6):963-978.
86. Grueber WB, Jan LY, & Jan YN (2002) Tiling of the Drosophila epidermis by multidendritic sensory neurons. *Development* 129(12):2867-2878.
87. Martin-Blanco E*, et al.* (1998) puckered encodes a phosphatase that mediates a feedback loop regulating JNK activity during dorsal closure in Drosophila. *Genes Dev* 12(4):557-570.
88. Hummel T, Krukkert K, Roos J, Davis G, & Klambt C (2000) Drosophila Futsch/22C10 is a MAP1B-like protein required for dendritic and axonal development. *Neuron* 26(2):357-370.
89. Kim AH*, et al.* (2009) A centrosomal Cdc20-APC pathway controls dendrite morphogenesis in postmitotic neurons. *Cell* 136(2):322-336.
90. Tapia M, Wandosell F, & Garrido JJ (2010) Impaired function of HDAC6 slows down axonal growth and interferes with axon initial segment development. *PLoS One* 5(9):e12908.
91. Pelled D, Riebeling C, van Echten-Deckert G, Sandhoff K, & Futerman AH (2003) Reduced rates of axonal and dendritic growth in embryonic hippocampal

neurones cultured from a mouse model of Sandhoff disease. *Neuropathol Appl Neurobiol* 29(4):341-349.
92. Mori Y, Matsui T, Furutani Y, Yoshihara Y, & Fukuda M (2012) Small GTPase Rab17 regulates dendritic morphogenesis and postsynaptic development of hippocampal neurons. *J Biol Chem* 287(12):8963-8973.
93. Chen L, Stone MC, Tao J, & Rolls MM (2012) Axon injury and stress trigger a microtubule-based neuroprotective pathway. *Proc Natl Acad Sci U S A* 109(29):11842-11847.
94. Tseng GF & Hu ME (1996) Axotomy induces retraction of the dendritic arbor of adult rat rubrospinal neurons. *Acta Anat (Basel)* 155(3):184-193.
95. Yawo H (1987) Changes in the dendritic geometry of mouse superior cervical ganglion cells following postganglionic axotomy. *J Neurosci* 7(11):3703-3711.
96. Crozatier M, Valle D, Dubois L, Ibnsouda S, & Vincent A (1996) Collier, a novel regulator of Drosophila head development, is expressed in a single mitotic domain. *Curr Biol* 6(6):707-718.
97. Warrior R (1994) Primordial germ cell migration and the assembly of the Drosophila embryonic gonad. *Dev Biol* 166(1):180-194.
98. Yamamoto AH, Komma DJ, Shaffer CD, Pirrotta V, & Endow SA (1989) The claret locus in Drosophila encodes products required for eyecolor and for meiotic chromosome segregation. *Embo J* 8(12):3543-3552.
99. Zhang J*, et al.* (2007) Thirty-one flavors of Drosophila rab proteins. *Genetics* 176(2):1307-1322.
100. Nestoras K, Lee H, & Mohler J (1997) Role of knot (kn) in wing patterning in Drosophila. *Genetics* 147(3):1203-1212.
101. Mohler J, Seecoomar M, Agarwal S, Bier E, & Hsai J (2000) Activation of knot (kn) specifies the 3-4 intervein region in the Drosophila wing. *Development* 127(1):55-63.
102. Kuo CT, Jan LY, & Jan YN (2005) Dendrite-specific remodeling of Drosophila sensory neurons requires matrix metalloproteases, ubiquitin-proteasome, and ecdysone signaling. *Proc Natl Acad Sci U S A* 102(42):15230-15235.
103. Barolo S, Castro B, & Posakony JW (2004) New Drosophila transgenic reporters: insulated P-element vectors expressing fast-maturing RFP. *Biotechniques* 36(3):436-440, 442.
104. Blochlinger K, Bodmer R, Jack J, Jan LY, & Jan YN (1988) Primary structure and expression of a product from cut, a locus involved in specifying sensory organ identity in Drosophila. *Nature* 333(6174):629-635.
105. Chen YR & Tan TH (2000) The c-Jun N-terminal kinase pathway and apoptotic signaling (review). *Int J Oncol* 16(4):651-662.
106. Hirai S*, et al.* (2006) The c-Jun N-terminal kinase activator dual leucine zipper kinase regulates axon growth and neuronal migration in the developing cerebral cortex. *J Neurosci* 26(46):11992-12002.
107. Fan G, Merritt SE, Kortenjann M, Shaw PE, & Holzman LB (1996) Dual leucine zipper-bearing kinase (DLK) activates p46SAPK and p38mapk but not ERK2. *J Biol Chem* 271(40):24788-24793.
108. Morrison DK & Davis RJ (2003) Regulation of MAP kinase signaling modules by scaffold proteins in mammals. *Annu Rev Cell Dev Biol* 19:91-118.

109. Dhanasekaran DN, Kashef K, Lee CM, Xu H, & Reddy EP (2007) Scaffold proteins of MAP-kinase modules. *Oncogene* 26(22):3185-3202.
110. Whitmarsh AJ (2006) The JIP family of MAPK scaffold proteins. *Biochem Soc Trans* 34(Pt 5):828-832.
111. Koushika SP (2008) "JIP"ing along the axon: the complex roles of JIPs in axonal transport. *Bioessays* 30(1):10-14.
112. Whitmarsh AJ & Davis RJ (1998) Structural organization of MAP-kinase signaling modules by scaffold proteins in yeast and mammals. *Trends Biochem Sci* 23(12):481-485.
113. Nihalani D, Meyer D, Pajni S, & Holzman LB (2001) Mixed lineage kinase-dependent JNK activation is governed by interactions of scaffold protein JIP with MAPK module components. *Embo J* 20(13):3447-3458.
114. Horiuchi D*, et al.* (2007) Control of a kinesin-cargo linkage mechanism by JNK pathway kinases. *Curr Biol* 17(15):1313-1317.
115. Verhey KJ*, et al.* (2001) Cargo of kinesin identified as JIP scaffolding proteins and associated signaling molecules. *J Cell Biol* 152(5):959-970.
116. Bowman AB*, et al.* (2000) Kinesin-dependent axonal transport is mediated by the sunday driver (SYD) protein. *Cell* 103(4):583-594.
117. Byrd DT*, et al.* (2001) UNC-16, a JNK-signaling scaffold protein, regulates vesicle transport in C. elegans. *Neuron* 32(5):787-800.
118. Horiuchi D, Barkus RV, Pilling AD, Gassman A, & Saxton WM (2005) APLIP1, a kinesin binding JIP-1/JNK scaffold protein, influences the axonal transport of both vesicles and mitochondria in Drosophila. *Curr Biol* 15(23):2137-2141.
119. Taru H, Kirino Y, & Suzuki T (2002) Differential roles of JIP scaffold proteins in the modulation of amyloid precursor protein metabolism. *J Biol Chem* 277(30):27567-27574.
120. Abe N & Cavalli V (2008) Nerve injury signaling. *Current opinion in neurobiology* 18(3):276-283.
121. Whitmarsh AJ, Cavanagh J, Tournier C, Yasuda J, & Davis RJ (1998) A mammalian scaffold complex that selectively mediates MAP kinase activation. *Science* 281(5383):1671-1674.
122. Jin Y & Garner CC (2008) Molecular mechanisms of presynaptic differentiation. *Annu Rev Cell Dev Biol* 24:237-262.
123. Goellner B & Aberle H (2012) The synaptic cytoskeleton in development and disease. *Dev Neurobiol* 72(1):111-125.
124. Chang L, Jones Y, Ellisman MH, Goldstein LS, & Karin M (2003) JNK1 is required for maintenance of neuronal microtubules and controls phosphorylation of microtubule-associated proteins. *Dev Cell* 4(4):521-533.
125. Tararuk T*, et al.* (2006) JNK1 phosphorylation of SCG10 determines microtubule dynamics and axodendritic length. *J Cell Biol* 173(2):265-277.
126. Roos J, Hummel T, Ng N, Klambt C, & Davis GW (2000) Drosophila Futsch regulates synaptic microtubule organization and is necessary for synaptic growth. *Neuron* 26(2):371-382.
127. Janke C & Kneussel M (2010) Tubulin post-translational modifications: encoding functions on the neuronal microtubule cytoskeleton. *Trends Neurosci* 33(8):362-372.

128. Ruiz-Canada C & Budnik V (2006) Synaptic cytoskeleton at the neuromuscular junction. *Int Rev Neurobiol* 75:217-236.
129. Eto K, Kawauchi T, Osawa M, Tabata H, & Nakajima K (2010) Role of dual leucine zipper-bearing kinase (DLK/MUK/ZPK) in axonal growth. *Neurosci Res* 66(1):37-45.
130. Bounoutas A*, et al.* (2011) Microtubule depolymerization in Caenorhabditis elegans touch receptor neurons reduces gene expression through a p38 MAPK pathway. *Proc Natl Acad Sci U S A* 108(10):3982-3987.
131. Hirai S, Banba Y, Satake T, & Ohno S (2011) Axon formation in neocortical neurons depends on stage-specific regulation of microtubule stability by the dual leucine zipper kinase-c-Jun N-terminal kinase pathway. *J Neurosci* 31(17):6468-6480.
132. Ghosh-Roy A, Goncharov A, Jin Y, & Chisholm AD (2012) Kinesin-13 and tubulin posttranslational modifications regulate microtubule growth in axon regeneration. *Dev Cell* 23(4):716-728.
133. Nix P, Hisamoto N, Matsumoto K, & Bastiani M (2011) Axon regeneration requires coordinate activation of p38 and JNK MAPK pathways. *Proc Natl Acad Sci U S A* 108(26):10738-10743.
134. Schoorlemmer J & Goldfarb M (2001) Fibroblast growth factor homologous factors are intracellular signaling proteins. *Curr Biol* 11(10):793-797.
135. Buchsbaum RJ, Connolly BA, & Feig LA (2002) Interaction of Rac exchange factors Tiam1 and Ras-GRF1 with a scaffold for the p38 mitogen-activated protein kinase cascade. *Mol Cell Biol* 22(12):4073-4085.
136. Lee CM, Onesime D, Reddy CD, Dhanasekaran N, & Reddy EP (2002) JLP: A scaffolding protein that tethers JNK/p38MAPK signaling modules and transcription factors. *Proc Natl Acad Sci U S A* 99(22):14189-14194.
137. Kelkar N, Standen CL, & Davis RJ (2005) Role of the JIP4 scaffold protein in the regulation of mitogen-activated protein kinase signaling pathways. *Mol Cell Biol* 25(7):2733-2743.
138. Han ZS*, et al.* (1998) A conserved p38 mitogen-activated protein kinase pathway regulates Drosophila immunity gene expression. *Mol Cell Biol* 18(6):3527-3539.
139. Adachi-Yamada T*, et al.* (1999) p38 mitogen-activated protein kinase can be involved in transforming growth factor beta superfamily signal transduction in Drosophila wing morphogenesis. *Mol Cell Biol* 19(3):2322-2329.
140. Suzanne M*, et al.* (1999) The Drosophila p38 MAPK pathway is required during oogenesis for egg asymmetric development. *Genes Dev* 13(11):1464-1474.
141. Zhuang ZH, Zhou Y, Yu MC, Silverman N, & Ge BX (2006) Regulation of Drosophila p38 activation by specific MAP2 kinase and MAP3 kinase in response to different stimuli. *Cell Signal* 18(4):441-448.
142. Inoue H*, et al.* (2001) A Drosophila MAPKKK, D-MEKK1, mediates stress responses through activation of p38 MAPK. *Embo J* 20(19):5421-5430.
143. Craig CR, Fink JL, Yagi Y, Ip YT, & Cagan RL (2004) A Drosophila p38 orthologue is required for environmental stress responses. *EMBO Rep* 5(11):1058-1063.

144. Sano Y, *et al.* (2005) Drosophila activating transcription factor-2 is involved in stress response via activation by p38, but not c-Jun NH(2)-terminal kinase. *Mol Biol Cell* 16(6):2934-2946.
145. Cully M, *et al.* (2010) A role for p38 stress-activated protein kinase in regulation of cell growth via TORC1. *Mol Cell Biol* 30(2):481-495.
146. Vrailas-Mortimer A, *et al.* (2011) A muscle-specific p38 MAPK/Mef2/MnSOD pathway regulates stress, motor function, and life span in Drosophila. *Dev Cell* 21(4):783-795.
147. Han ZS & Ip YT (1999) Interaction and specificity of Rel-related proteins in regulating Drosophila immunity gene expression. *J Biol Chem* 274(30):21355-21361.
148. Davis MM, Primrose DA, & Hodgetts RB (2008) A member of the p38 mitogen-activated protein kinase family is responsible for transcriptional induction of Dopa decarboxylase in the epidermis of Drosophila melanogaster during the innate immune response. *Mol Cell Biol* 28(15):4883-4895.
149. Ha EM, *et al.* (2009) Coordination of multiple dual oxidase-regulatory pathways in responses to commensal and infectious microbes in drosophila gut. *Nat Immunol* 10(9):949-957.
150. Shinzawa N, *et al.* (2009) p38 MAPK-dependent phagocytic encapsulation confers infection tolerance in Drosophila. *Cell Host Microbe* 6(3):244-252.
151. Park JS, Kim YS, & Yoo MA (2009) The role of p38b MAPK in age-related modulation of intestinal stem cell proliferation and differentiation in Drosophila. *Aging (Albany NY)* 1(7):637-651.
152. Chen X, *et al.* (2008) Antiapoptotic and trophic effects of dominant-negative forms of dual leucine zipper kinase in dopamine neurons of the substantia nigra in vivo. *J Neurosci* 28(3):672-680.
153. Itoh A, *et al.* (2011) ZPK/DLK, a mitogen-activated protein kinase kinase kinase, is a critical mediator of programmed cell death of motoneurons. *J Neurosci* 31(20):7223-7228.
154. Welsbie DS, *et al.* (2013) Functional genomic screening identifies dual leucine zipper kinase as a key mediator of retinal ganglion cell death. *Proc Natl Acad Sci U S A* 110(10):4045-4050.
155. Cavalli V, Kujala P, Klumperman J, & Goldstein LS (2005) Sunday Driver links axonal transport to damage signaling. *J Cell Biol* 168(5):775-787.
156. Hirai S, *et al.* (2002) MAPK-upstream protein kinase (MUK) regulates the radial migration of immature neurons in telencephalon of mouse embryo. *Development* 129(19):4483-4495.
157. Gelderblom M, Eminel S, Herdegen T, & Waetzig V (2004) c-Jun N-terminal kinases (JNKs) and the cytoskeleton--functions beyond neurodegeneration. *Int J Dev Neurosci* 22(7):559-564.
158. Correa SA & Eales KL (2012) The Role of p38 MAPK and Its Substrates in Neuronal Plasticity and Neurodegenerative Disease. *J Signal Transduct* 2012:649079.
159. Goedert M, *et al.* (1997) Phosphorylation of microtubule-associated protein tau by stress-activated protein kinases. *FEBS Lett* 409(1):57-62.

160. Reynolds CH, Utton MA, Gibb GM, Yates A, & Anderton BH (1997) Stress-activated protein kinase/c-jun N-terminal kinase phosphorylates tau protein. *J Neurochem* 68(4):1736-1744.
161. Reynolds CH, Nebreda AR, Gibb GM, Utton MA, & Anderton BH (1997) Reactivating kinase/p38 phosphorylates tau protein in vitro. *J Neurochem* 69(1):191-198.
162. Gdalyahu A*, et al.* (2004) DCX, a new mediator of the JNK pathway. *Embo J* 23(4):823-832.
163. Gordon-Weeks PR (2004) Microtubules and growth cone function. *J Neurobiol* 58(1):70-83.
164. Erez H*, et al.* (2007) Formation of microtubule-based traps controls the sorting and concentration of vesicles to restricted sites of regenerating neurons after axotomy. *J Cell Biol* 176(4):497-507.
165. Stone MC, Nguyen MM, Tao J, Allender DL, & Rolls MM (2010) Global up-regulation of microtubule dynamics and polarity reversal during regeneration of an axon from a dendrite. *Mol Biol Cell* 21(5):767-777.
166. Hur EM, Saijilafu, & Zhou FQ (2012) Growing the growth cone: remodeling the cytoskeleton to promote axon regeneration. *Trends Neurosci* 35(3):164-174.
167. Stronach B & Perrimon N (2002) Activation of the JNK pathway during dorsal closure in Drosophila requires the mixed lineage kinase, slipper. *Genes Dev* 16(3):377-387.
168. Sathyanarayana P*, et al.* (2003) Drosophila mixed lineage kinase/slipper, a missing biochemical link in Drosophila JNK signaling. *Biochim Biophys Acta* 1640(1):77-84.
169. Nguyen Q, Lee CM, Le A, & Reddy EP (2005) JLP associates with kinesin light chain 1 through a novel leucine zipper-like domain. *J Biol Chem* 280(34):30185-30191.
170. Arimoto M*, et al.* (2011) The Caenorhabditis elegans JIP3 protein UNC-16 functions as an adaptor to link kinesin-1 with cytoplasmic dynein. *J Neurosci* 31(6):2216-2224.
171. Sun F, Zhu C, Dixit R, & Cavalli V (2011) Sunday Driver/JIP3 binds kinesin heavy chain directly and enhances its motility. *Embo J* 30(16):3416-3429.
172. Morfini G*, et al.* (2006) JNK mediates pathogenic effects of polyglutamine-expanded androgen receptor on fast axonal transport. *Nature neuroscience* 9(7):907-916.
173. Stagi M, Gorlovoy P, Larionov S, Takahashi K, & Neumann H (2006) Unloading kinesin transported cargoes from the tubulin track via the inflammatory c-Jun N-terminal kinase pathway. *Faseb J* 20(14):2573-2575.
174. Morfini GA*, et al.* (2009) Pathogenic huntingtin inhibits fast axonal transport by activating JNK3 and phosphorylating kinesin. *Nature neuroscience* 12(7):864-871.
175. Reed NA*, et al.* (2006) Microtubule acetylation promotes kinesin-1 binding and transport. *Curr Biol* 16(21):2166-2172.
176. Eaton BA, Fetter RD, & Davis GW (2002) Dynactin is necessary for synapse stabilization. *Neuron* 34(5):729-741.

177. Hurd DD & Saxton WM (1996) Kinesin mutations cause motor neuron disease phenotypes by disrupting fast axonal transport in Drosophila. *Genetics* 144(3):1075-1085.
178. Pack-Chung E, Kurshan PT, Dickman DK, & Schwarz TL (2007) A Drosophila kinesin required for synaptic bouton formation and synaptic vesicle transport. *Nature neuroscience* 10(8):980-989.
179. Ghosh-Roy A, Wu Z, Goncharov A, Jin Y, & Chisholm AD (2010) Calcium and cyclic AMP promote axonal regeneration in Caenorhabditis elegans and require DLK-1 kinase. *J Neurosci* 30(9):3175-3183.
180. Muresan Z & Muresan V (2005) Coordinated transport of phosphorylated amyloid-beta precursor protein and c-Jun NH2-terminal kinase-interacting protein-1. *J Cell Biol* 171(4):615-625.
181. Huang C*, et al.* (2012) A permissive role of mushroom body alpha/beta core neurons in long-term memory consolidation in Drosophila. *Curr Biol* 22(21):1981-1989.
182. Budnik V*, et al.* (1996) Regulation of synapse structure and function by the Drosophila tumor suppressor gene dlg. *Neuron* 17(4):627-640.
183. Ritzenthaler S, Suzuki E, & Chiba A (2000) Postsynaptic filopodia in muscle cells interact with innervating motoneuron axons. *Nature neuroscience* 3(10):1012-1017.
184. Fujioka M*, et al.* (2003) Even-skipped, acting as a repressor, regulates axonal projections in Drosophila. *Development* 130(22):5385-5400.
185. Aberle H*, et al.* (2002) wishful thinking encodes a BMP type II receptor that regulates synaptic growth in Drosophila. *Neuron* 33(4):545-558.
186. Eresh S, Riese J, Jackson DB, Bohmann D, & Bienz M (1997) A CREB-binding site as a target for decapentaplegic signalling during Drosophila endoderm induction. *Embo J* 16(8):2014-2022.
187. Weber U, Paricio N, & Mlodzik M (2000) Jun mediates Frizzled-induced R3/R4 cell fate distinction and planar polarity determination in the Drosophila eye. *Development* 127(16):3619-3629.
188. Dietzl G*, et al.* (2007) A genome-wide transgenic RNAi library for conditional gene inactivation in Drosophila. *Nature* 448(7150):151-156.
189. Osterwalder T, Yoon KS, White BH, & Keshishian H (2001) A conditional tissue-specific transgene expression system using inducible GAL4. *Proc Natl Acad Sci U S A* 98(22):12596-12601.
190. Daniels RW*, et al.* (2004) Increased expression of the Drosophila vesicular glutamate transporter leads to excess glutamate release and a compensatory decrease in quantal content. *J Neurosci* 24(46):10466-10474.
191. Viquez NM, Li CR, Wairkar YP, & DiAntonio A (2006) The B' protein phosphatase 2A regulatory subunit well-rounded regulates synaptic growth and cytoskeletal stability at the Drosophila neuromuscular junction. *J Neurosci* 26(36):9293-9303.
192. Fuerst PG*, et al.* (2009) DSCAM and DSCAML1 function in self-avoidance in multiple cell types in the developing mouse retina. *Neuron* 64(4):484-497.

193. Fuerst PG, Koizumi A, Masland RH, & Burgess RW (2008) Neurite arborization and mosaic spacing in the mouse retina require DSCAM. *Nature* 451(7177):470-474.
194. Millard SS & Zipursky SL (2008) Dscam-mediated repulsion controls tiling and self-avoidance. *Current opinion in neurobiology* 18(1):84-89.
195. Schmucker D & Chen B (2009) Dscam and DSCAM: complex genes in simple animals, complex animals yet simple genes. *Genes Dev* 23(2):147-156.
196. Yamagata M & Sanes JR (2008) Dscam and Sidekick proteins direct lamina-specific synaptic connections in vertebrate retina. *Nature* 451(7177):465-469.
197. Schmucker D*, et al.* (2000) Drosophila Dscam is an axon guidance receptor exhibiting extraordinary molecular diversity. *Cell* 101(6):671-684.
198. Hattori D*, et al.* (2007) Dscam diversity is essential for neuronal wiring and self-recognition. *Nature* 449(7159):223-227.
199. Hattori D, Millard SS, Wojtowicz WM, & Zipursky SL (2008) Dscam-mediated cell recognition regulates neural circuit formation. *Annu Rev Cell Dev Biol* 24:597-620.
200. Zipursky SL & Sanes JR (2010) Chemoaffinity revisited: dscams, protocadherins, and neural circuit assembly. *Cell* 143(3):343-353.
201. Hughes ME*, et al.* (2007) Homophilic Dscam interactions control complex dendrite morphogenesis. *Neuron* 54(3):417-427.
202. Matthews BJ*, et al.* (2007) Dendrite self-avoidance is controlled by Dscam. *Cell* 129(3):593-604.
203. Wang J, Zugates CT, Liang IH, Lee CH, & Lee T (2002) Drosophila Dscam is required for divergent segregation of sister branches and suppresses ectopic bifurcation of axons. *Neuron* 33(4):559-571.
204. Chen BE*, et al.* (2006) The molecular diversity of Dscam is functionally required for neuronal wiring specificity in Drosophila. *Cell* 125(3):607-620.
205. Hummel T*, et al.* (2003) Axonal targeting of olfactory receptor neurons in Drosophila is controlled by Dscam. *Neuron* 37(2):221-231.
206. Millard SS, Lu Z, Zipursky SL, & Meinertzhagen IA (2010) Drosophila Dscam proteins regulate postsynaptic specificity at multiple-contact synapses. *Neuron* 67(5):761-768.
207. Zhu H*, et al.* (2006) Dendritic patterning by Dscam and synaptic partner matching in the Drosophila antennal lobe. *Nature neuroscience* 9(3):349-355.
208. Blank M*, et al.* (2011) The Down syndrome critical region regulates retinogeniculate refinement. *J Neurosci* 31(15):5764-5776.
209. Maynard KR & Stein E (2012) DSCAM contributes to dendrite arborization and spine formation in the developing cerebral cortex. *J Neurosci* 32(47):16637-16650.
210. Saito Y*, et al.* (2000) The developmental and aging changes of Down's syndrome cell adhesion molecule expression in normal and Down's syndrome brains. *Acta Neuropathol* 100(6):654-664.
211. Larsen DD & Callaway EM (2006) Development of layer-specific axonal arborizations in mouse primary somatosensory cortex. *J Comp Neurol* 494(3):398-414.

212. Shen L*, et al.* (2011) Altered expression of Dscam in temporal lobe tissue from human and experimental animals. *Synapse* 65(10):975-982.
213. Amano K*, et al.* (2008) Association study between the Down syndrome cell adhesion molecule (DSCAM) gene and bipolar disorder. *Psychiatric genetics* 18(1):1-10.
214. Wang J*, et al.* (2004) Transmembrane/juxtamembrane domain-dependent Dscam distribution and function during mushroom body neuronal morphogenesis. *Neuron* 43(5):663-672.
215. Hattori D*, et al.* (2009) Robust discrimination between self and non-self neurites requires thousands of Dscam1 isoforms. *Nature* 461(7264):644-648.
216. Zhan XL*, et al.* (2004) Analysis of Dscam diversity in regulating axon guidance in Drosophila mushroom bodies. *Neuron* 43(5):673-686.
217. Fulga TA & Van Vactor D (2008) Synapses and growth cones on two sides of a highwire. *Neuron* 57(3):339-344.
218. Wilkie GS, Dickson KS, & Gray NK (2003) Regulation of mRNA translation by 5'- and 3'-UTR-binding factors. *Trends Biochem Sci* 28(4):182-188.
219. Santoro MR, Bray SM, & Warren ST (2012) Molecular mechanisms of fragile X syndrome: a twenty-year perspective. *Annual review of pathology* 7:219-245.
220. Brown V*, et al.* (2001) Microarray identification of FMRP-associated brain mRNAs and altered mRNA translational profiles in Fragile X syndrome. *Cell* 107(4):477-487.
221. Darnell Jennifer C*, et al.* (2011) FMRP stalls ribosomal translocation on mRNAs linked to synaptic function and autism. *Cell* 146(2):247-261.
222. Laggerbauer B, Ostareck D, Keidel EM, Ostareck-Lederer A, & Fischer U (2001) Evidence that fragile X mental retardation protein is a negative regulator of translation. *Human Molecular Genetics* 10(4):329-338.
223. Zhang YQ*, et al.* (2001) Drosophila fragile X-related gene regulates the MAP1B homolog Futsch to control synaptic structure and function. *Cell* 107(5):591-603.
224. Ascano M, Jr.*, et al.* (2012) FMRP targets distinct mRNA sequence elements to regulate protein expression. *Nature* 492(7429):382-386.
225. Li W & Guan KL (2004) The Down syndrome cell adhesion molecule (DSCAM) interacts with and activates Pak. *J Biol Chem* 279(31):32824-32831.
226. Alves-Sampaio A, Troca-Marin JA, & Montesinos ML (2010) NMDA-mediated regulation of DSCAM dendritic local translation is lost in a mouse model of Down's syndrome. *The Journal of neuroscience* 30(40):13537-13548.
227. Houser CR*, et al.* (1990) Altered patterns of dynorphin immunoreactivity suggest mossy fiber reorganization in human hippocampal epilepsy. *J Neurosci* 10(1):267-282.
228. Marco P & DeFelipe J (1997) Altered synaptic circuitry in the human temporal neocortex removed from epileptic patients. *Exp Brain Res* 114(1):1-10.
229. Sutula T, Cascino G, Cavazos J, Parada I, & Ramirez L (1989) Mossy fiber synaptic reorganization in the epileptic human temporal lobe. *Annals of neurology* 26(3):321-330.
230. Musumeci SA*, et al.* (1999) Epilepsy and EEG findings in males with fragile X syndrome. *Epilepsia* 40(8):1092-1099.

231. Stafstrom CE (1993) Epilepsy in Down syndrome: clinical aspects and possible mechanisms. *American journal of mental retardation : AJMR* 98 Suppl:12-26.
232. Verkerk AJ*, et al.* (1991) Identification of a gene (FMR-1) containing a CGG repeat coincident with a breakpoint cluster region exhibiting length variation in fragile X syndrome. *Cell* 65(5):905-914.
233. Zhang YQ, Rodesch CK, & Broadie K (2002) Living synaptic vesicle marker: synaptotagmin-GFP. *Genesis* 34(1-2):142-145.
234. Bateman JR, Lee AM, & Wu CT (2006) Site-specific transformation of Drosophila via phiC31 integrase-mediated cassette exchange. *Genetics* 173(2):769-777.
235. Gordon MD & Scott K (2009) Motor control in a Drosophila taste circuit. *Neuron* 61(3):373-384.
236. Shi L, Yu HH, Yang JS, & Lee T (2007) Specific Drosophila Dscam juxtamembrane variants control dendritic elaboration and axonal arborization. *The Journal of neuroscience* 27(25):6723-6728.
237. Yuan JS, Reed A, Chen F, & Stewart CN, Jr. (2006) Statistical analysis of real-time PCR data. *BMC bioinformatics* 7:85.
238. Rall W (1964) *Theoretical significance of dendritic trees for neuronal input-output relations* (Stanford University Press) pp 73-97.
239. Spruston N (2008) Pyramidal neurons: dendritic structure and synaptic integration. *Nat Rev Neurosci* 9(3):206-221.
240. Strausfeld NJ (1976) *Atlas of an insect brain* (Springer).
241. Laurent G (1999) *Dendritic processing in invertebrates: a link to function.* (Oxford: Oxford University Press).
242. Grueber WB, Yang CH, Ye B, & Jan YN (2005) The development of neuronal morphology in insects. *Curr Biol* 15(17):R730-738.
243. Harris WA (2001) Temporal coordinates: the genes that fix cell fate with birth order. *Dev Cell* 1(3):313-314.
244. Hatten ME (1999) Central nervous system neuronal migration. *Annu Rev Neurosci* 22:511-539.
245. Orgogozo V & Grueber WB (2005) FlyPNS, a database of the Drosophila embryonic and larval peripheral nervous system. *BMC Dev Biol* 5:4.
246. Kim MD, Jan LY, & Jan YN (2006) The bHLH-PAS protein Spineless is necessary for the diversification of dendrite morphology of Drosophila dendritic arborization neurons. *Genes Dev* 20(20):2806-2819.
247. Ghannad-Rezaie M, Wang X, Mishra B, Collins C, & Chronis N (2012) Microfluidic chips for in vivo imaging of cellular responses to neural injury in Drosophila larvae. *PLoS One* 7(1):e29869.
248. Huang da W, Sherman BT, & Lempicki RA (2009) Systematic and integrative analysis of large gene lists using DAVID bioinformatics resources. *Nat Protoc* 4(1):44-57.
249. Allen MJ*, et al.* (1999) Targeted expression of truncated glued disrupts giant fiber synapse formation in Drosophila. *J Neurosci* 19(21):9374-9384.
250. Sherwood NT, Sun Q, Xue M, Zhang B, & Zinn K (2004) Drosophila spastin regulates synaptic microtubule networks and is required for normal motor function. *PLoS Biol* 2(12):e429.

251. Moore AW, Jan LY, & Jan YN (2002) hamlet, a binary genetic switch between single- and multiple- dendrite neuron morphology. *Science* 297(5585):1355-1358.
252. Nadarajah B & Parnavelas JG (2002) Modes of neuronal migration in the developing cerebral cortex. *Nat Rev Neurosci* 3(6):423-432.
253. Tsai LH & Gleeson JG (2005) Nucleokinesis in neuronal migration. *Neuron* 46(3):383-388.
254. Taghert PH*, et al.* (2001) Multiple amidated neuropeptides are required for normal circadian locomotor rhythms in Drosophila. *J Neurosci* 21(17):6673-6686.
255. Boylan KL & Hays TS (2002) The gene for the intermediate chain subunit of cytoplasmic dynein is essential in Drosophila. *Genetics* 162(3):1211-1220.
256. Smyth GK (2004) Linear models and empirical bayes methods for assessing differential expression in microarray experiments. *Stat Appl Genet Mol Biol* 3:Article3.
257. Kim JH, Wang X, Coolon R, & Ye B (2013) Dscam expression levels determine presynaptic arbor sizes in Drosophila sensory neurons. *Neuron* 78(5):827-838.
258. Gamberi C, Johnstone O, & Lasko P (2006) Drosophila RNA binding proteins. *Int Rev Cytol* 248:43-139.
259. Moore DL*, et al.* (2009) KLF family members regulate intrinsic axon regeneration ability. *Science* 326(5950):298-301.